Viral Antagonism of Extracellular cGAMP Responses



A thesis submitted by

Henry Titus Wigram Blest

St Edmund Hall

for the degree of

Doctor of Philosophy in Medical Sciences

to the

University of Oxford

Michaelmas Term 2022

Abstract

The presence of viral DNA outside of the nucleus is detected by the pattern recognition receptor cGAS during infection. cGAS then generates the cyclic dinucleotide 2'3'-cGAMP, which activates the central hub of DNA sensing – STING. This results in the production of proinflammatory cytokines, primarily type I interferons, driving antiviral responses.

Classically, 2'3'-cGAMP was thought to solely act within the cytosol, as its negative charge makes it membrane impermeable. Recently, five membrane spanning channels (ABCC1, SLC19A1, SLC46A2, P2X7 and LRRC8A:C/E) have been shown to import and export 2'3'-cGAMP allowing movement between cells. This finding implicates extracellular 2'3'-cGAMP in a range of functions: defence against viral invasion; T cell proliferation; natural killer cell recruitment; vaccine efficacy; cancer clearance; metastasis and immunotherapy. 2'3'-cGAMP may thus function like a cytokine to message between cells.

I theorised if exogenous 2'3'-cGAMP functions within the innate immune response then viruses would act to evade this mechanism. I screened viruses for the capacity to deplete cGAMP channels during infection. I found that viruses with dsDNA genomes deplete multiple cGAMP channels during infection, whereas no viruses with RNA genomes reduced cGAMP channel abundance. Remarkably, Herpes Simplex Virus 1 (HSV-1) degraded three of the five known cGAMP channels - P2X7, SLC46A2 and LRRC8A:C. Therefore, I chose HSV-1 as a model virus to study the effects of extracellular 2'3'-cGAMP.

By immunoprecipitating LRRC8C from HSV-1 infected cells and preforming mass spectrometry-based proteomics I identified UL56, as a viral interaction partner of LRRC8C. Overexpression of UL56 confirmed that it caused LRRC8A:C degradation. Unexpectedly I found UL56 also caused degradation of the P2X7 and SLC46A2 channels. Using the reverse approach, I found that HSV-1 lacking the *UL56* gene (HSV-1-ΔUL56) was unable to degrade cGAMP channels. This proves that UL56 is necessary and sufficient to degrade all three of the cGAMP channels. Mechanistically UL56 contains PPXY motifs that act as a platform for recruitment of NEDD-4 family ubiquitin ligases. I showed that mutation of the PPXY motifs to AAXA prevented degradation of cGAMP channels by UL56, both when UL56-AAXA was over-expressed or upon infection with AXAA mutated virus (HSV-1-AAXA). Consistent with degradation mediated by NEDD-4 ligases, chemical inhibition of the proteasome appeared to rescue LRRC8A:C abundance.

To show UL56 inhibits 2'3'-cGAMP import, I developed in *vitro* models of 2'3'-cGAMP uptake for LRRC8A:C, SLC46A2 and P2X7. This was done either by activating channels endogenously expressed by 293 cells (LRRC8A:C) or by stably overexpressing the channels (P2X7 and SLC46A2) to allow increased 2'3'-cGAMP uptake. In this system, import of 2'3'-cGAMP can be blocked with channel-specific inhibitors or by overexpression of UL56. This showed functionally that UL56 prevents 2'3'-cGAMP from being imported into cells and so inhibits IFN-β production. In summary I show for the first time that a virus antagonises cGAMP channels, likely to avoid the effects of exogenous 2'3'-cGAMP, thus adding to the recent and exciting body of literature describing the role of 2'3'-cGAMP as a signalling molecule between cells.

Acknowledgements

Firstly, I would like to thank the Rehwinkel lab both past (Dr Jonny Hertzog, Dr Lise Chauveau, Dr Natalia Sampaio, Dr Alice Mayer, Dr Valerie Odon, Dr Tamara Davenne, Dr Qiannan Tang, Dr Layal Liverpool, Jurgen Moonen and Astrid Hvidt) and present (Dr Anne Bridgeman, Dr Rachel Rigby, Dr Tanja Davis, Gerissa Fowler, Elizabeth Horton and Alexander Redmond) for their wonderful support. Particular thanks go to my supervisor Lise for her endless patience and uplifting nature. Jonny for being a constant fount of knowledge and for putting up with endless questions. Natalia for being a supportive force of nature particularly when the outlook was bleak. Anne not only for her direct scientific contributions but also her upbeat presence within the lab. My desk mate Rachel for her unparalleled technical insights and always encouraging me to push forwards. I would like to thank Tanja, Gerissa, Lizze, Jurgen and Alex for their camaraderie. Additionally, I am very grateful to have been able to supervise Jed Avissar, an extremely talented, Msc student who was willingly bossed around and contributed massively to the work presented on both P2X7 and SLC46A2. I would also like to thank my thesis committee (Professor Alexander Drakesmith, Professor Mads Gyrd-Hansen and Professor Jelena Bezbradica) and the Maelfait lab for their advice and encouragement.

I would like to acknowledge the greatly supportive teachers, university lectures and scientific mentors I have had the privilege of learning from over the years. In particular my school teachers Mr Nicholas Welford, Dr Richard Heal, Mrs Susan Haslam and Mrs Abigail Elliot. Not only for their lessons but also their pastoral support. My undergraduate supervisor Dr Jamel Mankouri whose encouragement gave me the confidence to pursue a PhD. Professor Richard Milne a lecturer who taught me the fundamental tenets of virology. My post-graduate supervisor Dr Rebecca Sumner who took the time to explain at length the techniques needed to study the innate immune response.

I would like to thank my family for their continuous support. Notably my father (Anthony Blest) and my mother (Caroline Sheldon) without whose constant encouragement this would not have been possible. My sibling Francesca Blest for being a source of stability and my

closest ally. My sisters Harriet, Julia and Anna and cousins Juliet, Tom, Lucy, Richie, Charles, and Sophie – for being borderline hilarious. And of course, to Mary for providing sanity.

I am truly Blest to be surrounded by supportive friends and would like to thank - Katherine Stoodley, Giles Docherty, Milly Sellers, Charlie Campbell, Helena Winston, Silvia Castro Torres, Jago Poynter, Molly Skinner, Fred Manning, Billy Metcalfe, Emily Everest-Phillips, Antonin Charet, Eloise Donovan and Panagiotis Karagkiozelis. I would also like to specifically thank my long-suffering flat mate – Federico Nebuloni – and I promise that I will do more cleaning after submission.

I would like to thank the MRC and WIMM DPhil studentship for funding me through my studies and our close collaborators Colin Crump and Jake Barker who provided us with many reagents that made the work possible.

At her own request (and quite rightly so), this thesis is dedicated to my oldest friend Elvira McCaldin. An individual who listened to me constantly whine about my siRNA transfected THP-1 cells being dead... again. Counselled me through the frustrations of COVID and has always made herself available at times of crisis. I thank you for your support.

Finally, and most importantly, I would like to thank Jan Rehwinkel for providing an exceptionally supportive environment in which to work. This would not have been possible without his guidance, and I am eternally grateful for the work and supervision he has put in. Specifically, I thank Jan for allowing me the freedom to test some of my own ideas and for being a committed mentor. It has been an enormous privilege to work with him.

Acronyms

2'3'-cGAMP	2',3'-cyclic-GMP-AMP
ABCC1	ATP Binding cassette subfamily C member 1
ABCG2	ATP Binding cassette subfamily G member 2
ADAR	Adenosine deaminase acting on RNA
AdV	Adenovirus
AGS	Aicardi-Goutières syndrome
AIM-2	Absent In melanoma 2
AL	Abundnace limit
AMP	Adenosine monophosphate
AMPK	AMP-activated protein kinase
ATP	Adenosine triphosphate
BLAST	Blasticidin
BMDC	Bone marrow-derived dendritic cell
BMDM	Bone-marrow-derived macrophage
BMM	Bone marrow-derived macrophage
cAMP	Cyclic adenosine monophosphate
Cas9	CRISPR-associated protein 9
CBD	cyclic dinucleotide binding domain
CDN	cyclic dinucleotide
CG	5'-CG-3' motif
cGAS	Cyclic GMP–AMP synthase
CNS	Central nervous system
COVID-19	Coronavirus disease 2019
CRISPR	Clustered Regularly Interspaced Short Palindromic Repeats
Cryo-EM	Cryogenic electron microscopy
CTT	C terminal tail
CVV	Crystal violet viability
CyHV-3	Cyprinid herpesvirus 3
DAMP	Damage associated molecular pattern
DC	Dendritic cell
DDX	DEAD-box helicase
DHX	DEAH-box helicase
DMEM	Dulbecco's Modified Eagle Medium
DNA-PK	The DNA-dependent protein kinase
dsDNA	Double stranded DNA
dsRNA	Double stranded RNA
DUB	Deubiquitinating enzymes
E2	Prostaglandin E2
EE	Early endosome

EEHV	Elephant Endotheliotropic Herpesvirus
EGFR	Epidermal growth factor receptor
EL	Extracellular loop
ENPP1	Ecto-nucleotide pyrophosphatase/phosphodiesterase
ERAD	Endoplasmic reticulum (ER)-associated protein degradation
ERGIC	Endoplasmic-reticulum–Golgi intermediate compartment
FACS	Fluorescence-activated cell sorting
FPRL-1	Formyl peptide G protein-coupled receptor
GABA	Gamma-aminobutyric acid
gB	Glycoprotein B
gC	Glycoprotein C
gD	Glycoprotein D
GFP	Green fluorescent protein
GJIC	Gap junctional intercellular communications
GTP	Guanosine-5'-triphosphate
HDP-RNP	HEXIM1-DNA-PK-paraspeckle components-ribonucleoprotein complex
HFF	Human foreskin fibroblast
HIV-1	Human Immunodeficiency Virus type 1
HIV-2	Human Immunodeficiency Virus type 2
HSPG	Heparan-sulphate proteoglycans
HSV-1	Herpes Simplex Virus type 1
HSV-2	Herpes Simplex Virus type 2
HUVEC	Human umbilical vein endothelial cells
IAV	Influenza
IFNAR	The interferon-α/β receptor
IL	Intracellular loop
IP3	Inositol trisphosphate
IRF	Interferon regulatory factors
ISG	Interferon stimulated gene
ISRE	IFN-stimulated response element
KSHV	Kaposi's Sarcoma-Associated Herpesvirus
LAT	Latency Associated Transcript
LPS	Lipopolysaccharides
LRR	Leucine-rich repeat
LRRC8A	Leucine-rich repeat-containing protein 8A
MAVS	Mitochondrial antiviral-signaling protein
MCMV	Murine Cytomegalovirus
MDA5	Melanoma differentiation-associated protein 5
MEF	Mouse embryonic fibroblast
MEM	Minimum Essential Medium
MerTK	MER proto-oncogene, tyrosine kinase
MHC	Major histocompatibility complex
MLF	Mouse lymphatic fibroblast

MTOC	Microtubule-organising center
NAD	Nicotinamide adenine dinucleotide
NBD1	Nucleotide-binding domain 1
NBD2	Nucleotide-binding domain 2
NF-kB	Nuclear factor-κB
NHEJ	Non-homologous end joining
NK cell	Natural killer cell
NLR	NOD-like receptor
NOD	NOD-like receptor
NPC	Nuclear pore complex
OAS	Interferon (IFN)-induced 2’-5’-oligoadenylate synthetase
OsHV-1	Oyster Herpesvirus type 1
P2A	Porcine teschovirus-1 2A
P2X7	Purinergic Receptor P2X 7
PAMP	Pathogen associated molecular pattern
PBMC	Peripheral blood mononuclear cell
PBS	Phosphate-buffered saline
pDC	Plasmacytoid dendritic cell
PI	Propidium iodide
pM	Peritoneal macrophage
PMA	Phorbol 12-myristate 13-acetate
PRR	Pattern recognition receptor
PS-cGAMP	Pulmonary surfactant mimetic liposomes
PURO	Puromycin
RIG-I	Retinoic acid-inducible gene I
RNF5	RING finger protein 5
RPMI	Roswell Park Memorial Institute
RR	Arginine-rich region
RT-qPCR	Quantitative reverse transcription PCR
S1P	Sphingosine-1-phosphate
SAVI	STING associated vasculopathy with onset in in infancy
sGAGs	Sulphated glycosaminoglycans
sgRNA	Single guide RNA
siRNA	Small interfering RNA
SLC19A1	Solute carrier family 19 member 1
SLC46A1	Solute carrier family 46 member 1
SLC46A2	Solute carrier family 46 member 2
SLC46A3	Solute carrier family 46 member 3
spCAS9	S. pyogenes Cas9
ssDNA	single stranded DNA
ssRNA	single stranded DNA
STING	Stimulator of interferon genes
T-VEC	Talimogene laherparepvec

TAM	Tumor-associated macrophage
TBK1	TANK binding kinase 1
TCT	Tracheal cytoxin
TIR	The toll-interleukin-1 receptor
TLR	Toll-like receptor
TM	Transmembrane
TMD0	Transmembrane domain 0
TMD1	Transmembrane domain 1
TMD2	Transmembrane domain 2
ULK1	Unc-51 Like Autophagy Activating Kinase 1
VACV	Vaccinia Virus
VL	Viability limit
VRAC	Volume-regulated anion channels
VZV	Varicella-Zoster Virus
WPRE	Woodchuck Hepatitis Virus post-transcriptional regulatory element
ZBP1	Z-DNA-binding protein 1
ZBP1	Z-DNA-binding protein 1
ZIKV	Zika Virus

Contents

Abstract i

Acknowledgement ii

Acronyms iv

I – Introduction 1

I.1 Immunology, Innate Immunity and Pattern recognition receptors 1

I.2 Toll-like receptors 4

I.3 Cytosolic RNA sensors 6

I.4 Cytosolic and Nuclear DNA sensors 10

I.5 STING 16

I.5.1 Regulators of STING trafficking 18

I.5.2 Regulation of STING by post translational modification 19

I.5.3 Atypical regulators of STING 21

I.5.4 STINGs relevance to autoimmune disease and therapeutic design 23

I.6 Signalling down stream of PRRs – the IFN response 25

I.7 Transfer of cGAMP between cells 26

I.7.1 ENPP1 27

I.7.2 Transfer through gap junctions 31

I.7.3 Transport by viruses 33

I.7.4 SLC19A1 33

I.7.5 SLC46A2 35

I.7.6 P2X7 36

I.7.7 Volume regulated anion channels (LRRC8A:C) 39

I.7.8 ABCC1 43

I.7.9 LL-37 45

I.8 HSV-1 47

I.8.1 HSV-1 Infection cycle 49

I.8.2 Detection of HSV-1 infection by PRRs 51

I.8.3 HSV-1 antagonises PRRs 52

I.9 Objective of the study 54

II – Materials and Methods 55

II.1 Materials 55

II.1.1 Cells 55

II.1.2 Plasmids 59

II.1.3 Oligonucleotides for cloning 63

II.1.4 Antibodies 64

II.1.5 TaqMan Probes 65

II.2 Methods 65

II.2.1 CRISPR screen 65

II.2.2 HSV-1 production and titration 65

II.2.3 Construction of lentiviral expression constructs 66
II.2.4 Construction of lentiCRISPRv2 plasmids 66
II.2.5 Lentivirus production 67
II.2.6 Transduction 67
II.2.7 Western blotting 67
II.2.8 Immunoprecipitation and proteomic mass spectrometry 68
II.2.9 RT-qPCR 68
II.2.10 Knockout cell line production 69
II.2.11 IFN Bioassay / One Glo Assay (3C11 cells) 69
II.2.12 Quanti-Luc assay 69
II.2.13 Dual luciferase assay 70
II.2.14 Flow cytometry 70
II.2.15 Fluorescence activated cell sorting 71
II.2.16 siRNA transfection 71
II.2.17 Crystal violet viability assay 71
II.2.18 YOPRO-1 assay 72

III – Screening for Regulators of STING 73
III.1 CRISPR Screen to identify regulators of STING 74
III.2 siRNA interference in THP-1 cells 77
III.3 Validation of CRISPR screen by siRNA interference 82
III.4 Overexpression of potential accessories of STING 84
III.5 Testing if overexpression of candidate genes enhances STING signalling 86
III.6 Discussion 88

IV – Screening for viral antagonists of cGAMP channels 91
IV.1 Screening for viruses that degrade endogenous LRRC8A:C 93
IV.2 Overexpression and resolution of P2X7, SLC46A2 and SLC19A1 95
IV.3 Screening for viruses that degrade overexpressed P2X7, SLC46A2 and SLC19A1 97
IV.4 Screening for viruses that degrade endogenous ABCC1 98
IV.5 Discussion 99

V – Antagonism of LRRC8A:C by HSV-1 103
V.1 HSV-1 targets human LRRC8A 104
V.2 Identifying HSV-1 genes potentially involved in LRRC8A:C depletion 105
V.3 UL56 degrades LRRC8A:C 109
V.4 LRRC8A:C is degraded by the proteasome 110
IV.5 In *vitro* LRRC8A:C 2’3’-cGAMP uptake assay 112
V.6 UL56 antagonises 2’3’-cGAMP uptake 113
V.7 Discussion 114

VI - Antagonism of SLC46A2 and P2X7 by UL56 119
VI.1 SLC46A2 is degraded by UL56 120
VI.2 Model of SLC46A2 mediated 2’3’-cGAMP transport 121
VI.3 UL56 antagonises SLC46A2 mediated 2’3’-cGAMP transport 123

VI.4 P2X7 is degraded by UL56 123
VI.5 UL56 antagonises P2X7 123
VI.6 UL56 antagonises P2X7 mediated 2'3'-cGAMP import 127
VI.7 Discussion 128

VII - Discussion 130
VII.1 Aim 1 – Regulators of STING (Chapter III) 130
VII.2 Aim 2 – Viral antagonism of cGAMP channels (Chapters IV, V and VI) 130
VII.3 Knowledge gaps 133
VII.4 Final thoughts 136

Bibliography 137

List of Figures I

Appendix (Supplementary Figures and Tables) IX

Chapter I

Introduction

The evolutionary game of cat and mouse between virus and host has created intriguing molecular narratives. This introduction will focus upon nucleic acid sensing during virus infection concentrating on cytosolic DNA sensing, as this is directly relevant to viral antagonism of 2'3'-cGAMP transport, which is described in the results chapters.

I.1 Immunology, Innate Immunity and Pattern recognition receptors

The innate immune system is commonly deemed non-specific or simple. Despite this "simplicity" our understanding of innate immunity has chronologically lagged behind adaptive immune responses. This is despite the first immunological finding being innate. In 1882 Élie Metchnikoff observed through a primitive microscope phagocytic cells trying to digest a rose thorn he pushed into a starfish larvae (Figure 1A) (Metchnikoff 1908). His discovery led to the rise of the cellularists who believed immunity mediated by cell clearance was the foremost mechanism of antimicrobial resistance. This early innate philosophy was quickly superseded in the 1900s with the field's focus shifting upon Emil Behring and Paul Ehrlich characterising humoral immunity. Behring initially observed that serum from infected animals, which we now know contains protective antibodies, had pathogen specific antibacterial properties (Behring 1890). Ehrlich went on to characterise antibodies in relation to complement and described them as side chains produced and secreted from cells to neutralise toxins (Figure 1B) (Ehrlich 1957). This placed cell free immunity at the forefront of immunological research for the first half of the 20th century resulting in the discovery and characterisation of B cells. In the 1960s Jacques Miller worked on the thymus; in his own words, this organ was thought to be - "a graveyard for dying lymphocytes" (Swan 2011). He proved it was in fact the site where tolerance to self was learned, making him the world's only living person to have discovered the function of a human organ (Miller 1961). His initial work led to the subsequent

discovery of T cells and put clonal selection into vogue (Miller and Mitchell 1968; Mitchell and Miller 1968a, 1968b). Further work characterised the mechanism of T cell activation by MHC molecules driven largely by studies looking at restricted antigen recognition during influenza virus infection (Townsend et al. 1986; Morrison et al. 1986). Remarkably towards the end of the 1980s the mechanics of somatic recombination, antibody production, antigen processing and MHC presentation had been laid out into what we consider fundamental immunology today. Yet the field of innate immune sensing was non-existent, until 1989, when Charles Janeway speculated at the Cold Spring Harbour Symposia on Quantitative Biology that the field was reaching an Asymptote – "a moment where future experimental questions are obvious but technically difficult to perform with results aiming to give a higher degree of understanding but not revolutionise understanding within the field". This is one of the few predictions he got wrong. His seminar moved away from clonal responses to focus upon the immunologist's "dirty little secret" - the adjuvant. Adjuvants are ground up bacteria or alum injected alongside the vaccine antigen critical to a vaccine's efficacy. He speculated: The adjuvant induces a secondary signal needed to drive clonal expansion of T and B cells. He reasoned this signal came about by germline encoded receptors recognising pathogen associated molecular patterns, possibly lipopolysaccharides (LPS), that are present in bacterial species but not the host (Figure 1C). Janeway termed these theorised receptors pattern recognition receptors (PRRs). Additionally, he believed PRRs predated the clonal immune system drawing on the similarities in the lytic machinery of innate natural killer (NK) and adaptive cytotoxic T lymphocytes, stating that adaptive mechanisms were likely built upon pre-existing innate immune capacity. Finally, he identified the drawback of germ line encoded receptors is the lack of immunological memory - a hall mark of the adaptive immune response (Janeway 1989). In 1999, TLR4, the first known PRR, was described and shown definitively to recognise LPS (Poltorak et al. 1998; Hoshino et al. 1999; Medzhitov, Preston-Hurlburt, and Janeway 1997; Lemaitre et al. 1996). Janeway had predicted not only the existence of PRRs but also their ligand and evolutionary standing point a decade before they came into human knowledge (Janeway 1989). This is surely one of history's greatest pieces of speculation and with that Janeway broke his own asymptote starting a new branch of immunology. At the time of writing, >30 PRRs have been identified in the human genome.

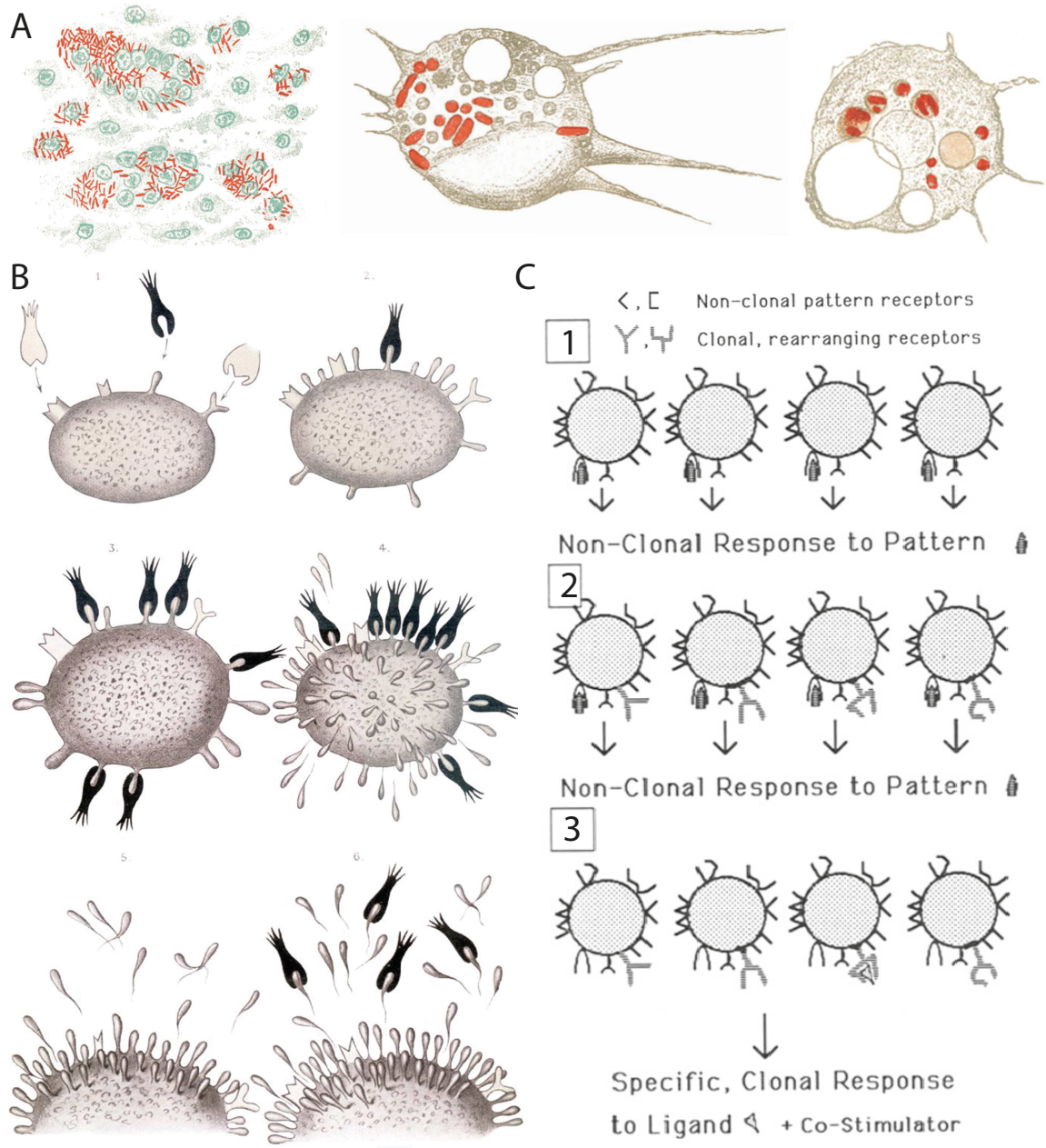


Figure 1 - Evolution of Immunology. A) Élie Metchnikov drawings of silver nitrate stained bacteria being digested by phagocytes (Metchnikoff 1902). B) Paul Ehrlich's drawings depicting side chain theory. His diagram shows cells producing many receptors. He thought side chains that bind toxins (in black) become so abundant they are released into the extracellular milieu providing protection to the host (Ehrlich 1957). C) Charles Janeway's remarkably accurate diagram of pattern recognition receptors from 1989. In: 1 – pre-vertebrates who only possess PRRs; 2 and 3 – vertebrates that possess both PRRs and clonal receptors (Janeway 1989).

This means it is now clear cells utilise an arsenal of PRRs which upon activation trigger an immune response integral to clearance of microbial invaders. Despite this Janeway's theory could not explain inflammation seen in sterile settings such as autoimmune disease or cancer. The answer came from Janeway's biggest rival, Polly Matzinger. She challenged the notion that microbial components are directly recognised by innate immune receptors. Instead

proposing danger theory, which states the immune response is likely triggered by “danger signals” released from damaged or distressed cells (Matzinger 1994, 2001; Matzinger 2002). Today it is clear the rivals were both correct as alongside PAMPs, damage associated molecular patterns (DAMPs) can also be recognised by PRRs, explaining sterile inflammation (Gong et al. 2020). All multicellular beings face threat of infection and hence PRRs evolved early in life’s history. For instance, homologs of PRRs found in humans can be seen widely across eukaryotes (e.g. corals possess many TLRs) and some even in prokaryotes (e.g. cGAS-STING homologs exist in bacterial defence islands and offer protection against bacteriophages) (Cohen et al. 2019; Palmer 2018). Additionally, paradigm shifting reports have described innate immune memory termed “trained immunity” formed through epigenetic remodelling, showing the innate immune system is far from simple (Netea et al. 2020). Instead, from an early point in evolution, PRRs have evolved to specifically detect erroneous structures and are one of the most diverse and complex molecular systems known to date.

I.2 Toll-like receptors

Toll-like Receptors (TLRs) were the first family of proteins found to fulfil Janeway’s criteria of a PRR and were initially identified in *Drosophila melanogaster* as a gene important for resistance to bacterial and fungal infections (Lemaitre et al. 1996). Structurally TLRs consist of an extracellular leucine rich repeat domain, which binds the PAMP, linked by a transmembrane region to the intracellular TIR domain (Figure 2A) (Asami and Shimizu 2021). TLRs form dimers working functionally as either homo or hetro -mers. The number of TLRs present in a species varies greatly - humans and mice have 10 and 12, respectively but *Strongylocentrotus purpuratus* (the purple sea urchin) encodes a staggering 253 (Tassia, Whelan, and Halanych 2017). TLRs can be broadly split into two categories; those that detect nucleic acids and exist endosomally (TLR3 - dsRNA, TLR7-ssRNA, TLR8-ssRNA, TLR9-unmethylated 5’-CG-3’ containing ssDNA) and those that broadly detect bacterial architecture and exist at the plasma membrane (TLR1:2 - triacylated lipoprotiens, TLR1:6 - diacylated lipoproteins, TLR4 – LPS and TLR5 - flagellin) (Fitzgerald and Kagan 2020). The final member, TLR10, has no clear ligand but is suggested to play a regulatory role (Fore et al. 2020). Upon PAMP recognition, the TIR domains dimerizes. From this point, TLR mediated

induction of proinflammatory cytokines follows two discrete signalling pathways: canonical or non-canonical. Canonically, the TIR domains of TLRs trigger the formation of a large protein complex termed the myddosome which drives NF-κB signalling. Non-canonical TLR signalling is exclusive to TLR3 and TLR4, which signal through the triffosome activating TBK1 to drive production of type I interferons (Figure 2B) (Asami and Shimizu 2021). As with many PRRs, dysregulation of TLRs is associated with autoimmune disease. TLRs have been implicated in atherosclerosis, rheumatoid arthritis, systemic lupus erythematosus, allergy, cancer, autoimmunity and inflammatory bowel disease making them an attractive therapeutic target (Hennessy, Parker, and O'Neill 2010). Interestingly, localisation of TLRs sensing nucleic acids is crucial to proportionate immune responses. For example, artificial re-localisation of TLR9 to the cell surface causes a lethal proinflammatory phenotype in mice (Mouchess et al. 2011; Barton, Kagan, and Medzhitov 2006). Few regulatory mechanisms have been found for TLRs that detect the molecular architecture of bacteria at the cell surface. Hence it has been suggested, at least in the case of TLRs, an evolutionary draw back to using nucleic acids as PAMPs is that numerous regulatory mechanisms must exist to allow for effective distinguishment between self and non-self (Fitzgerald and Kagan 2020).

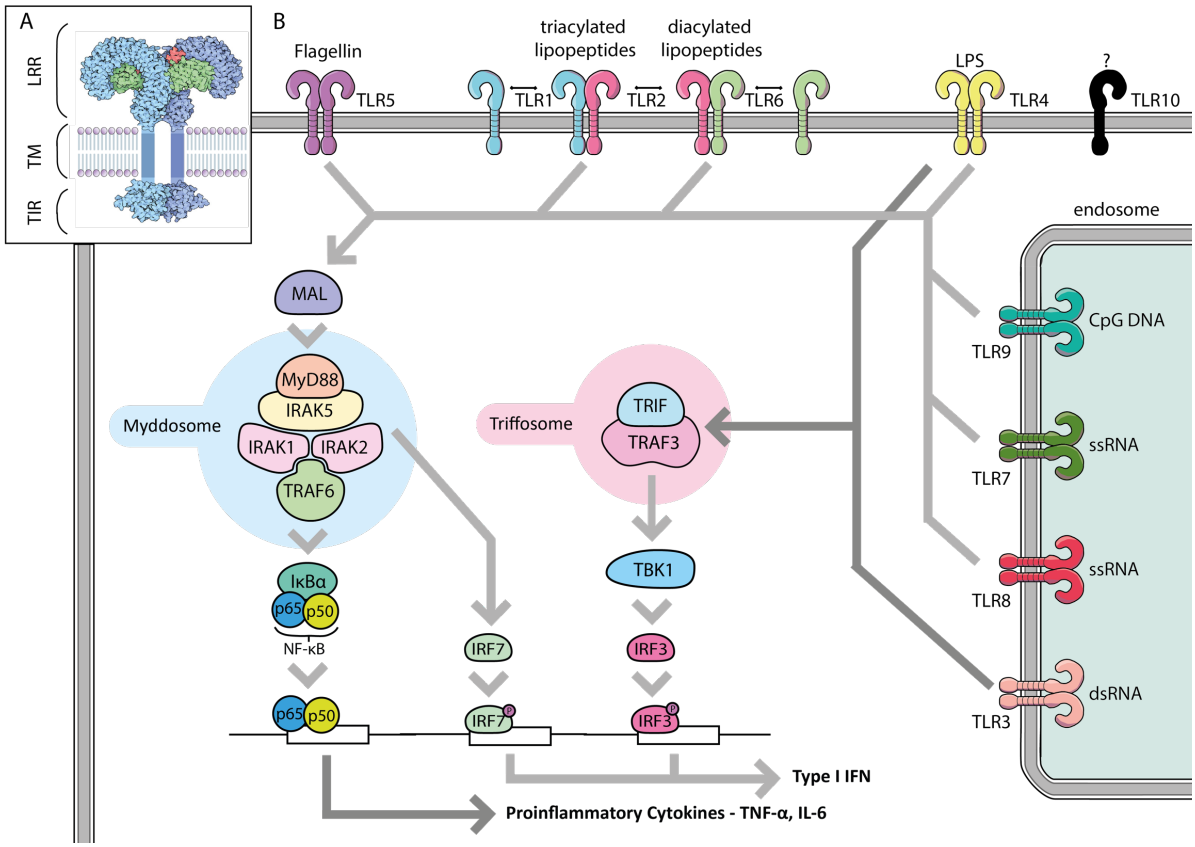


Figure 2 – Toll-like Receptor signalling. A) Structure of TLR4's LRR domain (blue) in complex with LPS (red) determined by X-Ray crystallography. MD-2, a TLR4 accessory required for detection of LPS is shown in green. The transmembrane domain and TIR domain are shown schematically. The Illustration is adapted from Goodsell (2011). B) The 10 human TLRs signal through the myddosome and triffosome to drive production of proinflammatory cytokines.

I.3 Cytosolic RNA sensors

The most notorious cytosolic RNA sensors are the retinoic-acid inducible gene-I (RIG-I) like receptors. They are part of the SF2 helicase superfamily of which the majority act as RNA helicases. Hence each possess a central helicase domain (Liu and Gack 2020). The first two-members, RIG-I and melanoma differentiation-associated protein 5 (MDA5), also possess CARD domains. RIG-I detects uncapped dsRNA with a 5' triphosphate (≥19 bp) distinct from eukaryotic cellular RNAs which possess a 5' 7-methylguanylate cap (Pichlmair et al. 2006; Hornung et al. 2006; Schmidt et al. 2009). MDA5 detects longer dsRNA (>300bp) although an exact motif has not been identified (Pichlmair et al. 2009; Kato et al. 2008). Upon ligand binding, both RIG-I and MDA5 recruit the central hub of RNA sensing MAVS, through their CARD domains, inducing MAVS oligomerisation at the mitochondria. Here TBK1, and IkB are recruited and drive activation of IRF3/7 and NF-κB, culminating in the production of

proinflammatory cytokines (Rehwinkel and Gack 2020). The final RIG-I like receptor - LGP2 - does not possess a CARD domain and so cannot signal through MAVS but instead plays a regulatory role. A number of mechanisms have been suggested by which LGP2 inhibits RIG-I signalling: blocking the interaction between MAVS and IKKε (Komuro and Horvath 2006); sequestering immunostimulatory RNAs (Rothenfusser et al. 2005) and preventing TRIM25 from adding activating K-63 linked polyubiquitin chains (Quicke et al. 2019). Conversely, LGP2 is known to aid MDA5 signalling by facilitating MDA5 oligomerisation onto dsDNA (Venkataraman et al. 2007; Satoh et al. 2010). Interestingly, ZCCHC3 has been identified as a co-receptor for both RIG-I and MDA5 as it facilitates dsRNA binding (Lian et al. 2018). The enzyme ADAR1 has also been shown to regulate RNA sensing and has recently become a focal point within the field. This enzyme edits bases within endogenous dsRNA from adenosine to inosine. This reduces the RNA's immunostimulatory potential by reducing its affinity to MDA5. Disruption of the *ADAR1* gene results in the chronic interferonopathy Aicardi-Goutières syndrome in humans (Rice et al. 2012; Liddicoat et al. 2015; Mannion et al. 2014; Pestal et al. 2015). This shows how stringent regulation of RNA sensing is crucial to prevent autoimmunity.

In addition to the RIG-I like receptors, the NOD-like receptors (denoted as NLRs or NODs) are a large family of RNA sensors. The majority (NLRP3, NLRP9b and NLRP1) induce inflammasome activation upon RNA binding. The inflammasome is a multi-subunit platform that recruits caspase 1 to cleave the precursors of IL-1β, IL-18 and gasdermin D into their active forms. Gasdermin D then forms a pore in the cell membrane through which the cytokines IL-1β and IL-18 exit the cell. This results in a type of proinflammatory cell death called pyroptosis (Deets and Vance 2021). Classically, NLRs depend upon recruitment of DEAH-Box helicase proteins to sense RNA. NLRP3 detects dsRNA through recruitment of DHX33 (Mitoma et al. 2013). NLRP9b detects short dsRNA by recruitment of DHX9 (Zhu et al. 2017). Recently, NLRP1 has also been shown to detect dsRNA although it is unclear if an accessory RNA binding protein is needed (Bauernfried et al. 2021). Many other DHX and related DEAD-Box Helicase (DDX) proteins have been proposed as RNA sensors (DHX9, DHX15, DDX1, DDX3, DHX29) although it is unclear if these work in unison with known receptors or as independent PRRs (Liu and Gack 2020). The final two members of the family – NOD2 and NLRP6 - trigger type I IFN production via MAVS rather than pyroptosis. NOD2 recognises

ssRNA whereas NLRP6 indirectly senses dsRNA by recruiting the DEAH-box RNA helicase DHX15 (Wang et al. 2015; Sabbah et al. 2009).

ZBP1 (also known as DAI or DLM1) is a recently discovered and intriguing sensor identified by efforts to find proteins that bind Z-form DNA (Z-DNA). This exists in a disordered right-handed helix unlike the left-handed helix formed by classical B-form DNA (Thapa et al. 2016). ZBP1 was originally proposed as a DNA sensor but recent evidence has shown it in fact detects Z-RNA formed during viral infection (Thapa et al. 2016; Maelfait et al. 2017; Kuriakose et al. 2016). Binding is mediated by the Z-DNA binding domains denoted Zα1 and Zα2. Upon Z-RNA binding, ZBP1 recruits RIPK3 and remarkably can trigger three forms of cell death - apoptosis is driven through caspase-8, pyroptosis is triggered by the NLRP3 inflammasome and necroptosis occurs by activation of MLKL to form cytotoxic pores. Interestingly, like with MDA5, editing by ADAR1 has also been shown to dampen ZBP1-dependent activation in models of autoimmune disease (de Reuver et al. 2022; Hubbard et al. 2022; Jiao et al. 2022).

ZAP is another RNA sensor found in a thought-provoking manner. 5’-CG-3’ dinucleotide (CG) sequences are known to appear within vertebrate genomes at a much lower frequency than in non-vertebrate genomes or in a random sequence. CG suppression was explained by CG specific DNA methyl transferases causing spontaneous methyl-cytosine deamination (C > T), which has accumulated throughout vertebrate evolution (Karlin and Mrázek 1997; Karlin, Doerfler, and Cardon 1994; Rima and McFerran 1997; Greenbaum et al. 2008). Surprisingly, many RNA viruses that are not substrates for DNA methyl transferases were seen to mimic CG suppression. ZAP was identified as an antiviral factor that binds to RNA containing CG

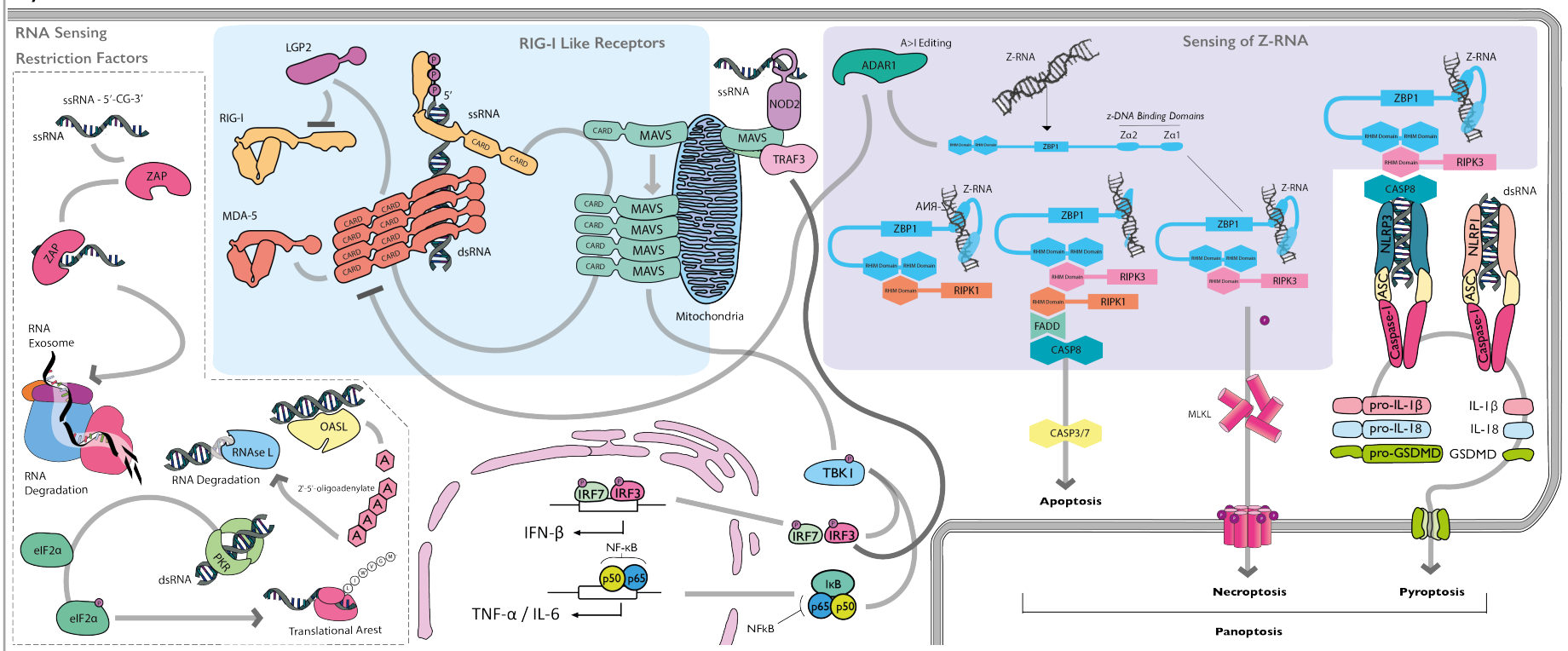


Figure 3 – Intracellular RNA sensors. A schematic showing known cytosolic RNA sensors discussed in section I.3. RNA PRRs are grouped into three classes - RNA sensing restriction factors, RIG-I like receptors and sensors of Z-RNA.

motifs targeting them for degradation by RNA exosomes (Takata et al. 2017; Guo et al. 2007). Seminal work has since shown that many RNA viruses suppress CG within their genomes to evade ZAP's activity, since artificial introduction of silent CG mutations limit viral replication in a ZAP dependent manner (Takata et al. 2017). CG motifs are also recognised by the DNA sensors TLR9, DHX9 and DHX36, discussed in the next section. The observed convergence upon CG motifs by PRRs is likely a common strategy to avoid detection of self. The RNA sensors described in this section are summarised in Figure 3.

I.4 Cytosolic and Nuclear DNA sensors

The inflammatory properties of dsDNA have been known since the 1960s as pre-treating cells with exogenous DNA limits viral replication (Rotem, Cox, and Isaacs 1963; Isaacs, Cox, and Rotem 1963). Only recently have the mechanisms by which DNA is detected been explored. The first DNA sensor identified was TLR9 (discussed in chapter I.2), which functions endosomally in dendritic cells and B cells to recognise unmethylated CG dinucleotides contained in ssDNA found in bacterial, viral, fungal and parasitic species (Hemmi et al. 2000; Bauer et al. 2001). Despite this, TLR9's activity could not explain why transfection of vertebrate dsDNA into the cytosol triggered IFN production, suggesting there was a cytosolic DNA sensor (Stetson and Medzhitov 2006a; Ishii et al. 2006). Over the past decade, many different intracellular DNA sensors have been proposed (DAI/ZBP1, RNA POL III, DNA-PK, IFI16, DHX9, DHX36, DDX41, DDX60, AIM2, MRE11/RAD50, LRRFIP1), which are discussed below (Dempsey and Bowie 2015). The major advance came with the discovery of 2'3'-cyclic GMP-AMP (2'3'-cGAMP); a cyclic dinucleotide produced in response to dsDNA in mammalian cells (Wu et al. 2013). Previously, cyclic dinucleotides (CDNs) were thought only to be signalling molecules produced by bacteria and were already known to be detected by another PRR – STING (discussed in chapter I.5) (Burdette et al. 2011; Ishikawa and Barber 2008). To identify the host cyclic GMP-AMP synthase (cGAS) the authors fractionated cellular lysates and assayed fractions for their ability to produce 2'3'-cGAMP upon introduction of dsDNA. The 2'3'-cGAMP producing fraction was then subjected to proteomic mass spectrometry and cGAS was identified (Sun et al. 2013). Since its discovery, cGAS, unlike other putative sensors of dsDNA, has emerged as the major sensor of B-form dsDNA in the cell cytoplasm. cGAS

activation ultimately results in the production of proinflammatory cytokines including type I interferons that facilitate: proximal cells entering an antiviral state; facilitation of cell death programmes; and priming of adaptive immune responses (Ablasser and Chen 2019). Notably, unlike other known PRRs, cGAS detects dsDNA indiscriminate of whether it is intrinsically (host) or extrinsically (pathogen) derived. Instead of detecting structural differences like classical PRRs (e.g. TLR9), it identifies the topological peculiarity of DNA in the cytosol. An overview of the cGAS-STING DNA sensing pathway is presented in Figure 4A.

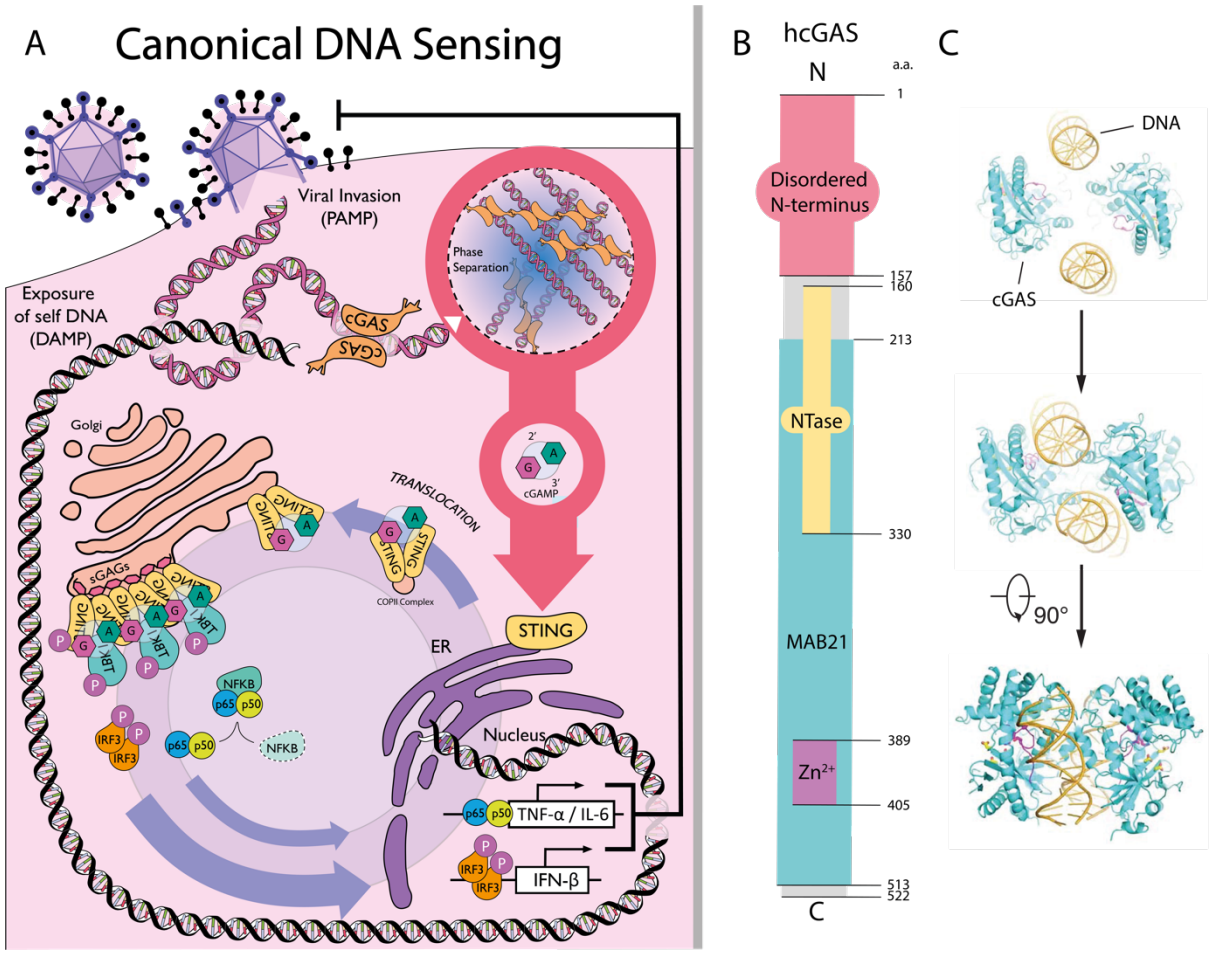


Figure 4 – DNA sensing by cGAS. A) The presence of mislocalised or pathogen associated dsDNA in the cytoplasm is detected by cGAS. Upon DNA binding, cGAS undergoes phase separation and generates the cyclic dinucleotide 2'3'-cGAMP required by the central hub of DNA sensing – STING – to translocate from the ER towards ERGIC. Here, STING recruits TBK1 to phosphorylate the master transcriptional regulators of innate immune activation - IRF3 and NF-κB. This results in the production of proinflammatory cytokines, primarily type I IFNs but also IL-6 and TNF-α. B) Schematic showing structural domains within human cGAS. C) Structure of human cGAS in complex with DNA resolved by X-ray crystallography. Adapted from Ablasser and Chen (2019).

Structurally, human cGAS's C-terminus has Mab-21 homology and contains a zinc ribbon domain, which binds DNA by two distinct sites. The central nucleotidyl-transferase domain

catalyses 2’3’-cGAMP formation and leads into a disordered and positively charged N-terminus which enhances cGAS activity (Figure 4B) (Hertzog and Rehwinkel 2020; Gao et al. 2013; Kranzusch et al. 2013; Civril et al. 2013). Interestingly, cGAS shares a close structural similarity with oligoadenylate synthase (OAS). Upon OAS detecting dsRNA during viral infection, it produces 2’-5’ oligoadenylate, which triggers RNase L to indiscriminately degrade host and viral mRNA, halting viral replication (Figure 3) (Kranzusch 2019; Hornung et al. 2014). cGAS binding dsDNA triggers rearrangement of the nucelotidyl tranferase domain allowing for binding of ATP and GTP. Initially, pppGpA is formed, then, this intermediate species twists within the active site to be circularised to 2’3’-cGAMP (Hooy et al. 2020; Civril et al. 2013; Gao et al. 2013; Hall et al. 2017). cGAS is also able to bind dsRNA and ssDNA but this does not induce 2’3’-cGAMP production, although there is evidence that DNA:RNA hybrids can bind to and activate cGAS (Civril et al. 2013; Gao et al. 2013; Mankan et al. 2014). Upon DNA binding, cGAS’s N-terminus polymerises, inducing phase separation, a phenomenon where liquids separate from each other forming distinct membrane-less compartments. Phase separation can be induced in the absence of DNA by modulating cation concentration (e.g. Zn^{2+}) and likely explains why other cations such as Mn^{2+} have been found to enhance cGAS’s activity (Hall et al. 2017; Du and Chen 2018).

Alongside cGAS, many accessory proteins modulate its function. G3BP1, ZCCHC3 and PCBP1 have all been shown to facilitate cGAS-DNA complex formation and are viewed as co-sensors (Liu et al. 2019; Liao, Lei, and Shu 2020; Lian et al. 2018). Additionally, PQBP1 and NONO have been reported to facilitate detection of dsDNA species by cGAS in the nucleus during HIV-1 infection (Lahaye et al. 2018). Mitotic kinases hyper-phosphorylate cGAS’s N-terminus during mitosis, preventing activation upon nuclear disintegration (Li, Huang, et al. 2021). Additionally, histones 2A/2B have been shown to lock cGAS into an inactive conformation, presumably preventing cGAS deposited in the nucleus during mitosis from being proinflammatory (Boyer et al. 2020; Kujirai et al. 2020; Michalski et al. 2020; Pathare et al. 2020; Zhao et al. 2020). In addition to phosphorylation, ubiquitination, SUMOylation, glutamylation and acetylation have all been reported to regulate cGAS’s function by an abundance of host enzymes reviewed in detail by Hertzog and Rehwinkel (2020).

Since its discovery, cGAS has been at the forefront of the cytosolic DNA sensing pathway, but other DNA sensors have also been described. Most notable are the inflammasome subunits AIM2 and IFI16. Both contain positively charged HIN domains that recognise the negatively charged backbone of dsDNA in a sequence independent manner (Jin et al. 2012). Binding results in inflammasome activation (discussed in chapter I.3) (Deets and Vance 2021). Like cGAS, AIM2 is known to sense mis-localised DNA within the cytosol and has been implicated in the detection of bacterial, viral and fungal infections (e.g. *l. monocytogenes*, *A. fumigatus* and VACV) (Rathinam et al. 2010; Wu, Fernandes-Alnemri, and Alnemri 2010; Karki et al. 2015). IFI16 recognises viral (KSHV or HIV-1) DNA or DNA damage within the nucleus and then translocates to the cytoplasm to drive inflammasome formation (Monroe et al. 2014; Kerur et al. 2011; Doitsh et al. 2014). This suggests that unlike AIM2, which exists in the cytosol, IFI16 possess selectivity for either damaged or pathogen derived DNA. However, how AIM2 distinguishes between host and erroneous DNA within the nucleus is unknown. Additionally, IFI16 has been shown to signal through STING. In keratinocytes, dsDNA breaks trigger IFI16 to form a complex with PARP-1, ATM, p53, which drives STING activation in manner independent of cGAS (Dunphy et al. 2018).

The DNA dependent protein kinase (DNA-PK) is a protein complex involved in the DNA damage response mediating non-homologous end joining (NHEJ). Alongside repairing DNA damage, DNA-PK also functions to sense dsDNA breaks. The functional sensor is made of three subunits: Ku70, Ku80 and DNA-PKcs. DNA-PK detects the ends of cytosolic and damaged nuclear dsDNA and then signals through both TBK1 and HSPA8/HSC70 to induce production of type I IFNs (Ferguson et al. 2012; Peters et al. 2013; Burleigh et al. 2020). DNA-PK has also been implicated in the HEXIM1-DNA-PK-paraspeckle components-ribonucleoprotein complex (HDP-RNP). This large complex containing SFPQ, PSPC1, NONO, HEXIM1 and the lncRNA NEAT1 and non-canonically responds to DNA by interacting with cGAS and its binding partner PQBP1. This is suggested to signal by enhancing STING activation (Morchikh et al. 2017). Due to conflicting reports, DNA-PK's relationship with STING remains contentious. What is clear about DNA-PK is it restricts viral replication being shown to act across all DNA coupled

Baltimore classes[1] (Hristova, Lauer, and Ferguson 2020). Therefore, DNA-PK is an intriguing DNA sensor but the mechanistic detail of how it functions is an exciting area for future investigation.

Many other sensors have been described that respond to cytosolic dsDNA but were largely regarded as "dead and buried" by leaders in the field after the discovery of cGAS. These genes were even treated to a funeral in a review by Russel Vance, the man who discovered STING binds CDNs (Figure 5A) (Vance 2016). Many of these are RNA helicases separated into the DEAH-box helicases (DHX) and DEAD-box helicases (DDX). DHX9 and DHX36 interact with, like TLR9, unmethylated CG motifs and function solely in plasmacytoid dendritic cells. Interestingly, DHX36 specifically binds A-form DNA[2] with CG motifs signalling through IRF7 to drive production of type I IFNs (Figure 5B) (Kim et al. 2010). These receptors, like cGAS, exist in the cytosol but little is known about their regulation. DDX41 was identified as a receptor during HSV-1 infection, like cGAS, detecting B-form DNA in the cytoplasm. dsDNA binding promotes an interaction between DDX41 and STING driving its activation and type I IFN production (Zhang et al. 2011). Interestingly, DDX41 has also been shown to bind and sense cyclic-di-GMP and cyclic di-AMP which are very similar in structure to 2'3'-cGAMP. The knockout of DDX41 also reduces STING driven responses to 2'3'-cGAMP, suggesting it may directly augment STINGs function (Parvatiyar et al. 2012). MRE11 is a molecule implicated in repair of dsDNA breaks and thought to signal through STING (Kondo et al. 2013). It is unclear if it is truly sensing DNA or as an enzyme with 3' to 5' exonuclease activity creates PAMPs, which can be detected by other sensors (Yuan et al. 2012). LRRFIP1 binds double stranded nucleic acids and signals through beta-catenin to phosphorylate IRF3 and drive IFN-β production (Yang et al. 2010). Collectively, these prehistoric DNA sensors are now regarded as putative PRRs. Prior to the discovery of cGAS, they were shown to enhance the response dsDNA. Today, it is unclear if they augment cGAS-STING signalling or if they function as PRRs in their own right. ZBP1, like the other putative DNA sensors, was initially a prominent DNA sensing candidate due to its two Z-DNA binding domains, before being "laid to rest"

[1] The Baltimore classification system is used to group viruses based upon the nucleic acids encoding their genome and their replication strategy. For instance virus genomes made up of dsDNA, dsRNA and (+)ssRNA constitute separate groups.

[2] A-form DNA exists in a right-handed helix like B-form DNA but is more tightly wound having a greater number of base pairs per turn. Structurally this results in the A-form helix being broad with a narrow major groove (Heinemann and Roske 2020).

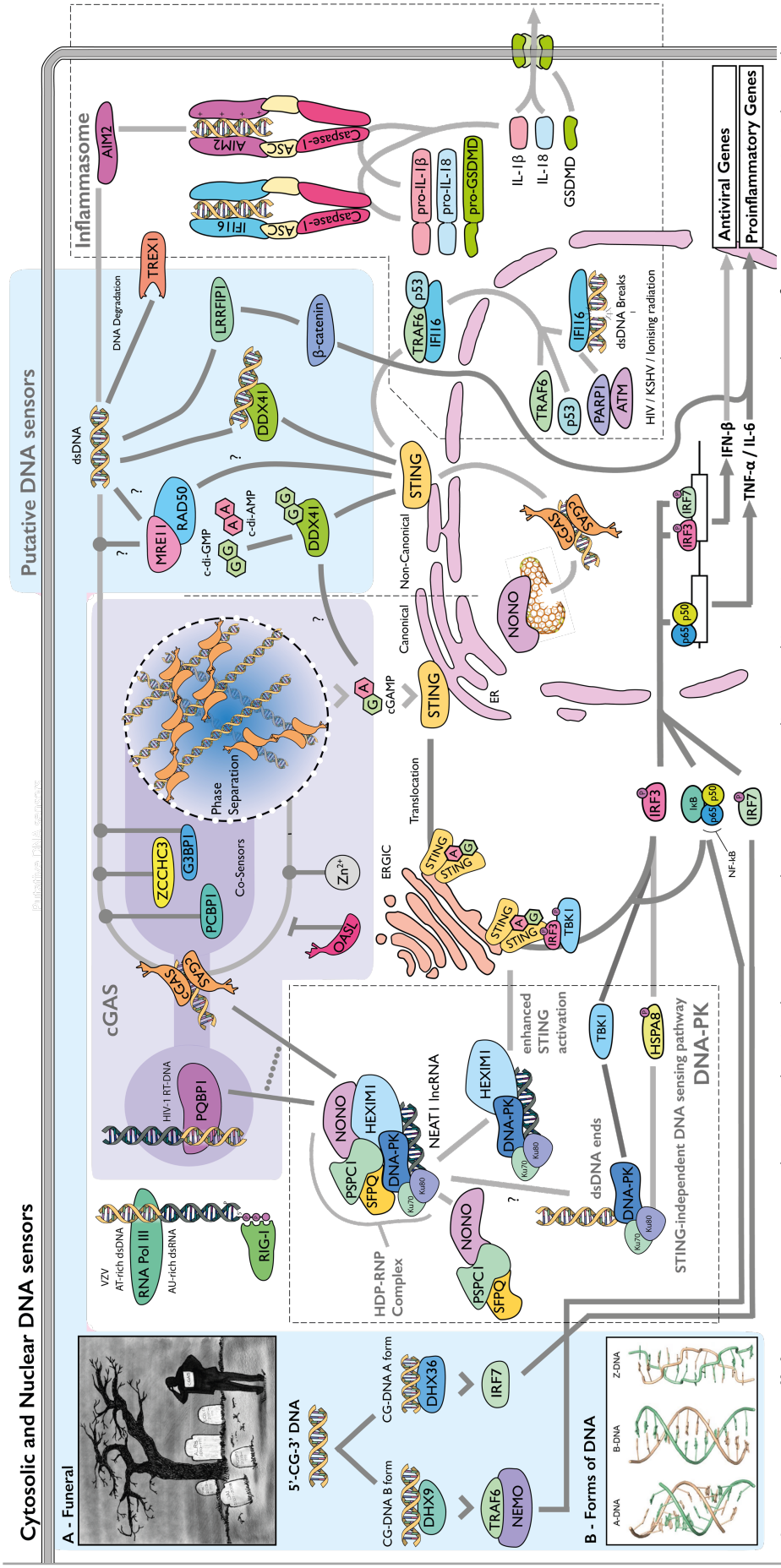


Figure 5 – Intracellular DNA sensors. A schematic showing known cytosolic DNA sensors discussed in section I.4. DNA PRRs are split into four groups - cGAS dependent sensors, putative DNA sensors, DNA-PK mediated sensing and inflammasome activators. A) Funeral given to putative DNA sensors after the discovery of cGAS lifted from Vance (2016). B) Crystal structure of A, B and Z -form DNA adapted from Heinemann and Roske (2020).

(discussed in chapter I.3) (Vance 2016). Now, ZBP1 has clearly "risen from the dead" being shown to detect Z-RNA and is at the leading edge of research into PRRs. This suggests further interrogation of these largely overlooked genes might deliver the next hot topic.

In less than a decade, our understanding of how DNA is sensed within the cell has increased exponentially. Despite this, there are many unanswered questions surrounding DNA sensing. For instance – How are DNA sensors aside from cGAS regulated during mitosis? Do cytosolic sensors for ssDNA exist? What role do the putative DNA sensors play? As cGAS has been widely implicated in both autoimmune disease and cancer, it seems clear that DNA sensors are an excellent target for therapeutic manipulation. Therefore, the rapid growth of academic and financial interest in the field of DNA sensing seems far from over. The DNA sensors described in this section are summarised in Figure 5.

I.5 STING

STING (also known as MITA, MPYS, ERIS or TMEM173), like many other components of the innate immune system, is highly conserved across eukaryotic organisms. Until recently, the most distant example was found in the starlet sea anemone (*Nematostella vectensis*), a species divergent from humans by >500 million years yet still possessing a STING homolog able to bind 2'3'-cGAMP (Figure 6A) (Kranzusch et al. 2015). New evidence derived from phylogenetic analysis of 38,167 microbial genomes predicts 52 C-terminal homologs of STING exist within prokaryotes. These cluster into bacterial defence islands proximal to prokaryotic cGAS known to defend against phage infection (Cohen et al. 2019). This suggests that STING and its antiviral functions originated in our most primitive ancestors. STING was initially identified as the protein required for induction of IFN-β upon either DNA transfection or HSV-1 infection (Ishikawa and Barber 2008). Subsequently, it was shown to sense bacterially derived cyclic dinucleotides (CDNs) used by prokaryotic species as signalling molecules (Burdette et al. 2011). Hence, STING is not just the central hub of DNA sensing but also functions as a PPR in its own right (Liu et al. 2021). Despite this, the question of how cytosolic DNA activates STING remained unanswered, until the discovery of cGAS which in humans produces 2'3'-cGAMP upon binding dsDNA (discussed in section I.4) (Sun et al. 2013; Wu et al. 2013). Structurally, STING has a short N-terminus followed by four transmembrane helices

connected to the cytosolic C-terminal cyclic dinucleotide binding domain (CBD) (Figure 6C and 6D). Functionally, the cytoplasmic domain forms a dimer undergoing conformational change upon 2'3'-cGAMP binding (Shang et al. 2019). Dimerisation initiates STING localised at the ER to translocate on COP-II vesicles into a complex network of tubulovesicular membranes peripheral to the Golgi known as the ER-Golgi intermediate compartment (ERGIC) (Dobbs et al. 2015; Ran et al. 2019). At ERGIC, STING dimers polymerise into high molecular weight chains with TBK1, a kinase that phosphorylates STING's C-terminus. STING then recruits IRF3 which is also phosphorylated by TBK1. IRF3 then dimerises and translocates into the nucleus initiating transcription of type I IFNs (Figure 4) (Zhang et al. 2019). Recruitment of TBK1 to STING also drives activation of the transcriptional factor NF-κB (classically measured by production of TNFα or IL-6) (Abe and Barber 2014). Broadly this results in a proinflammatory response and cells entering an antiviral state. STING that reaches ERGIC can traffic back to the ER on COP-I vesicles or be targeted into the endolysosomal system for degradation (Liu et al. 2022; Deng et al. 2020).

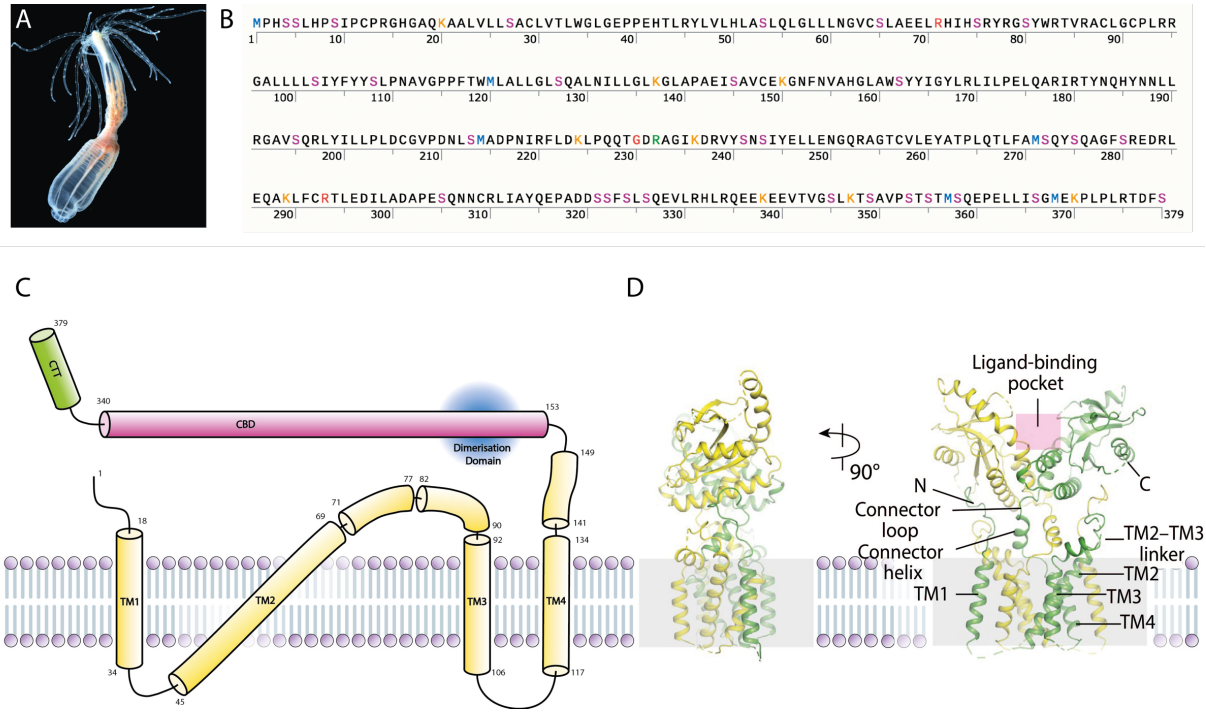


Figure - 6 structure of STING. A) picture of starlet sea anemone (*Nematostella vectensis*) lifted from Layden, Rentzsch, and Röttinger (2016). B) Amino acid sequence of STING showing: starts codons in blue, potential serine phosphorylation sites in purple, potential lysine ubiquitination sites in orange and polymorphic sites in red and green. C) Topological diagram of STING's domains, showing the cyclic dinucleotide binding domain (CBD) and C-terminal tail (CTT). D) Structure of human STING dimer resolved by cryo-EM. Individual subunits are coloured green and yellow, with the ligand binding pocket shown in pink. Figure adapted from Shang et al. (2019).

Aside from its role in DNA sensing, STING's N-terminus also functions as a regulator of autophagy. Autophagosome formation is initiated from STING associated ERGIC membranes, which serve as a site for LC3 lipidation, a process dependent on autophagosome biogenesis factors WIPI2 and ATG5 (Gui et al. 2019). STING's autophagic function also acts to negatively regulate type I IFN induction, since autophagosomes engulf and degrade the cytosolic DNA which activates cGAS (Gui et al. 2019). STING mediated autophagy directly restricts viral replication as truncated STING (1-340 a.a.), unable to activate TBK1, restricts HSV-1's replication in an ATG5 dependent manner, likely through digestion of viral particles (Gui et al. 2019). Interestingly, the aforementioned starlet sea anemone's STING induces autophagy but not IFN production in response to 2'3'-cGAMP, suggesting the autophagic function of STING predates its role as a signalling platform.

Over the last decade many accessory proteins have been characterised that regulate STING's function. At the time of writing, >50 have been reported, which I broadly separate into 3 categories:

1. Regulators of trafficking to ERGIC.
2. Regulation by posttranslational modification.
3. Atypical regulators.

In Chapter III we will consider a CRISPR screen performed by Alice Mayer looking to identify further regulators of STING. Due to the vast number of STING accessories known, I will discuss a few prototypic examples from each group to illustrate how STING signalling can be regulated. An overview of known STING accessories is presented in Figure 7 and in supplementary Table 1.

I.5.1 Regulators of STING trafficking

Several proteins are reported to associate with STING at the endoplasmic reticulum and are important for loading STING into COP-II vesicles for trafficking to ERGIC, most notably, iRhom2, SCAP, and YIPF5 (Luo et al. 2016; Wei et al. 2018; Chen et al. 2016). Additionally,

other proteins have been reported to anchor STING at the ER, preventing signal transduction. Individually ER associated STING accessories are well characterised, but evidence of how they cooperate is scarce. Therefore, a significant knowledge gap in the field is the exact mechanism by which STING exits from the ER.

YIPF5 a STING launch pad

YIPF5 is a member of the Yip family and directly interacts with STING and components of the COP-II complex (e.g. SAR1, SEC13, SEC23, SEC31). This leads to STING being incorporated into COP-II vesicles and transported to ERGIC for signal transduction. In accord, knockdown of YIP5 increases cellular susceptibility to HSV-1 due to reduced type I IFN production (Ran et al. 2019).

STIM1 is a STING anchor

STIM1 is a Ca^{2+} sensor within the endoplasmic reticulum and is essential to B and T cell function. Hence, deleterious mutations are a cause of severe combined immunodeficiency (Feske, Picard, and Fischer 2010). STIM1 also directly binds to STING retaining it in an inactive state at the ER. In line with this, STIM1 deficiency in patients and mice results in a spontaneous IFN signature (Srikanth et al. 2019).

I.5.2 Regulation of STING by post translational modification

Ubiquitin mediated regulation is ubiquitous among pattern recognition receptors and associated signalling molecules (e.g. cytosolic RNA sensors and TLR signalling) (Davis and Gack 2015). Classically, the ubiquitin system is viewed as a mechanism for targeting molecules for degradation, but recent findings clearly show a role for regulative and non-degradative ubquitination, which plays a crucial role in preventing overactive immune responses (Hu and Sun 2016). This is clearly demonstrated by the STING signalling pathway which is regulated by an extensive number of E3 ubiquitin ligases and deubiquitinatases (DUBs). There are eight different types of ubiquitination (linear, K6, K11, K27, K29, K33, K48, K63) classed depending on which lysine residues within ubiquitin links to form polyubiquitin chains (Davis and Gack

2015). Four of these have been observed to regulate STING signalling: K11, K27, K48 and K63 (Qin et al. 2014; Wang et al. 2014; Zhong et al. 2009; Zhang et al. 2012). In addition to ubiquitination, phosphorylation and SUMOylation have also been reported to regulate STINGs activity (Hu and Shu 2017; Konno, Konno, and Barber 2013; Zhong et al. 2009). A summary of post translation modifications shown to regulate STING is displayed in Figure 8.

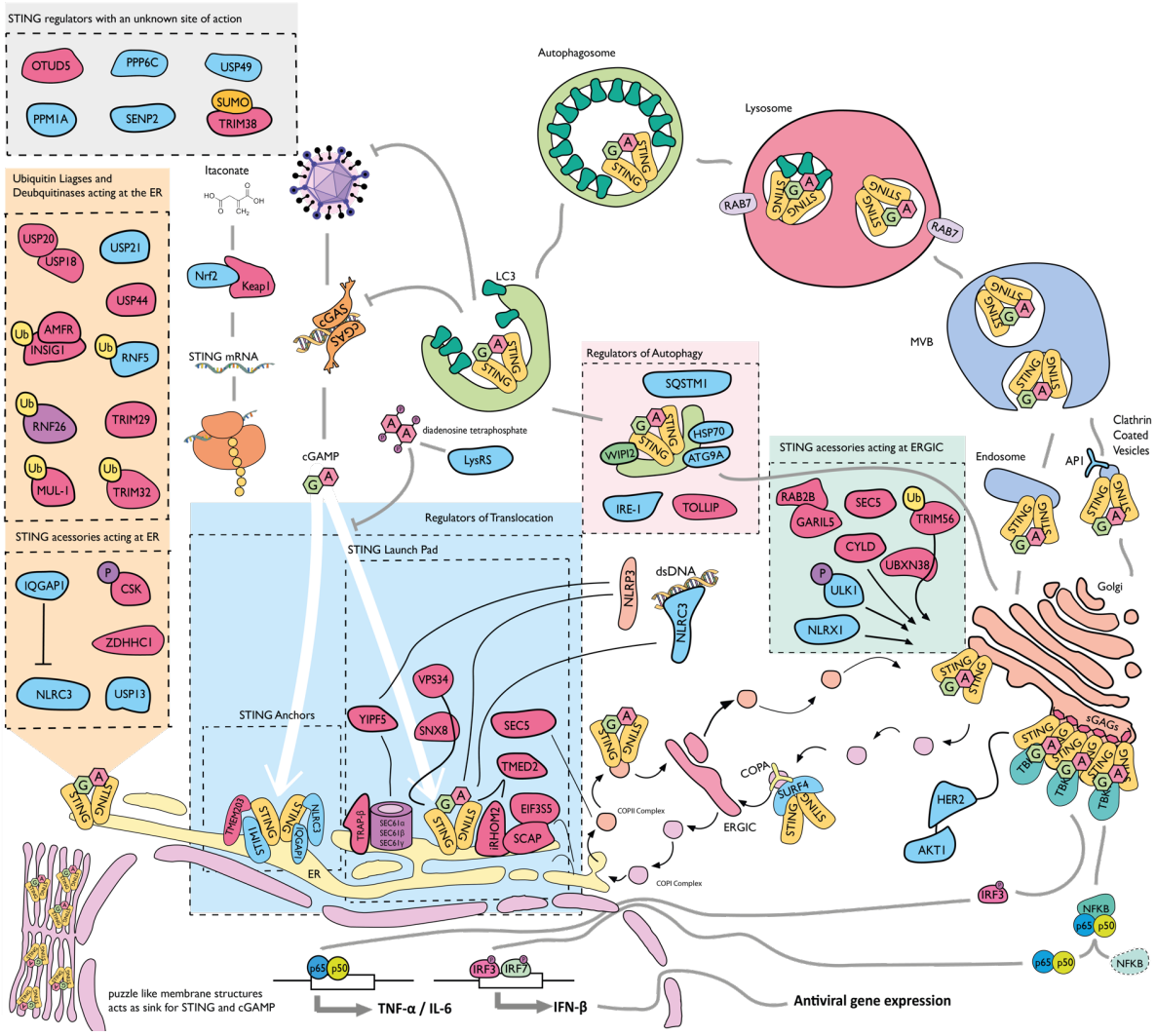


Figure 7 - Accessories of STING. Positive regulators of STING are shown in red and negative in blue. Where possible regulators are shown at their subcellular site of action. A description and reference for the individual STING regulators shown is given in supplementary Table 1.

Degradative ubiquitination of STING by RNF5

Ring Finger Protein 5 (RNF5) was the first E3 ubiquitin ligase shown to act on STING. It is primarily known for its role in the endoplasmic reticulum associated protein degradation

(ERAD) pathway. More recently, RNF5 has been shown to negatively regulate STING activation by attaching K48 linked polyubiquitin chains at lysine 150 leading to proteasomal degradation. In contradiction to conventional STING localisation, this is reported to happen exclusively at the mitochondria (Zhong et al. 2009).

Deubiquitination by CYLD rescues STING's activity

CYLD is a deubiquitinase (DUB) originally identified as a mutated tumour suppressor in familial cylindromatosi, a condition in which benign tumours called cylindromas form around the head and neck (Verhoeft, Ngan, and Lui 2016). CYLD is already documented to regulate innate immune signalling by removing K63 linked ubiquitin chains from RIG-I, which inhibits activation, and degradative K48 linked chains from TRAF2, a molecule crucial to TNF receptor signalling (Trompouki et al. 2003). More recently, it has been shown that knockdown of CYLD attenuates STING responses. Interestingly, CYLD co-immunoprecipitates with STING in the presence of RNF5. Subsequently, CYLD's DUB activity was shown to remove K48 linked chains deposited at lysine 150 by RNF5, preventing proteasomal degradation of STING and enhancing type I IFN production. Thereofore, CYLD and RNF5 exist in antithesis (Zhang, Wei, et al. 2018).

ULK1, a STING kinase

UNC-51-like kinase (ULK1), like ATG5, is a component of the autophagosome biosynthesis machinery and has been shown to phosphorylate STING at S366. This prevents signal transduction through IRF3 but not NF-κB. Interestingly, ULK1s activity is driven through AMP activated protein kinase (AMPK), which is activated by 2'3'-cGAMP, creating a negative feedback loop (Konno, Konno, and Barber 2013).

I.5.3 Atypical regulators of STING

Aside from post translational modification and trafficking, a series of STING regulators exist that operate outside of the binary.

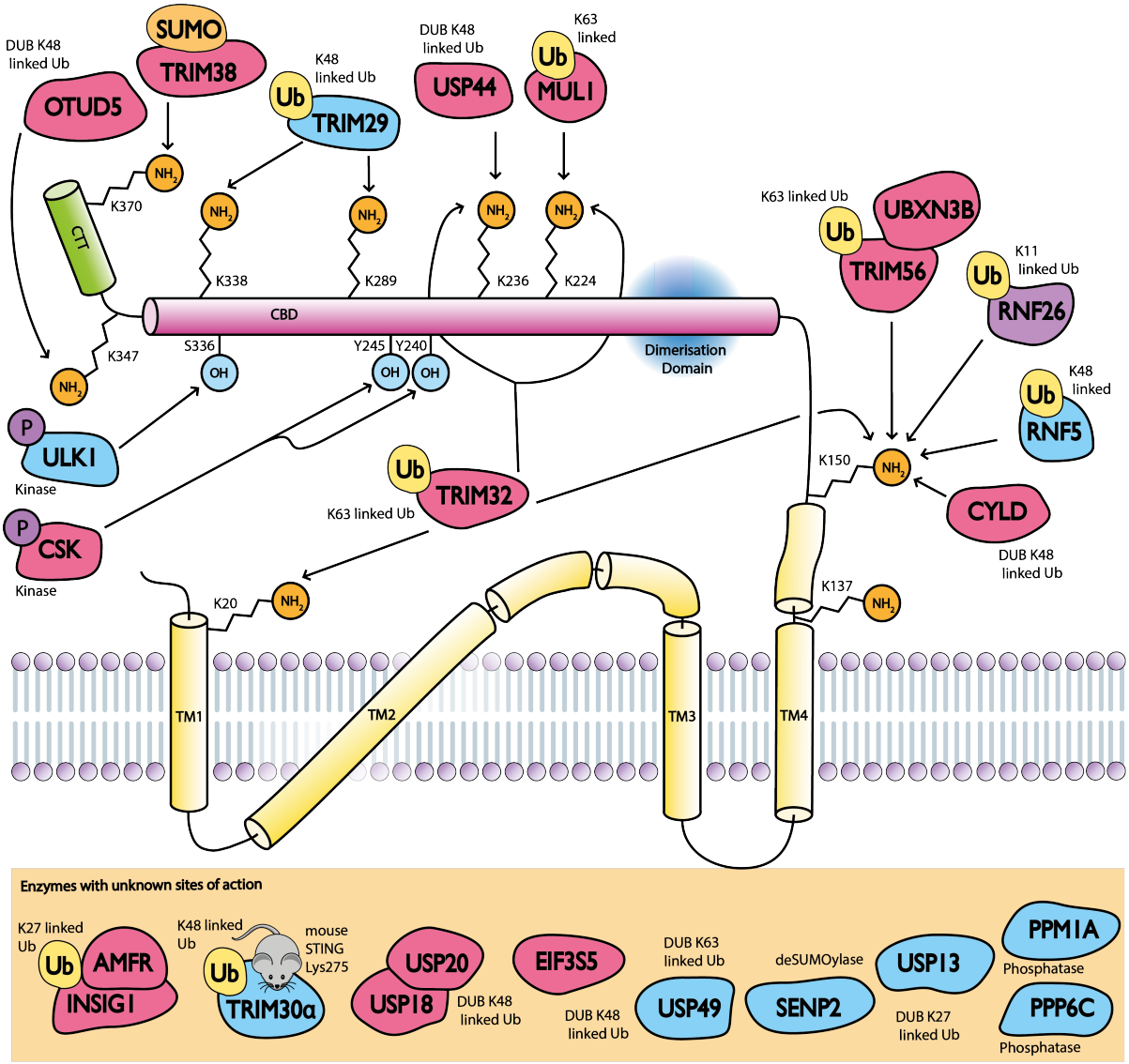


Figure 8 - Posttranslational modification of STING. Diagram showing the residues within STING targeted by ubiquitin ligases, SUMOylases, DUBs and kinases to regulate signalling. A description and reference for the individual STING regulators shown is given in supplementary Table 1.

sGAGs are a platform for STING signalling

Sulphated glycosaminoglycans (sGAGs) have been shown to aid STING signalling by providing a platform at the ER on which STING can polymerise to recruit TBK1 and subsequently IRF3. In accord, knockout of SLC35B2, an enzyme crucial to sGAG biosynthesis, causes a potent reduction in STING mediated signalling (Fang et al. 2021).

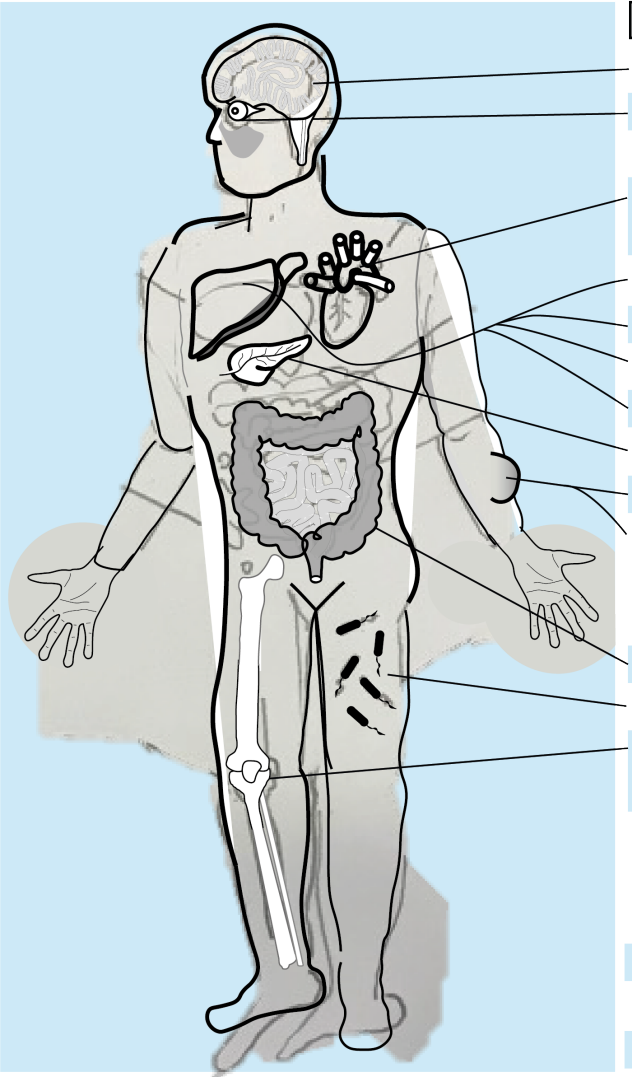
NRF2 destabilises STING's mRNA

NRF2 is a transcription factor thought to regulate the cellular response to oxidative stress. Mechanistically, NRF2 is associated with KEAP1 in an inactive state. Release from KEAP1 is triggered by the small metabolite itaconate. Unexpectedly, NRF2 activation also leads to destabilisation of the mRNA encoding STING and therefore to STING depletion and reduced signal transduction (Olagnier et al. 2018).

I.5.4 STING's relevance to autoimmune disease and therapeutic design

Although operational DNA sensing is required for protection from viral threat, overzealous responses drive chronic proinflammatory conditions, for example the debilitating interferonopathies: Aicardi-Goutières syndrome (AGS), STING associated vasculopathy with onset in in infancy (SAVI) and COPA Syndrome (Deng et al. 2020; Ahn, Ruiz, and Barber 2014; Liu et al. 2014). These are all caused by chronic activation of the STING pathway. AGS is caused by mutations in many different genes (*SAMHD1, ADAR1, TREX1, IFIH1, RNASEH2A, RNASEH2B, RNASEH2C, LSM11,* and *RNU7-1*) many of which lead to accumulation of DNA in the cytosol (Uggenti et al. 2020). SAVI is caused by gain for function mutation in the *STING* gene. COPA syndrome is a disease where mutations in COPA, a component of COP-1 vesicles, result in STING being unbale to traffic back from ERGIC (Deng et al. 2020). Moreover, in a wide range of more prevalent autoimmune disorders such as systemic lupus erythematosus, polyarthritis and Parkinson's disease, STING signalling is thought to contribute towards pathology (Sliter et al. 2018; An et al. 2017; Ahn et al. 2012). STING associated diseases are summarised in Figure 9.

The unmet medical need is profound since traditional drug screening approaches have struggled to produce STING antagonists and the few identified are yet to enter clinical trials (Haag et al. 2018; Hong et al. 2021; Hansen et al. 2018). Meanwhile, many STING associated diseases remain untreatable. Pharmaceutical manipulation of STING accessories could therapeutically alleviate the aforementioned autoimmune conditions. The identification of a metabolite, itaconate, that is an agonist of the negative STING regulator Nrf2 legitimises



Disease	Reference
Parkinson's disease	Sliter et al., 2018
Age-dependent macular degeneration	Kerur et al., 2018
Systemic lupus erythematosus	An et al., 2017
Myocardinal infraction	King et al., 2017
	Cao et al., 2018
Nonalcoholic steatohepatitis	Yu et al., 2019
Alcoholic liver disease	Petrasek et al., 2013
Steatohepatitis	Iracheta et al., 2014
Liver fibrosis	Iracheta et al., 2014
Acute pancreatitis	Zhao et al., 2018
Cancer	Ahn et al., 2014
Metastasis	Bakhoum et al., 2018
	Chen et al., 2016
	Zeng et al., 2017
Inflammatory bowel disease	Wottaw et al., 2021
Sepsis	Ahn et al., 2012
Polyarthritis	Gao et al., 2015
	Rodero et al., 2017
Neonatal anemia	Ahn et al., 2012
	Gao et al., 2015
	Rodero et al., 2017
Aicardi-Goutières syndrome	Gall et al., 2012
SAVI	Liu et al., 2014
COP-I Syndrome	Deng et al., 2020

Figure 9 - STING associated diseases. Schematic showing diseases where STING signalling is thought to contribute to pathology. The table is adapted from Ablasser and Chen (2019).

this concept, as exogenous itaconate treatment inhibits type I IFN production by STING in cultured primary fibroblasts derived from SAVI patients (Olagnier et al. 2018). Similarly, antagonism of the STING accessory STIM1 alleviates lupus pathology in mouse models (Prabakaran et al. 2021). STING agonists are also sought after for cancer immunotherapy as they show potent antitumor effects *in vivo* (e.g. in mouse models of metastatic melanoma, glioma and pancreatic cancer), either individually or in conjunction with other therapies (e.g. PD-1 blockade) (Nakamura et al. 2015; Ohkuri et al. 2014; Baird et al. 2016; Fu et al. 2015). Additionally, STING agonists have been shown to be excellent adjuvants within vaccines (Wang et al. 2020). Therefore, further study of STING and its accessories could generate highly sought-after and novel therapeutic strategies.

I.6 Signalling down stream of PRRs – the IFN response

Despite the vast heterogeneity seen in PRRs, most nucleic acid sensors signal through a relatively limited pool of transcription factors to induce proinflammatory cytokine expression, most notably IRF3, IRF7 and NF-κB. The reason for transcriptional convergence is unexplained but upon phosphorylation, the proinflammatory interferon regulatory factors (IRF3, IRF5, IRF7 and IRF8) dimerise into homo/heterodimers that translocate into the nucleus (Jefferies 2019). Here, they bind the promoter region of type I IFNs triggering expression. This encompasses 13 different subtypes of IFN-α in addition to IFN-β, IFN-ε, IFN-κ, and IFN-ω (Platanias 2005). Cytosolic DNA and RNA sensors principally activate IRF3 and IRF7. IRF3 is ubiquitously expressed but IRF7 expression is induced by IFN so it exists as a positive feedback loop (Marié, Durbin, and Levy 1998). The IRF species activated, and homo/heterodimers formed, govern the profile of cytokines induced. For example, overexpression of IRF5 leads to potent induction of IFN-α8 compared to IRF7 that favours expression of IFN-α1 (Barnes, Moore, and Pitha 2001). In addition to type I IFNs, IRFs also induce the expression of IFN associated cytokines – e.g. CXCL10, CCL5, IL-15 and IL-23 (Jefferies 2019). After release, IFNs act in both an autocrine and paracrine manner to activate the interferon receptor (IFNAR), made of two subunits, IFNAR1 and IFNAR2 (Ivashkiv and Donlin 2014).

Upon IFN binding, cytosolic accessories of IFNAR, JAK1 and TYK2 dimerise to form a kinase complex acting to phosphorylate STAT1 and STAT2. The STAT1-STAT2 dimer then translocates into the nucleus driving expression of genes downstream of an interferon stimulated response element (ISRE), known as interferon stimulated genes (ISGs) (Ivashkiv and Donlin 2014). Broadly, ISGs act to restrict viral replication. For instance, TRIM5 recognises the icosahedral symmetry of viral particles and prematurely disassembles capsids (Ganser-Pornillos and Pornillos 2019); Tetherin anchors viral particles to the plasma membrane preventing egress (Van Damme et al. 2008; Neil, Zang, and Bieniasz 2008); and ZAP acts to degrade viral RNA (Guo et al. 2007; Takata et al. 2017). In addition to driving the production of ISGs, type I IFN and its associated cytokines also activate adaptive immune responses. For example, type I IFNs act as costimulatory cytokines triggering T cell activation and aid cross

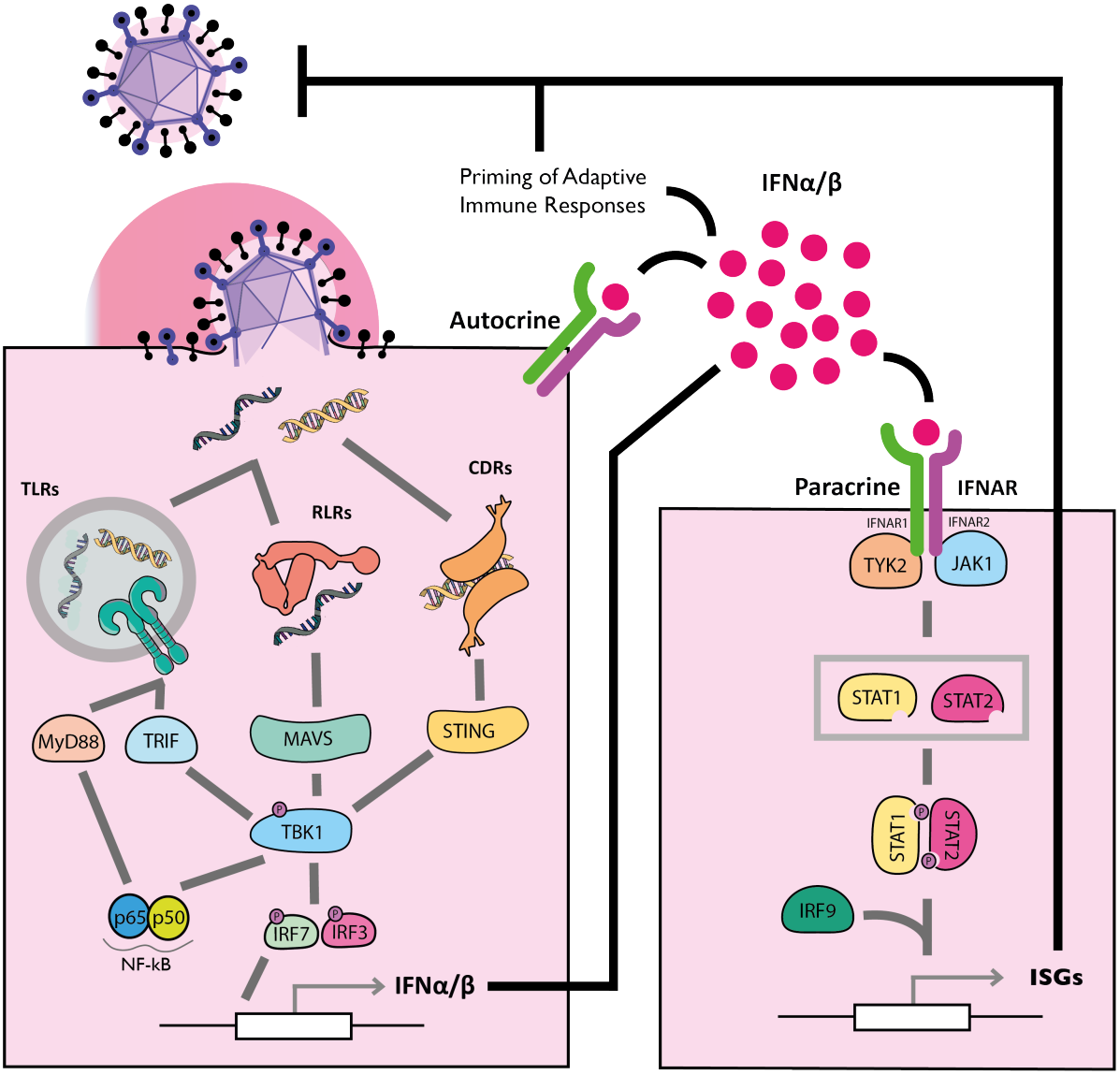


Figure 10 – Interferon signalling. Viral invasion releases nucleic acids into the cell cytosol that can be detected by toll-like receptors (TLRs), RIG-I like receptors (RLRs) and cytoplasmic DNA receptors (CDRs). This leads to the production of type I interferons, which act through the IFNAR receptor in both an autocrine and paracrine manner to drive ISG expression. ISGs then act to restrict viral replication.

presentation on MHC class I by dendritic cells (Stetson and Medzhitov 2006b). NF-κB functions alongside IRFs to drive production of IL-6 and TNF-α triggering the acute phase response and prime cell death pathways (Tanaka, Narazaki, and Kishimoto 2014; Idriss and Naismith 2000). An overview of the type I IFN signalling is presented in Figure 10.

I.7 Transfer of 2'3'-cGAMP between cells

The activity of 2'3'-cGAMP was previously considered topologically limited to its site of production, the cytosol, due to its molecular weight and negative charges preventing passive

movement through cell membranes and therefore spread between cells (Carozza et al. 2019). This is consistent with evidence showing 2'3'-cGAMP transfer can occur through GAP junctions and within viral particles, as these mechanisms effectively link the cytosol of one cell to the next (Ablasser et al. 2013; Gentili et al. 2015; Bridgeman et al. 2015). Only recently has the role of 2'3'-cGAMP outside of the cell been considered. For a decade, it had been known exogenous 2'3'-cGAMP could trigger IFN-β production by cells in *vitro* and reduce tumour growth by direct injection in *vivo* (Corrales et al. 2015; Ritchie et al. 2019; Luteijn et al. 2019). This led to the production of a series of 2'3'-cGAMP analogues for cancer treatment. Despite pharmaceutical success, it remained unclear how these cyclic dinucleotides (CDN) entered the cytosol to activate STING (Meric-Bernstam et al. 2021). This changed between 2019 -2021 when in quick succession five membrane transport proteins were shown to provide a route for CDNs to cross cell membrane - SLC19A1, SLC46A2, P2X7, LRRC8A:C and ABCC1 (Cordova et al. 2020; Ritchie et al. 2019; Luteijn et al. 2019; Lahey et al. 2020; Zhou, Chen, et al. 2020; Zhou, Fei, et al. 2020; Maltbaek, Snyder, and Stetson 2021). Although the dogma separates these proteins into channels (SLC19A1 and SLC46A2), transporters (ABCC1) and pores (P2X7) for simplicity I will collectively refer to them as cGAMP channels. In this section, I will consider the different mechanism by which 2'3'-cGAMP is transferred between cells (Figure 11). For reference, the primary and cancer cell lines in which these channels function and CDNs imported are summarised in Table 1.

I.7.1 ENPP1

To understand the role of extracellular 2'3'-cGAMP, we must first consider ecto-nucleotide pyrophosphatase/phosphodiesterase (ENPP1). ENPP1 is a hydrolase of CDNs and ATP. Studies overexpressing ENPP1 shows its action is limited to the extracellular space despite being present within the ER lumen (Carozza et al. 2019). Structurally, it contains a Ca^{2+} binding domain and chelates two Zn^{2+} ions into its catalytic site. These ions are required for ENPP1 function and supplementation has been shown to enhance hydrolase activity (Li et al. 2014). ENPP1's hydrophobic N-terminus can be cleaved, releasing the now soluble and hydrolysis active enzyme into the surrounding tissue fluid (Belli, van Driel, and Goding 1993). Notably, extracts from WT mouse spleen and liver can completely hydrolyse 2'3'-cGAMP but extracts

Channel	Agonists	Antagonists	cells using channel for import	cells not using channel for import	CDNs imported	CDNs not imported	Reference
Gap Junctions	Isoprenaline Tedisamil Ψ	Carbenoxolone Meclofenamate Tonostat 18β-glycyrhetinic acid Ψ	Monocytes *MEF* *L929* HEK293 THP-1		2'3'-cGAMP	NA	(Ablasser et al. 2013) (Pépin et al. 2020; Salameh and Dhein 2005)
SLC19A1	AICAR	Methotrexate Sulfasalazine	CD14+ Monocytes* K562 THP-1 NU-UL-1 U937	PBMCs *BMDMs* *dendritic cells* *spelnocytes.* Hela HEK293 *C1498* *L1210*	3'3'cGAMP 2'3'-cG^{S}A^{S}MP 2'3'cyclic AMP 2'3'cyclic-di-AMP 2'3' CDA	3'3'-CDA† 3'3'-CDG†	(Luteijn et al. 2019) (Ritchie et al. 2019; Ritchie, Cordova, and Li 2019)
SLC46A2		Sulfasalazine	CD14+ Monocytes	U937	2'3'-cGAMP 2'3'-CDA^{S} 2'3'-cG^{S}A^{S}MP 3'3'-cGAMP 3'3'-CDA†	3'3'-CDA† 3'3'-CDG†	(Cordova et al. 2021)
***P2X7*$^{\#}$**	ATP BzATP λ	A740003 λ	*BMDMs* *TAMs***	*CD103+ DC*** *CD11b+ DC***	2'3'-cGAMP$^{\#}$	$^{\#}$	(Zhou, Fei, et al. 2020; Müller and Namasivayam 2022)
LRRC8A:C	Hypotonicity S1P	Hypertonicity DCPIB	HUVEC TIME U937* HEK293*	CD14+ Monocytes DC NK CD4+ T Cells CD8+ T cells B Cells	2'3'-CDA†† 2'3'-cGAMP 2'3'-cG^{S}A^{S}MP 2'3'-CDA^{S}	3'3'-cGAMP 3'3'-CDA 3'3'-CDG	(Zhou, Chen, et al. 2020; Lahey et al. 2020; Concepcion et al. 2022; Green et al. 2020)
LRRC8A:E	Hypotonicity GTPγS cisplatin	DCPIB MONNA Carbenoxolone Tamoxifen Flufenamic acid Mefenamic acid NS3728	*MLF* *MEF* *BMDM* *pM* *L929*		2'3'-cGAMP 3'3'-cGAMP	FITC-cGAMP	(Zhou, Chen, et al. 2020; Lahey et al. 2020; Concepcion et al. 2022; Green et al. 2020)
ABCC1		MK-571 LY465803 LY475776 Reversan ω	HFF *BMM* *MEF* A549		2'3'-cGAMP		(Maltbaek, Snyder, and Stetson 2021)

Table 1 – The cell types in which cGAMP channels function and the CDNs they transport. Shown are cell types in which channel deficiency or specific chemical inhibitors prevent STING pathway activation in response to exogenous CDNs. FDA approved drugs are shown in red. Primary cell lines are shown in black and cancer cell lines in blue. Mouse cell lines and channels only tested in mice are shown in italics. * - Not major importer as knockout or chemical inhibition only marginally reduces CDN mediated STING activation. ** - Direct CDN uptake not proven in *vitro* but in *vivo* channel required for STING pathway activation in presence of exogenous CDNs. † - Unclear if imported. †† - Minimal effect of transporter on uptake. # - P2X7 forms a large non-selective pore for hydrophilic substances ~0.9 KDa in size therefore although not formally shown it is assumed there is no CDN specificity. Ψ reviewed by Salameh and Dhein (2005). λ reviewed by Müller and Namasivayam (2022). ω reviewed by Cole (2014).

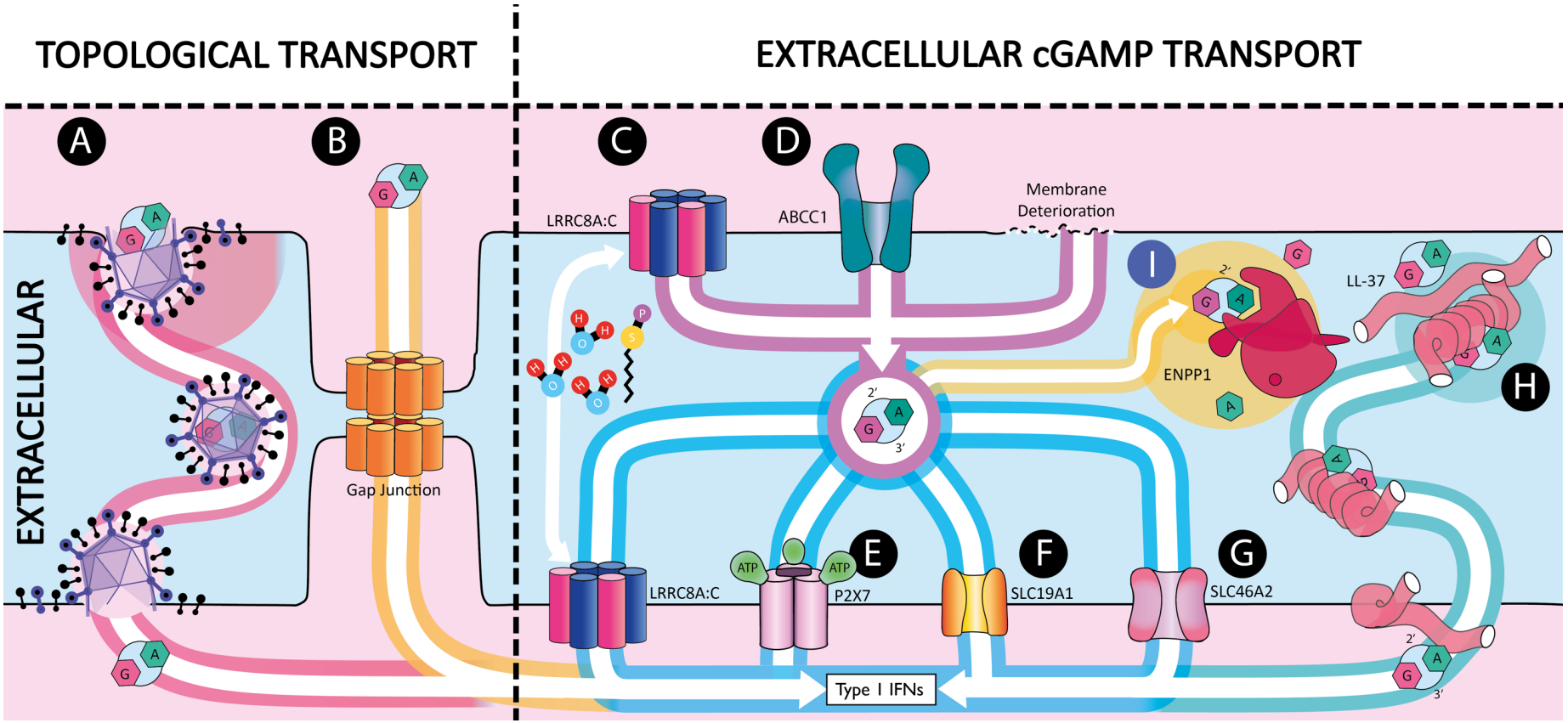


Figure 11 – Extracellular 2’3’-cGAMP transport. Schematic showing the mechanisms by which 2’3’-cGAMP can be transferred between cells. A) Within viral particles. B) Through gap junctions. C) Import and export through LRRC8A:C heterodimers which are activated by hypotonicity and S1P. D) Export through ABCC1. E) Transport through the ATP gated pore P2X7. F) Import through SLC19A1. G) Import through SLC46A2. H) 2’3’-cGAMP shuttling by LL-37. I) 2’3’-cGAMP hydrolysis by ENPP1.

from *Enpp1*-/- knockout mice show no detectable degradation. This demonstrates that at least in mice, Enpp1 is likely the dominant if not only 2'3'-cGAMP hydrolase (Li et al. 2014). Efforts have been made to produce non hydrolysable 2'3'-cGAMP analogues by replacement of phosphodiester linkages with phosphothioate linkages (e.g. 2'3-cG^{S}AMP, 2'3-cGA^{S}MP, 2'3'-cG^{S}A^{S}MP). This proved efficacious as phosphothioate analogues are 40 times more resistant to ENPP1 hydrolysis and induce more potent STING activation in cell culture (Li et al. 2014). Additionally, 3'3' linked species (e.g. 3'3'-cGAMP) produced by bacteria as secondary messengers have also shown resistance to ENPP1 mediated hydrolysis (Li et al. 2014). This paved the way for production of CDN based immunotherapeutics, which are currently in clinical trials. Notably, the CDNs 2'3'CDA^{S} (also known as ADU-S100) and MK-1454 are being tested for activity against advanced/metastatic solid tumours and lymphomas (trail IDs - NCT03172936 and NCT03010176) (Meric-Bernstam et al. 2021; Ritchie et al. 2019).

ENPP1 has also been shown to suppress antitumoral responses. Some cancer cells are known to have unstable nuclei due to incomplete chromosomal separation during mitosis. This leads to the formation of micronuclei, enclosing DNA within "leaky" membranes accessible by cGAS (Harding et al. 2017; Mackenzie et al. 2017). In cell culture, 2'3'-cGAMP efflux from many cancer cell lines can only be observed upon chemical inhibition or knockdown of ENPP1. In accord, *Enpp1*-/- mice unable to degrade 2'3'-cGAMP are resistant to tumour development in multiple models of cancer (Carozza et al. 2019). Tumour resistance is also observed in mice treated with ENPP1 inhibitors, an effect enhanced by simultaneous radiotherapy, a treatment known to increase erroneous chromosomal segregation and so augment detection of self-DNA by cGAS (Carozza et al. 2019; Mackenzie et al. 2017; Harding et al. 2017; Bakhoum et al. 2018; Bakhoum et al. 2015; Dou et al. 2017).

Overall, ENPP1 appears to potently suppress the proinflammatory effects of extracellular 2'3'-cGAMP. It is unclear if tissues lacking ENPP1 expression, or a yet to be identified regulator of this hydrolase, could allow for extracellular 2'3'-cGAMP accumulation and immune activation. However, it is clear that enhancement of immune responses triggered by extracellular 2'3'-cGAMP could provide effective cancer treatments, especially as upon ENPP1 inhibition endogenous 2'3'-cGAMP production would be localised to the tumour microenvironment.

This avoids dosing issues observed upon clinical administration of CDNs. The therapeutic window is narrow due to high CDN doses inhibiting the proliferation of T cells required for effective tumour rejection (Cordova et al. 2020; Gulen et al. 2017; Larkin et al. 2017; Cerboni et al. 2017; Concepcion et al. 2022). Systemic ENPP1 inhibitors also sidestep clinical concern regarding tumour disruption during CDN injection, which may physically dislodge cancerous cells encouraging metastasis. 2'3'-cGAMP and ATP degradation mediated by ENPP1 also contributes to the extracellular pool of adenosine, an immunosuppressant detected by the adenosine receptor. Extracellular adenosine produced by ENPP1 has been shown to enhance both tumour growth and metastasis (Li, Duran, et al. 2021). Therefore, ENPP1 inhibitors would act to simultaneously augment STING activation and prevent adenosine's anti-inflammatory properties. The tremendous therapeutic promise of ENPP1 inhibitors is well illustrated by swift financial interest from pharmaceutical investors. Professor Lingyin Li, the true pioneer of extracellular 2'3'-cGAMP responses, recently raised a $11.3 million in funding to create Angarus, a company focussed on the development of ENPP1 inhibitors, the first of which - AG-3132 - is about to enter phase 1 clinical trials (Crunchbase 2022).

I.7.2 Transfer through gap junctions

Gap junctions are intercellular channels which effectively link the cytoplasm of one cell to its neighbour. Their function is broad, playing a role in developmental signalling, electrical potentiation, cellular proliferation and differentiation (Totland et al. 2020). They are formed by connexins of which there are 21 known in humans. These form hexamers known as "hemichannels"(Laird 2006). A hemichannel on one cell links to another on an adjacent cell forming a gap junction, which assemble in clusters to form hundreds of intercellular channels, allowing for the passage of small and hydrophilic species (<~1.2 kDa), including signalling molecules, between cells (e.g. ATP, cAMP, IP_3, glucose, glutathione, glutamate, Ca^{2+}, K^+ and Na^+) (Vinken 2015). This constant exchange of metabolites and signalling molecules is called gap junction intercellular communication (GJIC) and allows a tissue to act as a collective. GJIC is a basic mechanism of tissue homeostasis and explains GAP junction's wide ranging physiological role.

It was known half a decade before the discovery of cGAS that GAP junctions facillitate IFN-β production in response to dsDNA. This was shown in the HEK293 cells expressing GFP under the the control of an IRF3 promoter. Upon dsDNA transfection, a striking visual pattern is seen where clusters of cells become GFP positive, suggesting stimulated cells might be instigating innate immune activation in their physically associated neighbours. This effect is lost on siRNA depletion of GAP junction components (Patel et al. 2009). Shortly after 2'3'-cGAMPs discovery, it was identified as the messenger responsible, as knocking out the only two connexins present in HEK293 cells (CX43 and CX45) prevented 2'3'-cGAMP transfer. Upon cellular reconstitution with other known connexins (CX26, CX31, CX32, CX40, CX52a and CX50) all but CX50 rescued 2'3'-cGAMP transfer. This is in line with the notion that gap junctions form pores with limited cargo specificity to redundantly facilitate 2'3'-cGAMP transfer between cells (Ablasser et al. 2013). Remarkably, gap junctions can also transfer 2'3'-cGAMP between non-static cells. In coculture experiments, HEK293 cells could transfer 2'3'-cGAMP to primary human monocytes, a process dependent on expression of CX43 and CX45 (Pépin et al. 2020). Additionally, in *vivo,* 2'3'-cGAMP coated in pulmonary surfactant mimetic liposomes (PS-cGAMP) can be taken up by alveolar macrophages and the 2'3'-cGAMP transferred to alveolar epithelial cells through GAP junctions (Wang et al. 2020). This passing of cyclic dinucleotides by non-static cells complicates the interpretation of in *vivo* models since the cells reacting to 2'3'-cGAMP may not be directly importing the 2'3'-cGAMP from the extracellular space.

Hemichannels at the cell surface have also been shown to have central roles in autocrine and paracrine, signalling, allowing exchange of small molecules between the cytoplasm and surrounding tissue fluid. This facilitates movement of small metabolites (e.g. ATP, glutamate, NAD^+, IP_3, prostaglandin E_2, and cAMP) across the cell membrane (Gossman and Zhao 2008; Valiunas 2013; Loiselle, Jiang, and Donahue 2013). The cyclic dinucleotide cAMP has a similar size and structure to 2'3'-cGAMP (~0.7 KDa) (Valiunas 2013). As of yet the role hemichannels play in 2'3'-cGAMP export / import has not been investigated.

I.7.3 Transport by viruses

Unexpectedly, 2'3'-cGAMP has also been shown to be transported between cells within viral particles. The Rehwinkel lab initially investigated if cGAS, like the RNA editing enzyme APOBEC3G, could be packaged into lentiviral virions (Bridgeman et al. 2015). Initially, they and others observed viruses (VACV, MCMV and HIV-1) produced in cGAS expressing cells triggered STING activation upon viral entry, although this was not due to cGAS packaging but rather 2'3'-cGAMP was shown to be incorporated within virions (Gentili et al. 2015; Bridgeman et al. 2015). These observations are remarkable as the volume of a viral particle is miniscule relative to a cell. Therefore, it is astonishing that enough 2'3'-cGAMP can be delivered to activate STING. These findings have found application in vaccine design as 2'3'-cGAMP loaded virus like particles coated with the influenza haemagglutinin induce higher levels of virus specific neutralising antibodies that protect mice from reinfection (Chauveau et al. 2020). Similarly, pulmonary surfactant mimetic microsomes containing 2'3'-cGAMP used as an adjuvant alongside influenza vaccination (H1N1) greatly enhanced humoral and $CD8^+$ T cell responses in mice. Additionally, in contrast to the currently available flu vaccines, they provided cross protection against distant and heterosubtypic flu strains, a remarkable and long sought-after accomplishment (Wang et al. 2020). This clearly illustrates the immense therapeutic potential of CDN containing vaccines.

I.7.4 SLC19A1

The first 2'3'-cGAMP channel to be reported was reduced folate carrier 1 (SLC19A1/RFC1). SLC19A1 was initially characterised as an anti-transporter and main importer of reduced folate into cells. This couples the uphill import of reduced/anti folates to the downhill export of inorganic phosphates (Zhao and Goldman 2013). The energy needed for folate accumulation is provided indirectly by the ATP expenditure needed to create inorganic phosphates. Folates are essential membrane impermeable B family vitamins required for cell proliferation, tissue repair and development (Zhao and Goldman 2013). Hence knockout of SLC19A1 in mice is embryonically lethal without continuous folate supplementation (Zhao et al. 2001). Additionally, SLC19A1 is of clinical relevance as the efficacy of the therapeutic antifolate, methotrexate, is positively correlated with SLC19A1's activity in patients with acute lymphoblastic leukaemia (Liu et al. 2017; Belkov et al. 1999; Kager et al. 2005).

Initially, SLC19A1's role in 2'3'-cGAMP transport was characterised in U937 and THP-1 monocytic cell lines. SLC19A1 knockout was seen to prevent STING activation in response to extracellular 2'3'-cGAMP. Chemical characterisation showed that methotrexate, a competitive inhibitor of SLC19A1 similarly prevented STING activation in response to exogenous 2'3'-cGAMP (Ritchie et al. 2019; Luteijn et al. 2019). Finally, a direct interaction between 2'3'-cGAMP and SLC19A1 has been shown; SLC19A1 precipitates with 2'3'-cGAMP immobilised on sepharose beads. This interaction is disrupted by free unbound 2'3'-cGAMP or methotrexate (Luteijn et al. 2019). More recently the structure of SLC19A1 in complex with 2'3'-cGAMP has been solved (Figure 12) (Zhang et al. 2022). Although SLC19A1's function has been observed in monocytic cell lines (THP1 and U937), only a minimal role in 2'3'-cGAMP uptake has been shown in primary human monocytes. This suggests SLC19A1 plays a non-dominant role in monocytic 2'3'-cGAMP import and highlights the caution and need for primary cell data to delineate the cell types in which these channels transport 2'3'-cGAMP in *vivo* (Ritchie et al. 2019).

Other cyclic dinucleotides in addition to 2'3'-cGAMP are imported into cells by SLC19A1, both synthetic (2'3'-RR CDA, 2'3'-cG^{S}A^{S}MP, 2'3'-CDA, 2'3'-CDA^{S}) and bacterially derived CDNs (3'3'-cGAMP). Although, some bacterially derived CDNs are imported poorly or not at all by SLC19A1 (e.g. 3'3'-CDA, 3'3'-CDG). The possibility that SLC19A1 shows specificity to the type of CDNs that are imported is exciting, as the knowledge of the cell types expressing SLC19A1 could allow for cell targeted CDN treatments based on CDN channel expression profiles (Ritchie et al. 2019).

Mouse SLC19A1 is not thought to import 2'3'-cGAMP, since efficient depletion of *Slc19a1* in mouse cell lines had no effect on 2'3'-cGAMP uptake. Similarly, in mouse primary BMM and BMDC cells, *Slc19a1* depletion does not reduce IFN-β mRNA levels upon CDN treatment. This suggests another importer is mediating mouse cell uptake of 2'3'-cGAMP (Luteijn et al. 2019). Therefore, without establishment of a suitable animal model to study this channel's role in the context of viral infection or cancer in *vivo,* it cannot be proven that it functions to enhance 2'3'-cGAMP driven immune responses, especially as it is possible that the wide variety of

natural SLC19A1 substrates may out compete 2'3'-cGAMP for import under physiological conditions. Therefore, future studies looking at viral antagonism in *vitro* or polymorphisms within patient cohorts will be key to provide evidence of its role at the physiological level.

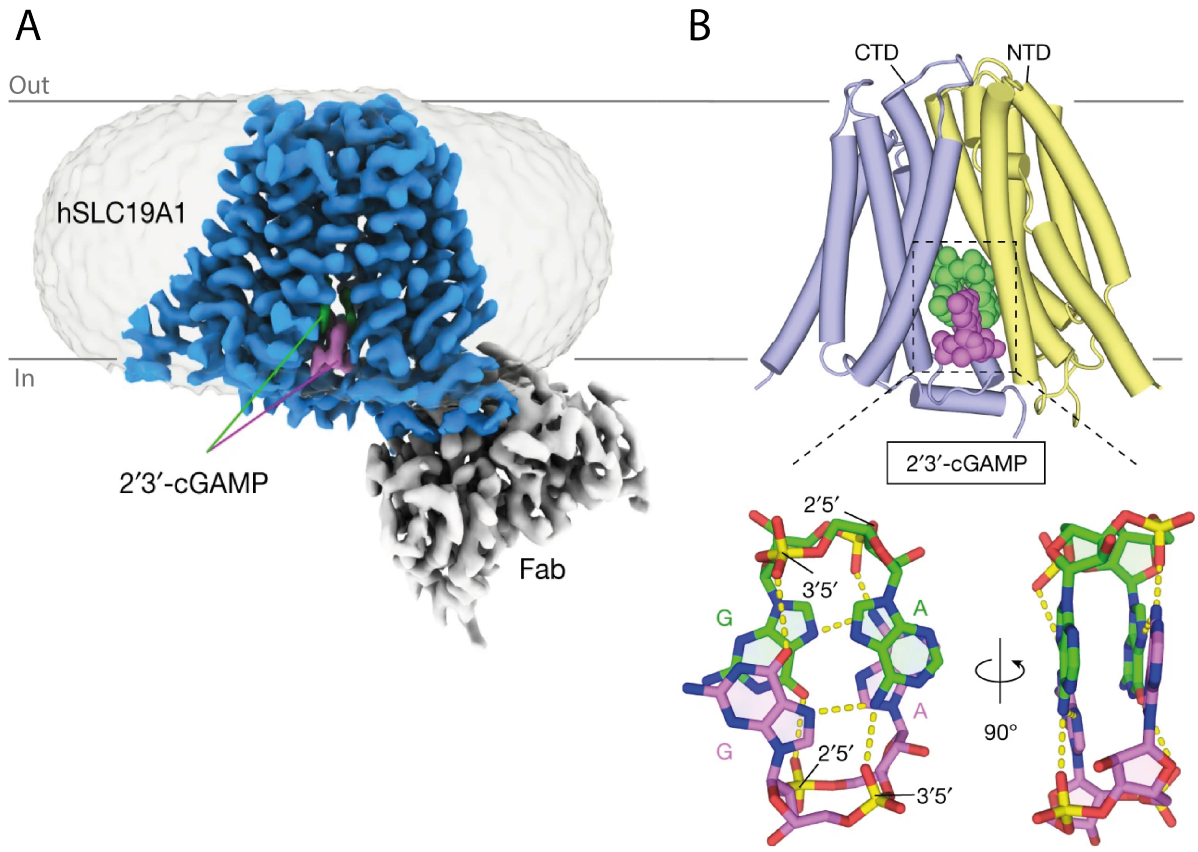


Figure 12 – Structure of SLC19A1 in complex with 2'3'-cGAMP. A) Cryo-EM density map of human SLC19A1(blue)-Fab(grey) complex bound to two molecules of 2'3'-cGAMP (green and purple). B) The overall structures of hSLC19A1 bound to 2'3'-cGAMP in the inward-open conformation. The N-terminal domain (NTD) is coloured yellow and C-terminal domain (CTD) coloured blue. Two bound 2'3'-cGAMP molecules are shown as a space-filling representation and are coloured (green and purple). Adapted from Zhang et al. (2022).

I.7.5 SLC46A2

SLC46A2 (TSCOT) is an orphan solute carrier with predominant expression known in the cortical epithelial cells of the murine thymus (Kim et al. 2015). It's only known substrate is foreign - the tracheal cytotoxin (TCT). This is produced by *Bordetella pertussis* and *Neisseria gonorrhoeae* entering mammalian cells and driving NOD1 activation and necrosis (Paik et al. 2017). Therefore, an endogenous role is yet to be assigned.

SLC46A2's role in 2'3'-cGAMP transport was initially identified by Cordova et al. who observed it is the dominant 2'3'-cGAMP importer in monocytes and macrophages. This was shown by

partial knockdown of SLC46A2, resulting in reduced STING activation in response to extracellular 2'3'-cGAMP in primary monocytes. Additionally, overexpression of human and murine SLC46A2 enhances STING activation in response to extracellular but not electroporated 2'3'-cGAMP. SLC46A2 is a member of the SLC46A solute transporter family, which has two other members: SLC46A1 and SLC46A3. SLC46A1, like SLC19A1, transports folate species into cells. Unlike SLC19A1, it functions optimally at low pH (~5.5) and is predominately responsible for intestinal folate uptake. SLC46A3, like SLC46A2, is an orphan solute carrier without known function (Qiu et al. 2006). Interestingly, SLC46A1 and SLC46A3 appeared as prominent hits in a previous screen looking to identify 2'3'-cGAMP importers (Luteijn et al. 2019). On overexpression, these proteins enhance STING activation in response to extracellular 2'3'-cGAMP. Despite this, effective depletion of SLC46A1 and SLC46A3 caused no or very minor inhibition of STING activation in monocytes. This is likely due to the redundant and highly efficient uptake through SLC46A2 (Cordova et al. 2021; Luteijn et al. 2019). As such SLC46A1 and SLC46A3 likely transport 2'3'-cGAMP but a physiological role is still to be explored. Research into whether SLC46A1 aids STING activation in the gut could answer this as it is highly expressed in the intestines, proximal to CDN producing bacteria and a site of autoimmune disease (Qiu et al. 2006).

Despite murine SLC46A2 being able to transport 2'3'-cGAMP, it is not responsible for uptake in murine macrophages, as SLC46A2 is poorly expressed in murine immune cells. SLC46A1 and SLC46A3 are expressed but have also been shown not to be the dominant transporter (Cordova et al. 2021). This suggests there is another mechanism of 2'3'-cGAMP uptake in murine macrophages (Cordova et al. 2021). Therefore, like with SLC19A1, there are clear differences in SLC46A2 mediated 2'3'-cGAMP uptake between humans and mice.

I.7.6 P2X7

Extracellular ATP functions in the synaptic cleft as a neurotransmitter, but widespread release is a renowned DAMP known to coordinate immune responses in various pathological settings (e.g. microbial invasion, tumour rejection and tissue damage) (Dou et al. 2018). Membrane disintegration of dying or damaged cells is thought to release ATP into the extracellular space. Additionally, channels transport ATP into secretory vesicles or directly into the extracellular

space (e.g. VRACs, pannexins, connexins) when triggered by various stimuli (e.g. Ca^{2+} currents, CO_2, mechanical deformation, hypoxia, heat and osmotic stress) (Lazarowski 2012). Remarkably, levels of ATP in the tumour microenvironment have been shown to be up to 1000 times greater than that of healthy tissue (Pellegatti et al. 2008). In mammals, released ATP is detected by two G-Protein coupled P2Y receptors (P2Y1R and P2Y11R) and by all 7 of the P2X ligand gated ion channels (P2X1-7) (Di Virgilio et al. 2018). The P2XRs are mainly expressed in excitable and immune cells, in line with ATP's role as both a neurotransmitter and DAMP. Notably, P2X7 is expressed in virtually all immune cells (including: Macrophages, Dendritic cells, granulocytes, T cells, B cells and NK cells) and confers resistance to bacterial, parasitic and viral infection (Di Virgilio et al. 2018). Under resting conditions P2X7 supports Na^+ and Ca^{2+} influx and minimal K^+ leakage out of the cell. Functionally, activation of P2X7 by ATP causes the opening of a non-selective pore for hydrophilic substances of up to ~0.9 KDa and passive K^+ efflux (Drill et al. 2021; Egan and Khakh 2004). Intracellular K^+ decline activates the NLRP3 inflammasome leading to the release of proinflammatory cytokines including IL-1β and IL-18 (Karmakar et al. 2016; Gombault, Baron, and Couillin 2013). For reference, 2'3'-cGAMP has a molecular weight of ~0.7 kDa, meaning passage through P2X7 is feasible (Li et al. 2014).

P2X7 was first implicated in 2'3'-cGAMP transport by Zhou et al. in a model of efferocytosis (Figure 13) (Zhou, Fei, et al. 2020). Efferocytosis is usually mediated when a cell displays Gas6 or ProS on the cell surface. These "eat me" molecules trigger monocytically expressed MerTK to induce phagocytosis and immunologically silent cell death. The authors observed in two mouse models of cancer (MC38 – colon adenocarcinoma and E0771 – a murine model of triple negative breast cancer) that blocking MerTK mediated efferocytosis by tumour associated macrophages causes release of 2'3'-cGAMP from dying cells. They speculate membrane integrity eventually becomes disrupted in cells not cleared and hence 2'3'-cGAMP is released into the extracellular medium. This manuscript also shows that in *vivo* MERTK antagonism reduces tumour size over time and acts cooperatively with other immunotherapies (e.g. PD-1 blockade) (Zhou, Fei, et al. 2020). This response requires the engrafted tumour to have active cGAS and the host to have STING. This is consistent with previous accounts of 2'3'-

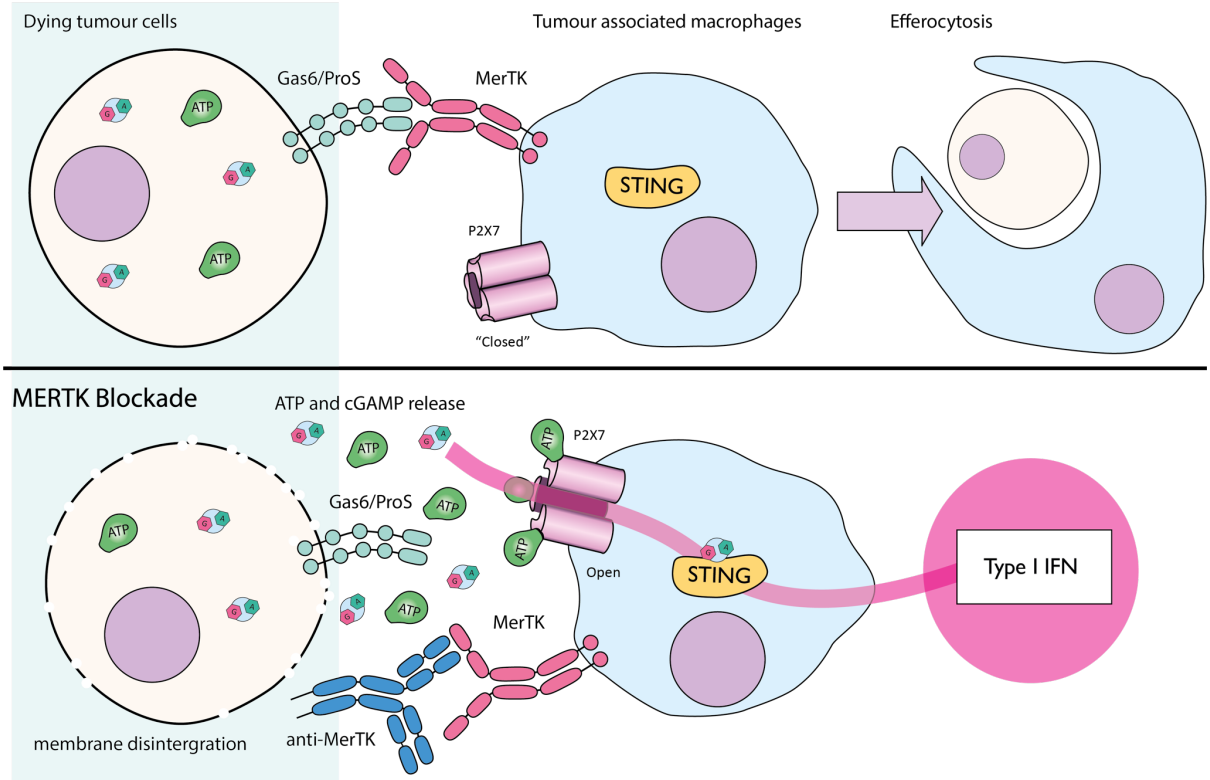


Figure 13 – P2X7 mediated 2'3'-cGAMP uptake during MERTK blockade. Dying cancer cells are cleared by efferocytosis where the MerTK receptor present on tumour associated macrophages (TAMs) recognises "eat me" signals Gas6/ProS. This leads to immunologically silent cell death by engulfment and digestion of the cellular corpse. Blockade of MerTK activity with an anti-MerTK antibody result in accumulation of dying cancer cells. Likely as a result of membrane disintegration, 2'3'-cGAMP and ATP are released into the tumour microenvironment. ATP activates the P2X7 pore expressed by TAMs allowing 2'3'-cGAMP to passively move across the plasma membrane and drive type I IFN production through STING.

cGAMP produced by tumours activating STING within healthy tissue to mediate tumour rejection (Carozza et al. 2019; Marcus et al. 2018). P2X7 was identified as the channel mediating exogenous 2'3'-cGAMP uptake, since P2X7 knockout prevented the ISG signature seen in the tumour microenvironment and stopped tumour regression in response to MERTK blockade. Additionally, in BMDMs ATP strikingly enhances STING activation upon treatment with extracellular 2'3'-cGAMP. This effect is nullified by the P2X7 specific inhibitor A740003, indicating murine P2X7 likely imports 2'3'-cGAMP. Whether human P2X7 also imports 2'3'-cGAMP is yet to be shown. Since ENPP1 hydrolyses both ATP and 2'3'-cGAMP this raises an exciting possibility that ENPP1 inhibitors could act synergistically with MERTK blockade to clear cancer, as the accumulation of extracellular ATP and 2'3'-cGAMP would maximise P2X7's function.

I.7.7 Volume regulated anion channels (LRRC8A:C)

Maintenance of cellular volume in response to extracellular osmotic change is critical to cellular homeostasis. Volume regulated anion channels (VRAC) are named after the observable efflux of Cl^- and organic solutes when cells are placed in a hypotonic (low salt) solution, which induce cell swelling (Hernández-Carballo et al. 2010; Cahalan and Lewis 1988). The release of anions induces the osmotic efflux of water and so reduces/maintains cellular volume (Figure 14A). Three decades after this electro-osmotic phenomenon was observed, the gene critical to VRAC function was identified - LRRC8A (SWELL1) (Voss et al. 2014; Qiu et al. 2014). Since then, the VRAC channels have been implicated in: neuronal signalling (Sirianant et al. 2016); cellular migration (Zhang, Deng, et al. 2018; Wong et al. 2018); apoptosis (Chen et al. 2019); sperm cell genesis and motility (Lück et al. 2018); T cell development (Kumar et al. 2014); insulin release (Stuhlmann, Planells-Cases, and Jentsch 2018); and adipocyte expansion (Zhang et al. 2017). VRAC's broad physiological relevance is likely due to its role in the import/export of signalling molecules. Structurally, LRRC8A forms a hexameric channel into which the other LRRC8 members - LRRC8B-E – are stochastically incorporated (Figure 14B). LRRC8A is the critical component and a heteromeric hexamer must be formed to efficiently mediate anion transport across membranes (Chen et al. 2019). All VRACs appear to convey small anions such as chloride, but hexamer composition determines the larger species transported. For instance, complexes containing LRRC8A:B mediate inorganic anion flux, whereas LRRC8A:C and LRRC8A:E also transport larger anionic osomolytes such as ATP, glutamate, and aspartate. Finally, LRRC8A:D has generally increased permeability for neutral and even positively charged osmolytes such as: taurine, lysine, serine, inositol, γ-aminobutyric acid (GABA) and the anticancer drug cisplatin (Table 2) (Schober, Wilson, and Mongin 2017; Planells-Cases et al. 2015; Gaitán-Peñas et al. 2016; Lutter et al. 2017). Due to LRRC8C being expressed in immune and LRRC8B being expressed in neuronal tissue they are predicted to play a role in immune and neuronal signalling (Abascal and Zardoya 2012).

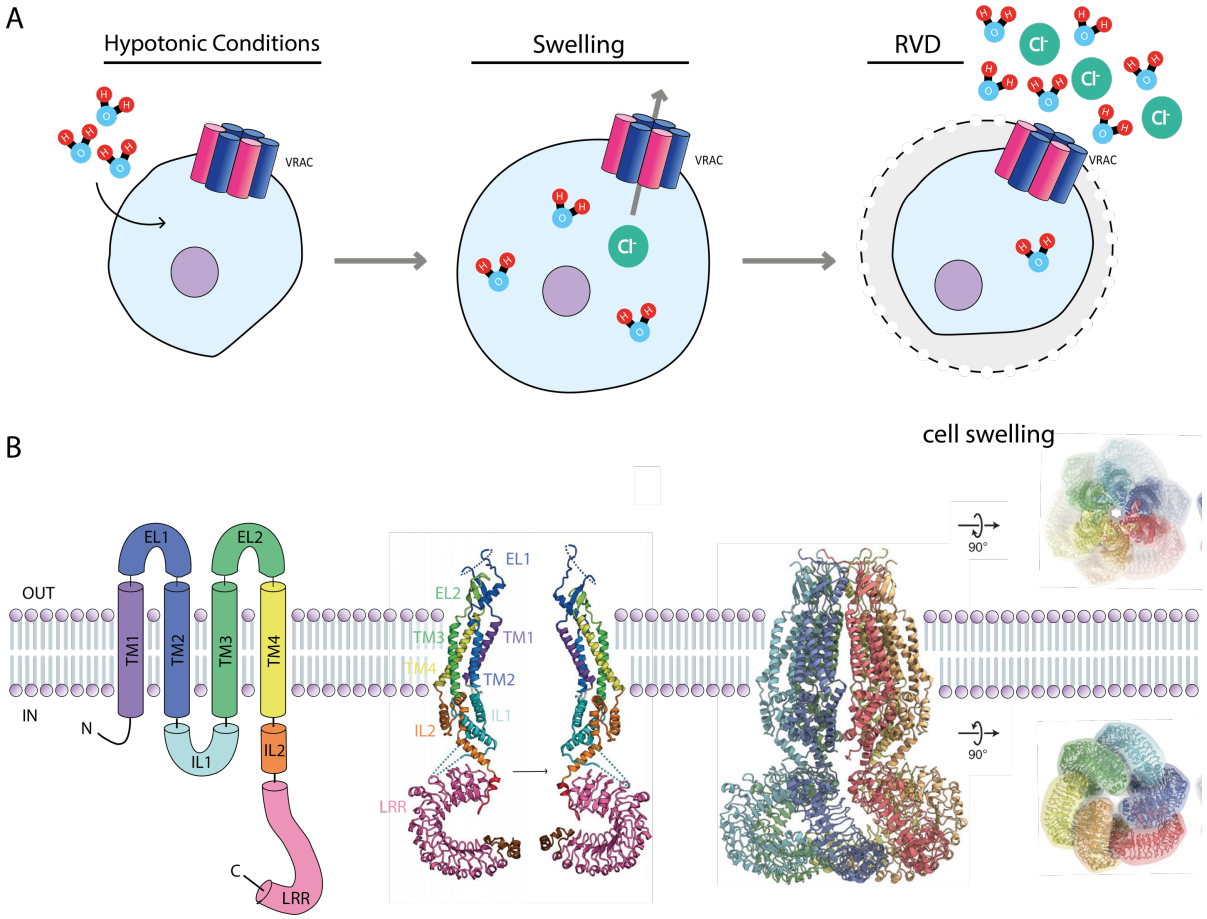


Figure 14 – Structure and function of VRACs. A) Diagram showing regulatory volume decrease. Hypotonic conditions cause cells to swell as water molecules cross the plasma membrane through osmosis. Cell swelling opens VRAC channels, leading to export of small anionic species such as Cl^-. The reduction in anionic solutes within the cell reduces its osmolarity and allows for cell shrinkage. B) Topology of LRRC8A. Depicted is the transmembrane domains, Extracellular loops (EL), intracellular loops (IL) and leucine rich repeats (LRR). Cryo-EM density map of hexameric channel formed by human LRRC8A. Structure adapted from Kasuya et al. (2018).

Overall, the permeability of individual hexamers is technically difficult to define, and it is likely that further substrates and hexameric VRAC configurations will be discovered. Interestingly, the LRRC8 proteins are closely related to pannexins, the vertebrate homolog of invertebrate gap junctions (Abascal and Zardoya 2012). Additionally, the cytoplasmic leucine rich repeat domain (LRR) is bioinformatically predicted to be a signalling platform (Abascal and Zardoya 2012).

A CRISPR screen aimed to identify the transporter mediating background 2’3’-cGAMP uptake in SLC19A1 KO cells identified VRACs as a potential 2’3’-cGAMP transporter (Lahey et al. 2020). Knockout of the VRAC subunits LRRC8A and LRRC8C reduces STING activation in response to exogenous 2’3’-cGAMP. In HEK293 cells, hypotonic buffers enhanced STING

activation in response to extracellular 2'3'-cGAMP in an LRRC8A:C dependent manner. Additionally, patch clamp analysis showed 2'3'-cGAMP was able to competitively inhibit the influx of Cl- ions through VRAC, suggesting 2'3'-cGAMP permeates LRRC8A:C (Lahey et al. 2020). Surprisingly, knockdown of LRRC8D increases STING activation in response to extracellular 2'3'-cGAMP, suggesting LRRC8D inhibits 2'3'-cGAMP transport through LRRC8A:C (Lahey et al. 2020). Mechanistically, LRRC8D likely competes with LRRC8C for the available pool of LRRC8A to form functional channels, which likely blocks negatively charged 2'3'-cGAMP from moving through the channel, since LRRC8D forms a pore with preference for neutral or positively charged species. To find cells in which the LRRC8A:C channel imports 2'3'-cGAMP under physiological conditions, Lahey et al. identify cell lines with high expression of LRRC8A and LRRC8C but low expression of the inhibitory subunit LRRC8D. Primary human umbilical vein endothelial cells (HUVECs) were found to fit this profile. Therefore, Initial reports suggest that in humans LRRC8A:C mediated 2'3'-cGAMP import is limited to vascular endothelial cells (Lahey et al. 2020). It remains to be explored if the endothelium within the lymphatic system proximal to many immune cells also utilises these channels. Structural work shows the narrowest region of the LRRC8A channel is gated by an arginine residue (R103), creating a strong positive charge at the extracellular face of the pore crucial to 2'3'-cGAMP

VRAC subunit	Substrate	Tissue localisation	Reference
LRRC8B	Small inorganic anions (e.g Cl^-)	Neuronal tissues, adrenal cotex, fallopian airway and bronchial epithelial cells, macrophages, platelets.	(Abascal and Zardoya 2012)
LRRC8C	Small inorganic anions and large anionic osmolytes (e.g. Glutamate, ATP, aspartate)	T cells, monocytes, macrophages, dendritic cells, chorion villus cells, endometrial and endothelial cells.	(Abascal and Zardoya 2012; Schober, Wilson, and Mongin 2017)
LRRC8D	Small inorganic anions and large osmolytes (e.g. taurine, lysine, serine, inositol, GABA, cisplatin, carboplatin)	Almost ubiquitous.	(Abascal and Zardoya 2012; Schober, Wilson, and Mongin 2017; Planells-Cases et al. 2015; Lutter et al. 2017)
LRRC8E	Small inorganic anions and large anionic osmolytes (e.g. Glutamate, ATP, aspartate)	Gingival epithelium, airway bronchial epithelial cells and the parotid gland.	(Abascal and Zardoya 2012; Schober, Wilson, and Mongin 2017)

Table 2– Substrate and tissue specificity of auxiliary VRAC subunits. LRRC8A is thought to be ubiquitously expressed. Tissue expression data was compiled from publicly available transcriptome databases by Abascal and Zardoya (2012).

transport (Lahey et al. 2020). In addition to osmotic gradients, VRACs are also activated by sphingosine-1-phospahte (S1P) via the G protein coupled receptor S1PR1. S1P, like hypotonicity, was shown to enhance 2'3'-cGAMP transport through LRRC8A:C, increasing STING activation (Lahey et al. 2020).

An independent study in mice showed murine VRACs also transport 2'3'-cGAMP. However, murine LRRC8A:E, rather than human LRRC8A:C channels transport 2'3'-cGAMP (Zhou, Chen, et al. 2020). Additionally, the endothelial tissue restriction in humans was not observed in mice, with MEFs, MLFs and BMDMs all utilising LRRC8A:E for 2'3'-cGAMP transport. *Lrrc8a* knockout in mice is embryonically lethal, but *lrrc8e* -/- mice were more susceptible to HSV-1 infection, showing in mice extracellular 2'3'-cGAMP transport through VRACs aids the antiviral immune response (Zhou, Chen, et al. 2020).

Despite efforts predominately focussing on import, VRACs have also been shown to act as 2'3'-cGAMP exporters. HEK293 cells overexpressing cGAS release 2'3'-cGAMP upon treatment with hypotonic buffers in an LRRC8A dependent manner (Lahey et al. 2020). The disproportionate focus on import means LRRC8A:C mediated 2'3'-cGAMP export is relatively understudied. Future work will be needed to test if LRRC8A:C can export 2'3'-cGAMP when cGAS is expressed endogenously and the physiological relevance of this.

It has been suggested that LRRC8A:C only functions under "artificial hypotonic conditions" and may not be physiologically relevant (Maltbaek, Snyder, and Stetson 2021). I believe, as osmotic pressure is relative, the import or export of osmolytes could trigger VRAC activity under physiological conditions. Additionally, the secondary channel agonist S1P exists endogenously and therefore provides a mechanism for LRRC8A:C activation in physiological settings. More recently, LRRC8A:C has been shown to import 2'3'-cGAMP into T cells where STING activation inhibits cell cycle progression and drives apoptosis. In accord, *Lrrc8c* -/- mice have hyperactive T cell responses in models of autoimmune encephalitis, demonstrating it is likely this channel functions more widely than was initially predicted (Concepcion et al. 2022). Since LRRC8A:C activity can be affected by osmotic disruption, studies looking to identify or characterise 2'3'-cGAMP channels should carefully consider if transport could occur indirectly

through LRRC8A:C, since over expression or knockout of ion channels could lead to disrupted osmotic homeostasis – a potential trigger for VRAC mediated 2'3'-cGAMP transport.

I.7.8 ABCC1

The ABC transporter family encompasses 49 members classified into 7 subfamilies (ABCA-G) (Vasiliou, Vasiliou, and Nebert 2009). Each ABC transporter contains two cytosolic nucleotide bindings domains (NBD1 and NBD2), which hydrolyse ATP to actively transport a broad range of substrates across the membrane. ABCC1 contains 17 transmembrane domains split into 3 domains: TMD0, TMD1 and TMD2 (Johnson and Chen 2017; Cole 2014). MSD1 and MSD2 form the pore through which substrates are moved, while the function of MSD0 remains uncertain (Figure 15) (Cole 2014). ABCC1 is also known as multidrug resistance protein 1 (MRP1). This alias is due to the transporter's direct relevance to pharmaceutical bioavailability as among its substrates are chemotherapeutic agents (e.g. doxorubicin, vinblastine and vincristine) to which ABCC1 provides resistance (Yin et al. 2009). ABCC1 also functions to export a wide variety of endogenous substrates: Leukotriene C4, lipid species including S1P, glucuronides, glutathione conjugates and free glutathione which are reviewed in detail by Cole (2014). Despite ABCC1 being the subject of intense research regarding drug resistance, its physiological role is ill defined. Some have suggested ABCC1 exports xenobiotics and toxic by-products of metabolism (Bakos and Homolya 2007). This is in line with ABCC1's polarised expression profile at barrier sites within the body such as, choroid cells, which maintain separation between the blood and cerebrospinal fluid, capillary endothelial cells forming the blood brain barrier and syncytiotrophoblasts within the placenta, which separate mother from foetus (Rao et al. 1999; St-Pierre et al. 2004; Nies et al. 2004). Therefore, ABCC1's potential action to expel toxic molecules could explain how it became an obstacle for clinicians trialling chemotherapeutic agents.

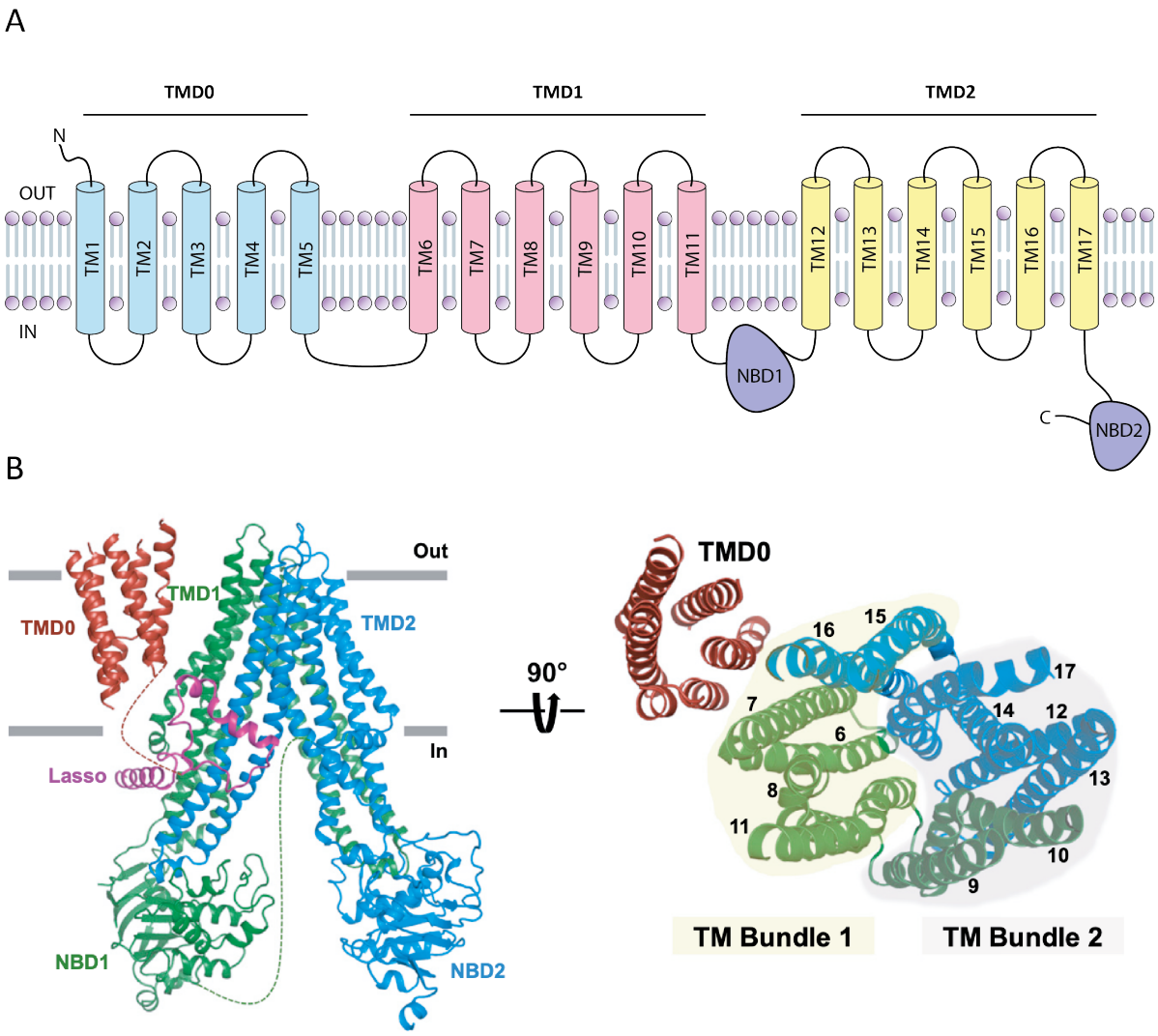


Figure 15 – Structure of ABCC1. A) Diagram depicting topology of ABCC1 with its transmembrane domains (TM) and nucleotide binding domains (NBD) shown. B) Cartoon showing structure of bovine ABCC1 based upon a Cryo-EM density map. Lifted from Johnson and Chen (2017).

ABCC1 was first implicated in 2'3'-cGAMP export by Maltbaek et al. who observed 2'3'-cGAMP export from cells after transfection with dsDNA then screened different classes of exporter to identify this transporter. ABCC1 is the only CDN transporter studied in the context of autoimmunity. TREX1 is a 3' → 5' exonuclease, which degrades any DNA that inadvertently reaches the cytosol under sterile conditions. Mutation of the *TREX1* gene leads to the chronic interferonopathy Aicardi-Goutières syndrome due to activation of cGAS (Stetson et al. 2008; Gao et al. 2015; Gray et al. 2015). In accord, *Trex1* -/- mice have a life span of on average ~110 days due to the associated severe autoimmune phenotype (Maltbaek, Snyder, and Stetson 2021; Gao et al. 2015). Maltbaek et al. show the type I IFN signature and immunopathology seen in *Trex1* -/- mice is exasperated when *ABCC1* is simultaneously knockedout. In *vitro,*

ABCC1 was shown to export 2’3’-cGAMP in an ATP dependent manner. ABCC1 mediated 2’3’-cGAMP export negatively regulates IFN induction by preventing 2’3’-cGAMP binding to STING (Maltbaek, Snyder, and Stetson 2021). Therefore, ABCC1 is the only 2’3’-cGAMP transporter shown to reduce IFN induction, since all the 2’3’-cGAMP importers are considered to function in a proinflammatory manner. Export of 2’3’-cGAMP leading to reduced STING activation aligns with the only known mechanism of 2’3’-cGAMP degradation - ENPP1 – being extracellular. Whether ABCC1 can also function to enhance 2’3’-cGAMP driven responses in settings of microbial invasion or cancer remains to be seen. Additionally, if 2’3’-cGAMP export through LRRC8A:C also acts to alleviate STING driven inflammation has not been investigated. A known substrate of ABCC1, S1P, is a known agonist of LRRC8A:C. Therefore, whether ABCC1 acts cooperatively with LRRC8A:C is an interesting possibility (Lahey et al. 2020; Takabe et al. 2010). Another ABC family member - ABCG2 - has been proposed as a 2’3’-cGAMP exporter and chemical inhibition was previously shown to prevent 2’3’-cGAMP export (Maltbaek, Snyder, and Stetson 2021). As ABCC1 and ABCG2 are the only ABC transporters known to export S1P, this further suggests a link between ABC and LRRC8A:C mediated 2’3’-cGAMP transport (Takabe et al. 2010). However, ABCC1 has been shown to export 2’3’-cGAMP from “inside out” vesicles derived from insect cell lines devoid of LRRC8A:C, indicating that ABCC1 is likely a 2’3’-cGAMP channel in its own right and not indirectly acting by opening LRRC8A:C via S1P (Maltbaek, Snyder, and Stetson 2021).

I.7.9 LL-37

Antimicrobial defence peptides (AMP) are small cationic amphipathic molecules found across all kingdoms of life. They are split broadly into two classes: cathelicidins and defensins (Zhang et al. 2021). The AMPs found in multicellular organisms resemble the offensive peptides released by prokaryotes to kill competing microorganisms and are likely one of the earliest forms of immune defence. LL-37 is the only human encoded member of the cathelicidin family and is only 4.4 kDa in size (Xhindoli et al. 2016). It exists as a proprotein, hCAP-18, and is expressed by front line immune cells such as neutrophils, macrophages, dendritic cells, NK cells, mast cells and epithelial cells (Vandamme et al. 2012). LL-37 is released into the site of inflammation by exocytosis and is cleaved by serine proteases into its active form (Yamasaki

et al. 2006; Sørensen et al. 2001). Within bacterial cell membranes, LL-37 forms a tetrameric pore leading to bacterial cell lysis (Turner et al. 1998; Lee et al. 2011; Sancho-Vaello et al. 2020). Host cell membranes are protected from pore formation due to elevated cholesterol levels, but high concentrations of LL-37 can still lead to membrane permeabilisation (Ding et al. 2013). This peptide acts widely against bacteria with >40 species restricted by its action (Vandamme et al. 2012). Meaning, LL-37 is short in size but not functionality as alongside direct antibacterial activity LL-37 also acts as: a chemoattractant for macrophages, dendritic cells and neutrophils; a catalyst of NLRP3 inflammasome activation; a trigger for degranulation of mast cells; and is a cytokine signalling through EGFR, FPRL-1 and even P2X7 (Yang et al. 2020; Yoon et al. 2021). Additionally, LL-37 can form a complex with extracellular dsDNA able to activate endosomal TLR9 in pDCs and drive STING activation through cytoplasmic DNA sensors in monocytes (Chamilos et al. 2012; Lande et al. 2007). The LL-37-dsDNA complex reaches endosomes through lipid raft and proteoglycan dependent endocytosis, but how it crosses the endosomal membrane to reach cytosolic DNA sensors is unknown (Sandgren et al. 2004). However, it has been suggested that the cationic amphipathic complex might be able to passively diffuse through the phospholipid bilayer (Chamilos et al. 2012; Vandamme et al. 2012).

A recent study has shown that LL-37 also transports 2’3’-cGAMP across the cell membrane, since in *vitro* treatment of cells with extracellular 2’3’-cGAMP and LL-37 enhances STING activation (Wei et al. 2022). In *vivo,* prophylactic treatment of mice with LL-37 and extracellular 2’3’-cGAMP has been shown to restrict HSV-1 replication and increase IFN driven responses (Wei et al. 2022). However, the mechanism by which exogenous LL-37 delivers 2’3’-cGAMP to the cytosol is unclear. 2’3’-cGAMP, like dsDNA, forms a complex with LL-37 potentially able to cross cell membranes (Wei et al. 2022). Equally, tetrameric pore formation could allow 2’3’-cGAMP to access the cytosol through nonspecific membrane disruption. Cells treated with LL-37 do not show increased permeability to propidium iodide (PI), suggesting in this context cellular membranes are not disrupted (Wei et al. 2022). As PI is a positively charged molecule, it may be unable to move through the positively charged LL-37 pore (Sancho-Vaello et al. 2020; Kirchhoff and Cypionka 2017). Therefore, whether 2’3’-cGAMP passes through LL-37 pores or moves through the membrane as a 2’3’-cGAMP-LL-37 complex

remains uncertain. Future work assessing if endogenously expressed LL-37 enhances 2'3'-cGAMP mediated responses will be crucial to prove a physiological role for LL-37 during cGAS-STING signalling. Interestingly, dsDNA-LL-37 complexes are resistant to nuclease degradation (Sandgren et al. 2004). Therefore, it remains to be determined if LL-37 protects 2'3'-cGAMP from ENPP1 mediated hydrolysis.

The field of 2'3'-cGAMP transport is in a period of exponential growth. cGAMP channels are novel components of the innate immune system. Although viral replication has been shown to be restricted by extracellular 2'3'-cGAMP it is unknown if viruses can antagonise 2'3'-cGAMP transport. Specifically in Chapters V and VI we will discuss if HSV-1 antagonises cGAMP transport during infection. To provide context the biology of this virus is described in the next section.

I.8 HSV-1

Herpesviruses are etched throughout human history - being named by Hippocrates ~400 B.C, appearing on the front cover of TIME magazine in 1982 and more recently in UK album charts (Lily Allen – track "knock em out") (Figure 16A and B) ("TIME" 1982; Mammas and Spandidos 2016; Allen 2006). *Herpesvirales* is a spectacular evolutionary success being arguably the most widespread virus order with distant relatives of primate herpesviruses found in oysters (Waltzek et al. 2009). Therefore, it is unsurprising the deleterious consequences of herpes infection are not limited to human health. 60% of endangered Asian elephants born in captivity die due to Elephant Endotheliotropic Herpesvirus (EEHV) (Jesus, Doherr, and Hildebrandt 2021). In 2008, Ostreid herpesvirus 1 (OsHV-1) caused mass mortality within French oyster beds (80-100%) leading the government to provide €135 million in expense relief (Fuhrmann et al. 2019). Recently, a vaccine against Cyprinid herpesvirus 3 (CyHV-3) has been developed and is being used to protect prized Koi carp, which hold enormous financial value, some over one million dollars (Figure 16C) (Klafack et al. 2022; Marugen 2018). Despite their discernible negative impact, herpesviruses usually cause a mild pathology within their host allowing for long term co-existence. The eight known human herpesviruses are split into the α, β and γ sub-classes. HSV-1 is an α herpesvirus associated with infection "above the belt", causing cold sores, while its closest relative HSV-2 acts "below the belt" to cause genital

herpes (Whitley and Baines 2018). Despite this waistline boundary, HSV-1 increasingly causes genital herpes, particularly in young populations due to changes in attitude towards sexual promiscuity (Roberts, Pfister, and Spear 2003). Interestingly, HSV-2 is one of two known cases of a herpesvirus, which are usually highly specific to their host, crossing species boundaries to infect humans. Phylogenetic evidence suggests that HSV-2 is derived from a herpesvirus infecting a chimpanzee and spread to humans 1.6 million years ago (Wertheim et al. 2014).



Figure 16 – (Natural) history of HSV-1. A) Depiction of Hippocrates (Unknown 13th Century). B) TIME magazine August 2nd, 1982 ("TIME" 1982). C) Kōhaku, the most expensive koi carp in the world, sold for $1.8 million (Marugen 2018). D) HSV-1 initially infects the oral mucosa, infecting sensory neurons and travelling by anterograde transport to the trigeminal ganglion, the site of viral latency. Further spread into the central nervous system can lead to encephalitis. Reactivation allows trafficking by retrograde transport back to the oral mucosa and lytic infection.

The second zoonotic herpes virus is Cercopithecine herpesvirus 1 (Herpes B virus) which causes asymptomatic disease in its natural host, the Asian macaques, but fatal disease in humans exposed to saliva from infected animals (Tischer and Osterrieder 2010). The final α herpesvirus is varicella-zoster virus (VZV) and the cause of both chicken pox and shingles (Zerboni et al. 2014). It is estimated globally 3752 million people are infected with HSV-1 and 491 million with HSV-2 (James et al. 2020). Aside from cold sores, HSV-1 can cause severe disease such as: herpes encephalitis (19.3% lethality), herpes keratitis, an infection of the cornea that can lead to blindness, and systemic infections in neonates that have a 31% lethality (Hansen et al. 2020; Kimberlin et al. 2001; Rowe et al. 2013). Despite severe cases being rare, the virus's high prevalence (67% globally) means the disease burden caused by HSV-1 is great (James et al. 2020). Therefore, an improved understanding of the viral lifecycle could aid treatment of HSV-1 driven disease.

I.8.1 HSV-1 Infection cycle

HSV-1 initially infects epithelial cells neighbouring the oral mucosa and then peripheral sensory neurons, traveling to the central nervous system by retrograde transport (Petti and Lodi 2019). Within neuronal cells there are two outcomes to infection: either lytic or latent. Latency is a characteristic feature of herpesvirus infection and in the case of HSV-1 is established in the trigeminal ganglia through epigenetic silencing of the HSV-1 genome by H3K9 and H3K27 methylation (Silva et al. 2008; Liang et al. 2009). During latency, the only highly expressed viral gene is the latency associated transcript (LAT), an RNA which broadly suppresses active replication (Nicoll et al. 2016; Suzich and Cliffe 2018). Establishment of a latent reservoir of virus leads to a lifelong infection where reactivation is triggered by a variety of stimuli (e.g. fever, menstruation, surgical resection, sunlight and psychological distress) that broadly induce host stress and leads to anterograde transport back to the epithelium and blister formation (Figure 16D) (Petti and Lodi 2019). Both primary infection and reactivation of latent virus can also lead to infection of the central nervous system (CNS), potentially causing herpes simplex encephalitis.

HSV-1 virions initially associate with the cell surface through interactions between glycoprotein B and C (gB and gC) with heparan-sulphate proteoglycans (HSPGs) (Satoh et al. 2008; Herold et al. 1991). Glycoprotein D (gD) then engages an entry receptor, either nectin-1 or nectin-2 or HVEM, to activeate gB through a gH-gL complex to fuse the virus envelope to the cell membrane (Whitbeck et al. 1997; Warner et al. 1998; Geraghty et al. 1998; Atanasiu et al. 2010). The viral capsid is then released into the cytosol where it can be trafficked along microtubules by the molecular motors dynein and kinesin-1 to the nuclear pore complex (Döhner et al. 2002; Radtke et al. 2010). Here, viral DNA is released through the virus's portal

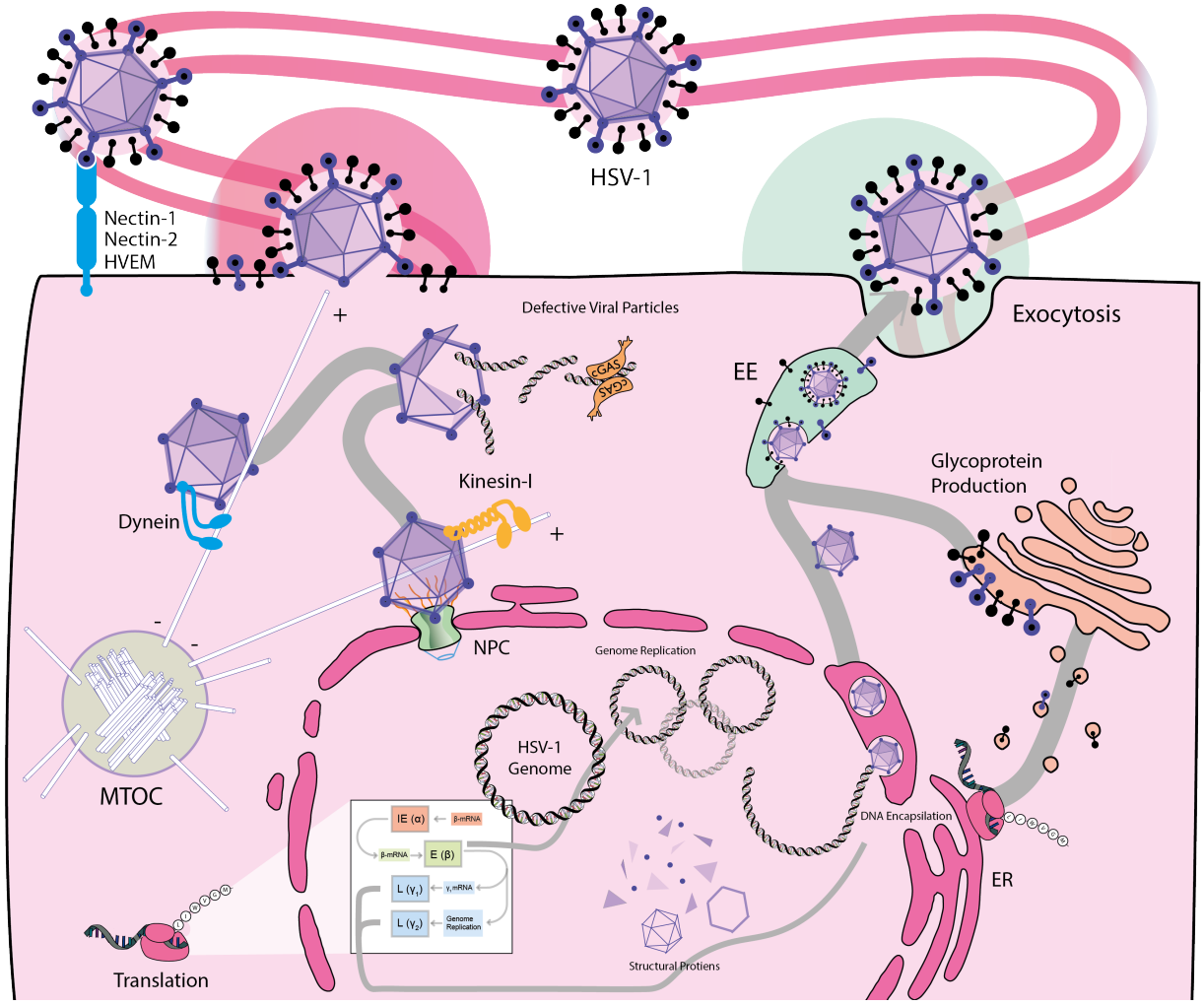


Figure 17 – HSV-1 replication cycle. HSV-1 associates with the cell surface through interaction with heparan-sulphate proteoglycans then binds to an entry receptor to trigger membrane fusion. Molecular motor proteins traffic virions through the microtubule-organising centre (MTOC) to the nuclear pore complex (NPC). HSV-1 genes are expressed temporally leading to the production of the structural proteins needed for capsid assembly which are loaded with viral genomes and then traffic to early endosomes (EE). Exocytosis allows for progeny viral particles to be released.

complex into the nucleus where the genome circularises (Sodeik, Ebersold, and Helenius 1997). Gene expression is then regulated temporally with genes allocated to kinetic classes of immediate early (α), early (β), leaky late (γ_1) and true late (γ_2) (Gruffat, Marchione, and Manet 2016). Infection starts with expression of immediate early genes, encoding proteins that transcriptionally control early gene expression. Early genes encode the machinery for viral genome replication and trigger the expression of late genes. Late genes are divided into two classes. Leaky late expressed directly after early genes and true late expressed only upon genome amplification and are broadly involved in construction of new virions (Gruffat, Marchione, and Manet 2016). After DNA replication has occurred, viral capsids are assembled within the nucleus and DNA genomes packaged. The prevailing hypothesis is that virions travel through the first nuclear membrane gaining an envelope which is then lost on fusion to the outer nuclear envelope (Ibáñez et al. 2018). The virus reaches early endosomes where it acquires tegument proteins and is enveloped. Trafficking to the plasma membrane allows for progeny virus to be released by exocytosis (Figure 17) (Ibáñez et al. 2018).

I.8.2 Detection of HSV-1 infection by PRRs

Innate immune sensing of HSV-1's nucleic acids during infection is well described. Within endosomes, TLR9 detects dsDNA and TLR3 detects dsRNA (Krug et al. 2004; Zhang et al. 2007). ZBP1, RIG-I and MDA5 have also been implicated in detection of erroneous RNA species generated during HSV-1 infection (Jeffries, Suptela, and Marriott 2022; Guo et al. 2018; Danastas, Miranda-Saksena, and Cunningham 2020). However, for all of the RNA sensors implicated during HSV-1 infection, the identity of the RNA detected is unknown (Danastas, Miranda-Saksena, and Cunningham 2020). cGAS is considered the preeminent sensor of HSV-1's dsDNA within the cytosol assumed to be released from defective virions that do not reach the nuclear pore (O'Connor and Sen 2021; Horan et al. 2013). Collectively, these sensors drive the production of type I IFNs restricting viral replication (discussed in section 1.6). Aside from canonical intracellular 2'3'-cGAMP signalling, extracellular 2'3'-cGAMP has also been shown to restrict HSV-1's replication. Mice expressing mutant ENPP1 (H362A) unable to degrade 2'3'-cGAMP have elevated extracellular 2'3'-cGAMP levels and are resistant to HSV-1 infection in a STING dependent manner (Carozza et al. 2022). Similarly, in mice LRRC8A:E (equivalent to human LRRC8A:C in terms of 2'3'-cGAMP transport) dependent 2'3'-cGAMP

uptake has been shown to confer resistance to HSV-1 infection in a manner dependent on STING (Zhou, Chen, et al. 2020).

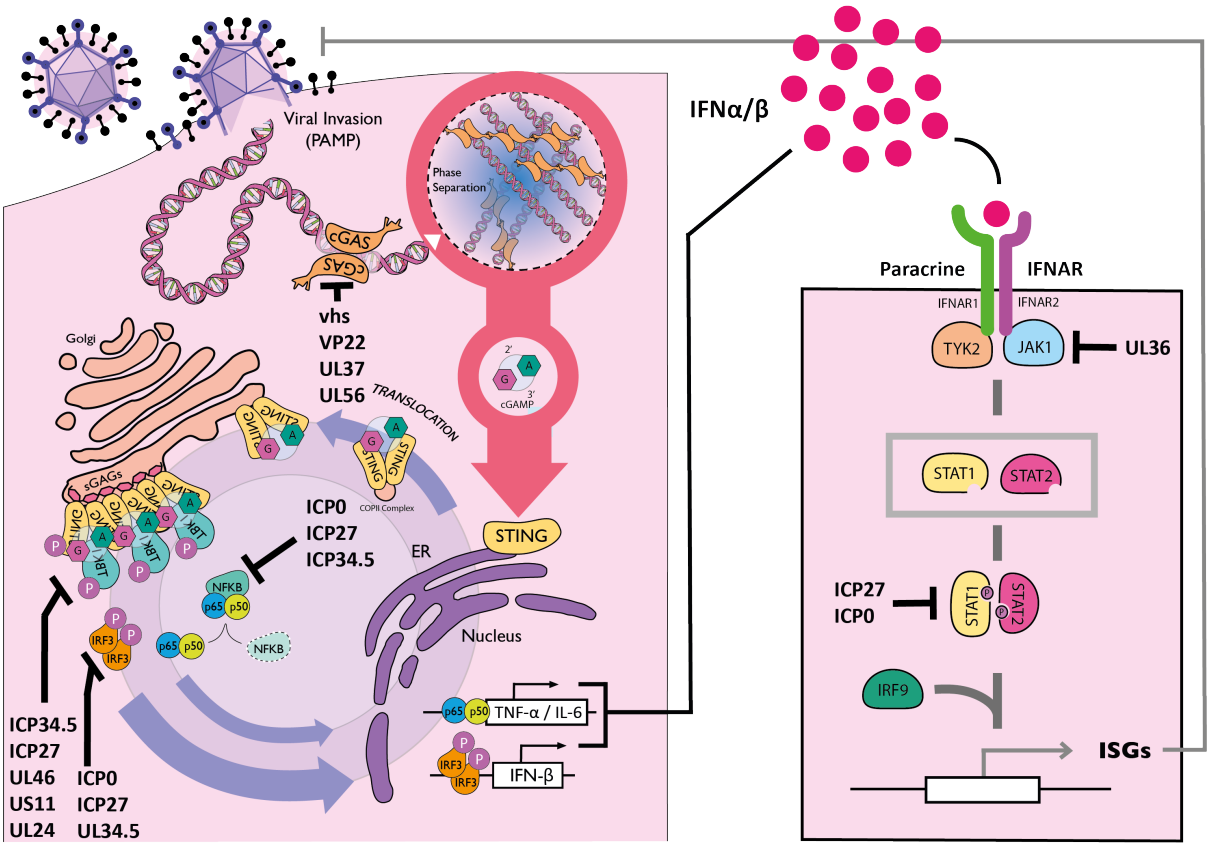


Figure 18 – Antagonism of cGAS-STING signalling by HSV-1. cGAS-STING pathway and the known antagonists encoded by HSV-1. Adapted from Danastas, Miranda-Saksena, and Cunningham (2020).

I.8.3 HSV-1 antagonises PRRs

Organisms are locked into an eternal battle where they must adapt, evolve and proliferate to keep up with their natural competition and persist (Van 1973). This is termed the red queen hypothesis named after a quote from Lewis Caroll's sequel to Alice in Wonderland - "Now, *here*, you see, it takes all the running you can do, to keep in the same place" (Carroll 1871). Nowhere is the evolutionary arms race more apparent than in virology with the viruses, total dependence on host's replication machinery, locking both into a molecular arms race. Therefore, almost all mechanisms developed by the host to restrict viral replication are antagonised by viruses to allow for unfettered replication. This is true for PRRs and can be illustrated by HSV-1 which encodes a myriad of Machiavellian molecules that antagonise nucleic acid sensors (Figure 18). Notably vhs, VP22, UL37 and UL56 inhibit 2'3'-cGAMP

production by cGAS upon binding of dsDNA (Danastas, Miranda-Saksena, and Cunningham 2020). Additionally, ICP0, ICP27 and ICP34.5 inhibit STING activation. Downstream of cGAS, many molecules target TBK1, IRF3/7 and components of the IFNAR pathway (Danastas, Miranda-Saksena, and Cunningham 2020; Zheng et al. 2022). The redundancy of HSV-1 encoded antagonists targeting the cGAS-STING pathway is stereotypical of large dsDNA viruses considered the tanks of the immunological world encoding hundreds of immunomodulators to shut down host defences. Despite HSV-1 being known to target all other components of the cGAS-STING pathway, no viral antagonist of 2'3'-cGAMP transfer pathways have been identified. This will be the focus of this thesis and is documented in chapters IV, V and VI.

I.9 Objective of the Study

Due to the immense therapeutic promise of the cGAS-STING signalling axis further characterisation of this pathway could aid therapeutic development of agonists for cancer immunotherapy, and antagonists for the treatment of autoimmune disease. My work broadly builds upon what is known about the cGAS-STING pathway and has two aims.

Aim 1 –Regulators of STING (Chapter III)

Initially, I supported the work of Alice Mayer, a post Doc in the lab. She performed a genome wide CRISPR screen to identify genes that augment STING's function. I developed a siRNA-based system in THP-1 cells to validate hits from the CRISPR screen. The intention was to characterise the molecular detail of how novel STING regulators support signalling. However, none of the hits could be validated convincingly.

Aim 2 – Viral antagonism of 2'3'-cGAMP channels (Chapters IV, V and VI)

The paradigm shifting discovery of channels that both import and export 2'3'-cGAMP represents an area within the cGAS-STING field that is relatively unexplored. I postulated, as virus and host are locked into a molecular arms race, if 2'3'-cGAMP channels function within the innate immune response then a viral antagonist must exist. A common strategy used by viruses to antagonise components of the hosts immune response is degradation. Therefore, I initially screened different viral families to determine if any degraded 2'3'-cGAMP channels during infection. I then unpicked the mechanism and biological consequences of viral antagonism.

Chapter II

Materials and Methods

II.1 Materials

II.1.1 Cells

Cells were maintained in a humidified incubator at 37°C at atmospheric oxygen levels and 5% CO_2. Adherent cells were regularly passaged using Trypsin-EDTA (Thermo Fischer Scientific – 25200056). Media was supplemented with 10% (v/v) foetal calf serum (Sigma-Aldrich) and 2mM L-glutamine (Gibco - 25030081).

HEK293 HEK cells are derived from female human embryonic kidney (HEK) tissue transformed with sheared adenovirus (Ad)5 DNA and are believed to be a neuronal cell type (Schmidt et al. 2009). Cells were maintained in Dulbecco's modified Eagel medium (Thermo Fischer Scientific – 41965-039) and were a kind gift from Caetano Reis e Sousa (The Francis Crick Institute, UK).

HEK293T HEK293T cells are HEK293 cells which stably express the large SV40 T antigen which allows for replication of plasmids containing the SV40 promoter (Reus et al. 2020). Cell lines that overexpress cGAMP channels or UL56 constructs were generated by stable transduction with lentiviral constructs (detailed in section II.2.6). Cells were maintained in the same manner as HEK293s and were kindly gifted by Caetano Reis e Sousa (The Francis Crick Institute, UK).

p125 HEK293 HEK293 cells stably transduced with a p125-Greenfire construct express both GFP and Luciferase from an IFN-β promoter are described in detail by Hertzog et al. (2018). LRRC8A and GOPC knockout cells

were produced as detailed in section II.2.11. Cells were maintained in the same manner as HEK293s.

3C11 3C11 cells are HEK293s which were stably transduced with the pGreenfire-ISRE construct and therefore express both GFP and Luciferase from an ISRE promoter. They are used as a type I IFN reporter cell line and are described in detail by Bridgeman et al. (2015). They were produced by Jonathan Maelfait and were maintained in the same manner as HEK293s.

THP-1 THP-1 cells are a monocytic cell line derived from a 1 year old human male with acute myeloid leukaemia (Tsuchiya et al. 1980). These cells can be easily differentiated into a macrophage like cell type on exposure to phorbol 12-myristate 13-acetate (PMA) (Tsuchiya et al. 1980). They grow in suspension and were maintained in Rosewell Park Memorial Institute medium (Thermo Fischer Scientific – 41965-039) and were a kind gift from Vincenzo Cerundolo (The University of Oxford, UK).

p125 THP-1 THP-1 cells were stably transduced with the p125-Greenfire construct and therefore express both GFP and Luciferase from an IFN-β promoter described in detail by Hertzog et al. (2018). They are resistant to blasticidin. Cells were maintained in the same manner as THP-1s.

THP-1 Lucia THP-1 Lucia Dual reporter cells (InvivoGen - thpd-nfis) secrete luciferase into the medium under the control of an ISG54 minimal promoter in conjunction with five IFN-stimulated response elements. Additionally, they secrete the embryonic alkaline phosphatase (SEAP) reporter gene under the control of a NF-κB consensus transcriptional response element conjoined to three copies of the c-Rel binding site.

This allows measurement of both IRF and NF-κB activity. These cells are resistant to blasticidin and zeomycin. Cell lines overexpressing genes identified in the CRISPR screen (Chapter III) were generated by stable transduction with lentiviral constructs (detailed in II.2.6). These cells were a kind gift from Søren Paludan (Aarhus University, Denmark) and were maintained in the same manner as THP-1s.

Immortalised MEFs Immortalised mouse embryonic fibroblasts (MEFs) were derived from murine embryos and cultured in Dulbecco's modified Eagel medium. They were produced by Elizabeth Horton.

Vero E6 Vero E6 cells are derived from the kidney epithelial cells of *Cercopithecus aethiops* (African Green Monkey). They display contact inhibition and so are suitable for propagating slowly replicating viruses. The cells were a kind gift from Alain Kohl (University of Glasgow, UK).

Viruses

HSV-1 HSV-1 (KOS) and mutant viruses (ΔUL56, AXAA-123) were a kind gift from Colin Crump (The University of Cambridge, UK). Viruses were propagated in Vero E6 cells and then titrated by plaque assay onto Vero E6 cells as described in section II.2.2.

HSV-2 HSV-2 infected HEK239T cell lysates were a kind gift from Søren Paludan (Aarhus University, Denmark).

VACV VACV (WR) was a kind gift from Michael Way (CRUK, LRI).

AdV-GFP	Adenovirus type 5 engineered to express GFP and the Cre recombinase was prepared by Anne Bridgeman in HEK293 cells.
HIV-1	HIV-1 (pNL4-3) was procured from NIH AIDs reagents (cat number - 11100). VSV-G pseudotyped single round replicative virus was produced in HEK293T cells as described in section II.2.5.
HIV-2	HIV-2- GFP Δenv Δnef (ROD9) was a kind gift from Nicholas Manel (Institut Curie, France). VSV-G pseudotyped single round replicative virus was produced in HEK293T cells as described in section II.2.5.
ZIKV	ZIKV (ZIKV/H.sapiens/Brazil/PE243/2015) was a kind gift from Alain Kohl (University of Glasgow, UK). Viruses were prepared by Mirjam Schilling in Vero E6 cells and then titrated onto A549 cells.
IAV	IAV (PR8) was a kind gift from Paul Digard (The University of Edinburgh, UK). Viruses were prepared by Rachel Rigby. Viral titres were determined using NP staining as previously described Powell et al. (2012) and TCID50 doses converted to pfu/ml by multiplying by 0.7.

II.1.2 Plasmids

Name	Description	Origin
Vector backbones		
pCDNA3	Protein expression construct driven by human cytomegalovirus promoter.	Gifted by James Chen (University of Texas, USA).
pCDNA3.2	Protein expression construct driven by human cytomegalovirus promoter.	Acquired from Thermo Fischer Scientific (12489019).
plenti6.2 -V5 (BLAST)	Lentiviral expression construct with C terminal V5 tag. PGK promoter drives expression of the *Blasticidin S deaminase* gene which offers resistance to blasticidin.	Acquired from Thermo Fischer Scientific (V36820).
plenti6.2 -V5 (PURO)	Lentiviral expression construct with C terminal V5 tag. PGK promoter drives expression of the *PuroR* gene which offers resistance to puromycin.	Constructed by Jonny Hertzhog. The *Blasticidin S deaminase* gene in plenti6.2 -V5 (BLAST) was exchanged for the *PuroR* gene.
lentiCRISPRv2	Construct for expression of a guide RNA driven by U6 promoter. EFS-NS promoter drives expression of the *PuroR* gene which offers resistance to puromycin. The EFS-NS promoter also drives expression of spCas9.	Gifted by Andrew Basset (Wellcome Trust Sanger Institute, UK). Described by Sanjana, Shalem, and Zhang (2014).
pEXP103	Protein expression construct with a N terminal GFP tag.	Gifted by David Koelle (The University of Cambridge, USA).
Dual Luciferase Assay		
pRL-TK	Constitutively expresses Renilla luciferase under the control of the thymidine kinase (TK) promoter.	Acquired from Promega (E2241).
p125-Luc	Expresses firefly luciferase under the control of the human IFN-β promoter.	Kind gift from Takashi Fujita described by Yoneyama et al. (2004).
pcDNA3.2 STING	Constitutively expresses human STING.	Constructed by Lise Chauveau.

Protein expression vectors		
pEXP103 GFP-UL56	Constitutively expresses the HSV-1 gene UL56 with a N terminal GFP tag.	Gifted by David Koelle (The University of Cambridge, USA).
pEXP103 GFP-UL6	Constitutively expresses the HSV-1 gene UL6 with a N terminal GFP tag.	Gifted by David Koelle (The University of Cambridge, USA).
pcDNA3 murine cGAS	Constitutively expresses murine cGAS.	Gifted by James Chen (University of Texas, USA).
pcDNA3.2 human cGAS	Constitutively expresses human cGAS.	Constructed by Lise Chauveau.
Lentivirus Production		
p8.91	Lentiviral packaging plasmid encoding - gag, pol tat and Rev.	Gifted by Greg Towers (University College London, UK).
pCMV-VSV-G	Constitutively expresses the vesicular stomatitis viruses G protein (VSV-G) from a human cytomegalovirus promoter for use in lentiviral pseudotyping.	Gifted by Bob Weinberg (Massachusetts Institute of Technology, USA).
Lentiviral constructs		
pNL4-3-deltaE-EGFP	Encodes replication deficient HIV-2-GFP Δenv Δnef (strain RPOD9) for production of single round replicative pseudotyped virus.	Acquired from NIH AIDs reagents (cat number - 11100).
pHIV-2 ROD9 dEnvdNef GFP+	Encodes replication deficient HIV-2-GFP Δenv Δnef (strain ROD9) for production of single round replicative pseudotyped virus.	Gifted from Nicholas Manel (Institut Curie, France).
plenti6.2 GFP-V5 (PURO)	Constitutively expresses GFP with a N terminal V5 tag.	Constructed by Jonny Hertzhog.
plenti6.2 LRRC8A-V5 (PURO)	Constitutively expresses human LRRC8A with a C terminal V5 tag.	Constructed by Henry Blest.
plenti6.2 LRRC8C-V5 (PURO)	Constitutively expresses human LRRC8C with a C terminal V5 tag.	Constructed by Henry Blest.
plenti6.2 P2X7-V5 (PURO)	Constitutively expresses human P2X7 with a C terminal V5 tag.	Constructed by Henry Blest.

plenti6.2 SLC19A1-V5 (PURO)	Constitutively expresses human SLC19A1 with a C terminal V5 tag.	Constructed by Henry Blest.
plenti6.2 SLC46A2-V5 (PURO)	Constitutively expresses human SLC46A2 with a C terminal V5 tag.	Constructed by Henry Blest.
plenti6.2 UL56-V5 (PURO)	Constitutively expresses untagged UL56 due to presence of STOP codon.	Gifted by Colin Crump (The University of Cambridge, UK).
plenti6.2 UL56-AAXA1-V5 (PURO)	Constitutively expresses untagged UL56 due to presence of STOP codon. PPXY motif 1 (see Figure 47) is mutated to AAXA.	Gifted by Colin Crump (The University of Cambridge, UK).
plenti6.2 UL56-AAXA2-V5 (PURO)	Constitutively expresses untagged UL56 due to presence of STOP codon. PPXY motif 2 (see Figure 47) is mutated to AAXA.	Gifted by Colin Crump (The University of Cambridge, UK).
plenti6.2 UL56-AAXA3-V5 (PURO)	Constitutively expresses untagged UL56 due to presence of STOP codon. PPXY motif 3 (see Figure 47) is mutated to AAXA.	Gifted by Colin Crump (The University of Cambridge, UK).
plenti6.2 UL56-AAXA123-V5 (PURO)	Constitutively expresses untagged UL56 due to presence of STOP codon. PPXY motif 1,2 and 3 (see Figure 47) are mutated to AAXA.	Gifted by Colin Crump (The University of Cambridge, UK).
plenti6.2 TBK1-V5 (PURO)	Constitutively expresses human TBK1 with a C terminal V5 tag.	Constructed by Henry Blest.
plenti6.2 COPS4-V5 (PURO)	Constitutively expresses human COPS4 with a C terminal V5 tag.	Constructed by Henry Blest.
plenti6.2 COPS8-160-V5 (PURO)	Constitutively expresses the 160 amino acid isoform of human COPS8 with a C terminal V5 tag.	Constructed by Henry Blest.
plenti6.2 COPS8-209-V5 (PURO)	Constitutively expresses the 209 amino acid isoform of human COPS8 with a C terminal V5 tag.	Constructed by Henry Blest.
plenti6.2 KIDINS220-V5 (PURO)	Constitutively expresses human KIDINS220 with a C terminal V5 tag.	Constructed by Henry Blest.
plenti6.2 MAT2A-V5 (PURO)	Constitutively expresses human MAT2A with a C terminal V5 tag.	Constructed by Henry Blest.

plenti6.2 PCBP1-V5 (PURO)	Constitutively expresses human PCBP1 with a C terminal V5 tag.	Constructed by Henry Blest.
plenti6.2 PHB-V5 (PURO)	Constitutively expresses human PHB with a C terminal V5 tag.	Constructed by Henry Blest.
plenti6.2 PHB2-V5 (PURO)	Constitutively expresses human PHB2 with a C terminal V5 tag.	Constructed by Henry Blest.
plenti6.2 RBBP6-V5 (PURO)	Constitutively expresses human RBBP6 with a C terminal V5 tag.	Constructed by Henry Blest.
plenti6.2 UBL5-V5 (PURO)	Constitutively expresses human UBL5 with a C terminal V5 tag.	Constructed by Henry Blest.
plenti6.2 XPR1-V5 (PURO)	Constitutively expresses human XRP1 with a C terminal V5 tag.	Constructed by Henry Blest.
plenti6.2 GFP-V5 (BLAST)	Constitutively expresses human GFP with a C terminal V5 tag.	Constructed by Henry Blest.
plenti6.2 P2X7-V5 (BLAST)	Constitutively expresses human P2X7 with a C terminal V5 tag.	Constructed by Henry Blest.
plenti6.2 SLC46A2-V5 (BLAST)	Constitutively expresses human SLC46A2 with a C terminal V5 tag.	Constructed by Henry Blest.
lentiCRISPR-v2 NT Guide-1	Expresses a non-targeting guide RNA (5'-ACGGAGGCTAAGCGTCGCAA-3') bioinformatically predicted to not align with the human genome and spCas9.	Gifted by Andrew Basset (Wellcome Trust Sanger Institute, UK).
lentiCRISPR-v2 NT Guide-2	Expresses a non-targeting guide RNA (5'-A CGCTTCCGCGGCCCGTTCAA -3') bioinformatically predicted to not align with the human genome.	Gifted by Andrew Basset (Wellcome Trust Sanger Institute, UK).
lentiCRISPR-v2 LRRC8A Guide-1	Expresses a guide RNA (5'-A GGATCCTGAAGCCGTGGT -3') targeting the *LRRC8A* gene.	Constructed by Henry Blest.
lentiCRISPR-v2 LRRC8A Guide-2	Expresses a guide RNA (5'-A GGCACCAGTACAACTACG -3') targeting the *LRRC8A* gene.	Constructed by Henry Blest.

lentiCRISPR-v2 GOPC Guide-1	Expresses a guide RNA (5'-A GGAACATGGATACCCCGCCA -3') targeting the *GOPC* gene.	Constructed by Henry Blest.

II.1.3 Oligonucleotides for cloning

Name	Primer Forward (5' → 3')	Primer Reverse (5' → 3')
P2X7	ATGCCGGCCTGCTGCAGC	GTAAGGACTCTTGAAGCCACTGTACTG
LRRC8A	ATGATTCCGGTGACAGAGCTCC	GGCCTGCTCCTTGTCAGC
LRRC8C	ATGATTCCCGTGACAGAATTCCGG	TTCTGTTTTCATTTGCTCCCGGAC
SLC19A1	ATGGTGCCCTCCAGCCC	CTGGTTCACATTCTGAACACCGTCG
SLC46A2	ATGAGCCCCGAGGTCACC	TTTCTCTATGATGTCTCCATATGGTGAC
TBK1	ATGCAGAGCACTTCTAATCATCTGTGG	AAGACAGTCAACGTTGCGAAGG
COPS4	ATGGCGGCAGCCGTG	CTGAGCCATCTGGGCTTCCA
COPS8-209	ATGCCAGTGGCGGTGATG	GTTTTCAAGGAAAGCCACATAATCCGTC
COPS8-160	ATGAATAATGCAAGATATCTTTGGAAAAG	GTTTTCAAGGAAAGCCACATAATCCGTC
KIDINS220	ATGTCAGTTTTGATATCACAGAGCGTCA	AAGAATGCTTTCTCTTTCTTCTCCAAAG
MAT2A	ATGAACGGACAGCTCAACGG	ATATTTAAGCTTTTTGGGCACTTCCCAT
PCBP1	ATGGATGCCGGTGTGACTGAAAG	GCTGCACCCCATGCCCTT
PHB	ATGGCTGCCAAAGTGTTTGAGT	CTGGGGCAGCTGGAGGA
PHB2	ATGGCCCAGAACTTGAAGGACTT	TTTCTTACCCTTGATGAGGCTGTCAC
RBBP6	ATGTCCTGTGTGCATTATAAATTTTCCT	CACAGTGACAGATTTCACTTTTTGGTCA
UBL5	ATGATCGAGGTTGTTTGCAACGAC	TTGATAATAAAGCTCCAGGTTCATCCCA
XPR1	ATGAAGTTCGCCGAGCACC	AGTGTTAGCTTCATCATCTGTGTCTTCT
LRRC8A Guide-1	CACCGGATCCTGAAGCCGTGGT	AAACACCACGGCTTCAGGATCC
LRRC8A Guide-2	CACCGGCACCAGTACAACTACG	AAACCGTAGTTGTACTGGTGCC
GOPC Guide-1	CACCGGAACATGGATACCCCGCCA	AAACTGGCGGGGTATCCATGTTCC

II.1.4 Antibodies

Target	Conjugate	Source	Manufacturer	Clone	Catalogue no.	Application	Dilution
LRRC8A	-	Mouse	Santa Cruz Biotechnology	8H9	sc-517413	WB	1:1000
LRRC8C	-	Rabbit	2B Scientific	polyclonal	MBS711316	WB	1:1000
STING	-	Rabbit	Cell Signaling	(D2P2F)	13647S	WB	1:1000
MAVS	-	Rabbit	ENZO Life Sciences	Polyclonal	ALX-210-929	WB	1:1000
V5[1]	HRP	Mouse	Invitrogen	(E10/V4RR)	MA5-15253-HRP	WB	1:1000
V5[2]	-	Mouse	Biolegend	7/4	680602	WB, IP	1:1000
VP5	-	Mouse	Santa Cruz Biotechnology	3B6	sc-56989	WB	1:1000
E3L	-	Mouse	Vincenzo Cerundolo (The University of Oxford, UK)	TW2.3	Produced by collaborator	WB	1:1000
GFP	-	Mouse	Sigma Aldrich	Monoclonal antibody mixture 7.1 and 13.1	11814460001	WB	1:1000
NS5	-	Rabbit	Andres Merit (University of Tartu, Estonia)	polyclonal	Produced by collaborator	WB	1:1000
PB2	-	Rabbit	GeneTex	polyclonal	GTX125925	WB	1:1000
ABCC1	-	Rabbit	Abcam	EPR22841-78	ab260038	WB	1:1000
V5	AF647	Mouse	Invitrogen	monoclonal	451098	Flow Cytometry	1:200
GOPC	-	Rabbit	Abcam	[EPR4080(2)]	Ab133472	WB	1:1000
ORF62	-	Mouse	Meridian Life Science	Monoclonal clonal antibody mixture SG1, SG1-1, SG2-2E6, SG3, SG4, NCP-1, IE-62.	C05107MA	WB	1:1000
UL56	-	Rabbit	Colin Crump (The university of Cambridge, UK)	polyclonal	Produced by collaborator	WB	1:1000
β -actin	HRP	Mouse	Sigma Aldrich	AC-15	A3854	WB	1:1000
*α*Mouse IgG	HRP	Sheep	GE Healthcare	Monoclonal	NA931V	WB	1:1000
*α*Rabbit IgG	HRP	Goat	Cell Signalling	Polyclonal	7074	WB	1:1000

[1] Used in chapters III and IV.
[2] Switched to this antibody in chapters V and VI as it had a lower background and did not non-specifically bind HSV-1 proteins see Chapter IV section 3.

II.1.5 TaqMan Probes

All TaqMan probes were acquired from InvitroGen

Gene	Protein	Assay ID
GAPDH	GAPDH	Hs02758991_g1
LRRC8A	LRRC8A	Hs01555916_m1
LRRC8C	LRRC8C	Hs00943621_m1
TBK1	TBK1	Hs00179410_m1

II.2 Methods

II.2.1 CRISPR screen (*in brevi*)

Lentiviral constructs encoding the GeCKO v2 library of sgRNAs were used to transduce p125 THP-1 cells. A comprehensive overview of the library is given by Sanjana, Shalem, and Zhang (2014). Puromycin selected cells were differentiated with PMA (5 ng/ml) and then 2'3'-cGAMP (Stratech - B8362-APE) was applied within a digitonin permeabilisation buffer (Sucrose 85 mM, Hepes HCl 50mM, KCl 100 mM, $MgCl_2$ 3 mM, 0.2% BSA, 1mM ATP, 0.1 mM GTP, digitonin 10 µg/ml, pH 7.4) for 30 minutes. 6 hours later cells were FACs sorted into GFP+ and GFP- populations. DNA was extracted and sgRNAs amplified by PCR using a U6 forward and EFS reverse primer. After sequencing a custom python pipeline was used to count sgRNA abundance within the GFP- and GFP+ populations. Statistical analysis designed to identify guides enriched within the GFP- population was performed with the analysis programme MAGeCK. A graphical representation of this is given in Figure 20A.

II.2.2 HSV-1 production and titration

To propagate HSV-1 stocks, Vero E6 cells were infected at an MOI of 0.003 in Minimum Essential Medium (MEM) until cells start to round up and detach from the flask after ~3-4 days. The supernatant was then spun at 21krpm for 2 hours at 4°C in the OPTIMA XPN-80 ultracentrifuge in a SW 32 Ti Swinging-Bucket Rotor. The pellet was resuspended in PBS and virus titred by overlaying Vero cells with serially diluted virus for 1.5 hours then removing the

medium and adding carboxylmethyl cellulose (1.5% w/v) in DMEM (10% FCS, 2mM L-G). Cells were left for 3 days and then fixed with 3.7% v/v PFA in PBS before crystal violet staining 5% v/v in dH_2O. Upon desiccation, plaques were counted and stock concentration determined in pfu/ml.

II.2.3 Construction of lentiviral expression constructs

To clone genes needed in overexpression constructs primers were designed (section II.1.3) based on the consensus sequences from the Ensemble genome browser (Flicek 2022). Targets were PCR amplified from cDNA libraries derived from various cell lines with Herculase II Fusion DNA Polymerase (Agilent Technologies – 600677-51). PCR reactions were resolved on 1% agarose gels and amplicons of correct size extracted using the QIAGEN gel extraction kit (QIAGEN - 28704). GoTaq (Promega– M780B) was used to add 5' A overhangs and the resulting DNA product inserted into the pCR8/GW/TOPO (Thermo Fisher Scientific – K250020) entry vector by the manufactures protocol. Genes were then shuttled into plenti6.2 -V5 (BLAST) or plenti6.2 -V5 (PURO) using a Gateway L-R recombination kit (Invitrogen – 12538120). Constructed plasmids were propagated in and then extracted from bacterial cultures derived from single clones of transformed 5-alpha compotent *E.coli* (New England Biolabs – C2987H) using both miniprep (QIAGEN - 27106) and maxi prep kits (QIAGEN – 12663). DNA concentration was measured using a nanodrop (Thermo Fischer Scientific) and then the sequence was verified by Sanger sequencing (Source Bioscience).

II.2.4 Construction of lentiCRISPRv2 plasmids

The lentiCRISPRv2 plasmid was linearised by incubation with BsmBI-v2 (New England Biolabs – R07395) in r3.1 buffer (New England Biolabs – B60035) for 1 hour at 55^{o}C. The digested product was then dephosphorylated by addition of alkaline phosphatase (thermos Fisher Scientific – EF0654) and incubated for 1 hour at 37^{o}C. The resulting DNA species was resolved on 1% agarose gel and extracted using the QIAGEN gel extraction kit (QIAGEN - 28704). Complementary primers encoding sgRNA were purchased (Merck) with a 5'-CACC overhang on the sense and 5'-AAAC overhang on the antisense strands. After primers were annealed, they were phosphorylated with T4 PNK (New England Biolabs – M0201S). The overhangs

create sticky ends enabling ligation by T4 ligase (New England Biolabs - B0202A) in T4 buffer (New England Biolabs – B0202A) into the linearised lentiCRISPRv2. The resulting vectors were propagated and verified in the same manner as described in section II.2.3.

II.2.5 Lentivirus production

Lentiviral particles were produced by transfection of HEK293T cells with either the plenti6.2 or lentiCRIPSRv2 construct together with pseudotyping (pCMV-VSV-G) and packaging (p8.91) vectors using the lipofectamine 2000 transfection reagent (Thermo Fisher Scientific - 11668030). Vector-containing supernatants were collected at 48h and 72h post-transfection and filtered through a 0.45µm Polyethersulfone (PES) membrane (Millex - SLHPO33RS).

II.2.6 Transduction

THP-1s were transduced at a concentration of $3x10^5$ cells per/ml in RPMI (10% FCS 2mM L-G) mixed 1:2 with lentiviral supernatant (described in section II.2.5) supplemented with 8µg/ml hexadimethrine bromide (Sigma-Aldrich – H9268). 293 cells were transduced by addition of DMEM (10% FCS 2mM L-G) mixed 1:5 with lentiviral supernatant. 48 hours post transduction, cells were put under either or both puromycin (THP-1 - 1.5µg/ml, HEK293 – 1 µg/ml) or blastcidin (HEK293 - 15µg/ml) selection and were used for experimentation after a flask of cells without antibiotic resistance had died.

II.2.7 Western blotting

For immunoblotting 50µl of NP-40 lysis buffer (50 mM Tris.H, 150 mM NaCl, 2mM EDTA, 5% (v/v) glycerol, 1 %, 1% (v/v) NP40, pH 7.4)[3] supplemented with protease inhibitors (cell signalling - 5871S) was added per $1x10^6$ cells. Insoluble cellular debris was pelleted, and supernatants prepared in NuPage loading buffer (Invitrogen - NP0007) supplemented with 5% β-mecaptoethanol. Except for where SLC19A1, SLC46A2 and ABCC1 are quantified, samples were boiled for 5 minutes at 70°C. Lysates were then subjected to SDS-PAGE on 4-12% Bis-Tris precast gradient gels (Thermo Fisher Scientific – NP0321). Proteins were transferred onto a nitrocellulose membrane (BioRad - 1620112) using a semi-dry transfer apparatus (BioRad – Trans-Blot Turbo) and blocked in TBS-N + 5% (w/v) dried milk powder

[3] In chapter IV, V, and VI NP40 lysis buffer is supplemented with 7M urea. This acts to denature transmembrane proteins that cannot be boiled. The explanation for this is given in Chapter IV, section IV.2.

(Merck - 70166), before being probed with primary and secondary antibodies diluted in TBS-N (NP-40 0.05%) + 5% (w/v) dried milk powder. Protein abundance was then visualised using the chemiluminescent HRP substate ECl (Perkin and Elmer – NEL104001EA) on the iBright FL1000 (Invitrogen). Band intensity was then quantified using the densitometry analysis software available within the Thermo Fisher Connect Platform.

II.2.8 Immunoprecipitation and proteomic mass spectrometry

293 cells were transduced with lentiviral vectors derived from plenti6.2 LRRC8A-V5 (PURO) and plenti6.2 LRRC8C-V5 (PURO) as detailed in section II.2.6. Cells were infected with HSV-1 at an MOI of 10 for 8 hours before lysis with NP-40 lysis buffer (50 mM Tris.H, 150 mM NaCl, 2mM EDTA, 5% (v/v) glycerol, 1 %, 1% (v/v) NP40, pH 7.4) supplemented with protease inhibitors (cell signalling - 5871S). Insoluble cellular debris was pelleted. Simultaneously dyanbeads (Invitrogen – 14311D) were coupled to 2.5ug of V5 targeting antibody (Biolegend – 680602) and added to each reaction. Input unbound and IP samples were collected and subjected to immunoblotting as descried in sections II.2.7. Additionally, immunoprecipitated samples were subjected to SDS-PAGE as described in II.2.7. Additionally silver nitrate staining was performed using the Pierce Silver Stain kit (Thermo Fisher Scientific – 24600). IP samples from LRRC8C-V5 overexpressing HEK293 cells were then submitted to the Benedikt Kessler group at the Target Discovery Institute for proteomic liquid chromatography coupled mass spectrometry. Data was analysed using the PEAKS software and identified peptides aligned to Human UniProt Swissprot database (Alignment ID -20210911_seq23155) and HSV-1 genome (NCBI database - NC_001806). Progenesis Label free quantitation software was then used to assign relative values of protein abundance.

II.2.9 RT-qPCR

RNA was extracted using the RNeasy Plus Mini Kit (Qiagen - 74136) and annealed to random hexamers (QIAGEN – 79236) to prime production of cDNA by SuperScript II reverse transcriptase (Thermo Fisher Scientific - 18064014) following the manufacturer's instructions. cDNA was diluted 1:5 in water, and then 2 µl were used as the template for real-time PCR using Taqman universal PCR master mix (Applied Biosystems - 4304437) and a Quant Studio 7 flex real-time PCR machine (Applied Biosystems). GAPDH was selected as the

constitutively expressed gene to which targets were normalised and then subsequently made relative to their respective mock treated control by the delta-delta Ct method described by Livak and Schmittgen (2001). The TaqMan probes used to quantify gene expression are documented in section II.1.5.

II.2.10 Knockout cell line production

p125 HEK293 cells were transduced with lentiviral vectors derived from lentiCRISPR-v2 constructs targeting LRRC8A and GOPC as described in section II.2.6. Puromycin selected cells were seeded by limiting dilution and single cell colonies grown out. Clones were then screened by immunoblotting and knockout cell lines selected.

II.2.11 IFN Bioassay / One Glo Assay (3C11 cells)

3C11 cells which express firefly luciferase from an interferon stimulated response element were overlaid with serially diluted cell culture supernatant for 24 hours. Luciferase expression was quantified using the One-Glo Luciferase Assay System (Promega - E6110) and GloMax-Multi+ Microplate Multimode Reader. The luminescence values were then converted to IFN values in U/ml using a recombinant IFN A/D standard from within the linear quantifiable range (R&D Systems - 11200-2). This is explained with an example in Chapter III, section III.2, Figure 24.

II.2.12 Quanti-Luc assay

$7.5x10^5$ lucia THP-1 cells stably transduced with genes identified in the CRISPR screen were differentiated with PMA (50 ng/ml) in a 24-well plate 24 hours prior to stimulation. Cells were stimulated with 2'3'-cGAMP (Stratech - B8362-APE) in three ways.

1. 2'3'-cGAMP was applied within a digitonin permeabilisation buffer (Sucrose 85 mM, Hepes HCl 50mM, KCl 100 mM, $MgCl_2$ 3 mM, 0.2% BSA, 1mM ATP, 0.1 mM GTP, digitonin 10 µg/ml, pH 7.4) for 30 minutes before replacement with RPMI (FCS 10%, L-G 2mM) and then supernatants harvested after 6 hours.

2. The vaccinia virus dsDNA (70bp) motif (Invivogen – tlrl-vav70n) was transfected with lipofectamine 2000 (1.75ul per well) (ref: 11668030).
3. High doses of exogenous 2'3'-cGAMP were added directly to the cell culture medium.

Supernatant from 2'3'-cGAMP treated Lucia THP-1 cells had luminescence measured using the GloMax-Multi+ Microplate Multimode Reader (Promega) on addition of the luciferase reagent Quanti-Luc (invivogen - rep-qlc1).

II.2.13 Dual luciferase assay

HEK293T ($1x10^4$) were seeded into 96 well plates and 24 hours later each well was transfected with p125-FLuc (20 ng) pRL-TK (5 ng) and pcDNA3.2-STING (10 ng) using lipofectamine 2000 (0.4ul). 48 hours after seeding, the cells were treated with 2'3'-cGAMP (Stratech - B8362-APE). For LRRC8A:C activation 2'3'-cGAMP was applied in either a isotonic (150 mM NaCl, 6 mM KCl, 1 mM $MgCl_2$, 1.5 mM $CaCl_2$, 10 mM glucose, 10 mM HEPES, pH 7.4) or hypotonic buffer with reduced NaCl concentration for 1 hour. For P2X7 activation 2'3'-cGAMP was applied with bzATP (Biotechne - 3312). In indicated conditions inhibitors of 2'3'-cGAMP transporters were applied - DCPIB (Cayman - 34064), A73004 (Merck - 5083170001) and sulphasaline (Cayman - 15025). Luminesce was then read using the dual luciferase assay kit (Promega – E1960) with firefly (indicative of IFN-β production) being divided by Renilla (consititively expressed) to normalise for transfection efficiency. The assay is shown graphically in Figure 50.

II.2.14 Flow cytometry

THP-1 cells stable transduced with genes identified in the CRISPR screen were stained with a violet live dead stain (Thermo Fischer Scientific ref: L34955) and fixed in 4% (v/v) paraformaldehyde in PBS. Cells were permeabilised by a 20-minute incubation in FACs buffer (PBS supplemented with 1% FCS, 2mM EDTA) containing 0.5% triton X-100. Cells were then stained with AF647-V5 before populations of GFP^+ and $V5^+$ cells were acquired on the attune NxT cytometer and analysed using the software package FlowJo.

II.2.15 Fluorescence activated cell sorting (FACS)

293 cells were transfected with either pEXP103 GFP-UL6 or pEXP103 GFP-UL56 with lipofectamine 2000 then after 24 hours trypsinised and stained with violet live dead stain (Thermo Fischer Scientific ref: L34955) in PBS. Cells were then sorted by a trained operator on the BD FACS Aria Fusion Flow Cytometer into GFP^+ and GFP^- populations. A small proportion of the sorted cells were re-run through the FACS Aria to check the purity of the sorted populations. Directly after sorting, cells were lysed for western blotting as described in section II.2.7. Data was analysed using the software package FlowJo.

II.2.16 siRNA transfection

Undifferentiated THP-1 cells were transfected with custom smart pool siRNA libraries (DharmaFECT) which encoding 4 different siRNA constructs per gene targeted. Individual siRNA sequences are provided in supplementary table 2. $2.5x10^5$ undifferentiated THP-1 cells were seeded into a 24 well plate. Each well was transfected with 60.5pmol of siRNA in complex with 1µl of Viromere® Blue (Lipocalxy – VB-01LB-O1) suspended in 45ul of the viromere blue buffer. 24 hours post transfection cells were differentiated with 50ng/ml of PMA (Sigma Aldrich – P1585). 48 hours post transfection 2'3'-cGAMP was applied within a digitonin permeabilisation buffer (Sucrose 85 mM, Hepes HCl 50mM, KCl 100 mM, $MgCl_2$ 3 mM, 0.2% BSA, 1mM ATP, 0.1 mM GTP, digitonin 10 µg/ml, pH 7.4) for 30 minutes before replacement with medium and then supernatants harvested after 6 hours. IFN was quantified using IFN Bioassay detailed in section – II.2.12.

II.2.17 Crystal violet viability assay

Cells were fixed in PFA 4% v/v in PBS and then stained with crystal violet 5% v/v in dH_2O. Upon desiccation the retained stain was dissolved in pure methanol and absorbance read at 570nm on the CLARIOstar plate reader (BMG Lab Tech).

II.2.18 YOPRO-1 assay

$1x10^5$ HEK293 cells were seeded into a flat bottomed 96 well plate pre-treated with 10% (v/v) collagen (Sigma – C8919) in PBS for 20 minutes before use. Assay buffer (2 mM KCl, 0.1 mM $CaCl_2$, 13 mM Glucose, 147 mM NaCl, 10 mM HEPES, pH 7.3) containing YO-PRO1 dye (Life Technologies – Y3603) was added to the cells. Then cells were excited with a laser (485-15 nm) and emission spectra (528-20 nm) measured from the bottom of the plate using the CLARIOstar plate reader's (BMG Lab Tech) orbital averaging function. After the first 10 minutes bzATP (Biotechne - 3312) was added and flourcence reading were taken at least every 60s until the end of the assay.

Chapter III

Screening for Regulators of STING

Although operational DNA sensing by the cGAS-STING pathway is required for protection from viral threat, overzealous responses drive chronic proinflammatory conditions (see Chapter I, section I.5.4, Figure 9). The unmet medical need for STING antagonists is profound as traditional drug screening approaches have struggled to identify inhibitors and the few identified are yet to enter clinical trials (Haag et al. 2018; Hong et al. 2021; Hansen et al. 2018). Additionally, STING agonists are sought after for cancer immunotherapy and as adjuvants in vaccines (Meric-Bernstam et al. 2021; Chauveau et al. 2020; Wang et al. 2020). Recently many genes have been shown to modulate STING signalling by encoding accessory proteins (see Chapter I.5.1, section I, Figure 7). This project aims to identify further genes that enhance STING signalling, as these could be novel pharmaceutical targets relevant to both therapeutic development and drug repurposing. Alice Mayer, a post-doctoral researcher within the Rehwinkel group, previously performed a CRISPR screen to identify molecules that augment STING signalling. She utilised a library of lentiviral constructs encoding the GeCKO v2 library of sgRNAs targeting 19050 genes and 1864 miRNAs (Figure 19) (Sanjana, Shalem, and Zhang 2014).

A CRISPR-v2 Plasmid



B The GeCKO v2 library of sgRNAs

Genes targeted	19,050
Targeting constructs per gene	6
miRNAs targeted	1,864
Targeting contructs per mRNA	4
Control (non-trargeting) RNAs	2,000
Total sgRNA constructs	123,411

Figure 19 - A) Schematic of the lentiviral construct used in the GeCKO v2 library. Showing the: U6 promoter, single guide RNA (sgRNA), elongation factor-1α short promoter (EFS), *Streptococcus pyogenes* CRISPR associated protein 9 (spCas9), FLAG octapeptide tag (FLAG), 2A self-cleaving peptide (P2A), puromycin selection marker (Puro) and post transcriptional regulatory element (WPRE). B) Composition of the GeCKO v2 library of sgRNAs.

After bioinformatic analysis, Alice identified 58 candidate genes potentially involved in STING mediated IFN-β production. To give context to subsequent work Alice's CRISPR screen is presented in Figures 20 and 21. After the 58 candidate genes were identified, I aimed to validate if any of them enhanced STING signalling. These could be novel pharmaceutical targets relevant to both therapeutic development and drug repurposing.

III.1 CRISPR Screen to identify regulators of STING

Clustered regulatory interspaced short palindromic repeats (CRISPR) technology has revolutionised genome editing by allowing for specific genes to be targeted by sgRNAs coupled to a CRISPR associated protein 9 (Cas9) (Jinek et al. 2012). Alice utilised the GeCKO V2 library of 123,411 sgRNAs which are packaged and then delivered to cells in lentiviral vectors (Figure 20A) (Sanjana, Shalem, and Zhang 2014). Off target effects or ineffective guides cause variability leading to both false positives and false negatives. Using 6 different sgRNAs per gene allows for greater statistical certainty at final analysis (Sanjana, Shalem, and Zhang 2014). The library also contains 1,864 sgRNAs targeting microRNAs (miRNAs) which play a key role in post-transcriptional regulation (Zhao et al. 2014). The monocytic THP-1 cell line was selected for the screen as they express functional cGAS and STING (Sun et al. 2013). These are also readily differentiated upon PMA treatment into a macrophage-like cell type (Tsuchiya et al. 1982).

The previously described p125 THP-1 cells were used, which express GFP under the control on an IFN-β promoter (Mayer et al. 2017). This allows for a fluorescent read out of IFN induction by flow cytometry. The cells were transduced with the GeCKO V2 library, puromycin selected and PMA differentiated. A digitonin permeabilisation buffer containing 2'3'-cGAMP was used to stimulate cells using a previously described method (Mayer et al. 2017). 6 hours after stimulation cells were separated into GFP- and GFP+ populations by fluorescence-activated cell sorting (FACS). DNA was extracted and sgRNAs amplified by PCR to be sequenced.

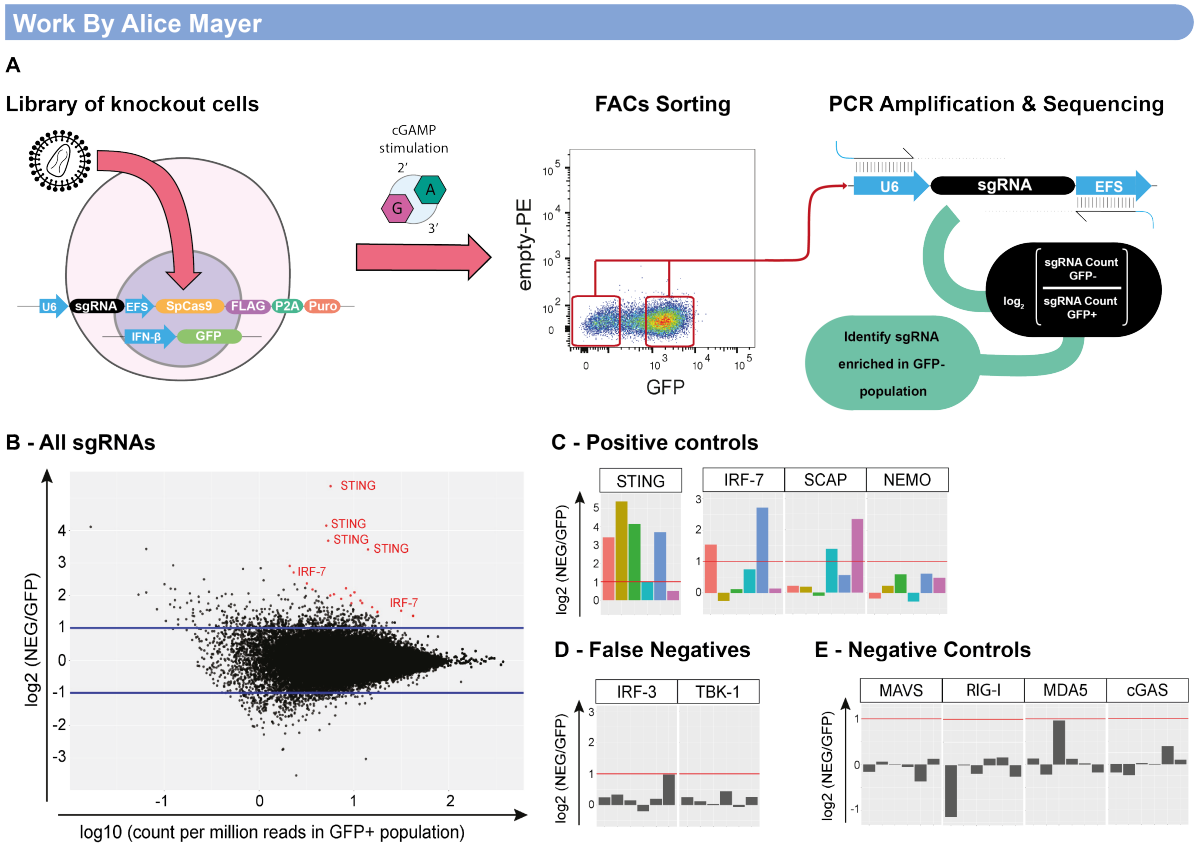


Figure 20 – CRISPR screen looking to identify regulators of STING. A) Lentiviral constructs encoding the GeCKO v2 library of sgRNAs were used to transduce p125 THP-1 cells engineered to express GFP from an IFN-β promoter. After puromycin selection cells were differentiated with PMA (5ng/ml) for 24 hours then permeabilised with digitonin buffer (0.001%) containing 2'3'-cGAMP (0.4 ng/ul). 6 hours later cells were then FACS sorted into GFP- and GFP+ populations. DNA was extracted and sgRNAs amplified by PCR using U6 forward and EFS reverse primers. A custom python pipeline was used to count sgRNA abundance within the GFP- and GFP+ populations. Statistical analysis designed to identify guides enriched within GFP- population was done with the statistical analysis programme MAGeCK. B) Negative bimodal model of guide enrichment. Each data point represents a sgRNA and those statistically significant are shown in red. STING and IRF7 are annotated. C) sgRNAs targeting genes known to enhance STING signalling that reach statistical significance. D) sgRNAs targeting genes known to augment STING signalling that don't reach statistical significance. E) sgRNAs targeting genes unrelated to 2'3'-cGAMP driven STING activation that don't reach statistical significance. Statistics at the individual sgRNA level was done using an alpha-modified robust rank aggregation method. Each bar represents one of the six sgRNAs used to target a gene. The bars show its individual enrichment score (n=1).

A custom python pipeline was used to extract and count guides within the GFP+ and GFP- populations. Enrichment of sgRNAs in the GFP- population would indicate that the targeted gene enhances STING signalling. Therefore, statistical analysis was performed with MAGeCK to identify genes that upon deletion prevent GFP production using an alpha-modified robust rank aggregation method (Kolde et al. 2012; Li et al. 2014) (Figure 20A). 4/6 sgRNAs targeting STING were found to be significantly enriched in the GFP- population (Figure 20B and C). Additionally, three proteins known to be involved in STING signalling reached statistical significance - IRF7, SCAP, NEMO (Figure 20C) (Ishikawa, Ma, and Barber 2009; Chen et al.

2016; Chen et al. 2017). Despite this IRF3 and TBK1 two molecules central to STING signalling did not reach statistical significance (Figure 20D). MAVS, RIG-I, MDA5 and cGAS which are not thought to activate STING in this context were assessed as negative controls and did not reach statistical significance (Figure 20E). This suggests functionally the screen has worked and may have identified unknown accessories to the STING pathway. Alongside the positive controls, 177 genes reached statistical significance. Gene ontology analysis revealed that 100 of these are involved in gene expression and 12 in mitochondrial function (data not shown). Disruption of these pathways will prevent protein translation and so GFP expression independent of STING signalling and so these genes were excluded. The remaining 58 genes were selected as potential accessories of STING and taken forward for validation (Figure 21).



Figure 21 – Statistical analysis of CRISPR screen. Gene ontology analysis revealed amongst 177 genes that reach statistical significance of these 100 are involved in gene expression and 12 in mitochondrial function or energy metabolism. These pathways are crucial to protein translation likely effecting GFP production independently of STING activation and so were excluded. This left 58 genes displayed in this figure that were investigated further. Statistics at the individual sgRNA level was done using an alpha-modified Robust Rank Aggregation Method. Each bar represents one of the six sgRNAs used to target a gene. The bars show the individual enrichment score (n=1).

III.2 siRNA interference in THP-1 cells

To validate the potential accessories of STING, I planned to use short interfering RNAs (siRNA) to transiently knockdown the 58 genes in THP-1 cells. This utilises the hosts RNA induced silencing complex (RISC) to target and degrade specific mRNAs/miRNAs. Classically siRNA knockdowns work well in non-hostile cell lines (e.g. HEK293 cells); however, for innate immune cells it is notoriously difficult (Li et al. 2015). This is because immune detection of dsRNA/ssRNA species present in siRNAs can induce cell death (Judge et al. 2005; Cekaite et al. 2007). Hence few siRNA based screens have been successful in studies of innate immunity (Li et al. 2015).

Preliminary work by Alice Mayer comparing many different transfection reagents showed that viromere blue maintained the highest cellular viability post siRNA delivery (data not shown). I next confirmed the siRNAs delivered by viromere blue resulted in knockdown of targeted genes. Cells were transfected with a pool of 4 different siRNAs targeting the same gene. I saw potent STING degradation at 72 hours post transfection in THP-1 cells differentiated with PMA (Figure 22A). I developed a simple method for measuring cellular viability as despite viromere blue mediating effective knockdowns it still resulted in significant cell death (data not shown). To do this I fixed and then stained THP-1 cells with crystal violet solution. Stain not retained by the cells was thoroughly washed away. After desiccation the stain was resolubilised in MeOH and an absorbance reading taken at 570nm. The principle being that intact cells on the bottom of the plate will retain the dye and give greater absorbance readings. I observed that crystal violet staining correlated well with the number of THP-1 cell seeded (Figure 22B). Additionally, treatment with the cytotoxic agent etoposide, which induces dsDNA breaks, reduced absorbance readings in a dose dependent manner (Figure 22B) (van Maanen et al. 1988; Dunphy et al. 2018). This shows the crystal violet viability assay (CVV) can assess cell death. From these readings I determined the viability limit (VL). Setting this as the point, a linear increase between cell number and absorbance reading began (Figure 22C).

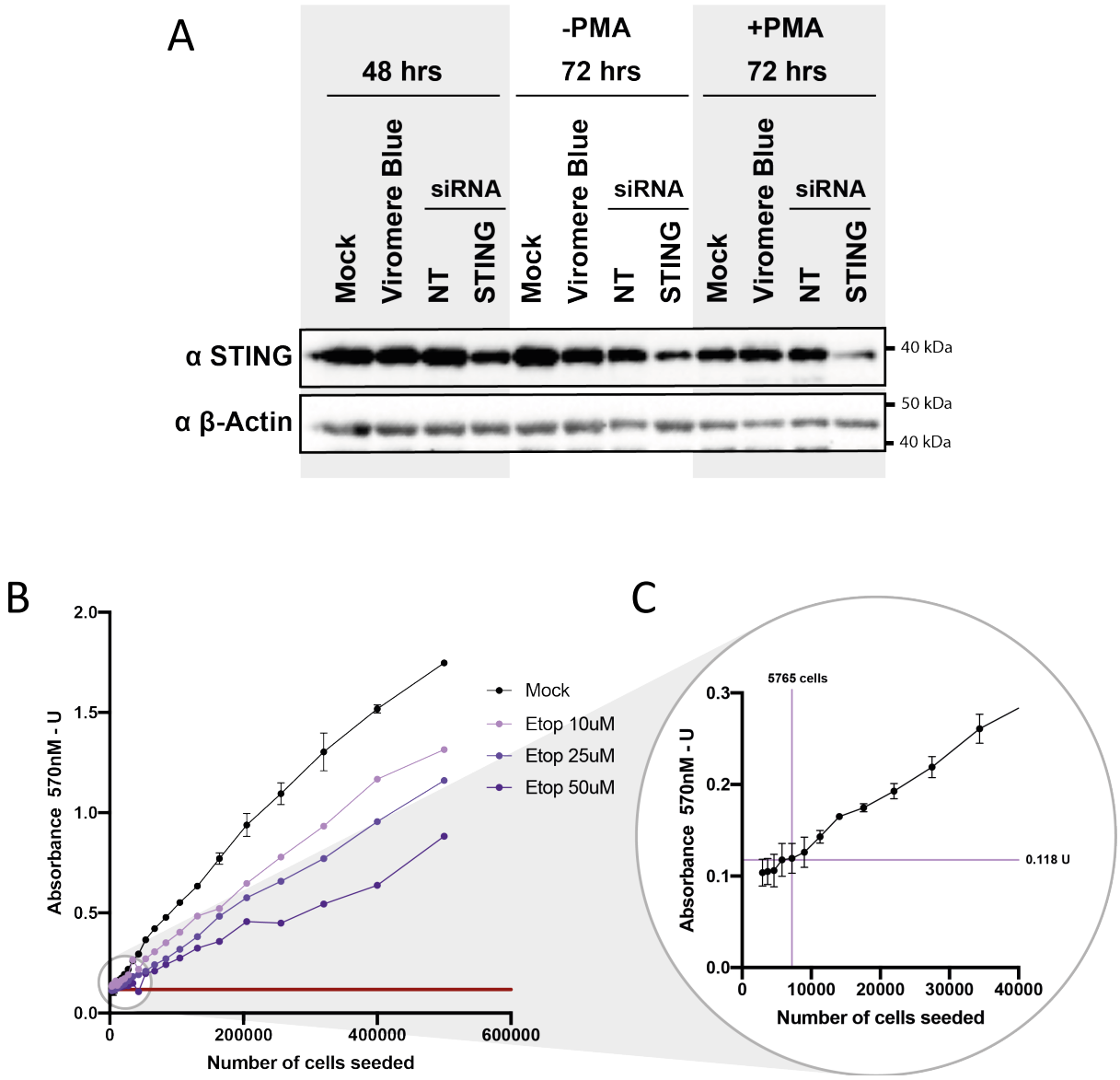


Figure 22 – siRNA knockdowns and crystal violet viability staining in THP-1 cells. A) THP-1 cells were transfected with non-targeting (NT) or STING targeting siRNAs using Viromere Blue. 48 hours post transfection the indicated cells were differentiated with PMA (50 ng/ml). The abundance of STING was assessed at the indicated time points by western blotting (n=1). B) The indicated number of THP-1 cells were differentiated with PMA (50ng/ml) in the presence or absence of etoposide. 24 hours later cells were fixed and stained with crystal violet dye. Retention of crystal violet was then measured by resolubilising the dye in MeOH and reading absorbance at 570nm. C) Point at which linear increase between cell number and absorbance started was determined (purple cross section). This was set as the minimum readable value. The mock is displayed as the mean of three technical replicates with error bars showing SEM. A single reading is displayed for the etoposide conditions hence no error bars are present (n=1).

I next tested if the successful siRNA knockdown of STING resulted in a reduction in STING signalling. To do this siRNA treated cells were stimulated with 2’3’-cGAMP in a digitonin permiabalisation buffer (Figure 23A) (Mayer et al. 2017). After 2’3’-cGAMP stimulation the cell supernatant was transferred to 3C11 cells that express luciferase under an interferon stimulated response element (Figure 23B). Using an IFN standard the IFN content of the supernatants can be determined. The viability of the cells was assessed by CVV (Figure 23C). Finally, I divided IFN value by CVV to normalise for cell number and allow comparison between different siRNAs (Figure 23D). I then tested the effect non-targeting (NT), STING and MAVS siRNAs had on IFN production after 2’3’-cGAMP stimulation. I observed treatment with all siRNAs resulted in roughly a ~3 fold reduction in viability (Figure 24A). Only STING siRNA was seen to reduce luminescence induction (Figure 24B). An IFN A/D standard was used to convert luminescence to IFN activity - U/ml (Figure 24C and supplementary Figure 1). STING knockdown also clearly reduced 2’3’-cGAMP activity after luminescence was converted to IFN and normalised to viability (Figure 24D and E). STING and MAVS targeting siRNA selectively reduced respective protein abundance (Figure 24F). This shows I have developed a system for siRNA knockdowns in THP-1 cells.

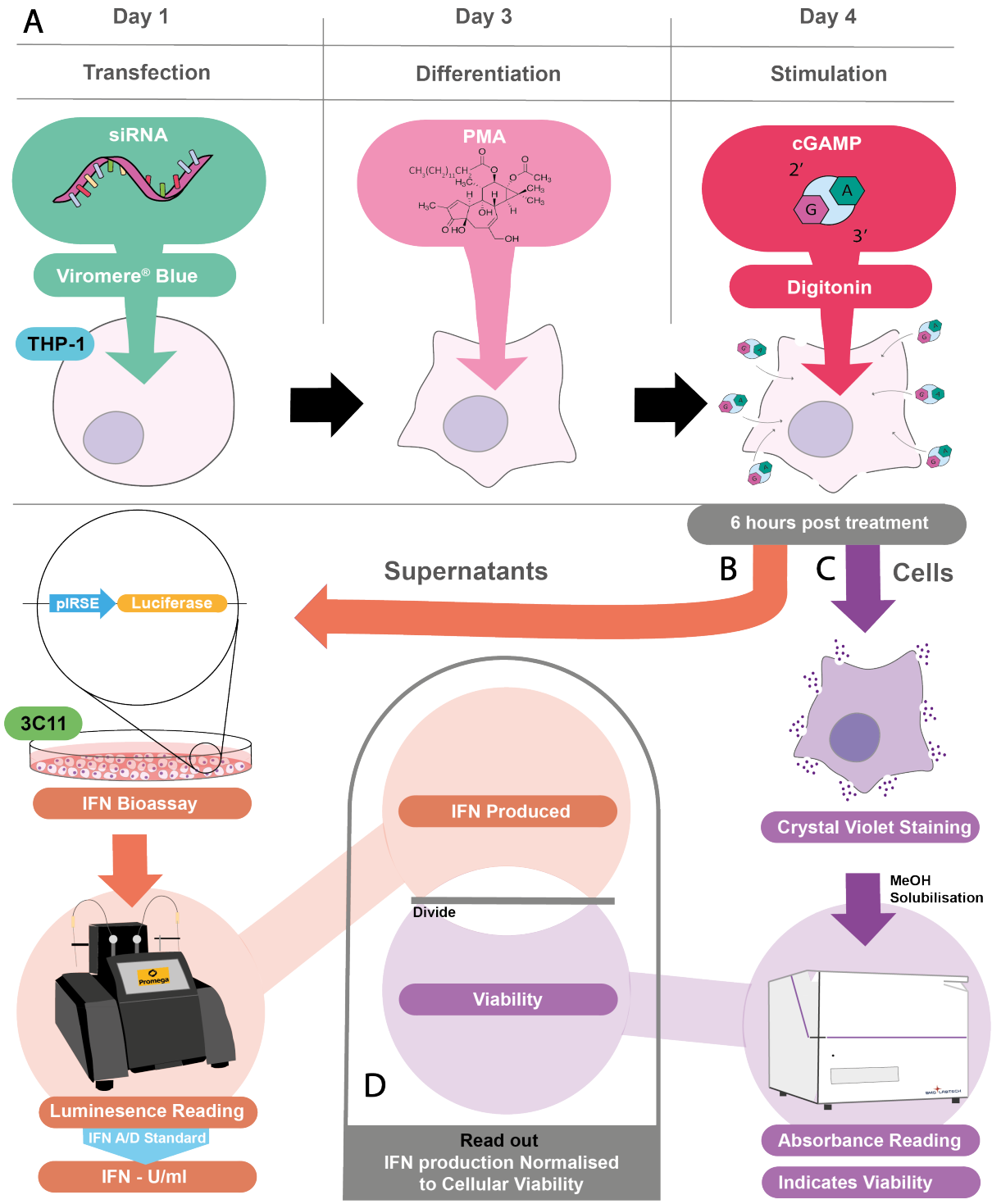


Figure 23 – Assessing IFN production by siRNA treated THP-1 cells (part 1). A) Cells were transfected with siRNA using Viromere Blue. 48 hours later cells were treated with PMA (50 ng/ml). Then at 72 hours post transfection stimulated with 2'3'-cGAMP (0.4 ng/ul) in permeabilisation buffer (0.001% digitonin). B) 6 hours after 2'3'-cGAMP stimulation supernatants were transferred onto 3C11 cells which express luciferase under an interferon stimulated response element (pIRSE). The recipient 3C11 cells were lysed and luminescence measured on addition of luciferin after 24 hours. Luminescence values were converted to IFN values using a IFN A/D standard. C) THP-1 cells were fixed and stained with crystal violet dye. Retention of crystal violet was then measured by resolubilising the dye in MeOH and reading absorbance at 570nm. D) IFN values were normalised by division to cellular viability.

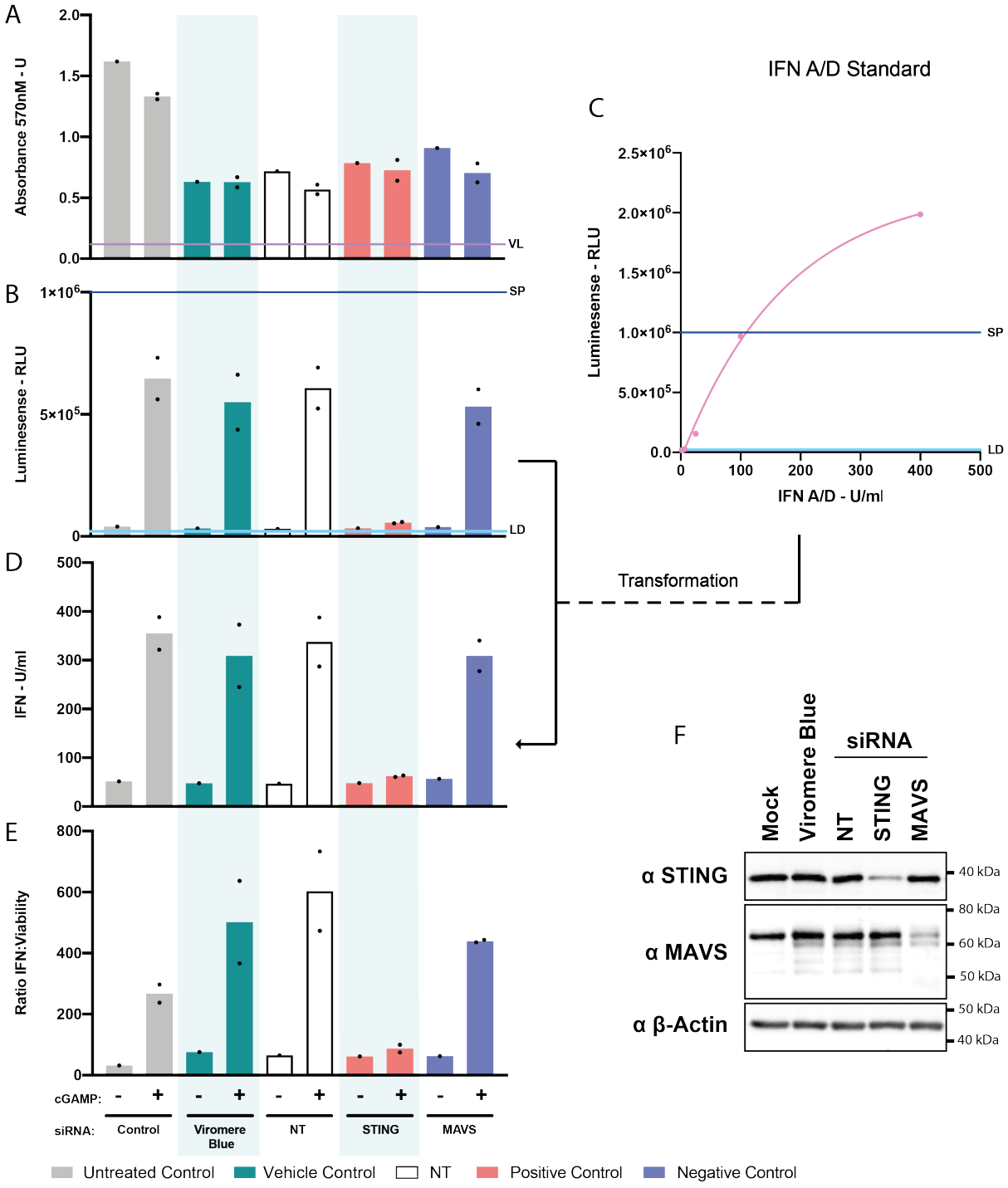


Figure 24 - Assessing IFN production by siRNA treated THP-1 cells (part 2). THP-1 cells were transfected with indicated siRNAs using Viromere Blue. 48 hours later cells were differentiated with PMA (50 ng/ml). Then at 72 hours post transfection stimulated with 2'3'-cGAMP (0.4 ng/ul) in permiabalisation buffer (0.001% digitonin). 6 hours after 2'3'-cGAMP stimulation supernatants were transferred onto 3C11 cells. A) Cell viability was measured using a crystal violet stain. The limit of detection (LD) defined as the minimum number of cells detectable is displayed. B) luminescence values. C) 3C11 were treated with an IFNA/D standard. Standards from individual bioassays were used to convert luminescence scores to IFN values. The limit of detection (LD) was defined as highest luminescence recorded for media with 0 U/ml of IFN A/D. The saturation point (SP) was defined as the value at which luminescence induction by IFN A/D moved outside of the linear range. Samples being tested were diluted to ensure they could be read within the SP and LD. A representative standard is shown.

(D) Luminescence values were converted to IFN values using the IFN A/D standard. (E) Total IFN production normalised by division to cellular viability. One representative experiment is shown with data points representing technical duplicates (n=3, biological repeats, representative graphs shown). F) STING and MAVS abundance was assessed by western blotting at 72 hours after siRNA treatment (n=2, biological repeats, representative blot shown).

III.3 Validation of CRISPR screen by siRNA interference

Using the methodology established in the previous section I screened the 58 potential accessories of STING from the CRISPR screen to test if knockdown reduces signalling. I used the limit of cellular detection determined in Figure 22B to exclude conditions with poor viability (Figure 25A). siRNA targeting positive controls (STING, IRF7, and SCAP) were found to supress normalised IFN production compared to the non-targeting and negative controls (MAVS and TLR4) (Figure 25C). A single negative control (cGAS) also showed reduced normalised IFN induction on STING stimulation. The 2'3'-cGAMP stimulus should circumvent the need for cGAS activity. Therefore, this is a false positive. It must be acknowledged that untreated cells and cells treated with the vehicle control viromere blue showed reduced IFN induction. I believe this may be an artefact of normalization, as untreated cells have a far greater viability which may skew the normalised values. The reduction in IFN production in viromere blue treated cells could be due to poor viability. Overall, it appears the siRNA-based screen has worked despite issues with viability and may have identified unknown accessories to the STING pathway. Alongside the positive controls, I identified 13 genes which appeared to have reduced IFN output after siRNA treatment (Figure 25C and supplementary Figure 2). To consider the viability of the 13 identified hits I plotted IFN values against CVV. 10 of the candidate genes clustered near the viability limit (PHB2, MAT2A, RBBP6, COPS8, KINDINS220, XPR1, MORC3, PHB, PPP1R2, PCBP1) (Figure 26). This indicates the reduced IFN production by some of the candidate genes may be due to poor viability. Only 3 of the 13 were above average viability (COPS4, EXOSC6 and UBL5). Of these, UBL5 was the only gene seen to down regulate IFN production to the same degree as siRNA targeting STING (Figure 26). I proceeded with testing the 13 identified genes by overexpression to see if any significantly enhanced STING signalling.

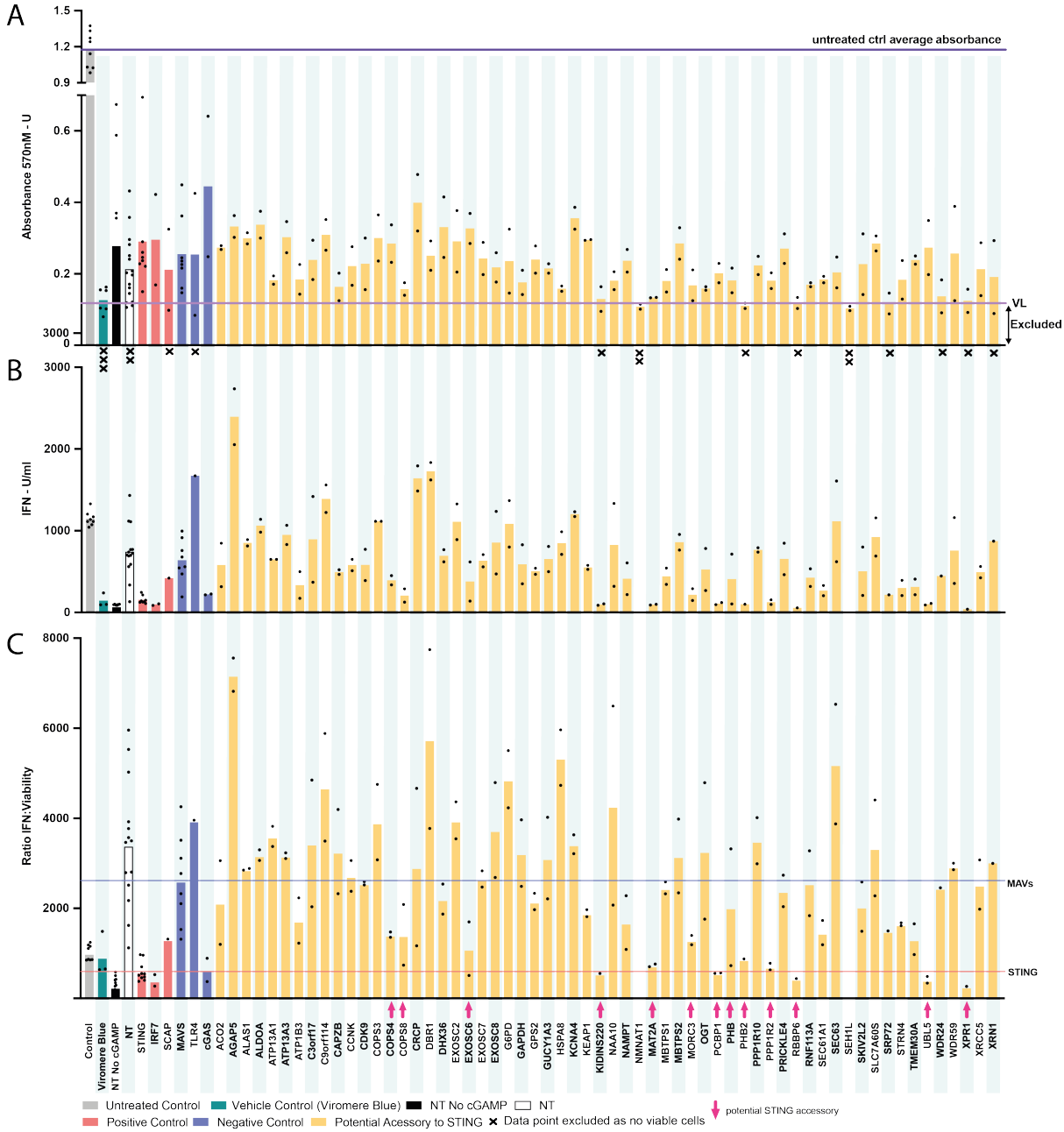


Figure 25 - siRNA Screen (Part 1) - THP-1 cells were transfected with indicated siRNAs using Viromere Blue as described in Figure 24. A) Cell viability was measured using a crystal violet stain. The average viability of the untreated wells and viability limit (VL) defined as the minimum number of cells detectable are displayed. An X indicates each data point excluded in subsequent analysis due to cells not meeting the viability limit (VL). B) Luminescence values were converted to IFN values using a IFN A/D standard. C) Total IFN production normalised to cellular viability. Technical duplicates were recorded and individual data points are displayed. The average value for the positive and negative controls STING and MAVS are displayed. Using these as a reference 13 genes of interest were identified for further testing indicated by pink arrows (n=1).

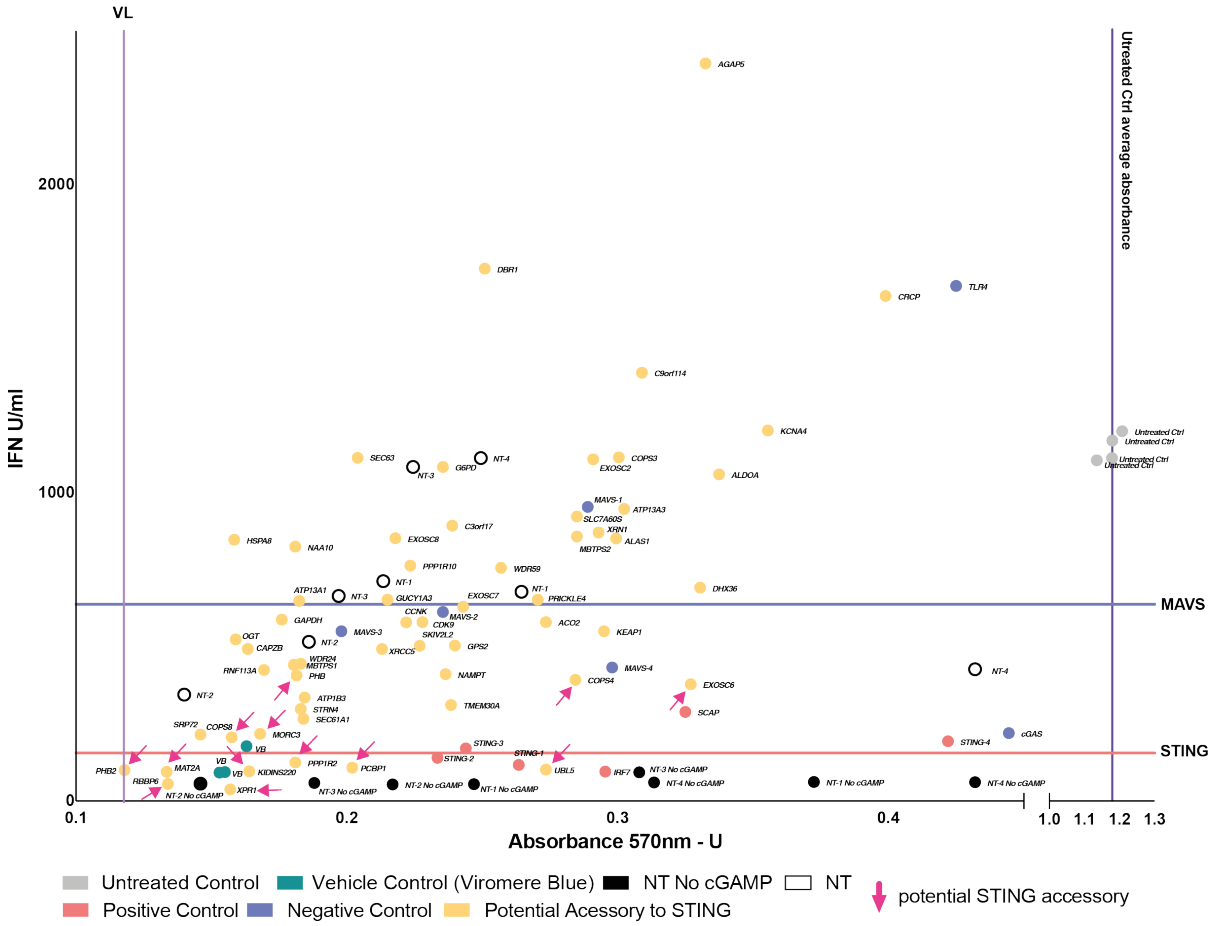
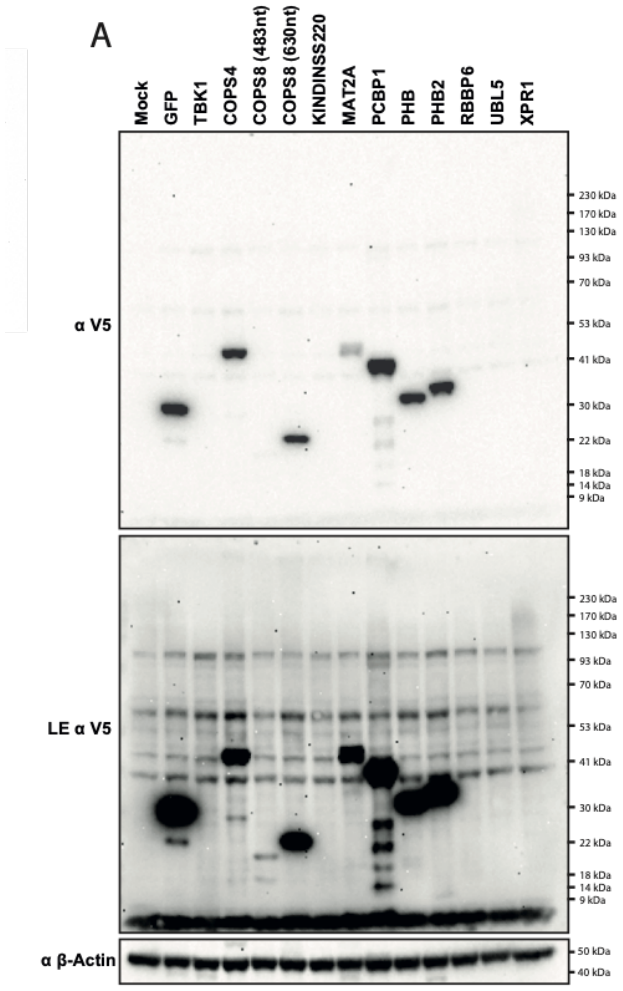


Figure 26 – siRNA screen (Part 2). Data from Figure 25 replotted as IFN vs Absorbance (viability). Data points show averages of technical duplicates with data points below the viability limit (VL) excluded. The average value for the positive and negative controls STING and MAVS are displayed. Using these as a reference 13 genes of interest were identified for further testing indicated by pink arrows (n=1).

III.4 Overexpression of potential accessories of STING

To perform gain-of-function assays, the 13 potential STING accessories identified in the siRNA screen were cloned into a lentiviral vector with a C-terminal V5 tag. For technical reasons EXOSC6, MORC3 and PPP1R2 could not be cloned. COPS8 exists as two isoforms. Isoform-1 which is 209 amino acids (COPS8-209) in length and isoform-2 which has a 49 amino acid N-terminal truncation (COPS8-160) due to an alternative start codon (Flicek 2022). Both isoforms were cloned and tested. Using these vectors, I transduced THP-1 Lucia cells. These secrete luciferase under the control of an IRF3-induced promoter giving a read out for STING activation. GFP and TBK1 were used as negative and positive controls for STING signalling. Western blotting confirmed expression of GFP, COPS4, COPS8-160, COPS8-209 MAT2A,

PCBP1, PHB and PHB2 at the expected sizes predicted by the database GeneCards (Figure 27A and B) (Center 2022). The remaining constructs (TBK1, KIDINS220, RBBP6, XRP1 and UBL5) could not be detected by Western blotting even after extended exposure (Figure 27A). Despite this RT-qPCR revealed a 3-fold increase in the level of *TBK1* mRNA (Figure 28A). Using flow cytometry as an alternative read out for protein expression, I show ~5% of TBK1 overexpressing cells are V5 positive (Figure 28B and supplementary Figure 3). This suggests TBK1 may be expressed at low levels.



B

Protein	Expected Size	Detected
GFP	28 kDa	Yes
TBK1	83.6 kDa	No
COPS4	46.3 kDa	Yes
COPS8 (483nt)	17.8 kDa	Yes
COPS8 (630nt)	23.2 kDa	Yes
KIDINS220	196.5 kDa	No
MAT2A	43.7 kDa	Yes
PCBP1	37.4 kDa	Yes
PHB	29.8 kDa	Yes
PHB2	33.3 kDa	Yes
RBBP6	33.3 kDa	No
UBL5	20.2 kDa	No
XPR1	81.5 kDa	No
V5 Tag	1.4 kDa	N/A

Figure 27 – Overexpression of potential STING acessories in THP-1 cells. A) THP-1 cells were transduced with lentiviruses stably expressing the indicated genes with a C terminal V5 tag and lysed. Protein abundance was then assessed by western blotting (n=1). B) Table showing whether proteins were detected at the expected size. Size predictions estimated by gene card.

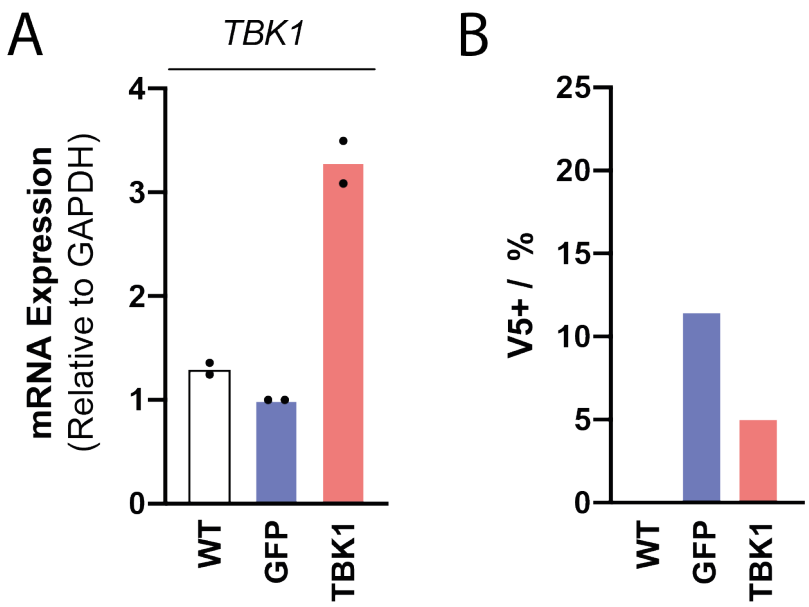


Figure 28 – Overexpression of TBK1 in THP-1 cells. (A) RNA was extracted from THP-1 Lucia cells stably expressing the indicated genes and RT-qPCR was performed for the *TBK1* gene. Technical duplicates shown (n=1). THP-1 Lucia cells stably expressing either GFP-V5 or TBK1-V5 were intracellularly stained for V5 and populations quantified by flow cytometry. Gating strategy shown in supplementary Figure 3 (n=1).

III.5 Testing if overexpression of candidate genes enhances STING signalling

I then assessed the capacity of each potential STING accessory to promote IRF3 activation. The THP-1 Lucia reporter cells were treated with three different STING stimuli: vaccinia virus DNA, 2'3'-cGAMP in digitonin permeabilisation buffer or a high dose of exogenous 2'3'-cGAMP. The three stimuli were titrated onto GFP (negative control) and TBK1 (positive control) overexpressing cell lines to find non-saturating doses. As expected, TBK1 overexpression increased IRF3 activation upon 2'3'-cGAMP and DNA stimulation by a modest ~2 fold compared to the GFP control (Figure 29A, B and C). A much greater increase in IFN production could be seen at baseline in TBK1 overexpressing cells (Figure 29A and B). Therefore, I initially tested if overexpression of the potential STING accessories increased baseline IRF3 activation in the absence of a stimulus. Vehicle controls were also tested, either lipofectamine or digitonin permeabilisation buffer. Of all the potential STING accessories COPS8-209 showed the greatest increase in IFN-β induction at baseline, ~4.8 fold greater than the GFP control (Figure 30A). Non-saturating doses of each stimulus were then applied to the overexpressing cell lines. Several candidate genes slightly augmented IRF3 activation in

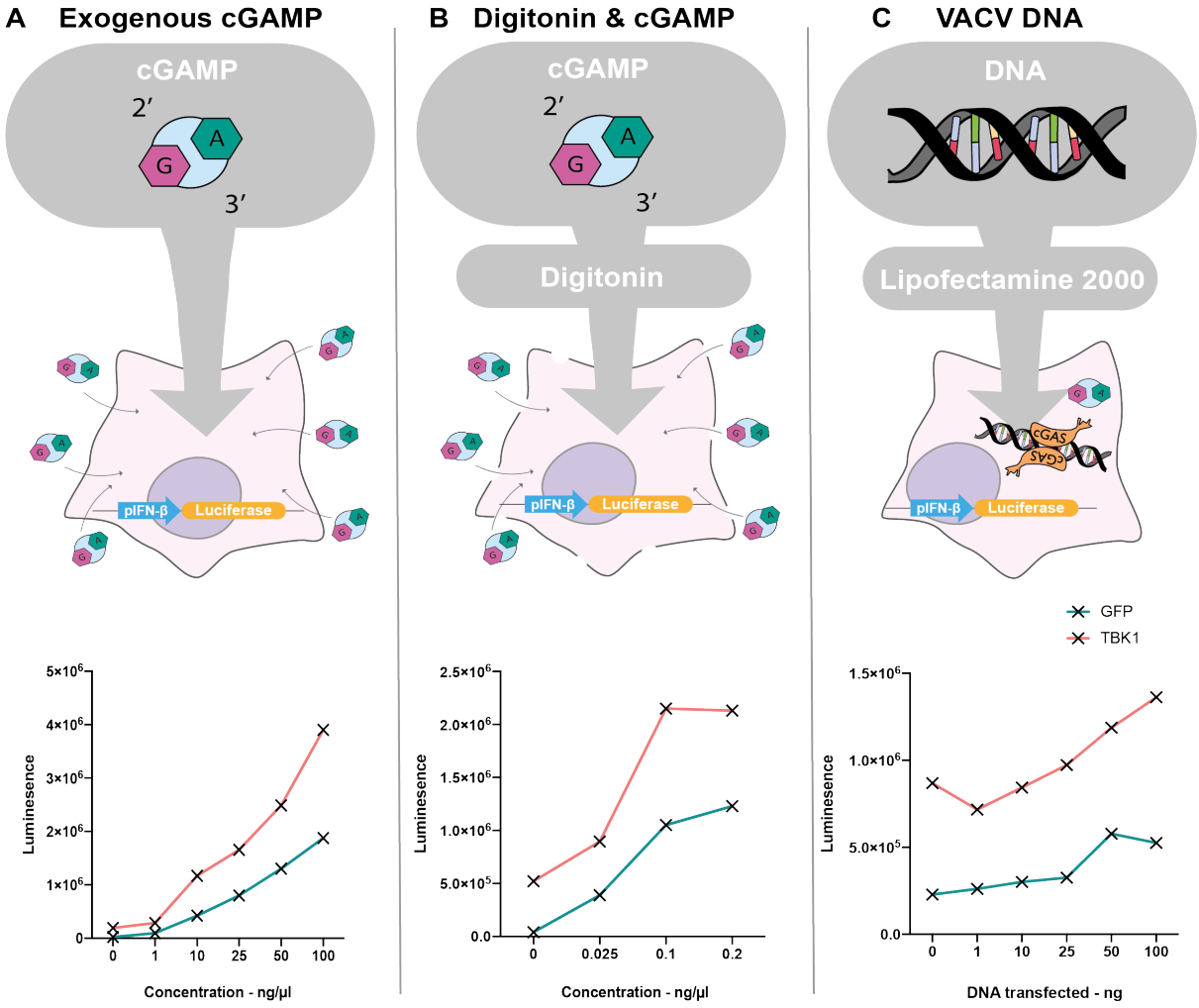


Figure 29 – Stimulation of THP-1 cells with 2'3'-cGAMP. THP-1 Lucia cells expressing luciferase under an IRF3-induced promoter were stably transduced with GFP or TBK1. THP-1 cells were differentiated with PMA (50 ng/ml) 24 hours prior to stimulation with: (A) exogenous 2'3'-cGAMP (n=3, biological repeats, representative graph shown); (B) 2'3'-cGAMP in a permeabilisation buffer (0.001% digitonin) (n=2, biological repeats, representative graph shown); (C) transfected VACV dsDNA (n=3, biological repeats, representative graph shown). 24 hours after stimulation luminometry was then used to assess luciferase production.

response to multiple stimuli, including COPS8-209 (average 1.4-fold increase), KINDINS220 (average 1.5-fold increase), MAT2A (average 1.3-fold increase) and RBBP6 (average 1.2-fold increase) (Figure 30B). Although the observed fold-changes are small, it is notable that overexpression of TBK1, a molecule central to DNA sensing, resulted only in a 2.7-fold increase in signalling upon stimulation (Figure 30B). Therefore, I titrated a wider range of exogenous 2'3'-cGAMP doses onto cells expressing the three most prominent hits - COPS8-209, KIDINS220 and MAT2A. In this context none of the hits were seen to increase IFN production suggesting they do not enhance STING signalling when overexpressed (Figure 31).

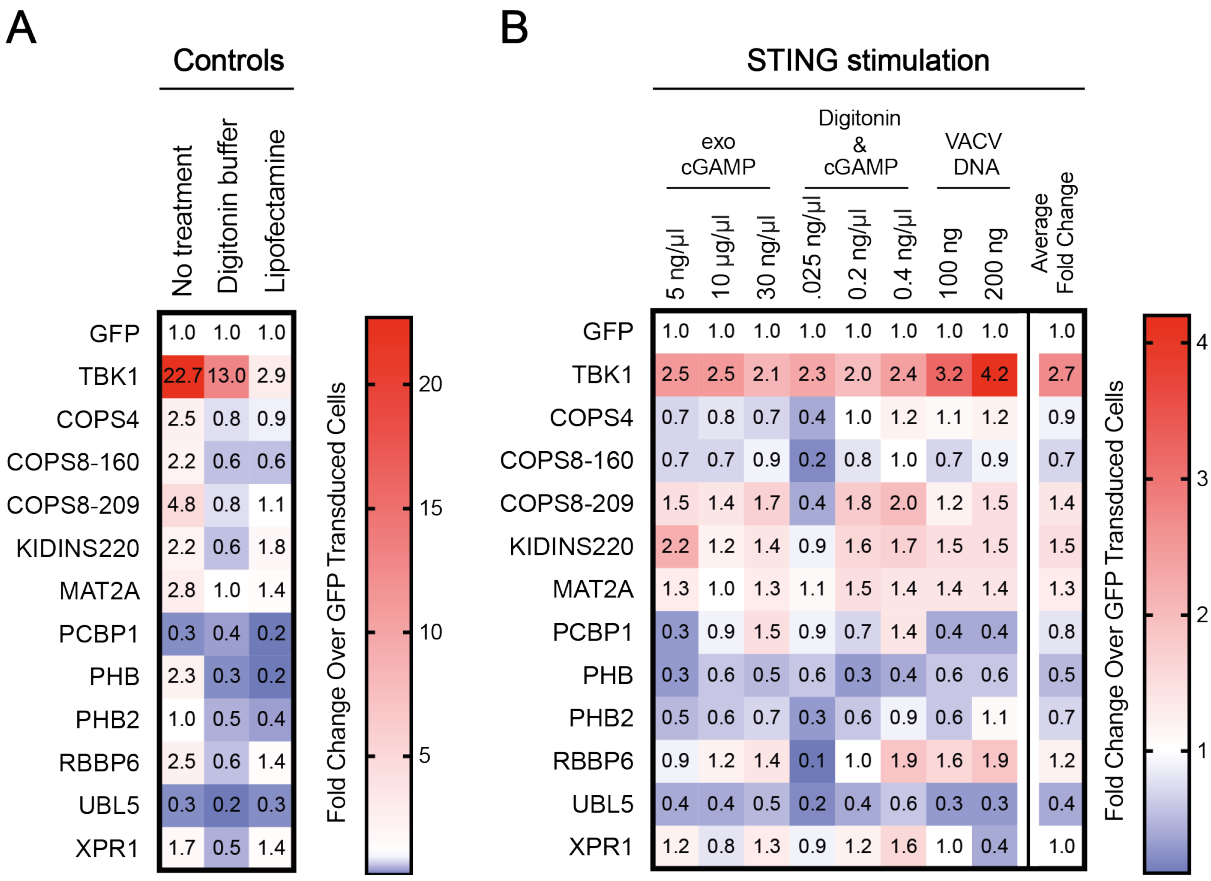


Figure 30 - Stimulation of THP-1 cells expressing potential STING accessories with 2'3'-cGAMP. THP-1 Lucia cells expressing luciferase under an IRF3-induced promoter were stably transduced with the indicated genes. THP-1 cells were differentiated with PMA (50 ng/ml) 24 hours prior to stimulation with: exogenous 2'3'-cGAMP, 2'3'-cGAMP in a permeabilisation buffer (0.001% digitonin) or transfected VACV dsDNA. 24 hours after stimulation luminometry was used to assess luciferase production. A) Heat map showing fold change of luciferase production relative to GFP for untreated and vehicle controls. B) Heat map showing fold change of luciferase production relative to GFP for different 2'3'-cGAMP stimuli. Left hand column displays average fold change across all stimuli and doses (n=2, average of biological repeats shown).

III.6 Discussion

Starting with a genome-wide library of 19,050 genes, Alice Mayer's CRISPR screen identified 58 potential accessories of STING. I first developed a method enabling siRNA knockdowns in THP-1 cells. This was done in a THP-1 cell line derived from a single cell clone, as the tested heterogenous line showed poor viability (data not shown). I showed clear siRNA knockdowns that reduced STING signalling in THP-1 cells. The limitation of the system being that viability is harshly reduced on siRNA treatment. I acknowledge this may produce false hits where reduced STING signalling is due to poor viability or cellular processes being disturbed. I would suggest future studies consider a different approach to do knockdowns in THP-1 cells. Where clonal selection of CRISPR cell lines is not possible shRNA delivery by

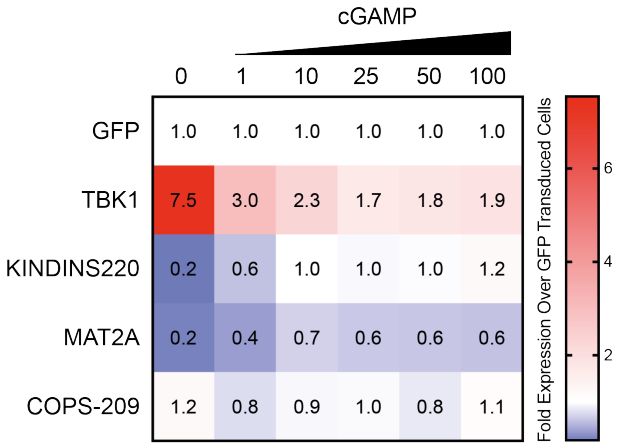


Figure 31 - Stimulation of THP-1 cells expressing potential STING accessories with exogenous 2'3'-cGAMP. THP-1 Lucia cells expressing luciferase under an IRF3-induced promoter were stably transduced with the indicated genes. The THP-1 cells were differentiated with PMA (50 ng/ml) 24 hours prior to stimulation with exogenous 2'3'-cGAMP at the indicated doses. 24 hours after stimulation luminometry was used to assess luciferase production (n=1).

lentiviral constructs may offer a higher throughput option producing a higher quality data. Additionally, a serious limitation I acknowledge is the lack of replicates in both the CRISPR and siRNA based screens. Despite the lack of replicates and viability issues, the siRNA based screen identified 13 genes which potentially enhanced STING signalling (COPS4, COPS8, EXOSC6, KIDINS220, MAT2A, MORC3, PCBP1, PHB, PHB2, PPP1R2, RBBP6, UBL5 and XRP1). Experiments overexpressing the potential accessories of STING were undermined by the lack of a convincing positive control. Initially I tried to overexpress STING itself, but cells died shortly after transduction (data not shown). I manged to get a small percentage of cells to express TBK1 (Figure 28A) although I could not show this by western blotting (Figure 27A). Suggesting overexpression of core components to the STING pathway leads to cytotoxicity. Overall, none of the potential STING accessories identified by the siRNA-based screen appeared to enhance STING signalling on overexpression. Unfortunately EXOSC6, MORC3 and PPP1R2 could not be tested in these assays. Additionally, as I cannot verify expression of KIDINS220, RBBP6, UBL5 and XRP1 for these genes no conclusions can be drawn.

Since the screens were performed, several of the potential STING accessories have been implicated in cGAS-STING signalling or IFN signalling in general. Keap1, a hit from the CRISPR screen, has been shown to antagonise Nrf2 by sequestration in THP-1 cells. This prevents Nrf2 mediated STING mRNA degradation and so Keap1 enhances STING signaling (Olagnier et al. 2018). The siRNA screen did not identify Keap1 as a positive regulator of STING as would be

expected. PCBP1, one of the 13 genes identified by the siRNA screen, has been shown to facilitate the binding between DNA and cGAS (Liao, Lei, and Shu 2020). The 2'3'-cGAMP stimulus within the siRNA based screen should circumvent the need for cGAS activity. Therefore, it is unclear why PCBP1 would be a positive hit unless it has an unknown role downstream of cGAS. MORC3 acts as a restriction factor of HSV-1 by epigenetically silencing latent genomes (Gaidt et al. 2021). The HSV-1 protein ICP0 degrades MORC3 allowing for active genome transcription. Recently it has been shown that a MORC3-regulated DNA element represses constitutive IFN-β expression. Degradation of MORC3 by HSV-1 therefore leads to IFN-β induction and viral restriction. Suggesting MORC3 is a "self-guarded" restriction factor as viral antagonism of its primary function (epigenetic silencing) leads directly to IFN-β expression (Gaidt et al. 2021). It is unclear why MORC3 was identified in both screens. As in this context MORC3 knockdown resulted in reduced IFN-β output which contradicts previous reports.

Despite the technical and logistical challenges during this project we successfully developed and preformed an siRNA-based screen in THP-1 cells. From this we identified 13 genes that are potentially involved in augmenting STING signalling. Unfortunately, my progress was halted at the start of the COVID-19 pandemic. Upon my return to the lab other more promising projects were prioritised. As such, no positive regulators of STING were identified by the work presented here. In the future work looking to validate the hits from the siRNA-based screen is justified. Particularly as the potential STING accessories were identified in the context of deletion. My work focussed upon overexpression a context in which these hits may not enhance STING signalling. Therefore, an alternative knockdown system which could offer greater cellular viability, such as shRNA or CRISPR could be used to assess if the hits from the siRNA-based screen truly enhance STING activation. Most notably experimental follow-up of the two top hits from the siRNA screen, namely UBL5 (a ubiquitin like protein known to aid pre-mRNA splicing) and EXOSC6 (a component of the exosome complex responsible for RNA degradation), is needed (Oka et al. 2014; Ammon et al. 2014; Kilchert, Wittmann, and Vasiljeva 2016). This is exciting as identification of a new regulator of STING signalling may allow for modulation of this pathway and treatment of the STING associated diseases presented in Figure 9.

Chapter IV

Screening for viral antagonists of cGAMP channels

In my previous chapter I detail my attempt to find auxiliary components of the STING signalling pathway. The remaining time as a PhD student was spent investigating cGAMP channels and their function during viral infection.

Until very recently 2'3'-cGAMP's activity was considered topologically limited to its site of production, the cytosol, as its large size and negative charge makes it membrane impermeable. Recently, and in quick succession, five channels have been shown to transport 2'3'-cGAMP across the cell membrane: ABCC1, SLC19A1, SLC46A2, P2X7 and LRRC8A:C/E heterodimers (see Chapter I, section I.7) (Zhou et al., 2020a, Lahey et al., 2020, Zhou et al., 2020b, Cordova et al., 2021, Ritchie et al., 2019, Luteijn et al., 2019, Maltbaek et al., 2021). A synopsis of their previously known functions and expression profile is given in Figure 32A. Despite 2'3'-cGAMP transport across the extracellular space being characterised over the past three years, some key open questions remain.

1. Which of the channels are functional under physiological conditions?

Differences in 2'3'-cGAMP uptake between mice and humans has prevented authors from showing some channels (SLC46A2 and SLC19A1) function physiologically (Cordova et al., 2021, Ritchie et al., 2019, Luteijn et al., 2019).

2. Which of these channels function in humans?

2'3'-cGAMP transport mediated by the P2X7 pore has only been shown in mice (Zhou et al., 2020b).

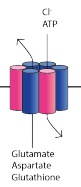
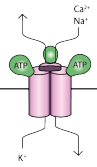
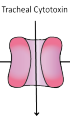
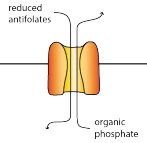
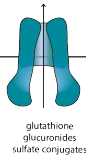
3. In which cell types and tissues are the channels functional?

LRRC8A:C/E only appears to transport 2'3'-cGAMP into endothelial cells. Despite this LRRC8A:C/E contributes to viral clearance of HSV-1 classically known to infect neuronal and epithelial cells, suggesting this channel may be relevant in more tissues than initially reported (Zhou et al., 2020a).

4. Is 2'3'-cGAMP export anti or proinflammatory?

Blocking 2'3'-cGAMP export through ABCC1 leads to intracellular 2'3'-cGAMP retention and enhanced STING signalling (Maltbaek et al., 2021). It is unknown whether ABCC1 also functions in a proinflammatory manner to promote cancer or microbial clearance like the other channels

A

	LRRC8A:C	P2X7	SLC46A2	SLC19A1	ABCC1
Channel					
Known function	Regulatory Volume Decrease Export/import of osmolytes	Non-selective pore ~0.9 kDa Neuronal signalling Inflammasome activation	Orphan transporter Import of tracheal cytoxin	Import of reduced antifolates Export of organic phosphates	Export of glutathione glucuronides and sulfate conjugates
Expression pattern	Endothilial Immune cell (T, B, macrophage).	Monocyte Neurons	Monocyte	Almost ubquitous expression	Almost ubquitous expression

B

Baltimore Classification	dsDNA			RT ssRNA(+)		ssRNA(+)	ssRNA(-)
Virus	HSV-1 	VACV 	AdV 	HIV-1 	HIV-2 	ZIKV 	IAV 
Family	Herpesviridae	Poxviridae	Adenoviridae	Retroviridae	Retroviridae	Flaviviridae	Orthomyxoviridae
Clinical manifestation	Cold Sore Encephalitis	Rarely Progressive Vaccinia	Conjunctivitis Respirtory infection Pneumonia	Acquired immunodeficientcy syndrome		Microcephaly	Flu
Cell types infected	Neuronal Epithelial Monocytic	Epithelial	Wide tropism	Macrophage Dendritic cells T cells Neurons		Neuronal Epithelial Endothelial	Respiratory Epithelial
Neucleic acid sensors triggered	cGAS (dsDNA) IFI16 (dsDNA) RIG-I (5'ppp-RNA) TLR3 (dsRNA)	cGAS (dsDNA) DNA-PK (dsDNA-ends) AIM2 (dsDNA) TLR9 (CpG-DNA)	cGAS (dsDNA) TLR9 (CpG-DNA) RIG-I (5'ppp-RNA)	cGAS (dsDNA) TLR9 (CpG-DNA) TLR8 (ssRNA)		RIG-I (5'ppp-RNA) MDA-5 (dsRNA) TLR3 (dsRNA)	cGAS (mtDNA) RIG-I (5'ppp-RNA) TLR7 (ssRNA) TLR3 (dsRNA)

Figure 32 - Synopsis of cGAMP channels and viruses tested. A) Synopsis of cGAMP channels based upon evidence presented in Chapter I, section I.7. B) Synopsis of viruses used adapted from Zahid et al. (2020).

The host's immune system acts to restrict viral invasion. Equally viruses encode antagonists of the host immune response to allow replication. Hence, if cGAMP channels function within the innate immune response viral antagonists should exist. Identification of a cGAMP channel antagonist would provide further evidence that these transporters are physiological relevant and subsequent characterisation could answer some of the aforementioned open questions. Therefore, we aimed to identify an antagonist of a cGAMP channel encoded by a human virus. To do this we screened viruses across different families and genome types. A synopsis of the viruses tested is provided in Figure 32B.

IV.1 Screening for viruses that degrade endogenous LRRC8A:C

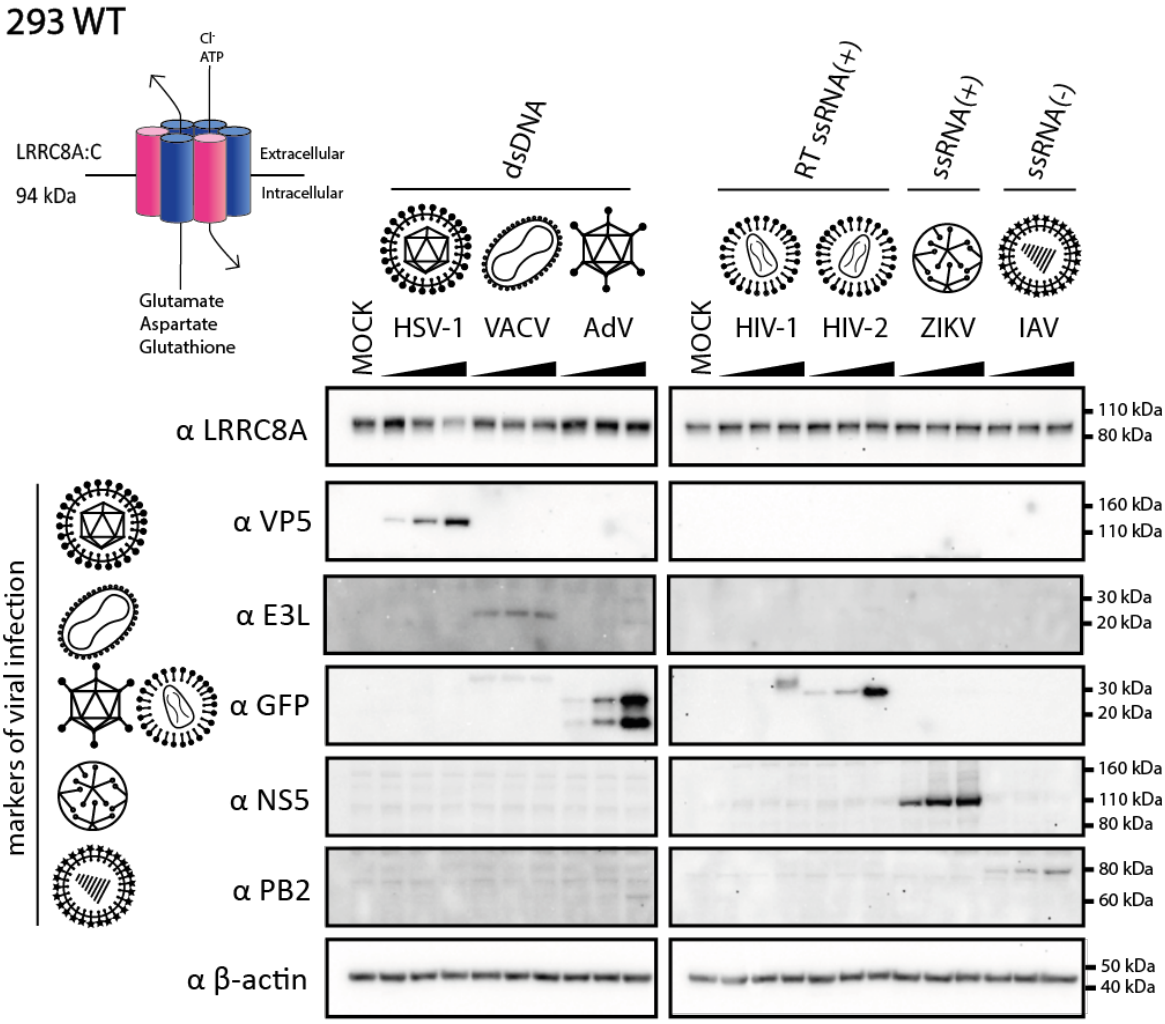


Figure 33 -Screening for viral degradation of LRRC8A. 293 cells were infected with HSV-1 (MOI – 0.02, 0.006, 0.002), VACV (MOI – 0.2, 0.066, 0.022), AdV (MOI – 1500, 150, 15), HIV-1 (1:10, 1:50, 1:250), HIV-2 (1:10, 1:50, 1:250), ZIKV (MOI – 1, 0.25, 0.06) and IAV (MOI – 10, 5, 2.5). 48 hours later, the cells were lysed and abundance of LRRC8A was assessed by western blotting (n=2, biological repeats).

Viruses commonly degrade components of the innate immune system to prevent antiviral responses and favour viral replication. We speculated that cGAMP channels could also be degraded by viruses. To test this, we infected HEK293 cells with herpes simplex virus 1 (HSV-1), vaccinia virus (VACV), Adenovirus (AdV), human immunodeficiency virus types 1 and 2 (HIV-1, HIV-2), Zika virus (ZIKV) and influenza A virus (IAV).

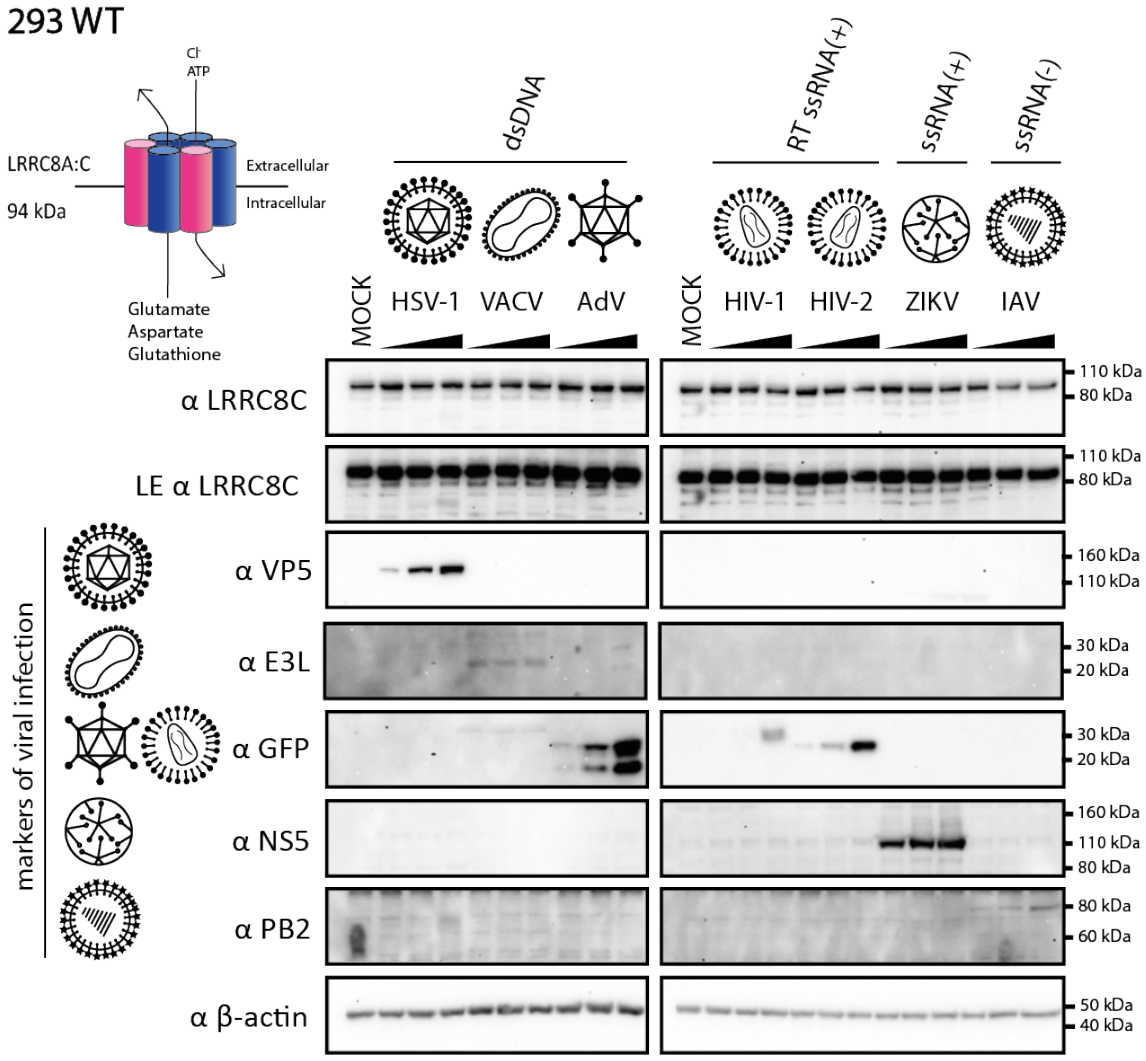


Figure 34 -Screening for viral degradation of LRRC8C. 293 cells were infected with HSV-1 (MOI – 0.02, 0.006, 0.002), VACV (MOI – 0.2, 0.066, 0.022), AdV (MOI – 1500, 150, 15), HIV-1 (1:10, 1:50, 1:250), HIV-2 (1:10, 1:50, 1:250), ZIKV (MOI – 1, 0.25, 0.06) and IAV (MOI – 10, 5, 2.5). 48 hours later, the cells were lysed and abundance of LRRC8C was assessed by western blotting. Secondary band indicated by * (n=2, biological repeats).

We then tested for channel levels by western blotting. Initially, we attempted to test all known cGAMP channels, but specific antibodies detecting endogenous protein were only available for LRRC8A and LRRC8C. We observed that of all the viruses tested only HSV-1 was

able to consistently down regulate LRRC8A (Figure 33). Interestingly, although the abundance LRRC8C was not greatly reduced by HSV-1, a smaller secondary band appeared at ~70kDa in lysates from HSV-1 infected cells (Figure 34). We speculate this could be an LRRC8C degradation product.

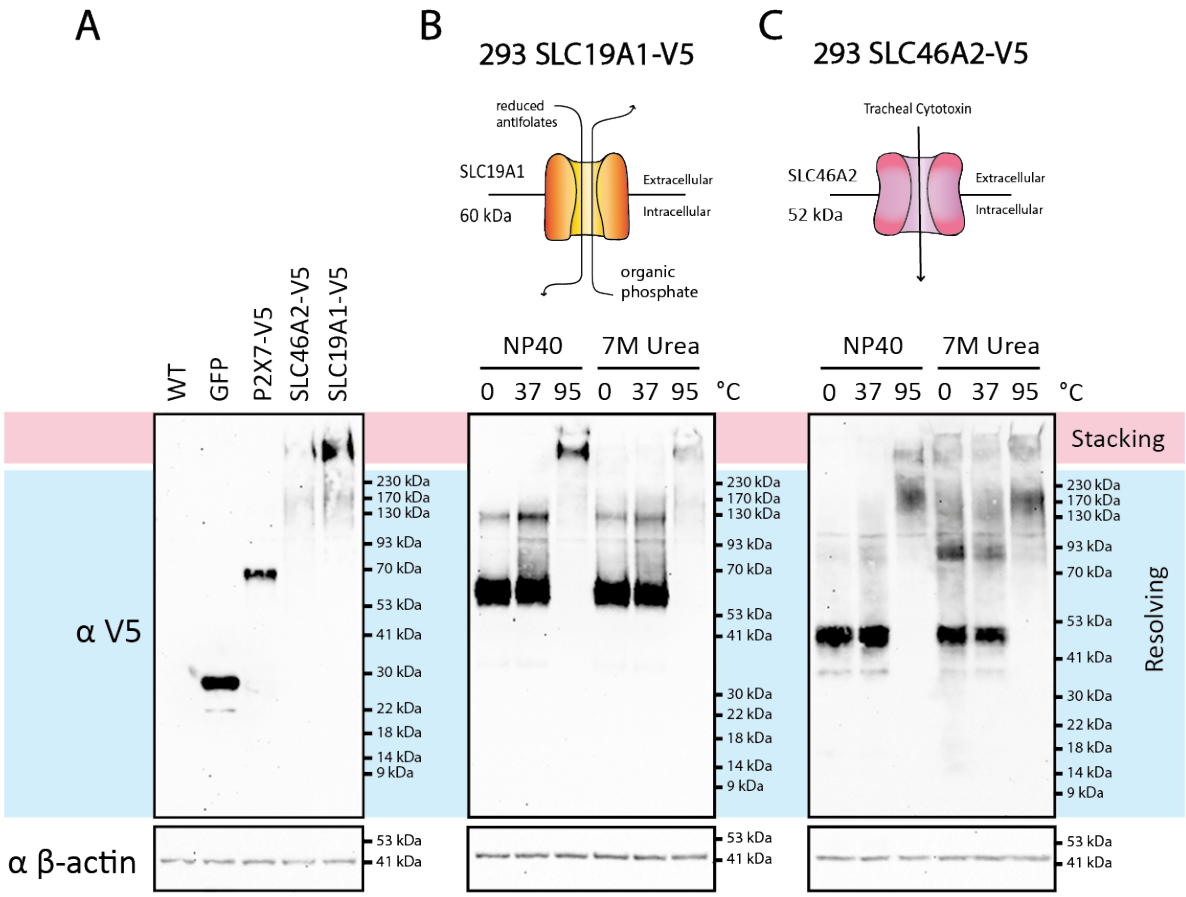


Figure 35 – Overexpression of P2X7, SLC19A1 and SLC46A2. A) A western blot of 293 cells stably transduced with P2X7-V5, SLC46A2-V5 and SLC19A1 (n=3, biological repeats). B/C) Western blots as in (A) boiled for 5 minutes at indicated temperatures and lysed in either NP40 buffer or NP40 buffer supplemented with 7M urea. Pink and blue boxes indicate the stacking and resolving portion of the gel (n=3, biological repeats).

IV.2 Overexpression and resolution of P2X7, SLC46A2 and SLC19A1

We were unable to reliably detect P2X7, SLC19A1, SLC46A1, SLC46A2 and SLC46A3 at endogenous levels (data not shown). Therefore, we created lentiviral expression vectors with a C-terminal V5 tag. We decided to focus upon SLC46A2 as although SLC46A1 and SLC46A3 also function to uptake 2'3'-cGAMP into macrophages the former is the dominant importer (Cordova et al., 2021). Upon over expression P2X7 was detected at the predicted size of ~68kDa (Figure 35A).

Initially SLC46A2 and SLC19A1 were not detectable. Within the stacking gel we were able to see that small amounts of V5 positive signal appeared around the gel pocket (Figure 35A). We hypothesised that aggregation might prevent entry into the gel, as many proteins with multi-pass transmembrane domains aggregate upon boiling (Tsuji, 2020). Therefore, I reduced the boiling temperature of the samples. This allowed visualisation both SLC19A1 and SLC46A2 at the expected size (Figure 35B and C). The reason for boiling western blotting samples is to unfold proteins allowing for total denaturation and exposure of linear epitopes recognised by many western blotting antibodies (Bass et al., 2017). Therefore, we chose to supplement our buffer with the strong denaturing agent Urea. Addition of Urea coupled with lack of boiling fully resolved SLC19A1 from pocket aggregation (Figure 35B).

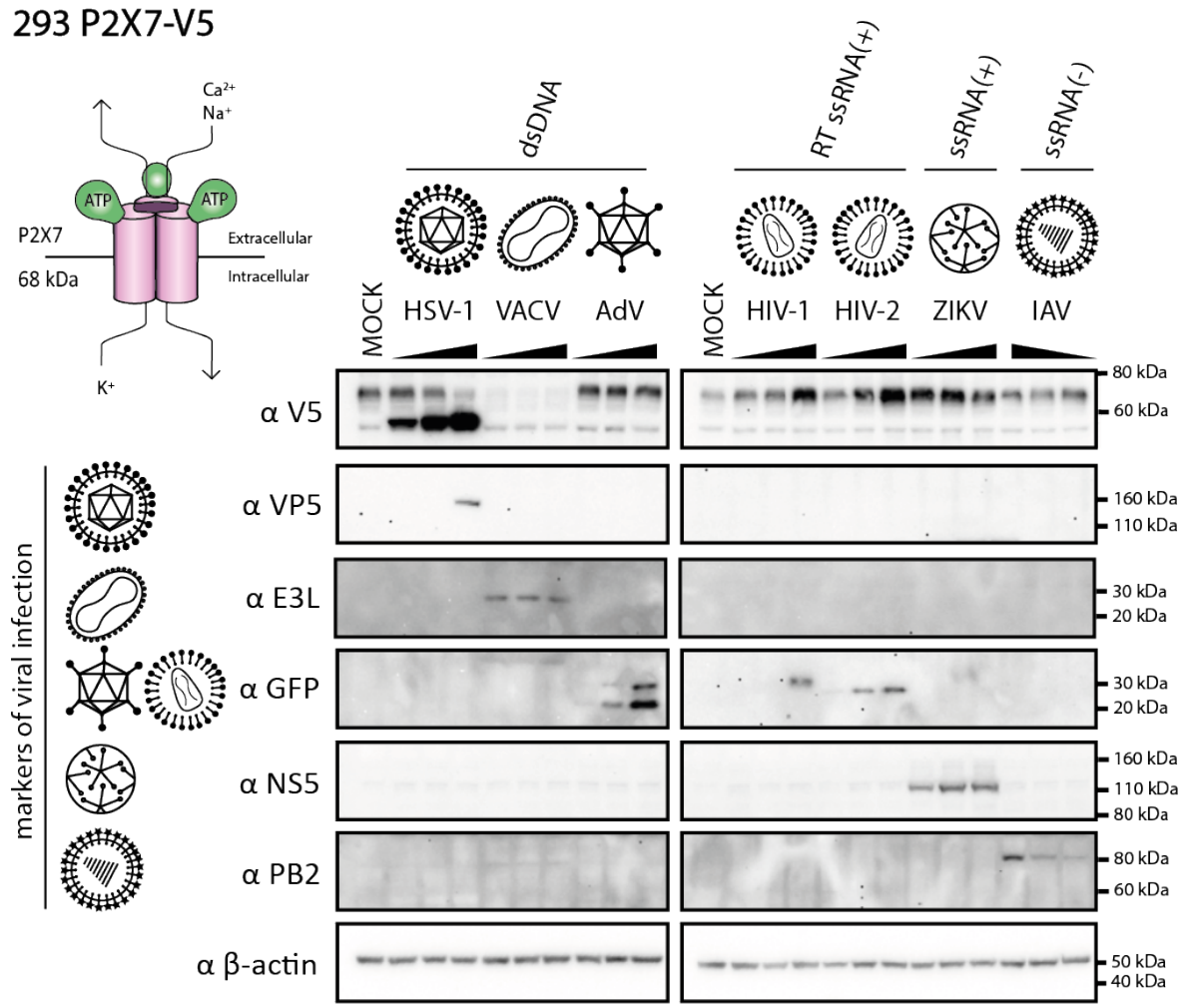


Figure 36 -Screening for viral degradation of P2X7-V5. 293 cells were infected with HSV-1 (MOI – 0.02, 0.006, 0.002), VACV (MOI – 0.2, 0.066, 0.022), AdV (MOI – 1500, 150, 15), HIV-1 (1:10, 1:50, 1:250), HIV-2 (1:10, 1:50, 1:250), ZIKV (MOI – 1, 0.25, 0.06) and IAV (MOI – 10, 5, 2.5). 48 hours later, the cells were lysed and abundance of P2X7-V5 was assessed by western blotting (n=2, biological repeats).

Conversely addition of Urea to SLC46A2 samples enhanced aggregation slightly (Figure 35C). We decided for both SLC19A1 and SLC46A2 lysates we would proceed with a NP40 lysis buffer supplemented with 7M urea. This maintains protein denaturation while still being able to clearly visualise both SLC19A1 and SLC46A2.

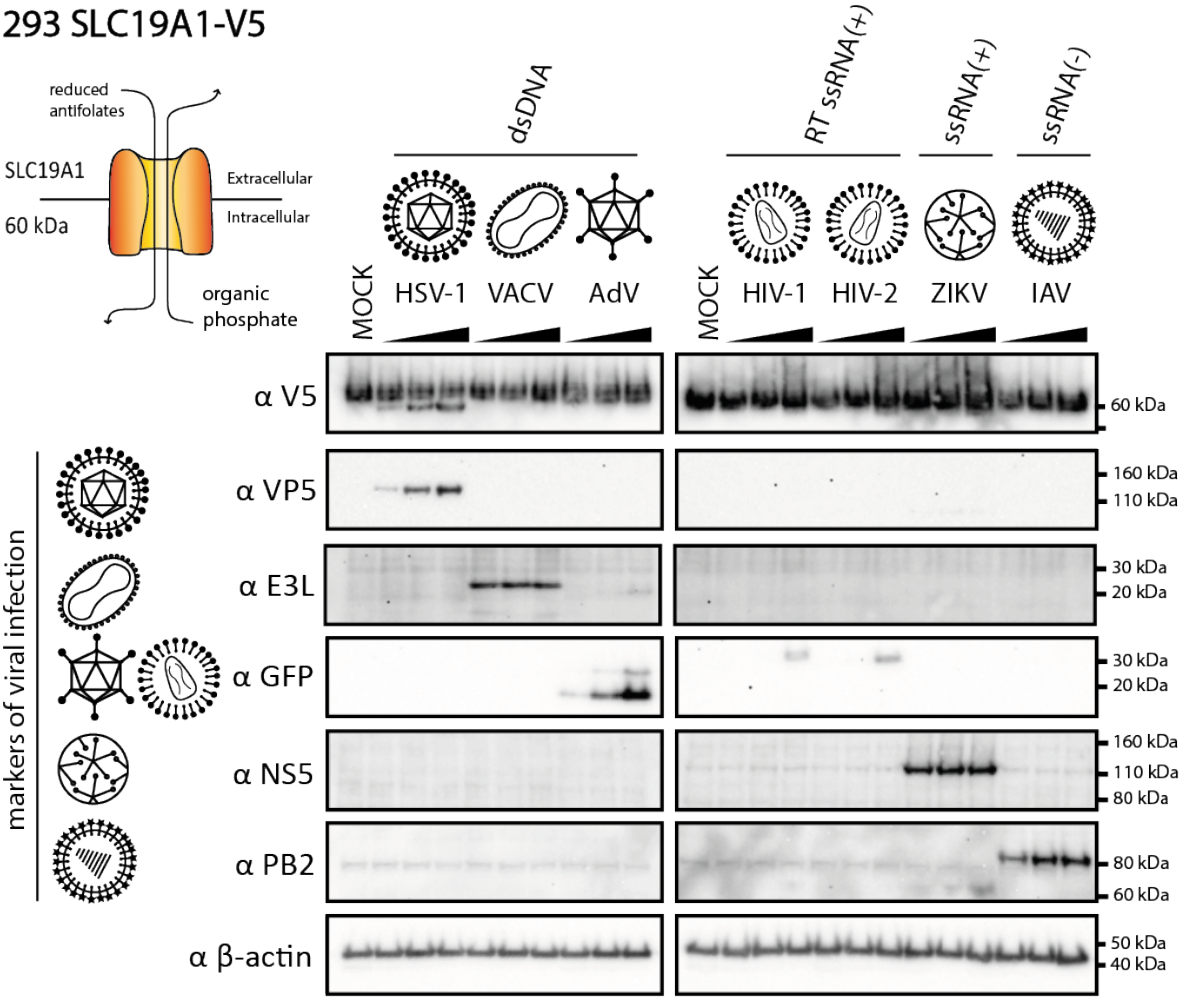


Figure 37 -Screening for viral degradation of SLC19A1-V5. 293 cells were infected with HSV-1 (MOI – 0.02, 0.006, 0.002), VACV (MOI – 0.2, 0.066, 0.022), AdV (MOI – 1500, 150, 15), HIV-1 (1:10, 1:50, 1:250), HIV-2 (1:10, 1:50, 1:250), ZIKV (MOI – 1, 0.25, 0.06) and IAV (MOI – 10, 5, 2.5). 48 hours later, the cells were lysed and abundance of SLC46A2-V5 was assessed by western blotting (n=1).

IV.3 Screening for viruses that degrade overexpressed P2X7, SLC46A2 and SLC19A1

Infection of HEK293 cells with HSV-1, VACV and IAV led to clear and reproducible degradation of P2X7-V5. Interestingly infection with HIV-1 and HIV-2 appeared to increase P2X7 expression (Figure 36). Infection of 293 cells overexpressing SLC19A1-V5 did not appear lead

to degradation by any of the viruses tested (Figure 37). Infection of HEK293 with HSV-1 and VACV led to clear and reproducible degradation of SLC46A2-V5 (Figure 38). A band at ~58 kDa in all HSV-1 infected samples was observed and is assumed to be non-specific binding.

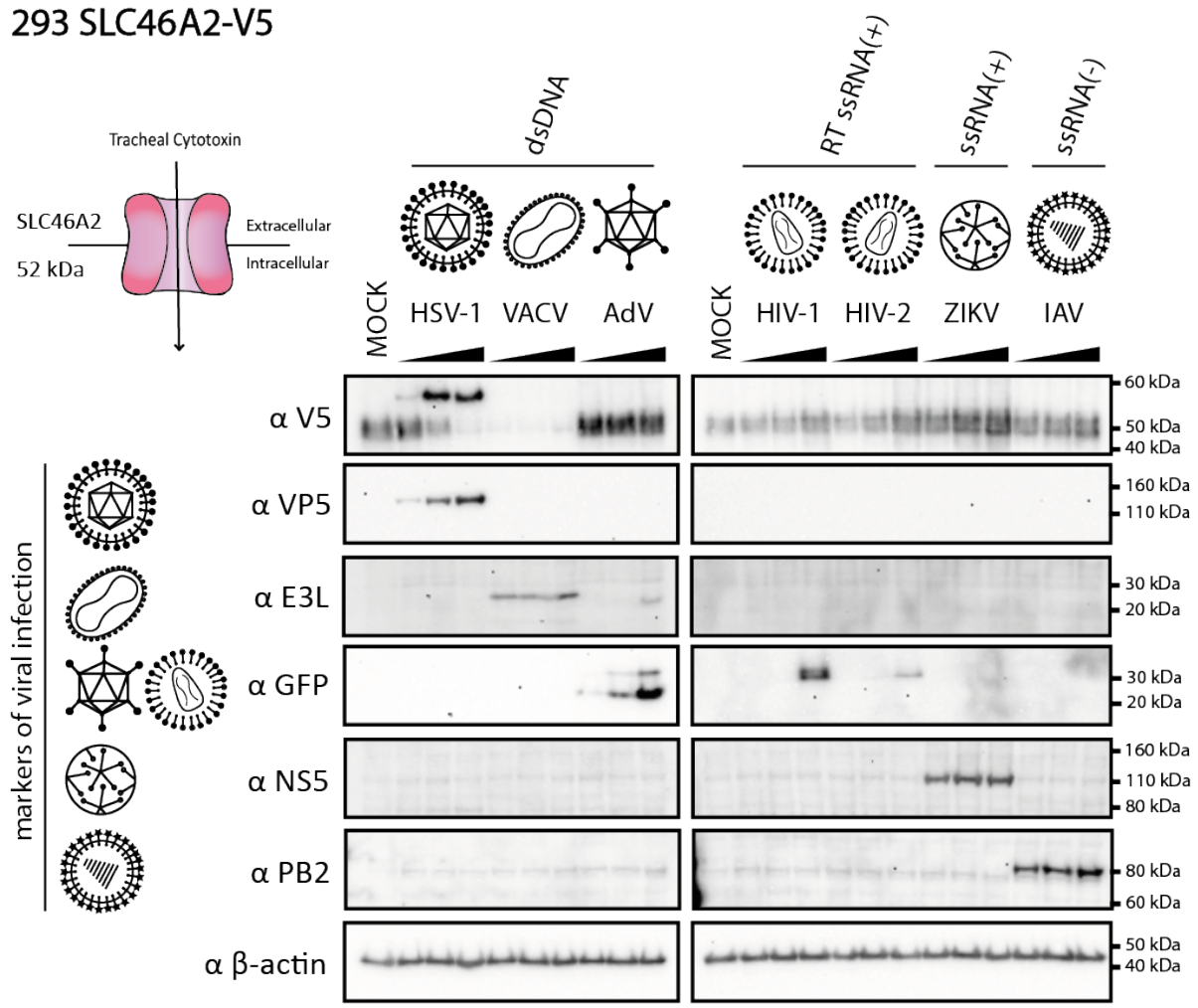


Figure 38 -Screening for viral degradation of SLC46A2-V5. 293 cells were infected with HSV-1 (MOI – 0.02, 0.006, 0.002), VACV (MOI – 0.2, 0.066, 0.022), AdV (MOI – 1500, 150, 15), HIV-1 (1:10, 1:50, 1:250), HIV-2 (1:10, 1:50, 1:250), ZIKV (MOI – 1, 0.25, 0.06) and IAV (MOI – 10, 5, 2.5). 48 hours later, the cells were lysed and abundance of SLC46A2-V5 was assessed by western blotting (n=1).

IV.4 Screening for viruses that degrade endogenous ABCC1

After the viral screens were completed ABCC1 was identified as an additional 2'3'-cGAMP exporter (Maltbaek et al., 2021). We were initially unable to detect endogenous expression of ABCC1. Therefore, we re-probed the membranes from Figure 35 to see if boiling causes aggregation like I observed with SLC19A1 and SLC46A2. We could see that not boiling the

samples significantly aided detection of ABCC1 by western blotting (Figure 39). We were then able to re-probe the membranes from Figures 37 and 38 to see if ABCC1 was degraded during viral infection. We found that none of the viruses tested effected ABCC1 abundance (Figure 40).

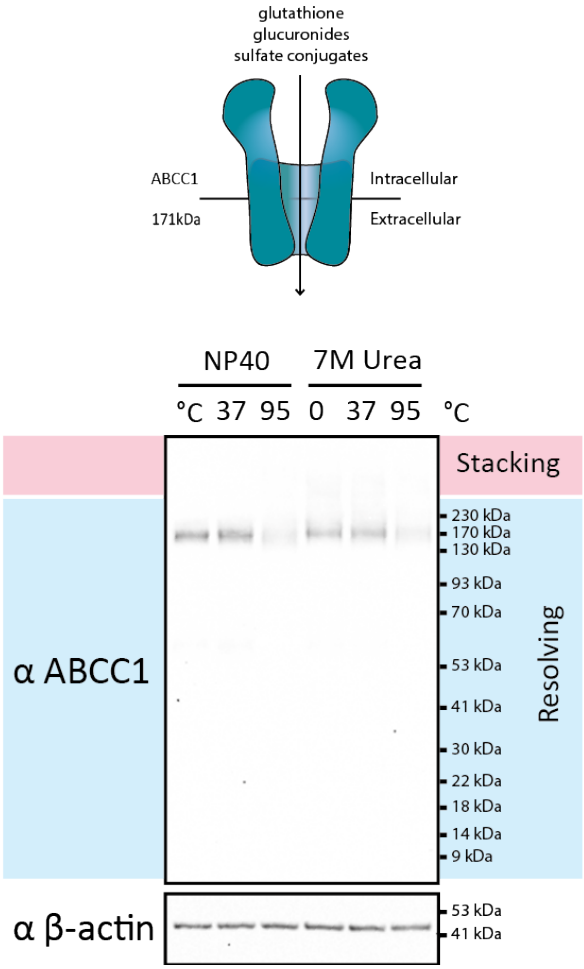


Figure 39 – Resolving ABCC1 by polyacrylamide gel electrophoresis. 293 cell lysates were boiled for 5 minutes at indicated temperatures after lysis in either NP40 buffer or NP40 buffer supplemented with 7M urea. Pink and blue boxes indicate the stacking and resolving portion of the gel (n=3, biological repeats).

IV.5 Discussion

Figure 41 gives a summary of the data presented in chapter IV. Initially we aimed to see if the expression levels of cGAMP channels were modulated during viral infection. Remarkably, many channels were seen to be down regulated during viral infection: P2X7 (by HSV-1, VACV, and IAV), SLC46A2 (by HSV-1, VACV) and LRRC8A:C (by HSV-1). This indicates that cGAMP channels are broadly targeted by viruses. Although it must be acknowledged some of the experiments will need to be repeated to achieve scientific certainty.

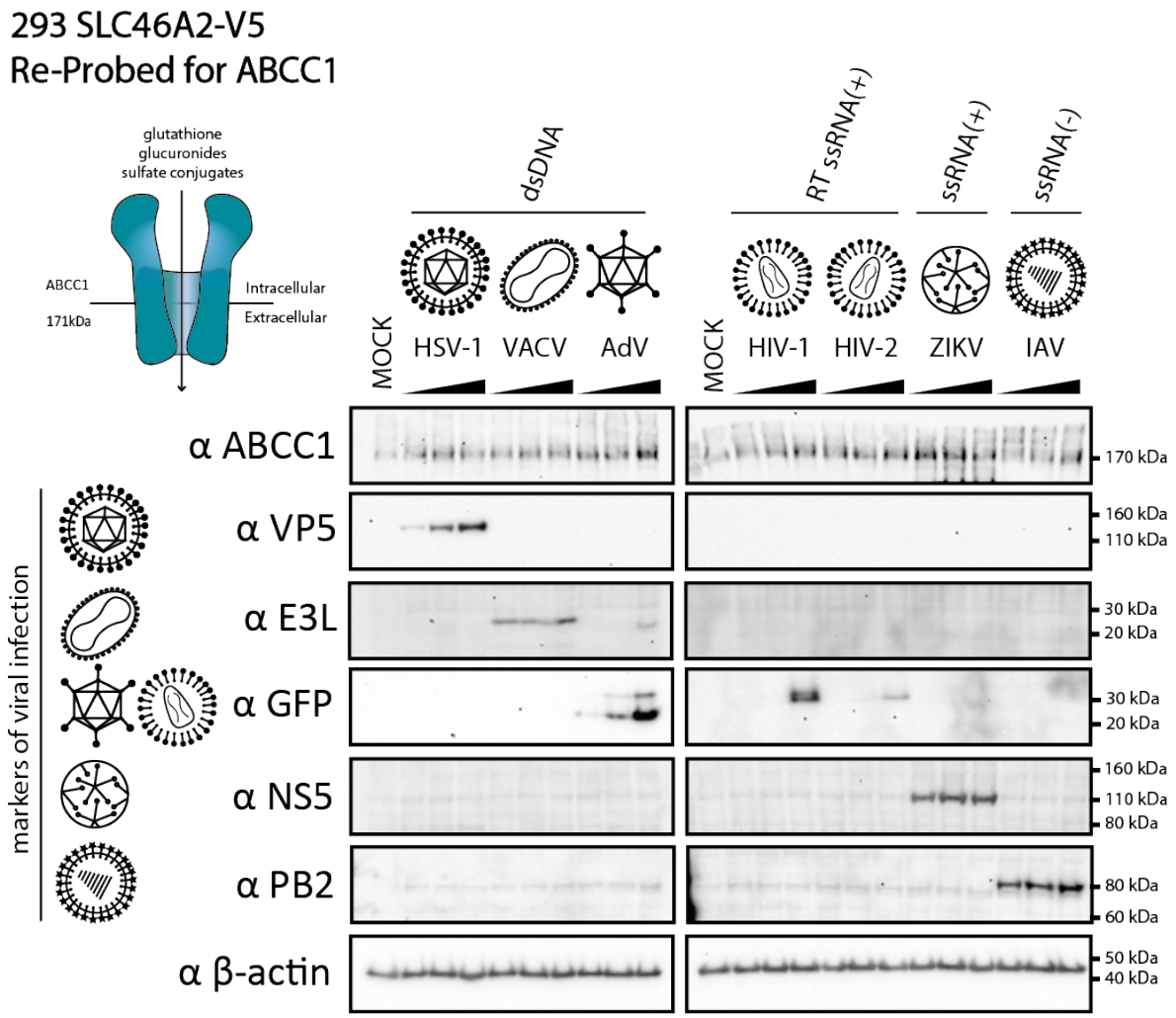


Figure 40 -Screening for viral degradation of ABCC1. 293 cells were infected with HSV-1 (MOI – 0.02, 0.006, 0.002), VACV (MOI – 0.2, 0.066, 0.022), AdV (MOI – 1500, 150, 15), HIV-1 (1:10, 1:50, 1:250), HIV-2 (1:10, 1:50, 1:250), ZIKV (MOI – 1, 0.25, 0.06) and IAV (MOI – 10, 5, 2.5). 48 hours later, the cells were lysed and abundance of ABCC1 was assessed by western blotting (n=2, biological repeats).

Unexpectedly some viruses were seen to increase channel expression upon infection: P2X7 (HIV-1, HIV-2) and SLC46A2 (ZIKV). All cases of viruses increasing channel abundance happened in models of overexpression from lentiviral constructs. Here expression is driven from a non-endogenous human cytomegalovirus promoter. Therefore, channel upregulation could be an artefact of the system used. Especially in the case of HIV-1 and HIV-2 whose encoded genes could directly interact with elements of the lentiviral constructs. How ZIKV increases expression of SLC46A2 remains less clear. Future work would be needed to establish if these viruses increase endogenous P2X7 and SLC46A2 levels and if so the biological consequence of this.

It is unclear why viruses target cGAMP channels not active in cell types they infect. For instance - VACV degrades SLC46A2, a channel only present in monocytes. This cell type is not thought to be infected by VACV (Figure 32). Therefore, what benefit does VACV receive from down regulating monocytically expressed SLC46A2 if it naturally infects neuronal and epithelial cells? There are two possible answers to this question:

1. VACV infects a wider range of cells than is currently known.
2. SLC46A2 is active in a wider range of cells than is currently known.

Similar mismatches between channel activity and viral tropism were observed. Notably HSV-1's downregulation of LRRC8A:C (active in endothelial cells and T cells) and VACV's down regulation P2X7. Future work using in *vivo* models will be crucial to ascertain in which tissues cGAMP channel act to restrict viral replication.

ABCC1 and SLC19A1 were not seen to be modulated during viral infection. Despite this we cannot rule out they are antagonised by another mechanism, or an untested group of viruses. Overall, the data indicates that LRRC8A:C, P2X7 and SLC46A2 are likely the most relevant cGAMP channels during viral infection.

Down regulation of these channel does not prove degradation is to evade cGAS-STING mediated responses. Therefore, it remains to be determined if channel degradation is to evade 2'3'-cGAMP transport or another channel function. For instance - five out of the seven viruses tested modulated the levels of P2X7 during infection. Viral antagonism of this channel may not only be to prevent 2'3'-cGAMP transport but also prevent P2X7 mediated NLRP3 inflammasome activation (Ferrari et al., 1997, Mariathasan et al., 2006, Perregaux and Gabel, 1994). While SLC46A2 was seen to be targeted by both VACV and HSV-1, it remains unknown if SLC46A1 and SLC46A3 are also targeted. If not, the SLC46A1/2/3 redundancy in monocytes may allow a level of 2'3'-cGAMP transport to remain active. Of the seven phenotypes showing channel down regulation six were by the large DNA viruses HSV-1 and VACV. This is likely because their DNA genomes are a more prominent PAMP than the DNA species produced during RNA virus infection, likely making exogenous 2'3'-cGAMP a greater block to viral

replication. Additionally, for both VACV and HSV-1, cGAS has been shown to restrict viral replication during infection (Figure 32) (Zahid et al., 2020, El-Jesr et al., 2020). Remarkably HSV-1 was able to down regulate four out of the five known cGAMP channels.

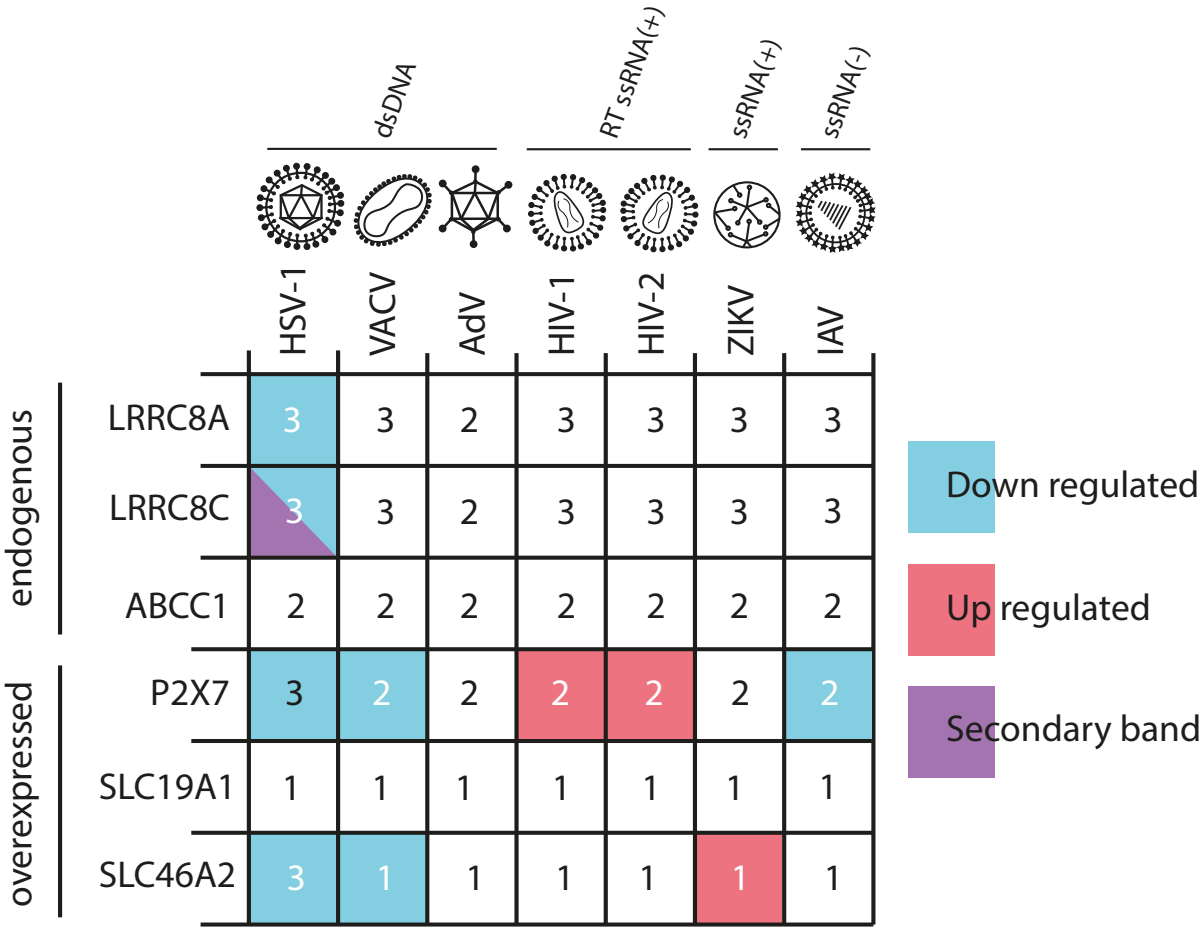


Figure 41 - Summary of cGAMP channel abundance during viral infection with viruses. Values indicate the number of times individual phenotypes were replicated.

Recently two studies have reported that HSV-1 is restricted by exogenous 2'3'-cGAMP. *Lrrc8e-/-* mice (equivalent in terms of 2'3'-cGAMP transport to LRRC8C in humans) are more susceptible to HSV-1 infection due to reduced IFN production (Zhou et al., 2020a). Additionally, mice with the *Enpp1*^{H362A} point mutation, which prevents exogenous 2'3'-cGAMP degradation, are resistant to HSV-1 infection (Carozza et al., 2022). We conclude that HSV-1 mediated degradation of the channels transporting exogenous 2'3'-cGAMP would likely facilitate viral replication. Therefore, we decided to use HSV-1 as a model in future chapters to study viral antagonism of exogenous 2'3'-cGAMP responses.

Chapter V

Antagonism of LRRC8A:C by HSV-1

In the previous section I showed that HSV-1 infection resulted in reduced abundance in three out of five (LRRC8A:C, SLC46A2 and P2X7) known cGAMP channels. HSV-1 most commonly manifests as the cold sore while its closest relative HSV-2 causes genital herpes (Whitley and Baines 2018). It is estimated globally 3752 million people are infected with HSV-1 and 491 million with HSV-2 (James et al. 2020). Aside from cold sores, HSV-1 can cause severe disease such as: herpes encephalitis (19.3% lethality), herpes keratitis, an infection of the cornea that can lead to blindness and systemic infections in neonates with 31% lethality (Hansen et al. 2020; Kimberlin et al. 2001; Rowe et al. 2013). Despite severe cases being rare the virus's high prevalence (67% globally) means the disease burden caused by HSV-1 is great (James et al. 2020). Therefore, an improved understanding of the viral lifecycle could aid treatment of HSV-1 driven disease.

Innate immune sensing of HSV-1's nucleic acids during infection is well described. Within endosomes, TLR2 detects dsDNA and TLR3 detects dsRNA. Within the cytosol, cGAS is considered the preeminent sensor of HSV-1 dsDNA during infection (O'Connor and Sen 2021), driving the production of IFN-β through production of 2'3'-cGAMP to restrict viral replication (see Chapter 1, section I.8.2). Aside from the canonical intracellular 2'3'-cGAMP signalling, extracellular 2'3'-cGAMP has also been shown to restrict HSV-1s replication, as mice possessing mutant ENPP1 (H362A) unable to degrade 2'3'-cGAMP have elevated extracellular 2'3'-cGAMP levels and are resistant to HSV-1 infection in a manner dependent on STING (Carozza et al. 2022). Additionally, in mice LRRC8A:E (equivalent to human LRRC8A:C in terms of 2'3'-cGAMP transport) dependent 2'3'-cGAMP uptake has been shown to confer resistance to HSV-1 infection in a manner dependent on STING (Zhou et al. 2020). Therefore, the down regulation of LRRC8A:C during HSV-1 infection could be a mechanism by which the virus antagonises extracellular 2'3'-cGAMP responses, a phenomenon not previously reported. I decided to use HSV-1 as a model to study viral restriction by extracellular 2'3'-cGAMP. Initially

I focused on HSV-1's antagonism of the LRRC8A:C as it is the only channel known to restrict HSV-1 replication (Zhou et al. 2020).

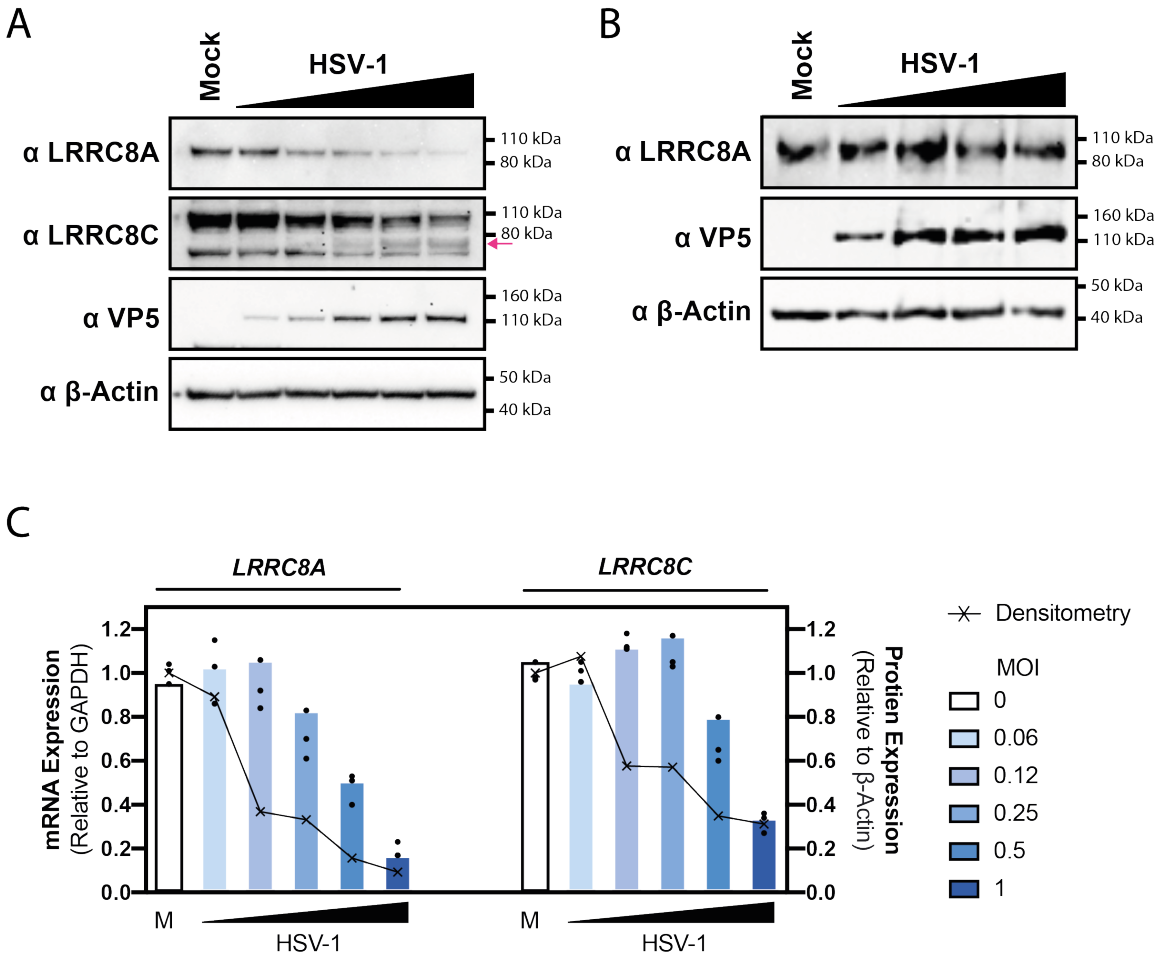


Figure 42 – Human LRRC8A:C is degraded by HSV-1. A) 293 cells were infected with HSV-1 at MOI - 0.06, 0.12, 0.25, 0.5 and 1. 24 hpi cells were lysed and LRRC8A:C abundance was quantification by immunblotting. A pink arrow shows the LRRC8C secondary band (n=3, biological repeats). B) MEFs were infected with HSV-1 at MOI – 1, 10, 30 and 100. 24 hpi cells were lysed and LRRC8A:C abundance was quatified by immunblotting (n=2, biological repeats). C) Total RNA was extracted from cells treated as in A. Expression levels of LRRC8A:C were determined by RT-qPCR with samples assayed in technical triplicates. Data were analysed by the comparative Ct method. Densitometry from A is plotted on the right hand Y axis (n=1).

V.1 HSV-1 targets human LRRC8A

I initially confirmed LRRC8A and LRRC8C abundance in HEK293 cells infected with HSV-1 is reduced in a dose-dependent manner (Figure 42A). Additionally, I observed a band at ~80 kDa that appears below LRRC8C upon HSV-1 infection (Figure 42A). I speculate this could be an LRRC8C degradation product. No down regulation of LRRC8A was detected in MEFs infected

with HSV-1 (Figure 42B), suggesting that HSV-1 could not down regulate murine LRRC8A. It is known HSV-1 encodes the virus host shut off protein (vhs), which indiscriminately degrades mRNAs to favour the translation of viral proteins (Oroskar and Read 1987; Read and Frenkel 1983). To test if vhs cause LRRC8A/C down regulation through global mRNA depletion I performed a dose titration of virus to determine the kinetics of mRNA vs protein degradation. I observed that the reduction in *LRRC8A* and *LRRC8C* mRNA was preceded by the reduction in protein abundance (Figure 42C). This suggested that vhs was not responsible for the initial reduction in LRRC8A and LRRC8C protein.

V.2 Identifying HSV-1 genes potentially involved in LRRC8A:C depletion

I next hypothesised that HSV-1 may encode a protein that targets LRRC8A:C for degradation. To identify the viral gene responsible for LRRC8A:C depletion, firstly, I aimed to identify the kinetic class the gene belongs to. Herpesviruses regulate gene expression temporally with genes allocated to kinetic classes of immediate early (α), early (β), leaky late (γ_1) and true late (γ_2). Infection starts with expression of immediate early genes encoding proteins that transcriptionally control early gene expression (Ibáñez et al. 2018). Early genes both instigate viral genome replication and regulate the expression of late genes. Late genes are divided into two classes: leaky late expressed directly after early genes and true late expressed only upon genome amplification (Figure 43) (Gruffat, Marchione, and Manet 2016). A time course of infection showed degradation of LRRC8A and LRRC8C and the appearance of the potential LRRC8C degradation product occurred at ~12 hpi. This coincides with expression of the prototypical late gene VP5 (Figure 43A, B and C). This suggested that the viral protein mediating LRRC8A degradation is in the late kinetic class. HSV-1 is one of three α herpesviruses that infect humans (Figure 44A). I considered whether the two other α herpesviruses – VZV and HSV-2 – also degraded LRRC8A. I found HSV-2 down regulated LRRC8A (Figure 44B). Despite the fluid within chicken pox and shingles blisters being highly infectious, VZV remains highly cell associated in *vitro* (Leclair et al. 1980; Josephson and Gombert 1988). Therefore, due to the lack of cell free VZV stocks at a significant titre co-

culture models are used (Caunt and Taylor-Robinson 1964; Grose and Brunel 1978). Here, VZV infected MeWo cells are seeded on top of uninfected MeWo cells. 1 hour after the cells have come into contact, the infected cells are removed by washing with PBS leaving VZV infection to progress. Using this model, I observed that VZV was unable to down regulate LRRC8A (Figure 44C). This suggests HSV-2 but not VZV degrades LRRC8A. I assumed the viral gene targeting LRRC8A:C was therefore likely present in HSV-1 and HSV-2 but not VZV. I compiled a list of the HSV-1, HSV-2 and VZV homologs and their reported kinetic classes (supplementary Table 3). There are 14 viral genes that are present in the HSV- 1 and HSV-2 genome but not in the VZV genome. 12 of these are in the late kinetic class.

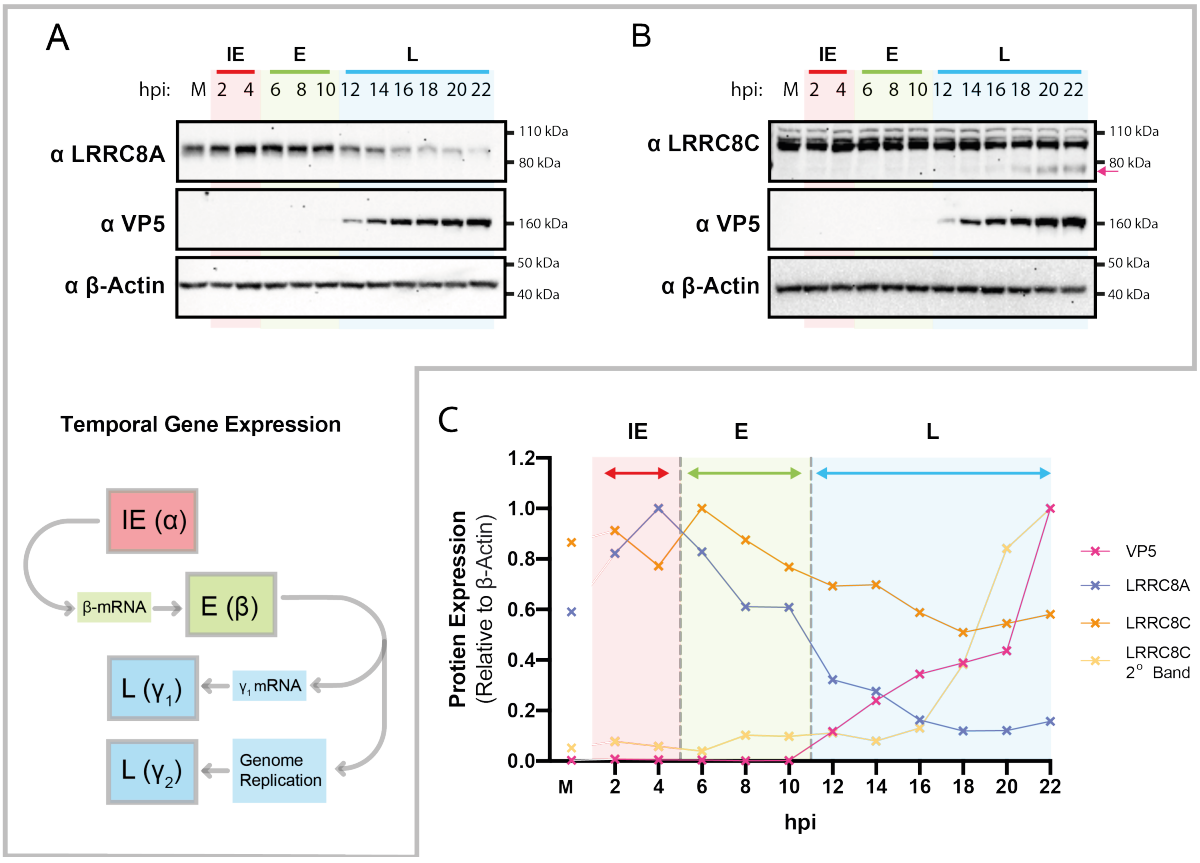


Figure 43 - LRRC8A:C is degraded late during HSV-1 infection. 293 cells were infected with HSV-1 at MOI 1 and lysed at the indicated time points. LRRC8A (A) and LRRC8C (B) abundance was then assessed by immunoblotting. A schematic showing the mechanism by which herpes viruses regulate there genome is also displayed (n=2, biological repeats). C) Densitometry from A and B.

I next aimed to immunoprecipitate LRRC8A and LRRC8C from HSV-1 infected cells to identify HSV-1 proteins interacting with LRRC8A:C during infection. In HEK293 cell lines that stably express LRRC8A and LRRC8C with a C-terminal V5 tag, immunoprecipitation was successful

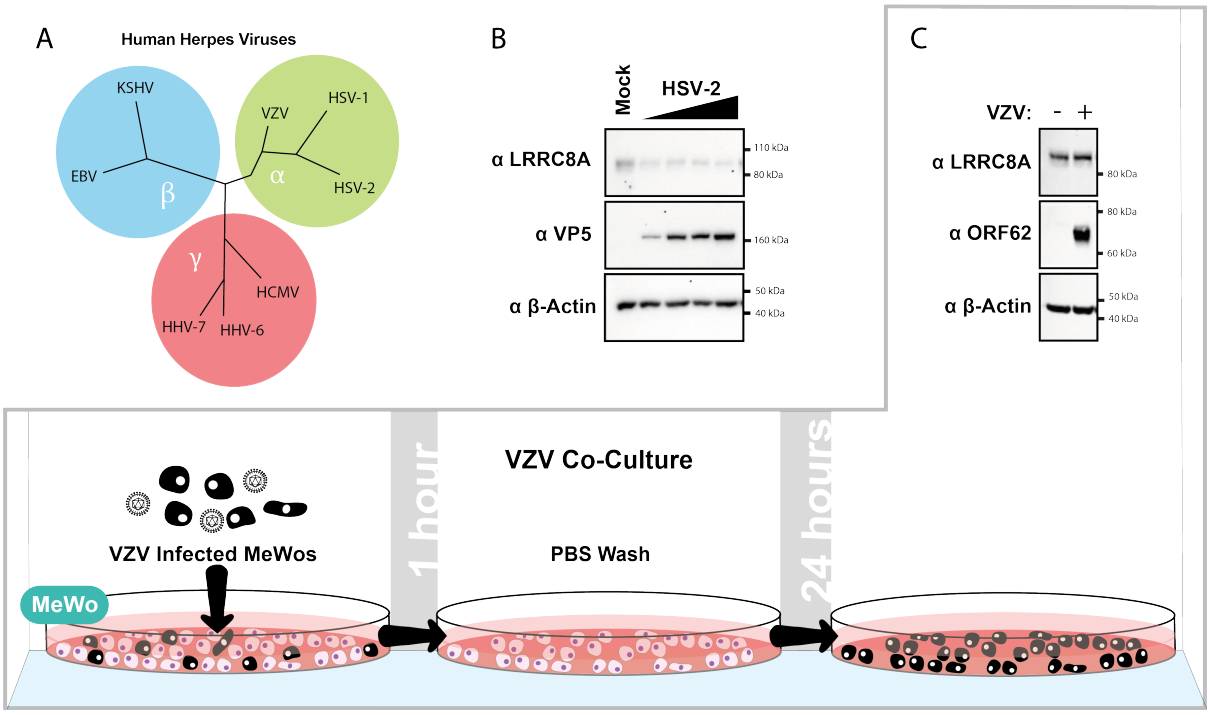


Figure 44 – HSV-2 but not VZV degrade LRRC8A:C. (A) Schematic showing phylogeny of human herpes viruses. (B) 293-T cells were infected with HSV-2 at MOI - 1, 3, 5, and 10. 24 hpi cells were lysed and LRRC8A:C abundance was assessed by immunblotting (n=2, biological repeats). (C) VZV infected MeWo cells were seeded on top of uninfected MeWo (1 infected cell : 5 seeded cells). 1 hour later the infected MeWos were washed off with PBS. 24 hours after VZV exposure cells were lysed and LRRC8A:C abundance was assessed by immunoblotting (n=3, biological repeats).

following HSV-1 infection (Figure 45A and B). The samples were resolved on polyacrylamide gels and stained with silver nitrate to visualise co-immunoprecipitating proteins. LRRC8A did not appear to precipitate with any other proteins upon HSV-1 infection (Figure 45A). In contrast, LRRC8C precipitated with many unidentified proteins not present in uninfected cells (Figure 45B). I then used quantitative mass spectrometry to identify the peptides associated with LRRC8C in HSV-1 infected cells (Figure 45C and supplementary Table 4). Known binding partners LRRC8C were highly enriched within the IP – LRRC8A, LRRC8D and LRRC8E. Additionally, many of other peptides were identified. Notably G3BP1 PCBP1 and ZCCHC3, which are known as co-sensors for cGAS (Lian et al. 2018; Liao, Lei, and Shu 2020; Liu et al. 2019). Also detected were peptides associated with the DNA-PK complex - NONO, PSPC1 and SFPQ (Figure 45 and supplementary Table 4) (Morchikh et al. 2017). 40 HSV-1 proteins were detected in the infected IP, all of which were enriched upon infection. This is not surprising as in the uninfected sample HSV-1 peptides will be absent. As many HSV-1 proteins were present at low abundance, I excluded genes within the lowest 3% of host proteins abundance scores, setting this as the abundance limit (AL) to remove background HSV-1 proteins

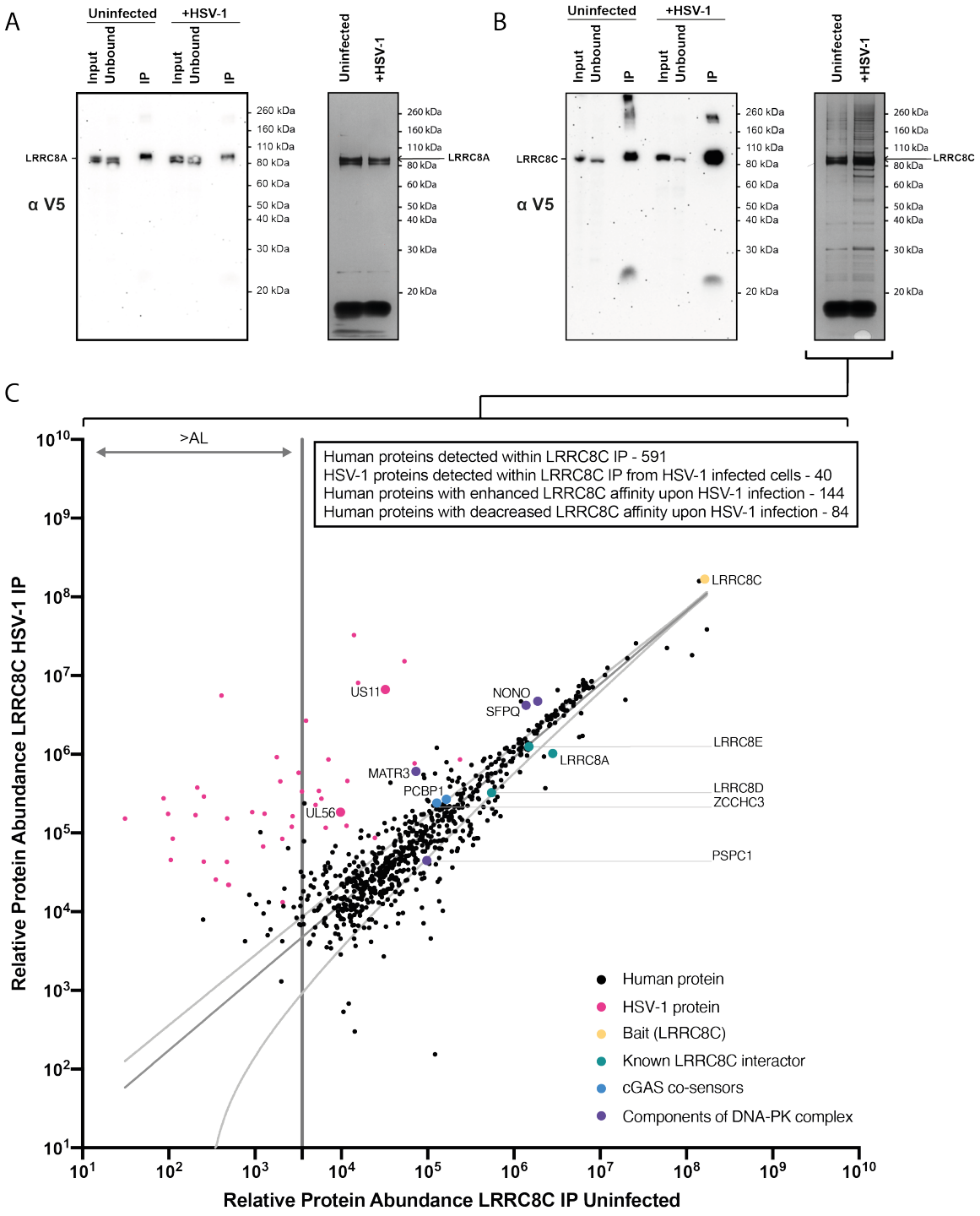


Figure 45 – Immunoprecipitation of LRRC8C from HSV-1 infected cells. HEK239 cells stably over expressing LRRC8A-V5 (A) or LRRC8C-V5 (B) were infected with HSV-1 at MOI 10. 8 hpi cells were lysed and immunoprecipitated with an α-V5 antibody. Input unbound and IP were subjected to immunoblotting (n=2, biological repeats). The LRRC8C IP samples were analysed by mass spectrometry. PEAKS software was used to identify peptides and align them to the Human UniProt Swissprot database (Alignment ID - 20210911_seq23155) and HSV-1 genome (NCBI database - NC_001806). The progenesis label free quantification software was used to assign relative values of protein abundance. The abundance limit (AL) was set to exclude lowest 3% of host proteins. Nonlinear regression shows average protein abundance where proteins above are enriched and below depleted in HSV-1 infected cells. Peripheral lines show the 95% confidence limits. Proteins associated with DNA-PK, cGAS or LRRC8C are annotated (n=1).

detectable but not truly associated with LRRC8C. Of the 12 viral proteins of interest, 3 appeared to be pulled down with LRRC8C from HSV-1 infected cells – UL56, US6 and US11 (Figure 46 and Supplementary Table 3).

V.3 UL56 degrades LRRC8A:C

The information gathered in Figures 43, 44 and 45 identified 3 genes potentially involved in LRRC8A:C degradation (Figure 46). UL56 has previously been reported to target multiple cellular proteins for proteasomal degradation by recruiting NEDD4 E3 ubiquitin ligases through its PPXY motifs (Soh et al. 2020). Most notably, UL56 degrades GOPC which traffics many transmembrane proteins from the Golgi apparatus to the plasma membrane (Figure 47) (Cheng et al. 2002). This leads to global down regulation of transmembrane proteins at the cell surface. As LRRC8A and LRRC8C have transmembrane domains and are expressed at the cell surface, I initially tested if UL56 was responsible (Deneka et al. 2018). To do this, a UL56 construct with an N terminal GFP tag was transfected into HEK293 cells. To exclude bulk effects, cells were then sorted into GFP+ and GFP- populations by fluorescence activated cell sorting (FACS). UL6, the viral portal complex was included as a negative control. UL56 but not UL6 was observed to degrade both LRRC8A and LRRC8C (Figure 48A). An engineered HSV-1 kindly donated by Colin Crump missing *UL56* was shown to be unable to degrade LRRC8A and

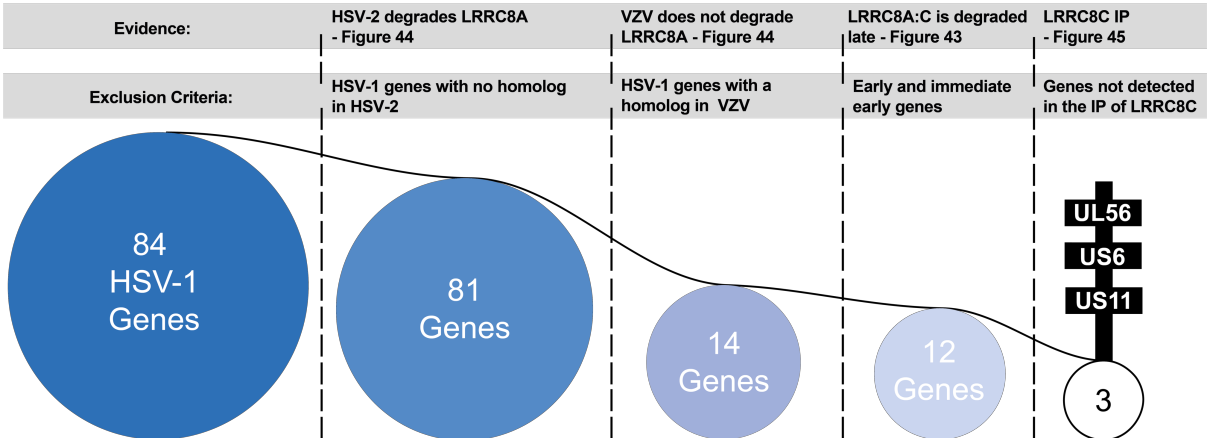


Figure 46 – Narrowing down HSV-1 genes responsible for LRRC8A:C degradation. Schematic showing how the pool of 84 HSV-1 genes was narrowed down to 2 candidate genes using the information gathered in Figure 43, Figure 44, and Figure 45.

LRRC8C during infection (Figure 48B). This shows that *UL56* is both necessary and sufficient for degradation of LRRC8A:C during HSV-1 infection. Additionally, mutation of UL56's three PPXY motifs to AAXA rescued LRRC8A and LRRC8C levels (Figure 48B). This suggests that E3 ligase recruitment is crucial to channel degradation.

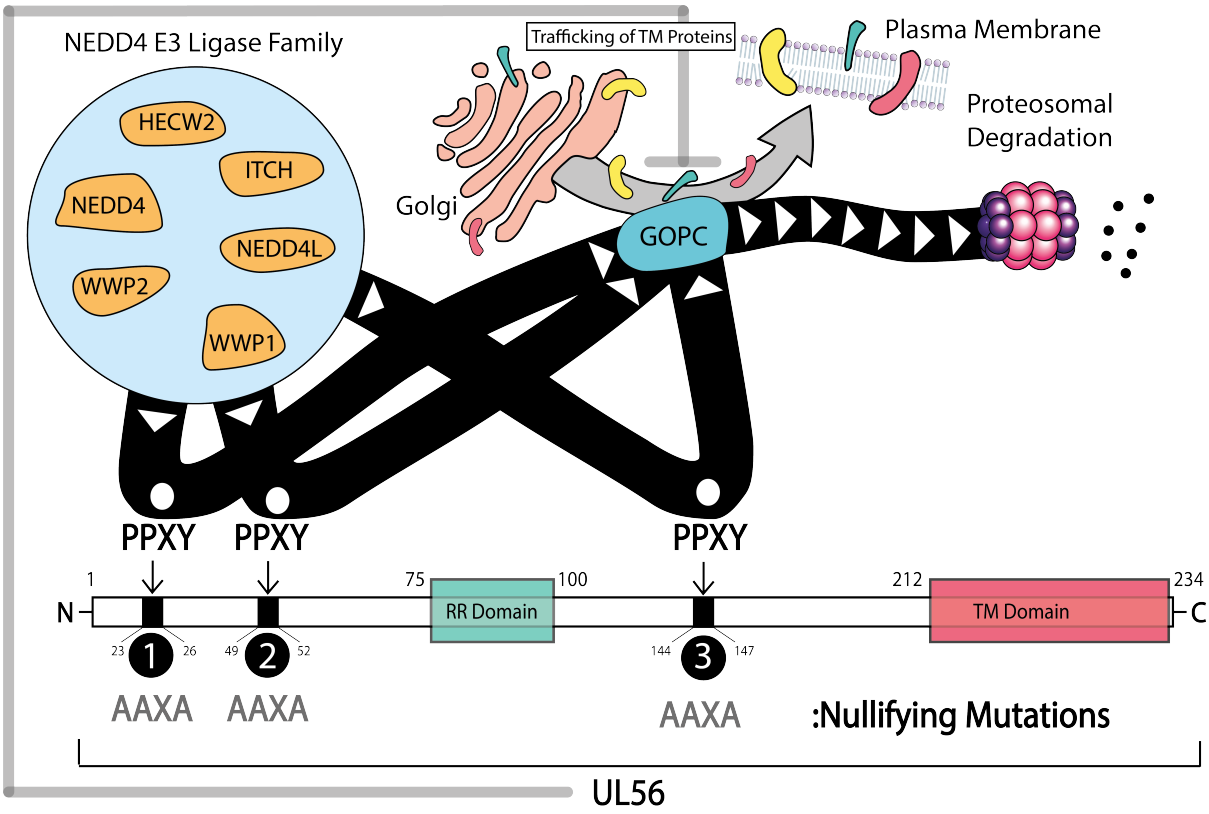


Figure 47 – Known functionality of UL56. The arginine rich region (RR) and transmembrane (TM) domain are annotated. PPXY motifs recruit NEDD4 family E3 ligases to ubiquitinate multiple cellular targets. One known target, the trafficking molecule GOPC, is targeted for proteasomal degradation. Mutation of PPXY motifs to AAXA nullifies UL56 mediated NEDD4 E3 ligase activity.

V.4 LRRC8A:C is degraded by the proteasome

Degradation of GOPC by UL56 leads to depletion of many transmembrane proteins unable to traffic towards the cell membrane (Figure 47). Therefore, I tested if GOPC expression was crucial to LRRC8A:C expression. I generated GOPC KO HEK293 single cell clones using lentivirally encoded CRISPR constructs and tested if LRRC8A and LRRC8C were expressed. GOPC KO was not observed to effect expression of LRRC8A and LRRC8C (Figure 49A). Therefore, during HSV-1 infection LRRC8A and LRRC8C degradation is unlikely to be caused by the absence of GOPC. This suggests that LRRC8A and LRRC8C are likely directly targeted

for degradation by UL56. To test if like GOPC LRRC8A and LRRC8C were proteasomally degraded, I treated HSV-1 infected cells with the proteasome inhibitor lactacystin (Fenteany et al. 1995). Drug treatment partially rescued LRRC8A and LRRC8C abundance suggesting UL56 may direct LRRC8A and LRRC8C for proteasomal degradation (Figure 49B). Although it must be acknowledged lactacystin also reduced the abundance of the viral protein VP5 indicating HSV-1's replication may be inhibited. Therefore, in terms of the degradative mechanism no firm conclusion can be drawn.

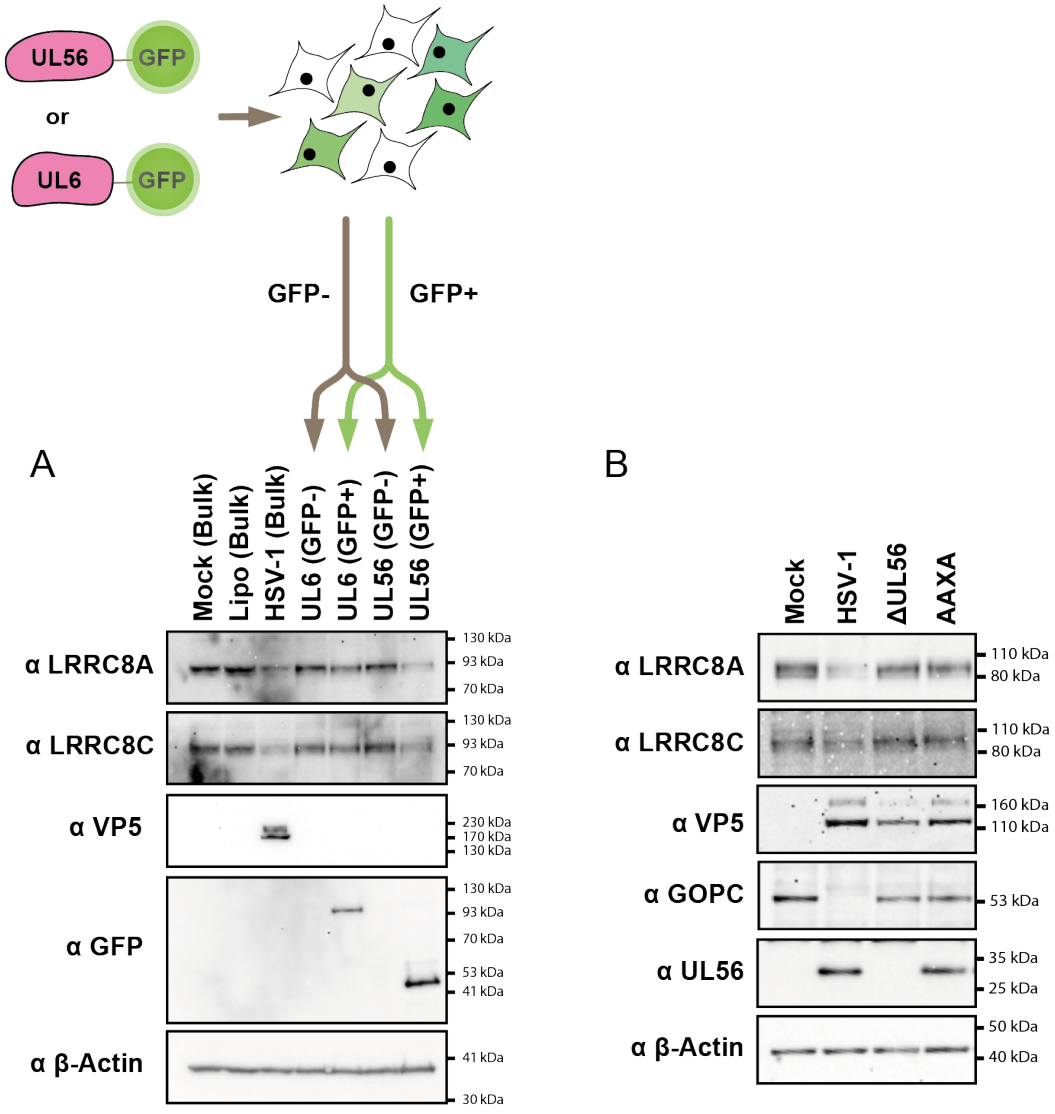


Figure 48 – UL56 is necessary and sufficient for LRRC8A:C degradation. A) HEK293 cells were transiently transfected with constructs expressing UL56-GFP or UL6-GFP. To exclude bulk effects, 24 hours after transfection cells were sorted into GFP- and GFP+ populations by FACS sorting. Gating strategy is shown in supplementary Figures 4 and 5. Mock, lipofectamine treated and HSV-1 infected cells (MOI 3 for 24 hours) were lysed without sorting (n=3, biological repeats). B) HEK239 cells were infected with the indicated HSV-1 genotypes (MOI 3) for 24 hours before lysis (n=3, biological repeats). In both cases western blotting was used to assess LRRC8A:C abundance.

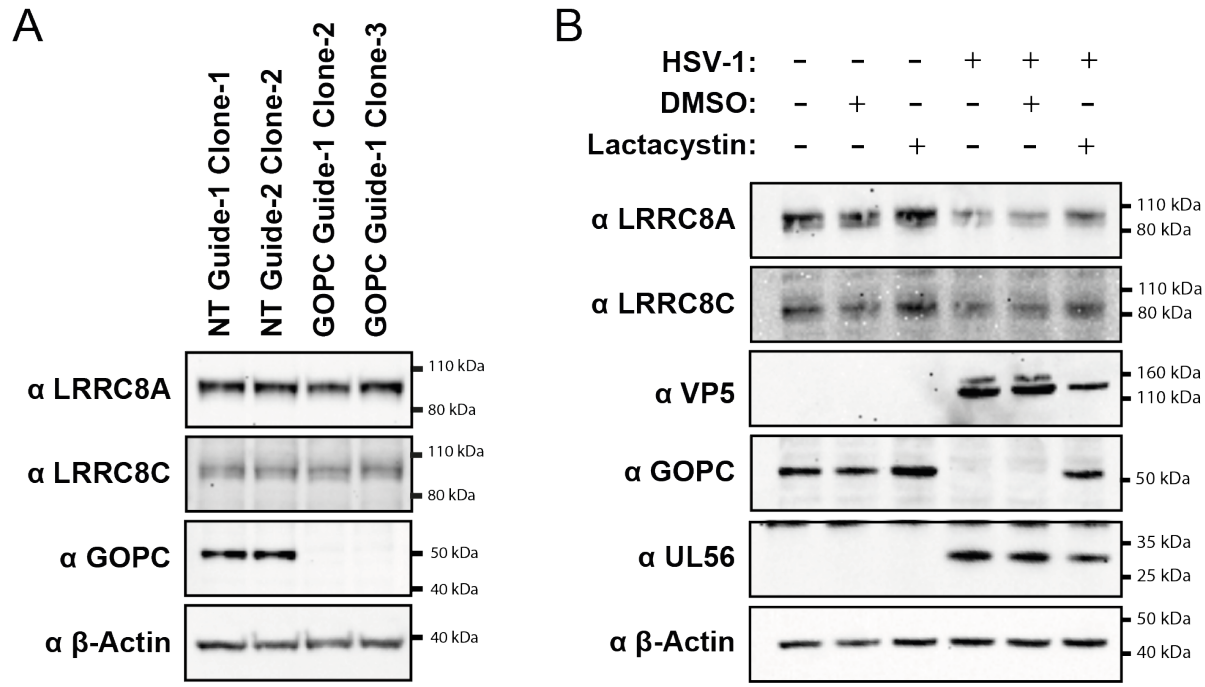


Figure 49 – LRRC8A:C is potentially proteasomally degraded. HEK293 GOPC knockout cell lines were lysed and western blotting was used to assess LRRC8A:C abundance (n=3, biological repeats). HEK293 cells were infected with HSV-1 (MOI 3) and one hour later treated with the proteasomal inhibitor lactacystin (20μm). 24 hpi western blotting was used to assess LRRC8A:C abundance (n=2, biological repeats).

V.5 In *vitro* LRRC8A:C 2'3'-cGAMP uptake assay

Having shown UL56 overexpression leads to LRRC8A:C degradation, I aimed to show this results in reduced 2'3'-cGAMP uptake and IFN-β induction. To do this, I utilised a previously described dual luciferase assay to measure IFN-β promoter induction upon 2'3'-cGAMP treatment (Bridgeman et al. 2015). Here, 293T cells are transfected with 3 plasmids. The first, pRL-TK, constitutively expresses renilla luciferase. The second, p125-F-Luc, expresses firefly luciferase under the control of a minimal IFN-β promoter. Therefore, firefly luminescence is a read out for IFN-β induction. Firefly values are divided by renilla readings to normalise for transfection efficiency. Cells are simultaneously transfected with pcDNA3.2 STING, which expresses STING that is endogenously absent from HEK293Ts. The LRRC8A channel is activated by reduced osmolarity (Qiu et al. 2014; Voss et al. 2014). Therefore, cells were treated with low salt buffer containing 2'3'-cGAMP to test if this increased IFN-β induction (Figure 50). I observed reducing salt and increasing 2'3'-cGAMP concentration synergised to promote IFN-β production (Figure 51). This could be significantly inhibited with the LRRC8A

specific inhibitor DCPIB (Figure 51) (Friard et al. 2017). I also produced LRRC8A KO HEK293 single cell clones using lentivirally encoded CRISPR constructs (Figure 52A). LRRC8A KO prevented IFN-β induction in response to 2'3'-cGAMP (Figure 52B). This demonstrates I have developed a model for LRRC8A:C mediated 2'3'-cGAMP uptake in HEK293T cells.

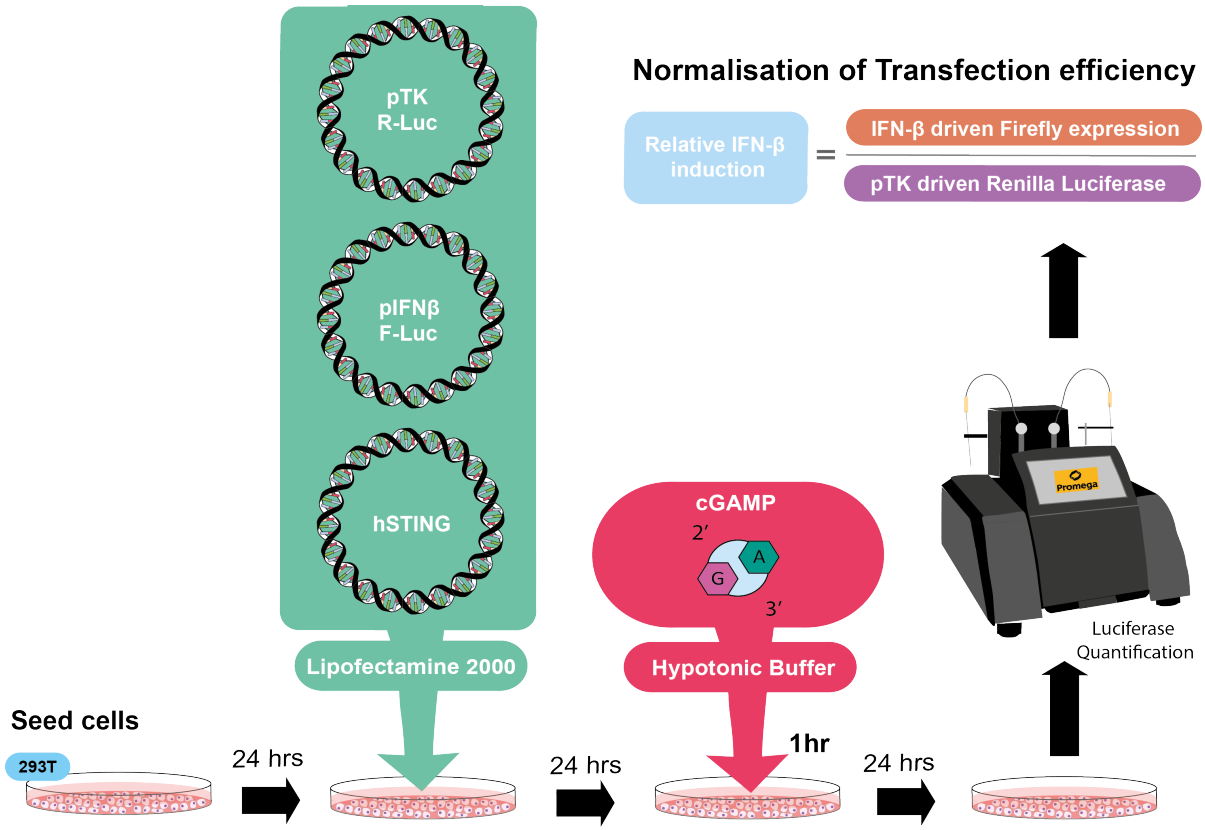


Figure 50 - Schematic showing dual luciferase assay. HEK293T cells were transfected with p125-FLuc expressing firefly luciferase under an IFN-β promoter, pRL-TK expressing renilla luciferase under an TK promoter and pcDNA3.2-STING constitutively expressing STING. 24 hours after transfection cells were then treated with 2'3'-cGAMP in a hypotonic buffer to active LRRC8A:C. Luminesce was then read with firefly (indicative of IFN-β production) being divided by renilla to normalise for transfection efficiency.

V.6 UL56 antagonises 2'3'-cGAMP uptake

Using the model of LRRC8A:C mediated 2'3'-cGAMP uptake developed in the previous section, I tested if UL56 blocked 2'3'-cGAMP import. For this purpose, I produced HEK293T cells that stably overexpress UL56 or UL56 PPXY motif mutants (Figure 53A). Overexpression of UL56 was observed to significantly reduce LRRC8A abundance which was rescued if all three PPXY motifs were muted to AAXA (Figure 53A and B). Similarly, IFN-β induction by low salt buffers

containing 2'3'-cGAMP was significantly reduced in cells overexpressing UL56 and rescued if all three PPXY motifs were mutated to AAXA (Figure 53C). This suggests that the three PPXY motifs are redundant in function, and each contribute to LRRC8A:C degradation. Importantly, this experiment demonstrates that UL56 prevented 2'3'-cGAMP import into cells. Unexpectedly although all UL56 constructs were detected some were expressed to higher levels than others (Figure 53A). Notably the UL56-AAXA123 construct was expressed to a much higher level. Speculatively, this may be because UL56 is proteasomally degraded alongside host proteins it targets, an effect that would be dependent upon PPXY motif mediated recruitment of NEDD4 ligases. Despite differences in expression level, as UL56-AAXA-123 was expressed to the highest level and had no effect on LRRC8A:C degradation or 2'3'-cGAMP uptake I do not believe this affects the conclusions made.

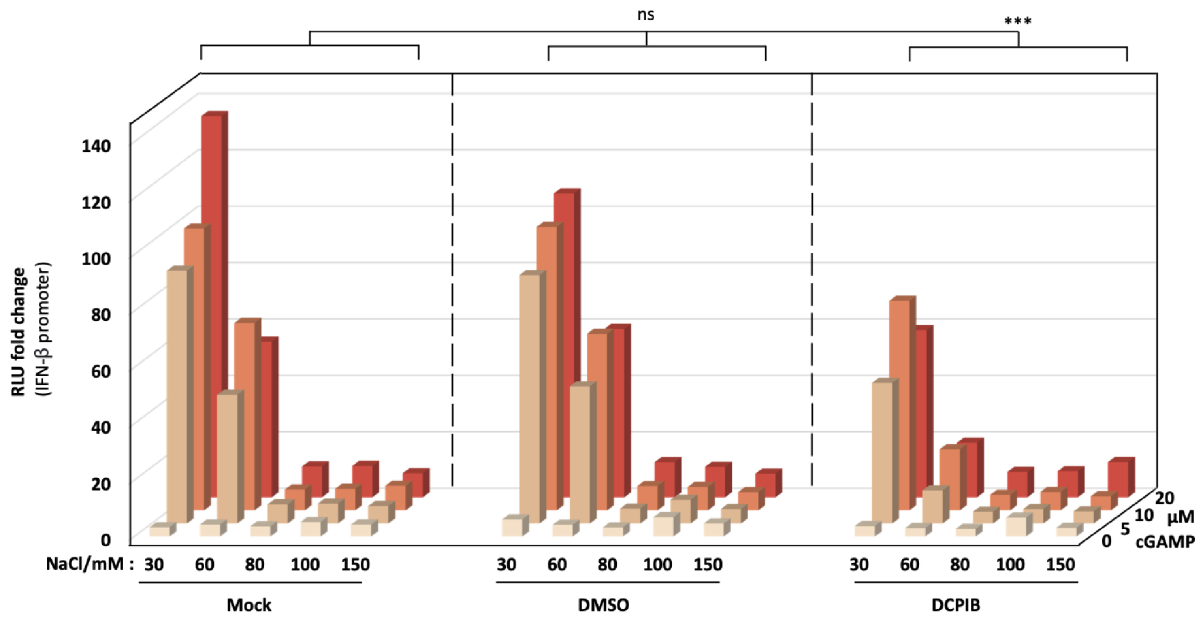


Figure 51 – Chemical inhibition of LRRC8A:C mediated 2'3'-cGAMP uptake. HEK293T cells were transfected with p125-FLuc (IFNβ promoter reporter), pRL-TK (constitutively expresses renilla luciferase) and pcDNA3.2 STING. IFN-β production was then assessed in response to low salt (NaCl) buffers containing 2'3'-cGAMP. Cells were also treated with DCPIB (20uM) or the vehicle control (DMSO). Graphs display average of three technical replicates statistically evaluated with grouped two-way ANOVA – Tukey. *=p<0.05, **=p<0.01, ***=p<0.001, ****=p<0.0001, ns=not significant (n=3, biological repeats, representative dataset).

V.7 Discussion

I was initially able to show that HSV-1 depletes LRRC8A:C in a mechanism independent of vhs. Coupling proteomic mass spectrometry with in *vitro* analysis of HSV-1's close relatives (VZV and HSV-2) and the kinetics of LRRC8A:C degradation, I identified UL56. Interestingly, I also

observed that LRRC8C immunoprecipitated with three known cGAS co-sensors (G3BP1, PCBP1 and ZCCHC3) and components of the DNA-PK complex (PSPC1, NONO and SFPQ) (Liu et al. 2019; Liao, Lei, and Shu 2020; Lian et al. 2018; Morchikh et al. 2017). This was unexpected and, although the proteomic mass spectrometry needs to be validated, it is interesting to speculate that LRRC8A:C activity may be modulated by the DNA sensing machinery. Using both overexpression and reverse genetics (HSV-1 ΔUL56), I was able to show UL56 was necessary and sufficient for LRRC8A:C degradation. Additionally, I was able to show by mutation UL56's three PPXY motifs were crucial for LRRC8A:Cs degradation. UL56 globally down regulates transmembrane protein expression at the plasma membrane by degradation of the trafficking molecule GOPC (Soh et al. 2020). I showed LRRC8A:C expression was not

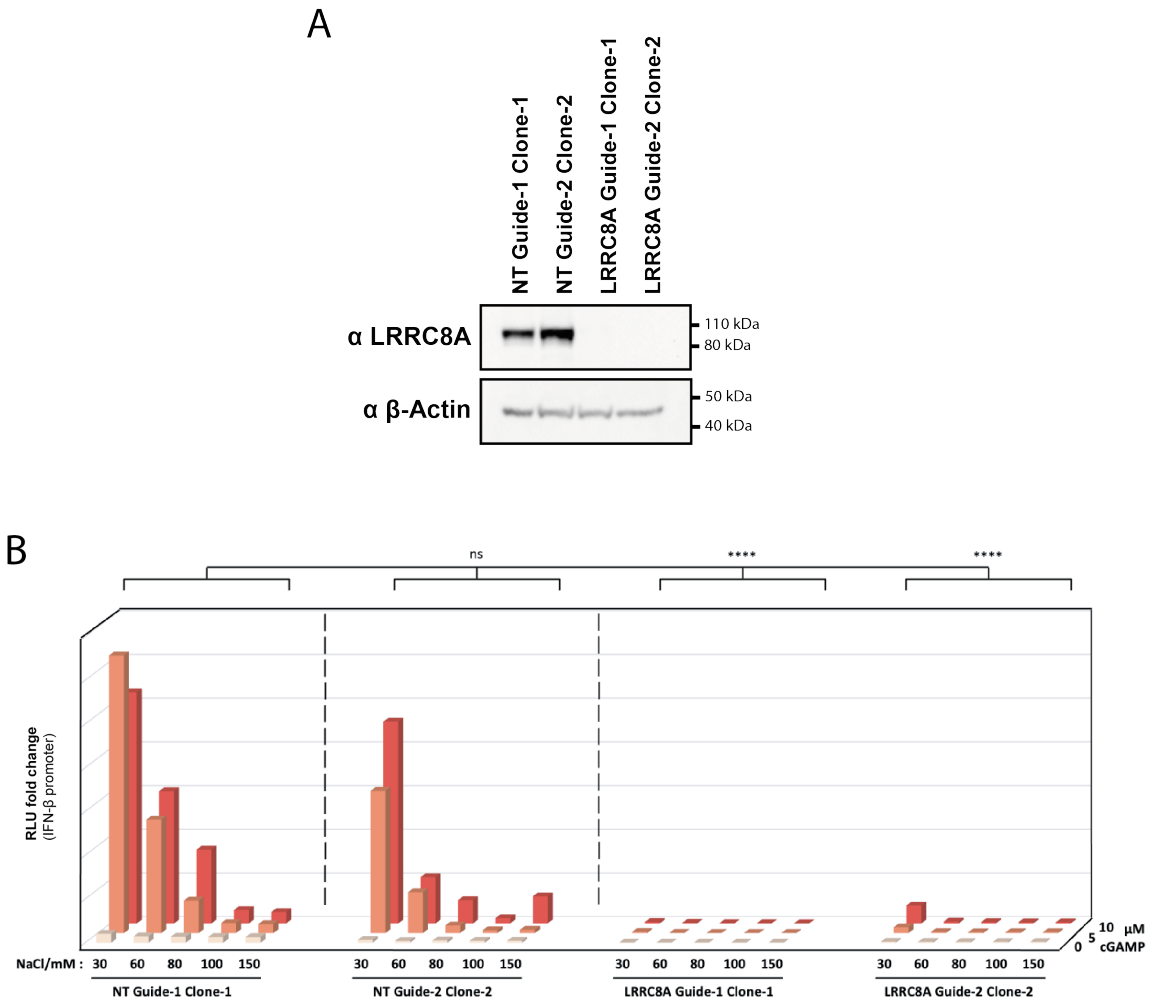


Figure 52 – LRRC8A is required for 2'3'-cGAMP uptake. A) HEK293 LRRC8A knockout single cell clones were lysed and western blotting was used to assess LRRC8A abundance (n=3, biological repeats). B) HEK293 LRRC8A KO cells were transfected with p125-FLuc (IFNβ promoter reporter), pRL-TK (constitutively expresses renilla luciferase) and pcDNA3.2-STING. IFN-β production was then assessed in response to low salt (NaCl) buffers containing 2'3'-cGAMP. Graphs display average of three technical replicates statistically evaluated with grouped two-way ANOVA – Tukey. *=p<0.05, **=p<0.01, ***=p<0.001, ****=p<0.0001, ns=not significant (n=3, biological repeats, representative data set).

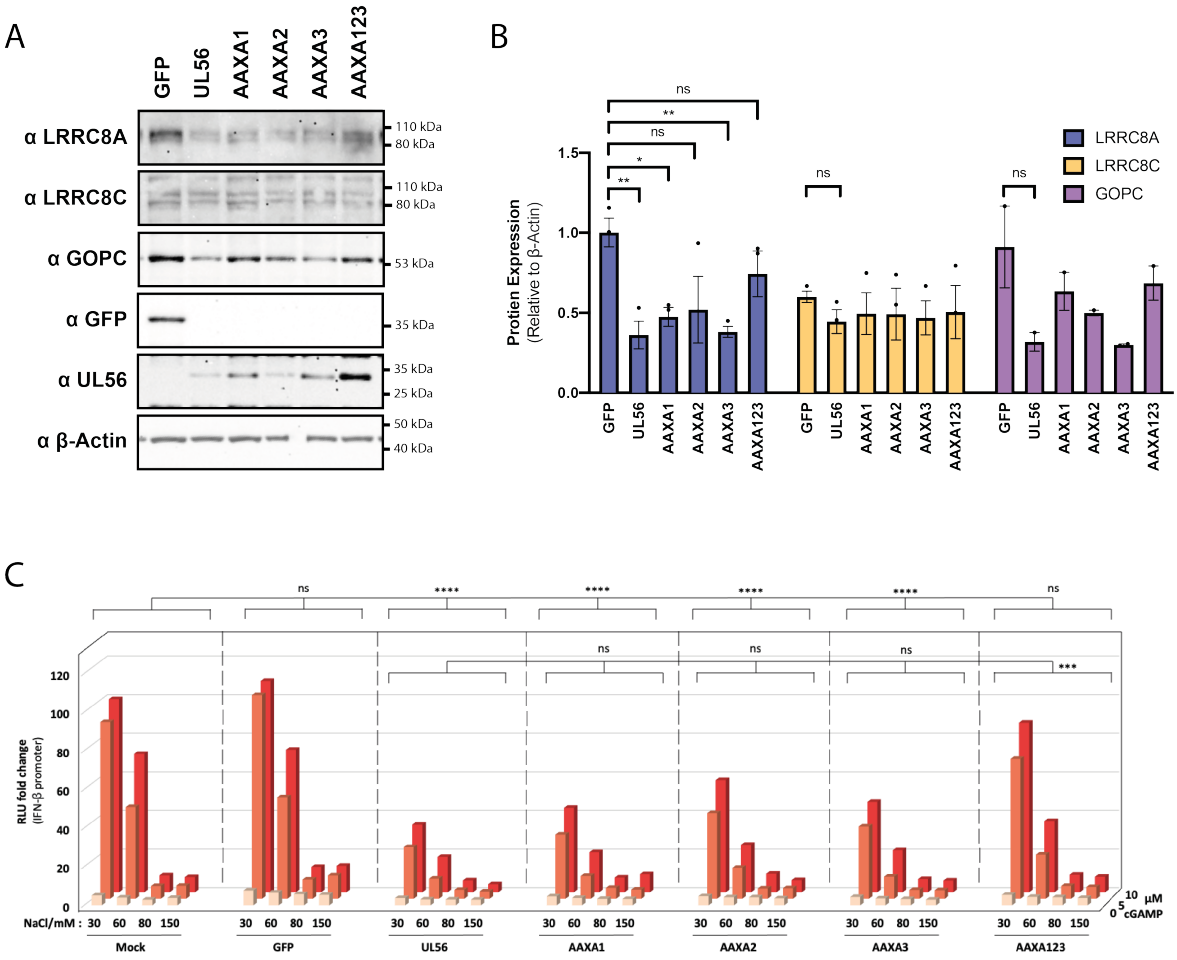


Figure 53 – UL56 inhibits LRRC8A:C mediated 2'3'-cGAMP uptake. A) HEK293T stably over expressing UL56 and UL56 AXAA mutant constructs were lysed and western blotting (A) was used to assess LRRC8A:C abundance. Densitometry was used to quantify the results (B). Graphs display average (±SEM) of three independent biological repeats statistically evaluated with two-way ANOVA – Tukey (n=3, biological repeats). B) HEK293T cells stably expressing indicated UL56 constructs were transfected with p125-FLuc (IFNβ promoter reporter), pRL-TK (constitutively expresses renilla luciferase) and pcDNA3.2-STING. IFN-β production was then assessed in response to low salt (NaCl) buffers containing 2'3'-cGAMP. Graphs display average of three independent biological repeats statistically evaluated with grouped two-way ANOVA – Tukey. *=p<0.05, **=p<0.01, ***=p<0.001, ****=p<0.0001, ns=not significant (n=3, biological repeats, pooled data for 3 individual experiments shown).

effected in GOPC knockout cells and so degradation must occur by a GOPC independent mechanism. As UL56's PPXY motifs recruit NEDD4 ubiquitin ligases, it is likely E3 ligases either directly or indirectly mediate LRRC8A:C degradation. By chemical inhibition of the proteasome I was able to partially rescue LRRC8A:C levels during HSV-1 infection. Suggesting LRRC8A:C is proteosomally degraded. Future work could test whether LRRC8A:C is directly ubiquitinated during HSV-1 infection. Additionally, the NEDD4 E3 ligase family could be

screened to identify if a E3 ligase is responsible for degradation. Finally, I developed an in *vitro* system of LRRC8A:C mediated 2'3'-cGAMP uptake. This was validated by both chemical inhibition of LRRC8A:C and LRRC8A knockout. Using this system, I showed LRRC8A:C degradation by UL56 functionally inhibits 2'3'-cGAMP uptake. As would be expected, preventing LRRC8A:C degradation by mutating every PPXY motif rescues 2'3'-cGAMP uptake. Interestingly, mutation of individual PPXY motifs could not prevent UL56's inhibition of 2'3'-cGAMP uptake through LRRRC8A:C. Suggesting the PPXY motifs act redundantly to inhibit LRRC8A:C activity. Having shown in *vitro* UL56 antagonise LRRC8A:C, there are three open questions I want to address.

1 – Does UL56 inhibit LRRC8A:C mediated 2'3'-cGAMP export as well as import?
2 – Does 2'3'-cGAMP release into the extracellular space inhibit HSV-1 ΔUL56 replication?
3 – In *vivo* is HSV-1 ΔUL56 attenuated due to STING dependent responses?

Unfortunately, with the current tools assembled this has not been possible. One complication is that UL56 has recently been suggested to directly inhibit cGAS (Zheng et al. 2022). I was able to confirm UL56 antagonises 2'3'-cGAMP production by both human and murine cGAS in a manner independent of its PPXY motifs (Supplementary Figure 6). Currently, I do not have a UL56 mutant unable to antagonise cGAS. This is important as studying UL56's effect on 2'3'-cGAMP export through LRRC8A:C requires expression of cGAS and UL56 in the same cell. In cells expressing UL56 and cGAS a reduction in extracellular 2'3'-cGAMP could be due to either reduced cGAS activity or reduced LRRC8A:C activity, or both. Hence, currently export studies are not possible. For the same reason in *vitro* studies of viral replication and in *vivo* work are also precluded. Future work could aim to identify the motifs within UL56 that mediate cGAS antagonism. Identification of a UL56 mutant unable to inhibit cGAS but still able to degrade LRRC8A:C could disassociate the phenotypes. An additional hurdle to in *vivo* work is that HSV-1 does not appear to degrade murine LRRC8A. An α herpes virus that naturally infects mice has not been identified (Ehlers et al. 2007). Additionally, the UL56 gene exists in a unique region specific to HSV strains meaning there are no homologs in the β or γ families (Koshizuka et al. 2002). Therefore, established in *vivo* models of herpes virus infection where mice are

the natural host (e.g. murine cytomegalovirus - MCMV) cannot be used to study UL56s effect on extracellular 2'3'-cGAMP responses.

I must acknowledge antagonism of LRRC8A:C by HSV-1 may not have evolved to avoid 2'3'-cGAMP mediated responses. LRRC8A:C has been shown to play a role in epithelial differentiation, a process HSV-1 may subvert (Friard et al. 2019). Additionally, LRRC8A:C has recently been shown in mice to activate the NLRP3 inflammasome in response to hypotonic buffers but is not needed for the response to classical stimuli (e.g. ATP, nigericin, silica or imiquimod) (Green et al. 2020). The NLRP3 inflammasome has been shown to restrict HSV-1's replication, but whether hypotonic inflammasome activation is relevant during HSV-1 infection is unknown (Karaba et al. 2020; Hayes et al. 2021). Therefore, the in *vivo* models needed to prove UL56's degradation of LRRC8A:C acts to prevent extracellular 2'3'-cGAMP from restricting HSV-1s replication are currently not feasible. Despite these short comings it is clear functionally expression of UL56 inhibits LRRC8A:C activity. It is possible this is to evade extracellular 2'3'-cGAMP responses as previously both LRRC8A:C and extracellular 2'3'-cGAMP have been shown to inhibit viral replication in *vivo* (Carozza et al. 2022; Zhou et al. 2020).

Chapter VI

Antagonism of SLC46A2 and P2X7 by UL56

In the previous section, I showed LRRC8A:C is degraded by UL56, functionally resulting in reduced extracellular 2'3'-cGAMP uptake. In Chapter IV (Figure 36 and 38) I observed, alongside LRRC8A:C, SLC46A2 and P2X7 are also down regulated during HSV-1 infection.

SLC46A2 is an orphan solute carrier protein with predominant expression known in the murine thymic cortex. It's only known substrate is foreign - the tracheal cytoxin (TCT). Produced by *Bordetella pertussis* and *Neisseria gonorrhoeae,* this toxin enters mammalian cells and drives NOD1 activation and necrosis (Paik et al. 2017). Therefore, 2'3'-cGAMP is SLC46A2's first endogenous substrate. This was initially identified by Cordova et al., who observed it is the dominant 2'3'-cGAMP importer in human but not murine monocytes and macrophages (Cordova et al. 2021). SLC46A1 and SLC46A3 have also been shown to increase IFN-β responses to extracellular 2'3'-cGAMP on overexpression but effective depletion caused no inhibition of STING activation in primary human monocytes (Cordova et al. 2021). Therefore, the physiological role, if any, of these channels during 2'3'-cGAMP import is unclear.

P2X7 is expressed in virtually all immune cells (including: Macrophages, Dendritic cells, granulocytes, T cells, B cells and NK cells) and confers resistance to bacterial, parasitic and viral infection (Di Virgilio et al. 2018). Under resting conditions P2X7 supports Na^+ and Ca^{2+} influx and K^+ efflux (Riedel, Schmalzing, and Markwardt 2007). Functionally activation of P2X7 causes the opening of a non-selective pore for hydrophilic substances up to 900 Da and allowing passive K^+ efflux (De Salis et al. 2022). Intracellular K^+ decline triggers the NLRP3 inflammasome leading to the release of proinflammatory cytokines, primarily IL-1β (Ghiringhelli et al. 2009). P2X7 was first implicated in 2'3'-cGAMP transport by Zhou et al. in

a mouse model of efferocytosis (Zhou et al. 2020). Here “eat me” molecules (Gas6 or Protein S) trigger monocytic phagocytosis and immunologically silent cell death (Boada-Romero et al. 2020). The authors observed that blocking efferocytosis causes release of 2’3’-cGAMP from dying cells. They speculate membrane integrity eventually becomes disrupted in dying cells leading to release of 2’3’-cGAMP and ATP into the extracellular medium. Tumour derived 2’3’-cGAMP is taken up by macrophages through the ATP gated P2X7 pore and contributes to cancer clearance (Zhou et al. 2020). This shows that, in mice, P2X7 functions to import 2’3’-cGAMP. It is yet to be shown in humans if P2X7 imports 2’3’-cGAMP in a similar manner.

In this section we focus on the consequence of SLC46A2 and P2X7 depletion during HSV-1 infection. Where indicated in the figure legends, experimental data was collected with the help of the Msc student Jed Avissar and my colleague Alex Redmond.

VI.1 SLC46A2 is degraded by UL56

LRRC8A:C is degraded by UL56. I therefore tested if the other 2’3’-cGAMP channels down regulated during HSV-1 infection (SLC46A2 and P2X7, see Chapter IV, Figure 36 and 38) were also degraded by UL56. To do this, a UL56 construct with an N-terminal GFP tag (pEXP103 GFP-UL56 and pEXP103 GFP-UL6) was transfected into HEK293T cells stably overexpressing SLC46A2. To exclude bulk effects, cells were then sorted into GFP+ and GFP- populations by fluorescence activated cell sorting (FACS). UL56 expressing cells contained reduced levels of SLC46A2 (Figure 54A). Additionally, HSV-1 ΔUL56 infection partially rescued SLC46A2 levels (Figure 54B). Thus, *UL56* is a viral gene mediating SLC46A2 degradation during HSV-1 infection. Additionally, mutation of HSV-1’s three PPXY domains to AAXA partially rescued SLC46A2 levels (Figure 54B), suggesting that E3 ligase recruitment aids channel degradation.

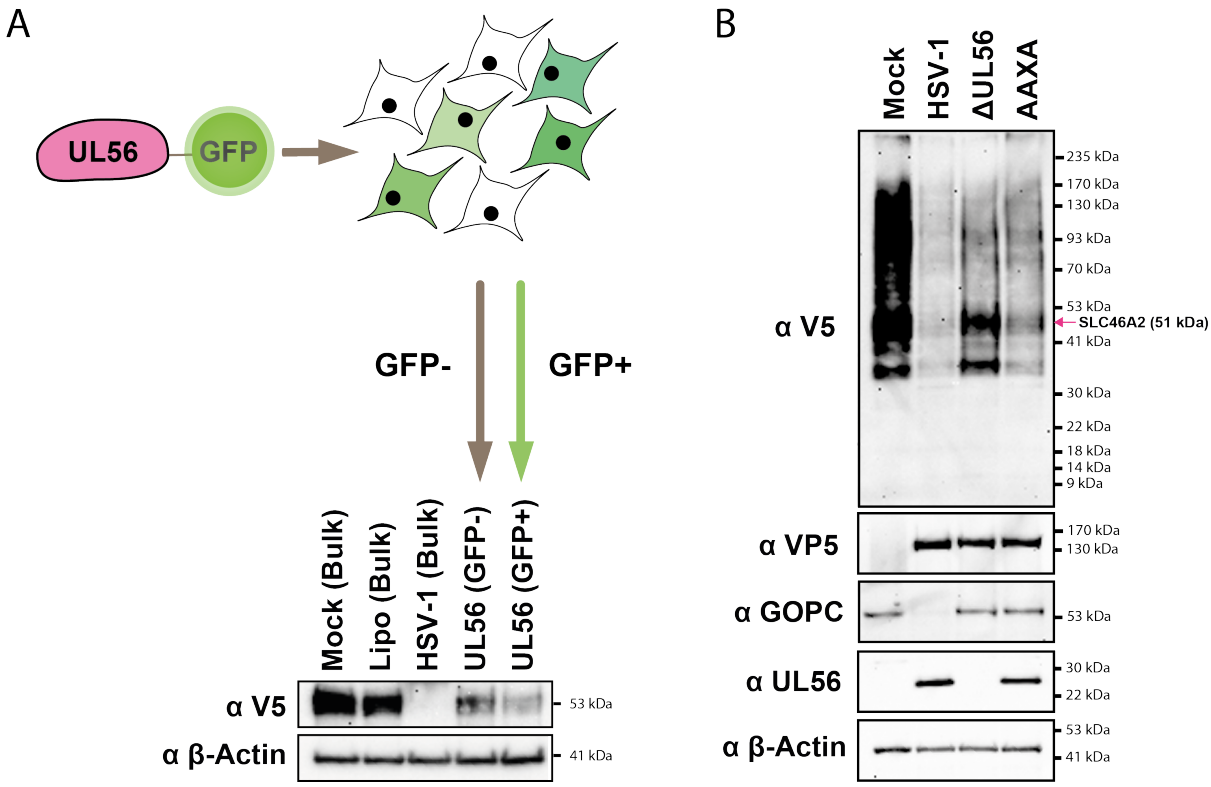


Figure 54 – UL56 degrades SLC46A2. A) HEK293T cells stably expressing SLC46A2 with a C-terminal V5 tag were transiently transfected with a construct expressing UL56-GFP. To exclude bulk effects, cells were FACS sorted into GFP- and GFP+ populations as, shown in supplementary Figure 4 and 5 (n=1, biological repeats). B) HEK293T SLC46A2-V5 cells were infected with the indicated HSV-1 genotypes (MOI 3) for 24 hours before lysis (n=3, biological repeats) (Experiment performed by Jed Avissar under my close supervision). In both A and B western blotting was used to assess LRRC8A:C abundance.

VI.2 Model of SLC46A2 mediated 2'3'-cGAMP transport

Having shown UL56 degrades SLC46A2 I aimed to show this results in reduced 2'3'-cGAMP uptake and IFN-β induction. To do this, we utilised a previously described (see Chapter V, section V.5, Figure 50) dual luciferase assay to measure IFN-β induction upon 2'3'-cGAMP treatment (Bridgeman et al. 2015). HEK293T cells stably expressing SLC46A2-V5 were treated with extracellular 2'3'-cGAMP to test if channel expression increased IFN-β induction (Figure 55A). SLC46A2-V5 expression significantly increased IFN-β production compared to the GFP control (Figure 55A). This could be significantly inhibited with the SLC46A2 inhibitor Sulfasalazine (SSZ) (Figure 55A) (Cordova et al. 2021). SSZ also significantly inhibited background IFN-β production from GFP expressing cells. This is likely because HEK293T cells endogenously express another cGAMP channel, SLC19A1, which is also inhibited by SSZ

(Figure 55A and B) (Cordova et al. 2021). Overall, this demonstrates we have developed an overexpression model for SLC46A2 mediated 2'3'-cGAMP uptake in HEK293T cells.

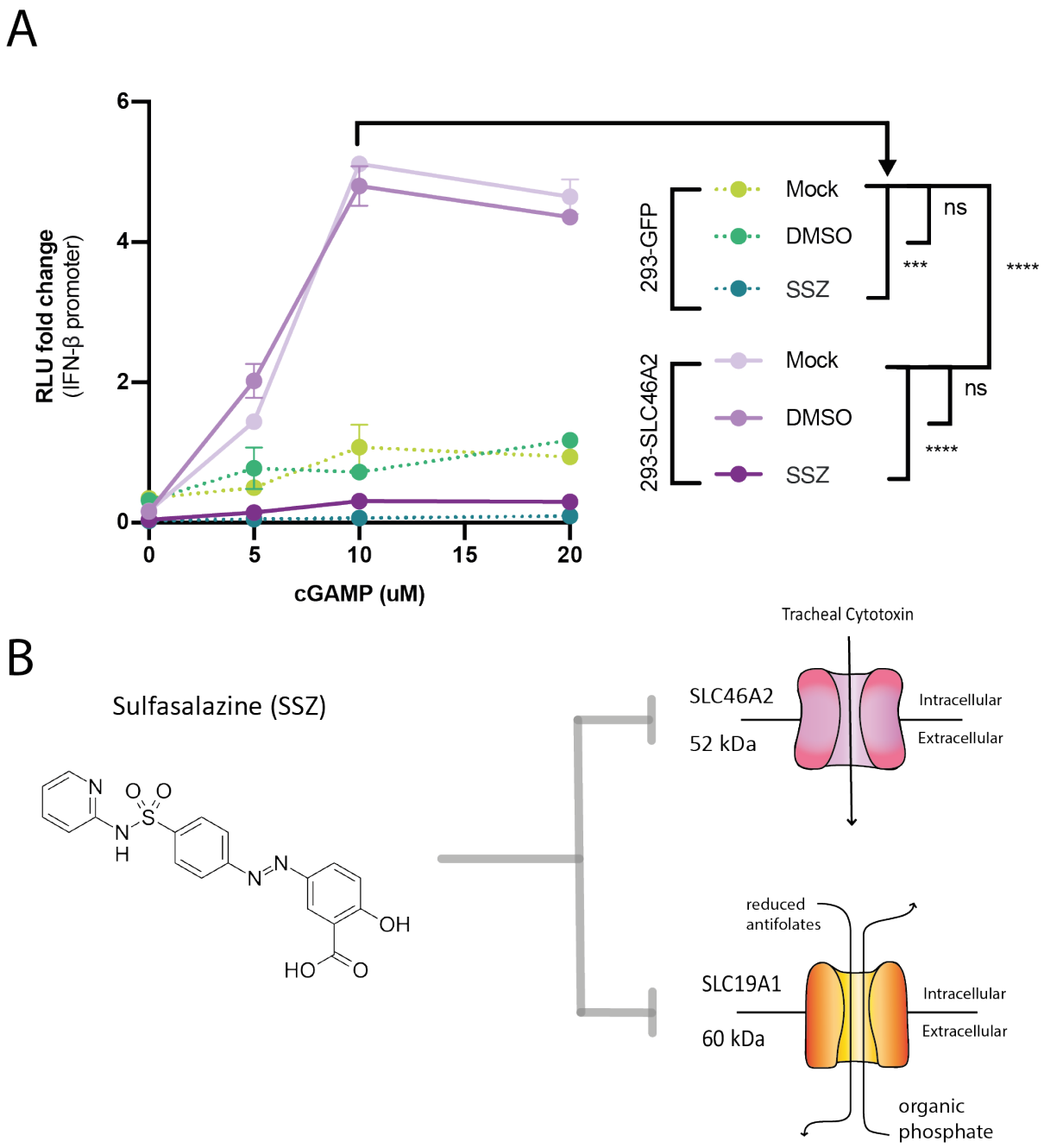


Figure 55 – A model of SLC46A2 mediated 2'3'-cGAMP uptake. A) HEK293T cells stably transduced with SLC46A2-V5 were transfected with p125-FLuc (IFNβ promoter reporter), pRL-TK (constitutively expresses renilla luciferase) and pcDNA3.2-STING. IFN-β production was then assessed in response to extracellular 2'3'-cGAMP. Cells were also treated with SSZ (1mM) or the vehicle control (DMSO). Graphs display average (±SEM) of three technical replicates statistically evaluated with two-way ANOVA – Tukey. *=p<0.05, **=p<0.01, ***=p<0.001, ****=p<0.0001, ns=not significant (n=3, biological repeats, representative dataset) (Experiment performed by Jed Avissar under my close supervision). B) Schematic showing sulfasalazine an antagonist of both SLC46A2 and SLC19A1.

VI.3 UL56 antagonises SLC46A2 mediated 2’3’-cGAMP transport

Using the model of SLC46A2 mediated 2’3’-cGAMP uptake developed in the previous section, we tested if UL56 blocked 2’3’-cGAMP import. To do this, UL56 or UL56 PPXY domain mutants were over expressed from a construct conferring puromycin resistance in HEK293T SLC46A2-V5 cells, which are blasticidin resistant (supplementary Figure 7). Overexpression of UL56 slightly reduced SLC46A2 abundance, which appeared to be rescued if any of the PPXY motifs were muted to AAXA (Figure 56A). In accord, IFN-β induction by extracellular 2’3’-cGAMP was significantly reduced in cells overexpressing UL56 and significantly rescued if any of PPXY domains were mutated to AAXA (Figure 56B). This suggested that activity of all three PPXY domains was required to degrade SLC46A2 and showed functionally that UL56 prevented SLC46A2 mediated 2’3’-cGAMP import into cells.

VI.4 P2X7 is degraded by UL56

Similarly, to SLC46A2 and LRRC8A:C, HSV-1 was seen to degrade P2X7 (Chapter IV, section IV.3, Figure 36). Remarkably overexpression of UL56 also resulted in degradation of the P2X7 pore (Figure 57A). P2X7-V5 levels were partially rescued during HSV-1 ΔUL56 infection (Figure 57B). This shows that UL56 contributes to P2X7 degradation during HSV-1 infection. Additionally, mutation of HSV-1’s three PPXY domains to AAXA partially rescued P2X7 levels (Figure 57B), suggesting that E3 ligase recruitment aids P2X7 degradation.

VI.5 UL56 antagonises P2X7

Having demonstrated that UL56 degrades P2X7 I next tested if this results in reduced P2X7 activity. To do this, I utilised a YO-PRO-1 uptake assay developed by Karasawa and Kawate (2018). YO-PRO-1 is a membrane impermeable dye that fluoresces upon binding DNA. Therefore, P2X7 activity can be measured in real time by recording the fluorescent output of YO-PRO-1 reaching the nucleus. I treated HEK293T cells stably expressing P2X7-V5 with

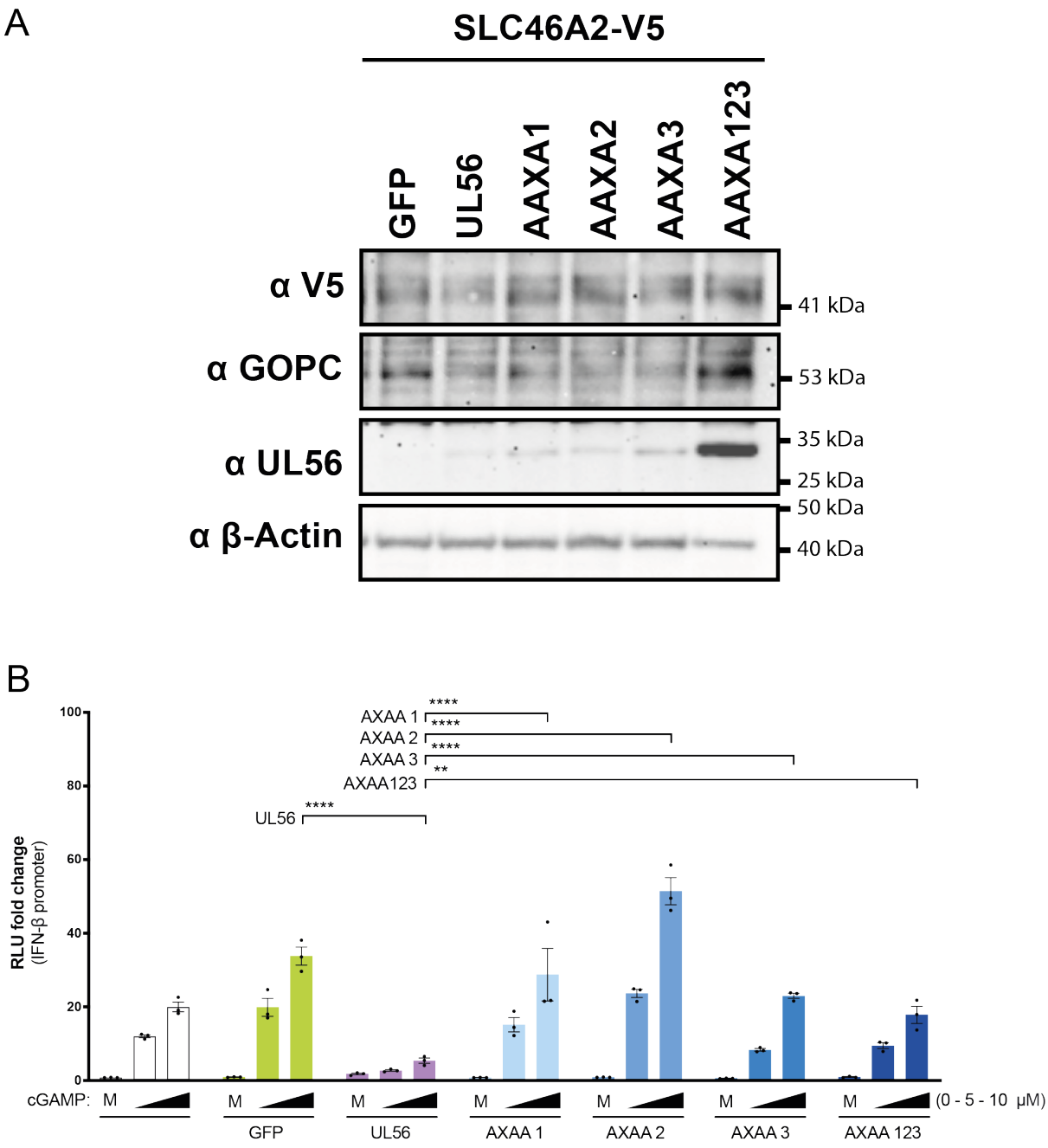


Figure 56 – UL56 inhibits SLC46A2 mediated 2'3'-cGAMP uptake. A) HEK293T SLC46A2-V5 stably over expressing UL56 and UL56 AXAA mutant constructs were lysed and western blotting was used to assess V5 abundance (n=2, biological repeats). B) HEK293T SLC46A2-V5 cells stably expressing the indicated UL56 constructs were transfected with p125-FLuc (IFNβ promoter reporter), pRL-TK (constitutively expresses renilla luciferase) and pcDNA3.2-STING. IFN-β production was then assessed in response to extracellular 2'3'-cGAMP. Graphs display average (±SEM) normalised to R-Luc and then the average of unstimulated groups of three technical replicates statistically evaluated with grouped two-way ANOVA – Tukey. *=p<0.05, **=p<0.01, ***=p<0.001, ****=p<0.0001, ns=not significant (n=3, biological repeats, representative data set shown) (Experiment performed by Jed Avissar under my close supervision).

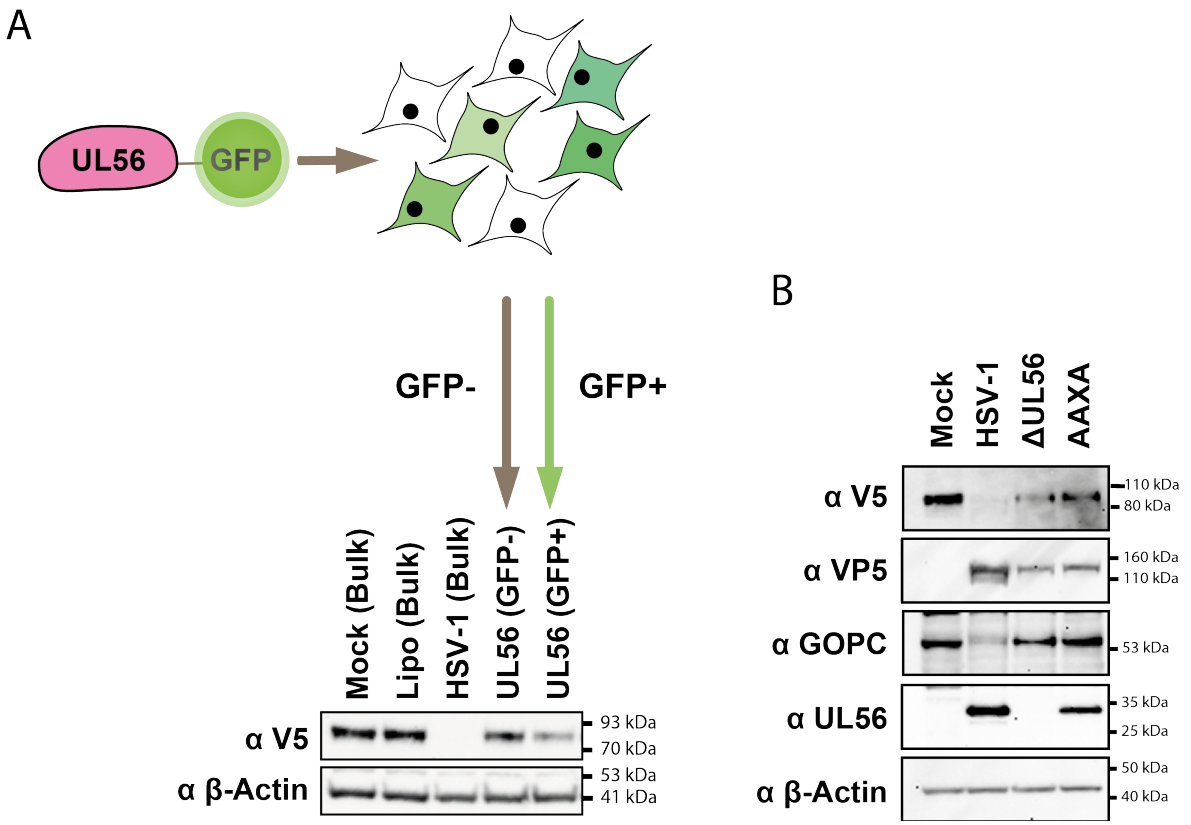


Figure 57 – UL56 degrades P2X7. A) HEK293T cells stably expressing P2X7 with a C-terminal V5 tag were transiently transfected with a construct expressing UL56-GFP. To exclude bulk effects cells were FACS sorted into GFP- and GFP+ populations as, shown in supplementary Figure 4 and 5 (n=3, biological repeats). B) HEK293T P2X7-V5 cells were infected with the indicated HSV-1 genotypes (MOI 3) for 24 hours before lysis (n=3, biological repeats) (Experiment performed by Jed Avissar under my close supervision). In both A and B, western blotting was used to assess LRRC8A:C abundance.

YO-PRO1 and the P2X7 agonist BzATP (Donnelly-Roberts et al. 2009). I observed in P2X7-V5 expressing cells that BzATP significantly increased YO-PRO1 uptake compared to the BzATP treated GFP-V5 expressing control cells (Figure 58). Additionally, the P2X7 inhibitor A73004 completely blocked YO-PRO1 uptake (Allsopp et al. 2018). This demonstrates that overexpression of P2X7 results in significantly enhanced P2X7 activity in HEK293T cells.

Next, I tested if UL56 expression reduced YO-PRO-1 uptake. To do this, UL56 or UL56 PPXY domain mutants were over expressed from a construct conferring puromycin resistance in HEK293T P2X7-V5 cells, which are blasticidin resistant (supplementary Figure 7). This work is currently ongoing and as of this moment we have been unable to confirm the expression of UL56 in these cell lines. Despite this, no uptake of YO-PRO-1 was observed in UL56

overexpressing cells, an effect partially rescued in the AAXA triple mutant (Figure 59B). This shows UL56 likely inhibits the activity of P2X7.

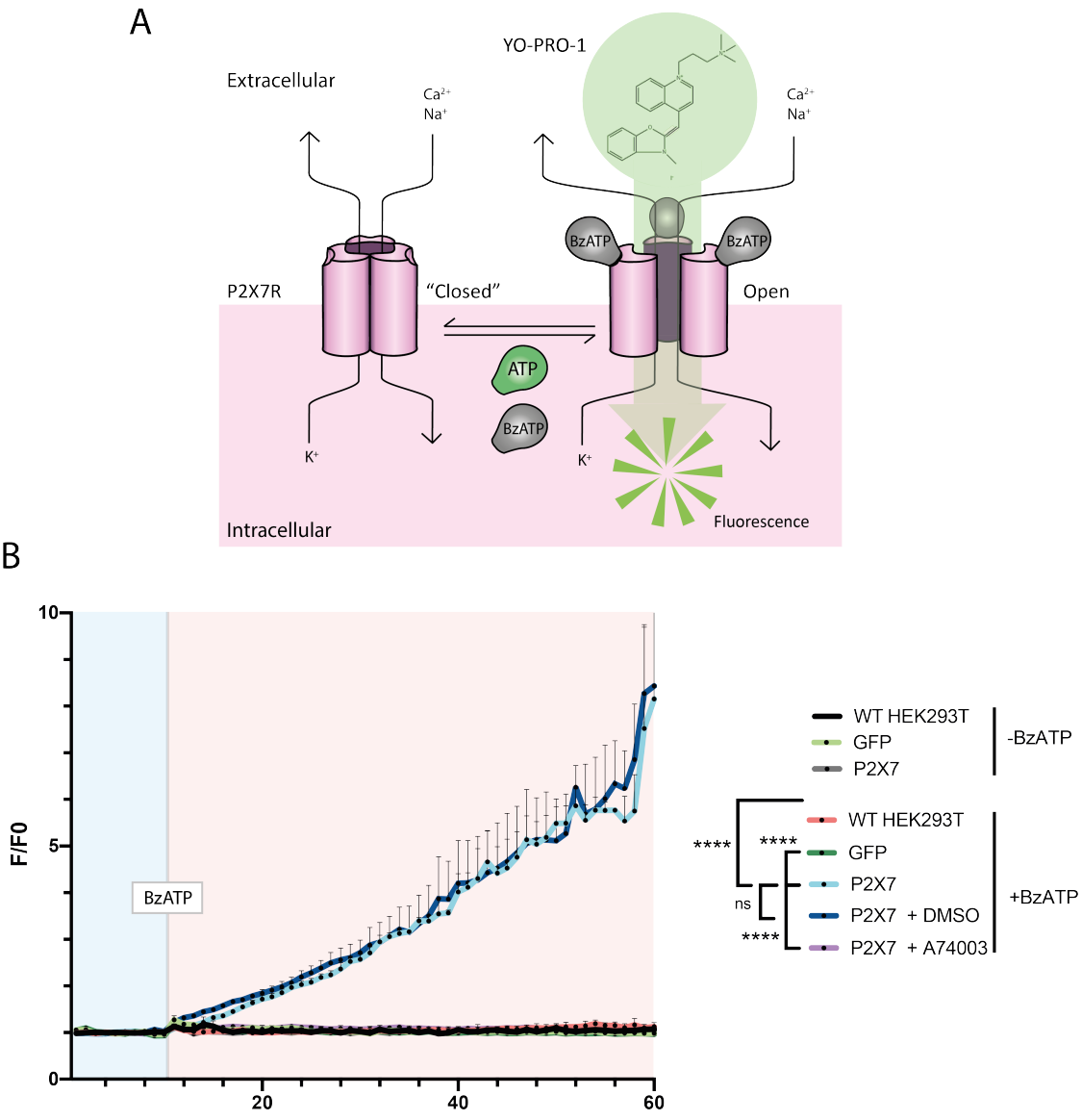


Figure 58 – P2X7 activity assay. A) Schematic showing YO-PRO-1 uptake through P2X7. B) Indicated HEK293 cells were treated with BzATP (80 µM) in the presence of YO-PRO-1. Immediately after YO-PRO-1 addition, green fluorescence was measured at 45 second intervals before and BzATP was added at 10 minutes indicated by a grey line. Fluorescence levels were normalised to the average fluorescence before BzATP was added (F/F0). Data was statically evaluated with grouped two-way ANOVA – Tukey. *=p<0.05, **=p<0.01, ***=p<0.001, ****=p<0.0001, ns=not significant (n=3, biological repeats, representative data set shown) (Experiment performed by Alex Redmond under my close supervision).

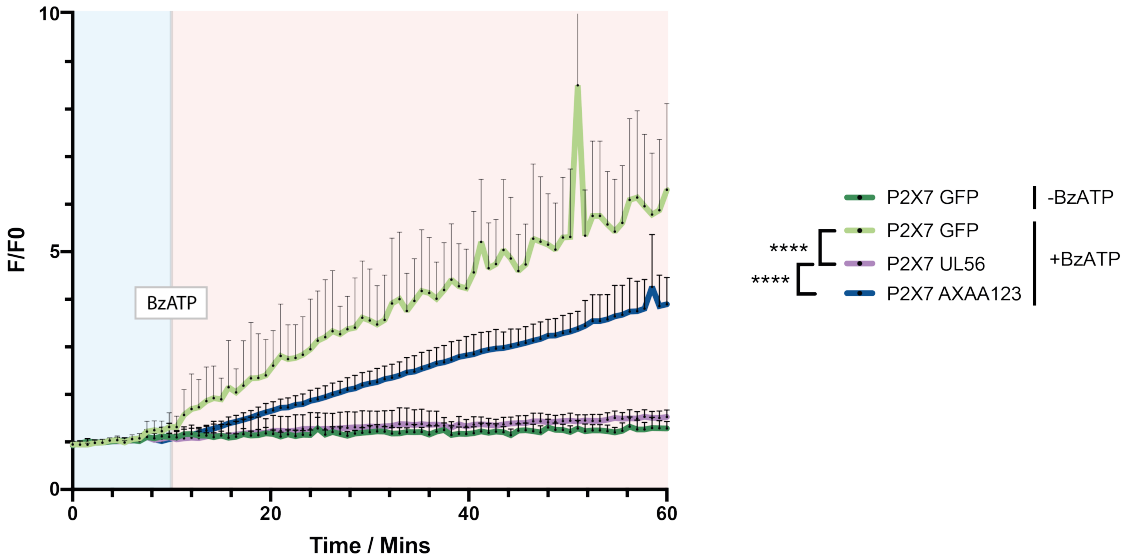


Figure 59 – UL56 inhibits P2X7's activity. HEK293T P2X7-V5 stably over expressing UL56 and UL56 AXAA mutant constructs were treated with BzATP (80 µM) in the presence of YO-PRO-1. Immediately after YO-PRO-1 addition, green fluorescence was measured at 45 second intervals before and BzATP was added at 10 minutes indicated by grey line. Fluorescence levels were normalised to the average fluorescence before BzATP was added (F/F0). Data was statically evaluated with grouped two-way ANOVA – Tukey. *=p<0.05, **=p<0.01, ***=p<0.001, ****=p<0.0001, ns=not significant (n=3, biological repeats, representative data set shown) (Experiment performed by Jed Avissar under my close supervision).

VI.6 UL56 antagonises P2X7 mediated 2'3'-cGAMP import

Having shown UL56 antagonises P2X7 I next tested if this results in reduced 2'3'-cGAMP uptake and IFN-β induction. To do this, I utilised a previously described (see Chapter V, section V.5, Figure 50) dual luciferase assay to measure IFN-β induction upon 2'3'-cGAMP treatment (Bridgeman et al. 2015). HEK293T cells stably expressing P2X7-V5 were treated with extracellular 2'3'-cGAMP and BzATP. I observed 2'3'-cGAMP and BzATP synergised to increase IFN-β induction (Figure 60A). Finally, I tested if, like YO-PRO-1, the uptake of 2'3'-cGAMP was prevented by UL56. It appeared that IFN-β induction by extracellular 2'3'-cGAMP was reduced in cells overexpressing UL56 and rescued if all three of PPXY domains were mutated to AAXA (Figure 60B). No rescue was observed if individual PPXY domains were mutated, suggesting the activities of all three PPXY domains are required to antagonise P2X7. However, further replicates and confirmation of UL56 expression will be required to state with certainty that UL56 antagonises P2X7 mediated 2'3'-cGAMP import into cells.

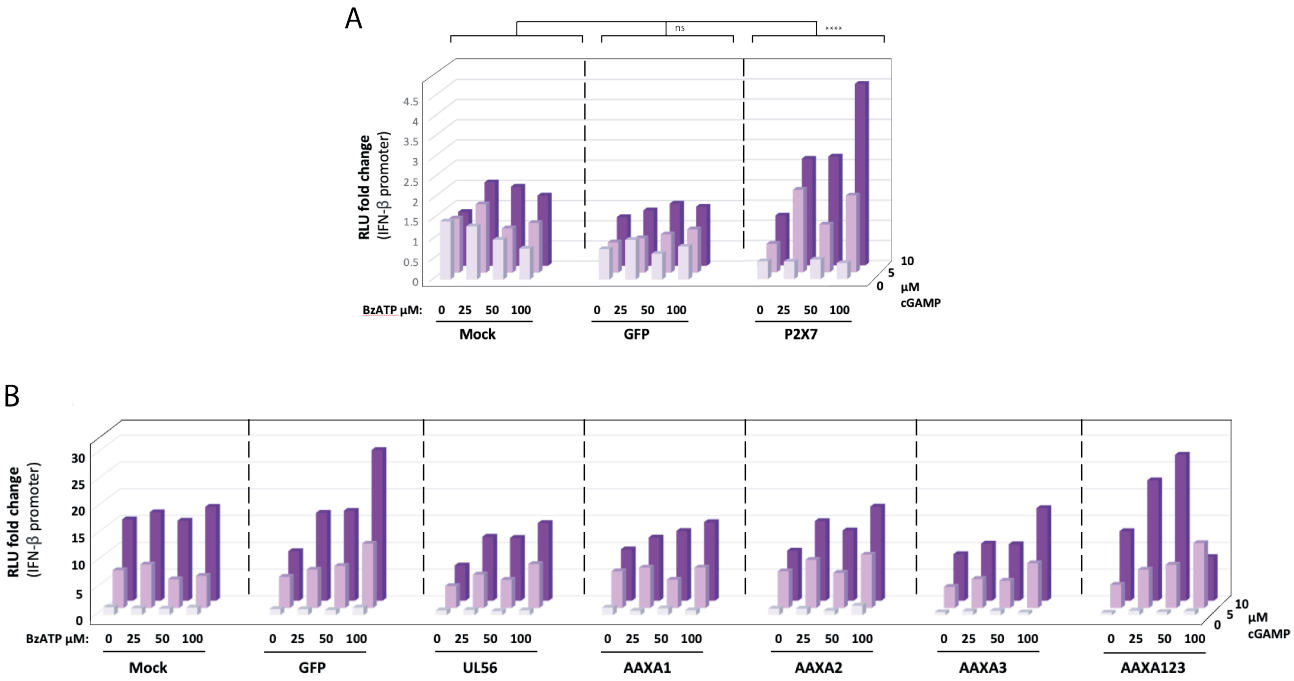


Figure 60 – UL56 inhibits 2'3'-cGAMP uptake through P2X7. A) HEK293T GFP-V5 or P2X7-V5 cells were transfected with p125-FLuc (IFNβ promoter reporter), pRL-TK (constitutively expresses renilla luciferase) and pcDNA3.2-STING. IFN-β production was then assessed in response to extracellular 2'3'-cGAMP and BzATP at the indicated doses. F-Luc is normalised to R-Luc and then the average of unstimulated groups. Data was statically evaluated with grouped two-way ANOVA – Tukey. *=p<0.05, **=p<0.01, ***=p<0.001, ****=p<0.0001, ns=not significant (n=3, biological repeats, representative data set shown). B) HEK293T P2X7-V5 cells stably expressing the indicated GFP or UL56 constructs were assessed for IFN-β induction as is A (n=1).

VI.7 Discussion

Being unable to detect endogenous P2X7 and SLC46A2, we had to rely on overexpression models to study these channels. I have shown that UL56 is able to degrade of both P2X7 and SLC46A2. As with LRRC8A:C, UL56 inhibited 2'3'-cGAMP uptake through both SLC46A2 and P2X7 in a PPXY dependent manner, suggesting NEDD4 ligase recruitment is needed for channel antagonism. Additionally, for the first time we have shown that human P2X7 is able to import 2'3'-cGAMP as the previous studies had been based on murine models. While SLC46A2 overexpression showed a large increase in 2'3'-cGAMP uptake (~4 fold), in comparison expression of P2X7 only enhanced IFN-β induction modestly (~2 fold). The reason why P2X7 induces much lower induction of IFN-β is difficult to explain. We reason it may be important to test if the opening of large P2X7 pores may trigger indirect 2'3'-cGAMP import through LRRC8A:C due to disrupted osmotic homeostasis. This could explain the minor

phenotype observed. In the future, it will be interesting to test if UL56 also degrades or antagonises SLC46A1 and SLC46A3, which are closely related to SLC46A2 (Cordova et al. 2021). The largest draw back of the presented work is that we have been unable to study SLC46A2 and P2X7 function endogenously. Unfortunately, cell lines expressing SLC46A2 and P2X7 are not known. Therefore, to study the function of UL56 at the endogenous level would likely require primary macrophages and monocytes, a cell type in which overexpression and knockdown work is particularly difficult. Therefore, with the present data set we conclude UL56 antagonises SLC46A2 and P2X7 in an overexpression setting.

Chapter VII

Discussion

VII.1 Aim 1 – Regulators of STING (Chapter III)

Reflecting on the aims of the study, we were able to develop a system to perform siRNA knockdowns in THP-1s, a cell line notoriously hard to transfect (Li et al. 2015). Using this method, I evaluated whether the genes identified in Alice Mayer's CRISPR screen augment STING's function. I identified 13 candidates. Despite the positive (siRNA targeting STING) and negative (siRNA targeting MAVS) controls indicating the siRNA-based screen worked functionally, I would not recommend the technique. The high levels of cell death seen likely led to many false positives and caused technical difficulties when it came to replication. Therefore, lentiviral CRISPR or shRNA-based approaches would likely have produced a higher quality data set. The majority of the 13 candidate genes were then tested in the context of overexpression to assess if they augment STING signalling. None were seen to consistently augment STING activation to a significant degree. It is important to note these proteins could still relate to STING signalling if knocked - down/out the context in which they were initially identified. Two of the most promising hits – EXOSC6 and UBL5 - from the siRNA screen could not be tested by overexpression due to technical constraints. Therefore, further work maybe warranted to decipher if novel STING regulators have been found within this screen.

VII.2 Aim 2 – Viral antagonism of cGAMP channels (Chapters IV, V and VI)

My second aim, to identify a viral antagonist of cGAMP channels, has been more productive. I initially showed in chapter IV that many viruses appear to deplete cGAMP channels during infection. Most notably the DNA viruses HSV-1 and VACV, which are both known to be detected by cGAS (Zahid et al. 2020). This is not surprising as these viruses have large genomes encoding a plethora of immunomodulators known to shut down the host's immune response (Danastas, Miranda-Saksena, and Cunningham 2020). Rather than down regulation

being a by-product of HSV-1's vhs protein shutting down host mRNA translation, I found a single gene, *UL56*, acts to degrade LRRC8A:C (Oroskar and Read 1987). Remarkably, UL56, which is also a known antagonist of cGAS, was able to degrade SLC46A2 and P2X7 and therefore acts against three out the five known cGAMP channels as discussed in Chapter IV section IV.5 (Zheng et al. 2022). Functionally, I observed in overexpression models that UL56 antagonises LRRC8A:C, SLC46A2 and likely P2X7 mediated 2'3'-cGAMP uptake as discussed in sections V.6 and VI.4. Although this study has been successful, I acknowledge its limitations. Most notably, I cannot currently show that our findings are of physiological relevance or even relevant to viral replication in *vitro*. This is largely due to the fact UL56 also acts to directly inhibit 2'3'-cGAMP production by cGAS, a finding we were able to validate (Zheng et al. 2022). Therefore, without a UL56 mutant unable to antagonise cGAS, it is hard to distinguish between STING modulation caused by cGAS antagonism and cGAMP channel degradation. In *vitro,* this complicates experiments showing extracellular 2'3'-cGAMP limits viral replication. Similarly, in *vivo* experiments to test if HSV-1 ΔUL56 elicits greater STING activation are precluded. The UL56 triple PPXY mutant (AAXA) is unable to degrade cGAMP channels but still antagonises cGAS (supplementary Figure 6). A UL56 mutant that cannot antagonise cGAS but still degrades cGAMP channels would therefore be of use to future work. This could be identified by alanine scanning. Here many UL56 mutant constructs would be produced with short stretches of amino acids replaced with alanine (Lefèvre, Rémy, and Masson 1997). Each mutant construct would then be tested to see if they antagonise cGAS to find the residues within UL56 responsible for cGAS antagonism. Despite this prospect in *vivo* studies are further complicated as LRRC8A appears not to be degraded by HSV-1 in murine cells. An α herpesvirus that naturally infects mice has not been identified (Ehlers et al. 2007). Additionally, the UL56 gene exists in a unique region specific to HSV strains meaning there are no homologs in the β or γ herpesvirus families (Koshizuka et al. 2002). Therefore, established in *vivo* models of herpes virus infection where mice are the natural host (e.g. murine cytomegalovirus - MCMV) cannot be used to study UL56's effect on LRRC8A:C mediated 2'3'-cGAMP responses. Although it is beyond the scope of this study, future in *vivo* work could investigate VACV, which appears to downregulate P2X7 and SLC46A2. It is possible that an antagonist found in this virus may not be complicated by dual functionality. Additionally, we have not been able to study the effect of UL56 on 2'3'-cGAMP export through LRRC8A:C as this would require

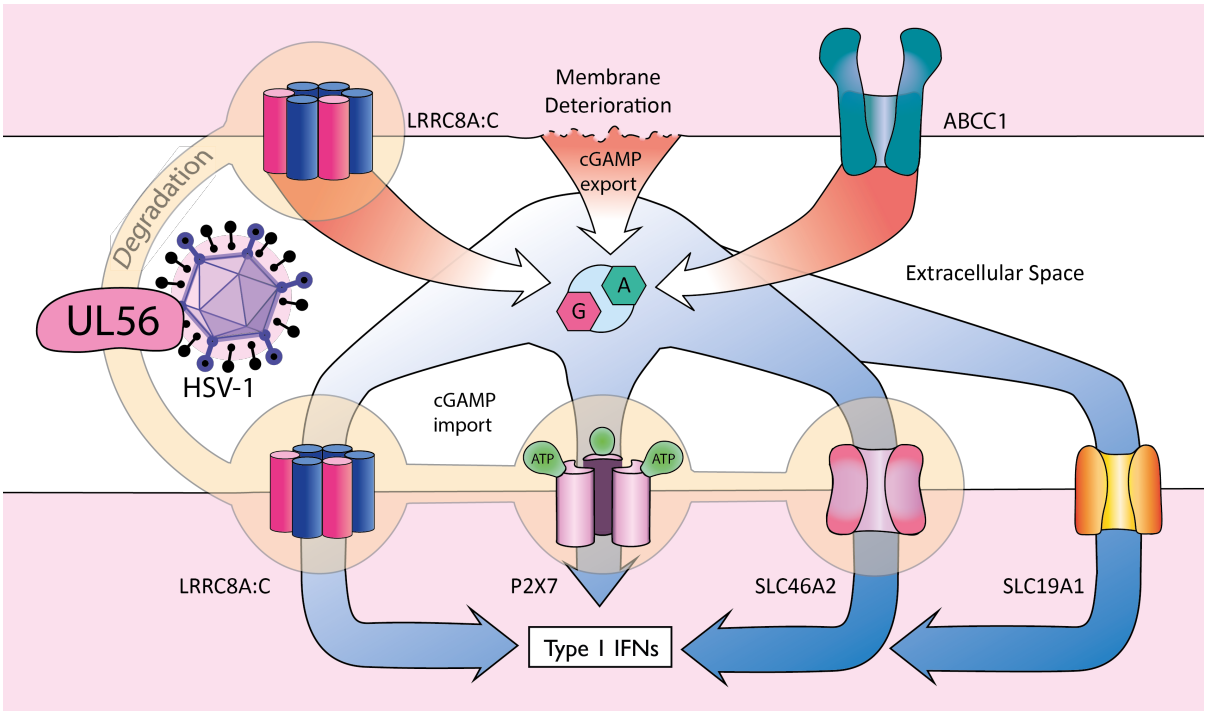


Figure 61 – UL56 targets multiple cGAMP channels. The *UL56* gene from HSV-1 targets LRRC8A:C, P2X7 and SLC46A2 for degradation and so antagonises 2'3'-cGAMP transport. Described in Chapters IV, V and VI.

expression of cGAS and UL56 within the same cell. To enable export work, I am considering using cGAS homologs from a distant species (e.g. *Drosophila melanogaster*) or a bacterial derived enzyme producing CDNs known to be transported by LRRC8A:C (e.g. 3'3'-cGAMP), both of which will likely not be inhibited by UL56 (Slavik et al. 2021; Whiteley et al. 2019). One aspect of the data set we would like to explore in greater depth is the mechanism by which cGAMP channels are degraded by UL56. I observed that chemical inhibition of the proteasome partially prevented degradation of LRRC8A:C by HSV-1. However, the drug used (lactacystin) also inhibited HSV-1's replication; it is thus impossible to draw a firm conclusion. I am currently optimising the time point of lactacystin treatment and HSV-1 infection to more definitively answer if proteasomal inhibition rescues LRRC8A:C abundance. Additionally, I have not explored if P2X7 and SLC46A2 are degraded due to UL56-mediated GOPC degradation, leading to global disruption of transmembrane protein trafficking, or if, like LRRC8A:C, they are more directly targeted by UL56. Additionally, we want to determine if any of the known NEDD4 E3 ligases are required for degradation of the cGAMP channels by UL56. This work is ongoing. As both LRRC8A and P2X7 can also activate the inflammasome, which acts to inhibit HSV-1's replication, we acknowledge that their degradation might not have

evolved to avoid extracellular 2'3'-cGAMP responses but instead inflammasome activation (Green et al. 2020; Karmakar et al. 2016). Presently, with the tools available, we are unable to unpick this. Despite these limitations, I am excited to report the first example of a viral gene, *UL56,* that antagonises cGAMP channel function, a phenomenon summarised in Figure 61.

It is worth consideration how the findings of this study could be applied to therapeutics. Recently, the company Arangarus attracted $11.3 million in funding to develop 2'3'-cGAMP localised therapies by developing small molecule inhibitors of ENPP1 (Crunchbase 2022). The advantage of this treatment is that 2'3'-cGAMP produced endogenously by the tumour will be localised to the tumour microenvironment. We speculate that 2'3'-cGAMP localised therapy could enhance the effects of oncolytic viruses. The only approved oncolytic viral therapy (T-VEC) is used to treat melanoma with a 26% overall response rate (Andtbacka et al. 2015). In short, this therapy uses HSV-1 engineered to selectively replicate in tumours as an "in situ" vaccine, designed to stimulate adaptive immune recognition of tumour derived epitopes leading to complete tumour clearance (Andtbacka et al. 2015). HSV-1's broad cell tropism may allow treatment of a wide range of cancers (Thomas et al. 2019). The virus does not have to be directly injected into the tumour and could be therefore used to treat cancers that are not surgically accessible, which would also avoid the need for direct tumour disruption (Thomas et al. 2019). We reason engineering HSV-1 to be more immunogenic by removing the *UL56* gene could greatly enhance this "in situ vaccine", as 2'3'-cGAMP has previously been shown to be a potent adjuvant (Wang et al. 2020).

VII.3 Knowledge gaps

My observation that mouse LRRC8A appears not to be degraded by UL56 adds to a broader body of evidence showing work on cGAMP channels in *vivo* is precluded by vast differences in 2'3'-cGAMP transport seen between humans and mice. For example, murine SLC19A1 is not a 2'3'-cGAMP transporter, LRRC8A:E (not LRRC8A:C) transports 2'3'-cGAMP in mice and murine SLC46A2 appears to transport 2'3'-cGAMP but does not function in murine monocytes and macrophages like human SLC46A2 (Cordova et al. 2021; Zhou et al. 2020; Ritchie et al.

2019; Luteijn et al. 2019). It is very important that future studies consider this as conclusions drawn solely from mice will likely be misleading. Many studies looking at 2'3'-cGAMP import have focussed upon the cell types and CDN species that move through the channels ex *vivo*. Therefore, a shift of focus towards research on cGAMP channels in humans could be crucial to understanding their physiological relevance. Hence, in the future, we aim to study polymorphisms in cGAMP channels within patient cohorts potentially allowing cGAMP channel function to be correlated to human disease. Interestingly, two common polymorphisms within P2X7, H155Y and A348T, are known to drastically increase pore activity (Bradley et al. 2011). Therefore, it is an interesting possibility to see whether these common polymorphisms lead to increased 2'3'-cGAMP uptake and may correlate in the human population with resistance to cancer or infection. In our study, we found that two cGAMP channels appeared not to be targeted by viruses: SLC19A1 and ABCC1. Of all the cGAMP channels, SLC19A1 is the most well characterised as a crystal structure in complex with 2'3'-cGAMP reveals the exact mechanism by which 2'3'-cGAMP moves through the ion conductance pathway (Zhang et al. 2022). Therefore, it was surprising that this ubiquitously expressed channel that likely functions in the innate immune response was not seen to be targeted by viruses. I acknowledge a drawback of testing degradation is that this does not identify viral antagonists acting by other mechanisms. For instance, if HSV-1 encoded a gene that acted as a "cork" for SLC19A1, we would have overlooked this. Therefore, future work to identify a viral antagonist of SLC19A1 is warranted to dissect its physiological role. This would be an important finding as SLC19A1 cannot be studied in mice so would provide the evidence for its role in *vivo* (Luteijn et al. 2019; Ritchie et al. 2019). If ABCC1 as a 2'3'-cGAMP exporter acts to dampen STING activation, as proposed by Stetson and co-workers, it makes sense the only anti-inflammatory transporter is not targeted by viruses (Maltbaek, Snyder, and Stetson 2021). Future work will be needed to show whether ABCC1 can also function in a proinflammatory manner and further if a viral antagonist exists. This also creates a contradiction as the proinflammatory 2'3'-cGAMP importers only have access to 2'3'-cGAMP if it has been delivered to the extracellular environment. Thus, depending on context, it is likely ABCC1 could act as both a proinflammatory and antinflammatory transporter. It remains to be seen if, like ABBC1, the only other known 2'3'-cGAMP exporter, LRRC8A:C, can

also act to supress STING signalling as currently it has only been shown to act in a proinflammatory manner (Zhou et al. 2020; Lahey et al. 2020).

Another unexpected finding during my study is the possibility that components of the DNA sensing pathway, both cGAS co-sensors and DNA-PK co-factors, are associated with LRRC8C (see Chapter 5, section V.2, Figure 45). Interestingly, before LRRC8C was shown to function as a 2'3'-cGAMP channel, it was bioinformatically predicted to function within the immune system due to its expression profile within immune cells (Abascal and Zardoya 2012). In the same study, it was also predicted that the cytosolic LRR domain is likely a signalling platform (Abascal and Zardoya 2012). Hence, it is interesting to speculate that cytosolic DNA might modulate LRRC8C's function via DNA binding proteins, which could synergise to allow 2'3'-cGAMP release at sites of infection. Since LRRC8A:C activity can be affected by osmotic disruption, studies to identify or characterise cGAMP channels should carefully consider if transport could occur indirectly through LRRC8A:C. Indeed, over expression or knockout of ion channels could lead to disrupted osmotic homeostasis – a trigger for VRAC mediated 2'3'-cGAMP transport.

Outside the scope of our project, but within the view of 2'3'-cGAMP transport research, there are many exciting questions that have not been answered. Notably, as FDA approved inhibitors of cGAMP channels already exist, could they be used to dampen STING activation in models of the many known STING associated diseases (see Chapter I, section 5.4, Figure 9). For instance, the inhibitors sulfasalazine and carbenoxolone are both known to target multiple cGAMP channels (see Chapter 1, section 1.7, Table 1). As these antagonists are known to inhibit murine as well as human channels, they could be used in the *Trex1*-/- model of AGS to test if they reduce IFN production and dampen pathology. This would then give a rationale for treating AGS, COPA and SAVI patients with these drugs as STING activation is the predominant underlying cause. Additionally, these drugs could be of use in more prevalent diseases where STING is thought to underlie the pathology (e.g. Parkinson's disease, SLE and polyarthritis) (Ablasser and Chen 2019). Another open question relates to LL-37's function during 2'3'-cGAMP transport. Most importantly it needs to be shown whether endogenous LL-37 can transport 2'3'-cGAMP (Sancho-Vaello et al. 2020). Studying the role of LL-37 during

viral infection could provide the answer to this. Additionally, SLC46A1 and SLC46A3 have been shown to transport 2'3'-cGAMP in *vitro* but cell types in which they function, or a physiological role, is yet to be established (Luteijn et al. 2019; Cordova et al. 2021). The only cGAS homolog in humans is OASL and senses RNA to produce 2'5'-linked oligoadenylate activating RNase-L to indiscriminately cleave RNA (Hu et al. 2018). This acts to restrict viral replication but whether 2'5'-linked oligoadenylate, like 2'3'-cGAMP, can be transported through channels, within viral particles, or even spread between cells has not been investigated. Previously, the Rehwinkel lab has shown that 2'3'-cGAMP is packaged into viral particles leading to a type I IFN response on entry to a new cell (Bridgeman et al. 2015; Gentili et al. 2015). It has been previously shown that some viruses (e.g. HIV-1, IAV and SARS-CoV2) encode channels termed viroporins that are incorporated into their envelope (Breitinger et al. 2022). It is unknown if viroporins or host channels incorporated into the viral envelope could act to export 2'3'-cGAMP from virions to evade 2'3'-cGAMP packaging.

VII.4 Final thoughts

The initial idea to use lysates from infected cells to identify a virus that degrades 2'3'-cGAMP transporters was inspired by Eaglesham et al., who theorised a viral 2'3'-cGAMP hydrolase must exist as a "strong selective pressure would exist for viruses to specifically destabilise 2'3'-cGAMP". They went on to discover poxins by screening a panel of viral lysates across different Baltimore classes for the ability to degrade 2'3'-cGAMP, which is usually a highly stable molecule (Eaglesham et al. 2019). It is an interesting question if poxins or other more recently identified virally encoded 2'3'-cGAMP hydrolases (C129R and EP364R) could act extracellularly (Dodantenna et al. 2022). We have recapitulated these experiments in the context of 2'3'-cGAMP transport, showing yet again the evolutionary arms race between virus and host consistently provides viral antagonists of the host's innate machinery. Overall, we believe that the import and export of 2'3'-cGAMP provides new pastures for research into cGAS-STING signalling. I look forward to seeing the exciting developments and therapeutic avenues which lie ahead, particularly as drugs targeting these channels are already available and could be relevant to the wide range of STING associated diseases.

Bibliography

Abascal, F., and R. Zardoya. 2012. 'LRRC8 proteins share a common ancestor with pannexins, and may form hexameric channels involved in cell-cell communication', *Bioessays*, 34: 551-60.

Abe, T., and G. N. Barber. 2014. 'Cytosolic-DNA-mediated, STING-dependent proinflammatory gene induction necessitates canonical NF-κB activation through TBK1', *J Virol*, 88: 5328-41.

Ablasser, A., and Z. J. Chen. 2019. 'cGAS in action: Expanding roles in immunity and inflammation', *Science*, 363.

Ablasser, Andrea, Jonathan L. Schmid-Burgk, Inga Hemmerling, Gabor L. Horvath, Tobias Schmidt, Eicke Latz, and Veit Hornung. 2013. 'Cell intrinsic immunity spreads to bystander cells via the intercellular transfer of cGAMP', *Nature*, 503: 530-34.

Ahn, J., D. Gutman, S. Saijo, and G. N. Barber. 2012. 'STING manifests self DNA-dependent inflammatory disease', *Proc Natl Acad Sci U S A*, 109: 19386-91.

Ahn, J., P. Ruiz, and G. N. Barber. 2014. 'Intrinsic self-DNA triggers inflammatory disease dependent on STING', *J Immunol*, 193: 4634-42.

Allen, Lily. 2006. "Knock 'Em Out." In *Alright Still*.

Allsopp, Rebecca C., Sudad Dayl, Anfal Bin Dayel, Ralf Schmid, and Richard J. Evans. 2018. 'Mapping the Allosteric Action of Antagonists A740003 and A438079 Reveals a Role for the Left Flipper in Ligand Sensitivity at P2X7 Receptors', *Molecular Pharmacology*, 93: 553.

Ammon, T., S. K. Mishra, K. Kowalska, G. M. Popowicz, T. A. Holak, and S. Jentsch. 2014. 'The conserved ubiquitin-like protein Hub1 plays a critical role in splicing in human cells', *J Mol Cell Biol*, 6: 312-23.

An, J., L. Durcan, R. M. Karr, T. A. Briggs, G. I. Rice, T. H. Teal, J. J. Woodward, and K. B. Elkon. 2017. 'Expression of Cyclic GMP-AMP Synthase in Patients With Systemic Lupus Erythematosus', *Arthritis Rheumatol*, 69: 800-07.

Andtbacka, R. H., H. L. Kaufman, F. Collichio, T. Amatruda, N. Senzer, J. Chesney, K. A. Delman, L. E. Spitler, I. Puzanov, S. S. Agarwala, M. Milhem, L. Cranmer, B. Curti, K. Lewis, M. Ross, T. Guthrie, G. P. Linette, G. A. Daniels, K. Harrington, M. R. Middleton, W. H. Miller, Jr., J. S. Zager, Y. Ye, B. Yao, A. Li, S. Doleman, A. VanderWalde, J. Gansert, and R. S. Coffin. 2015. 'Talimogene Laherparepvec Improves Durable Response Rate in Patients With Advanced Melanoma', *J Clin Oncol*, 33: 2780-8.

Asami, Jinta, and Toshiyuki Shimizu. 2021. 'Structural and functional understanding of the toll-like receptors', *Protein Science*, 30: 761-72.

Atanasiu, D., W. T. Saw, G. H. Cohen, and R. J. Eisenberg. 2010. 'Cascade of events governing cell-cell fusion induced by herpes simplex virus glycoproteins gD, gH/gL, and gB', *J Virol*, 84: 12292-9.

Baird, J. R., D. Friedman, B. Cottam, T. W. Dubensky, Jr., D. B. Kanne, S. Bambina, K. Bahjat, M. R. Crittenden, and M. J. Gough. 2016. 'Radiotherapy Combined with Novel STING-Targeting Oligonucleotides Results in Regression of Established Tumors', *Cancer Res*, 76: 50-61.

Bakhoum, S. F., L. Kabeche, M. D. Wood, C. D. Laucius, D. Qu, A. M. Laughney, G. E. Reynolds, R. J. Louie, J. Phillips, D. A. Chan, B. I. Zaki, J. P. Murnane, C. Petritsch, and D. A. Compton. 2015. 'Numerical chromosomal instability mediates susceptibility to radiation treatment', *Nat Commun*, 6: 5990.

Bakhoum, S. F., B. Ngo, A. M. Laughney, J. A. Cavallo, C. J. Murphy, P. Ly, P. Shah, R. K. Sriram, T. B. K. Watkins, N. K. Taunk, M. Duran, C. Pauli, C. Shaw, K. Chadalavada, V. K. Rajasekhar, G. Genovese, S. Venkatesan, N. J. Birkbak, N. McGranahan, M. Lundquist, Q. LaPlant, J. H. Healey, O. Elemento, C. H. Chung, N. Y. Lee, M. Imielenski, G. Nanjangud, D. Pe'er, D. W. Cleveland, S. N. Powell, J. Lammerding, C. Swanton, and L. C. Cantley. 2018. 'Chromosomal instability drives metastasis through a cytosolic DNA response', *Nature*, 553: 467-72.

Bakos, Éva, and László Homolya. 2007. 'Portrait of multifaceted transporter, the multidrug resistance-associated protein 1 (MRP1/ABCC1)', *Pflügers Archiv - European Journal of Physiology*, 453: 621-41.

Barnes, B. J., P. A. Moore, and P. M. Pitha. 2001. 'Virus-specific activation of a novel interferon regulatory factor, IRF-5, results in the induction of distinct interferon alpha genes', *J Biol Chem*, 276: 23382-90.

Barton, G. M., J. C. Kagan, and R. Medzhitov. 2006. 'Intracellular localization of Toll-like receptor 9 prevents recognition of self DNA but facilitates access to viral DNA', *Nat Immunol*, 7: 49-56.

Bass, J. J., D. J. Wilkinson, D. Rankin, B. E. Phillips, N. J. Szewczyk, K. Smith, and P. J. Atherton. 2017. 'An overview of technical considerations for Western blotting applications to physiological research', *Scand J Med Sci Sports*, 27: 4-25.

Bauer, S., C. J. Kirschning, H. Häcker, V. Redecke, S. Hausmann, S. Akira, H. Wagner, and G. B. Lipford. 2001. 'Human TLR9 confers responsiveness to bacterial DNA via species-specific CpG motif recognition', *Proc Natl Acad Sci U S A*, 98: 9237-42.

Bauernfried, Stefan, Matthias J. Scherr, Andreas Pichlmair, Karl E. Duderstadt, and Veit Hornung. 2021. 'Human NLRP1 is a sensor for double-stranded RNA', *Science*, 371: eabd0811.

Behring, Emil. 1890. 'Ueber das Zustandekommen der Diphtherie-Immunität und der Tetanus-Immunität bei Thieren.', *Dt med Wochenschrift*, 49:1113–4.

Belkov, Vladimir M., Eugene Y. Krynetski, John D. Schuetz, Yuri Yanishevski, Eric Masson, Susan Mathew, Susana Raimondi, Ching-Hon Pui, Mary V. Relling, and William E. Evans. 1999. 'Reduced Folate Carrier Expression in Acute Lymphoblastic Leukemia: A Mechanism for Ploidy but not Lineage Differences in Methotrexate Accumulation', *Blood*, 93: 1643-50.

Belli, S. I., I. R. van Driel, and J. W. Goding. 1993. 'Identification and characterization of a soluble form of the plasma cell membrane glycoprotein PC-1 (5'-nucleotide phosphodiesterase)', *Eur J Biochem*, 217: 421-8.

Boada-Romero, Emilio, Jennifer Martinez, Bradlee L. Heckmann, and Douglas R. Green. 2020. 'The clearance of dead cells by efferocytosis', *Nature Reviews Molecular Cell Biology*, 21: 398-414.

Boyer, Joshua A., Cathy J. Spangler, Joshua D. Strauss, Andrew P. Cesmat, Pengda Liu, Robert K. McGinty, and Qi Zhang. 2020. 'Structural basis of nucleosome-dependent cGAS inhibition', *Science*, 370: 450.

Bradley, Helen J., Jocelyn M. Baldwin, G. Ranjan Goli, Brian Johnson, Jie Zou, Asipu Sivaprasadarao, Stephen A. Baldwin, and Lin-Hua Jiang. 2011. 'Residues 155 and 348 Contribute to the Determination of P2X₇ Receptor Function via Distinct Mechanisms Revealed by Single-nucleotide Polymorphisms *', *Journal of Biological Chemistry*, 286: 8176-87.

Breitinger, Ulrike, Noha S. Farag, Heinrich Sticht, and Hans-Georg Breitinger. 2022. 'Viroporins: Structure, function, and their role in the life cycle of SARS-CoV-2', *The international journal of biochemistry & cell biology*, 145: 106185-85.

Bridgeman, A., J. Maelfait, T. Davenne, T. Partridge, Y. Peng, A. Mayer, T. Dong, V. Kaever, P. Borrow, and J. Rehwinkel. 2015. 'Viruses transfer the antiviral second messenger cGAMP between cells', *Science*, 349: 1228-32.

Burdette, Dara L., Kathryn M. Monroe, Katia Sotelo-Troha, Jeff S. Iwig, Barbara Eckert, Mamoru Hyodo, Yoshihiro Hayakawa, and Russell E. Vance. 2011. 'STING is a direct innate immune sensor of cyclic di-GMP', *Nature*, 478: 515-18.

Burleigh, Katelyn, Joanna H. Maltbaek, Stephanie Cambier, Richard Green, Michael Gale, Richard C. James, and Daniel B. Stetson. 2020. 'Human DNA-PK activates a STING-independent DNA sensing pathway', *Science Immunology*, 5: eaba4219.

Cahalan, M. D., and R. S. Lewis. 1988. 'Role of potassium and chloride channels in volume regulation by T lymphocytes', *Soc Gen Physiol Ser*, 43: 281-301.

Carozza, Jacqueline A., Volker Böhnert, Khanh C. Nguyen, Gemini Skariah, Kelsey E. Shaw, Jenifer A. Brown, Marjan Rafat, Rie von Eyben, Edward E. Graves, Jeffrey S. Glenn,

Mark Smith, and Lingyin Li. 2019. 'Extracellular 2’3’-cGAMP is an immunotransmitter produced by cancer cells and regulated by ENPP1', *bioRxiv*: 539312.

Carozza, Jacqueline A., Anthony F. Cordova, Jenifer A. Brown, Yasmeen AlSaif, Volker Böhnert, Xujun Cao, Rachel E. Mardjuki, Gemini Skariah, Daniel Fernandez, and Lingyin Li. 2022. 'ENPP1’s regulation of extracellular cGAMP is a ubiquitous mechanism of attenuating STING signaling', *Proceedings of the National Academy of Sciences*, 119: e2119189119.

Carroll, Lewis. 1871. 'Through the Looking-Glass'.

Caunt, A. E., and D. Taylor-Robinson. 1964. 'CELL-FREE VARICELLA-ZOSTER VIRUS IN TISSUE CULTURE', *J Hyg (Lond)*, 62: 413-24.

Cekaite, L., G. Furset, E. Hovig, and M. Sioud. 2007. 'Gene expression analysis in blood cells in response to unmodified and 2'-modified siRNAs reveals TLR-dependent and independent effects', *J Mol Biol*, 365: 90-108.

Cerboni, S., N. Jeremiah, M. Gentili, U. Gehrmann, C. Conrad, M. C. Stolzenberg, C. Picard, B. Neven, A. Fischer, S. Amigorena, F. Rieux-Laucat, and N. Manel. 2017. 'Intrinsic antiproliferative activity of the innate sensor STING in T lymphocytes', *J Exp Med*, 214: 1769-85.

Chamilos, G., J. Gregorio, S. Meller, R. Lande, D. P. Kontoyiannis, R. L. Modlin, and M. Gilliet. 2012. 'Cytosolic sensing of extracellular self-DNA transported into monocytes by the antimicrobial peptide LL37', *Blood*, 120: 3699-707.

Chauveau, Lise, Anne Bridgeman, Tiong Kit Tan, Ryan Beveridge, Joe Frost, Isabela Pedroza-Pacheco, Thomas Partridge, Persephone Borrow, Hal Drakesmith, Alain Townsend, and Jan Rehwinkel. 2020. 'cGAMP loading enhances the immunogenicity of VLP vaccines', *bioRxiv*: 2020.01.03.893586.

Chen, L., B. König, T. Liu, S. Pervaiz, Y. S. Razzaque, and T. Stauber. 2019. 'More than just a pressure relief valve: physiological roles of volume-regulated LRRC8 anion channels', *Biol Chem*, 400: 1481-96.

Chen, W., S. Li, H. Yu, X. Liu, L. Huang, Q. Wang, H. Liu, Y. Cui, Y. Tang, P. Zhang, and C. Wang. 2016. 'ER Adaptor SCAP Translocates and Recruits IRF3 to Perinuclear Microsome Induced by Cytosolic Microbial DNAs', *PLoS Pathog*, 12: e1005462.

Chen, Yi-An, Yi-Ling Shen, Hsuan-Yu Hsia, Yee-Peng Tiang, Tzu-Ling Sung, and Liuh-Yow Chen. 2017. 'Extrachromosomal telomere repeat DNA is linked to ALT development via cGAS-STING DNA sensing pathway', *Nature Structural & Molecular Biology*, 24: 1124-31.

Cheng, Jie, Bryan D. Moyer, Michal Milewski, Johannes Loffing, Masahiro Ikeda, John E. Mickle, Garry R. Cutting, Min Li, Bruce A. Stanton, and William B. Guggino. 2002. 'A Golgi-associated PDZ Domain Protein Modulates Cystic Fibrosis Transmembrane

Regulator Plasma Membrane Expression*', *Journal of Biological Chemistry*, 277: 3520-29.

Civril, Filiz, Tobias Deimling, Carina C. de Oliveira Mann, Andrea Ablasser, Manuela Moldt, Gregor Witte, Veit Hornung, and Karl-Peter Hopfner. 2013. 'Structural mechanism of cytosolic DNA sensing by cGAS', *Nature*, 498: 332-37.

Cohen, Daniel, Sarah Melamed, Adi Millman, Gabriela Shulman, Yaara Oppenheimer-Shaanan, Assaf Kacen, Shany Doron, Gil Amitai, and Rotem Sorek. 2019. 'Cyclic GMP–AMP signalling protects bacteria against viral infection', *Nature*, 574: 691-95.

Cole, Susan P. C. 2014. 'Multidrug Resistance Protein 1 (MRP1, ABCC1), a "Multitasking" ATP-binding Cassette (ABC) Transporter*', *Journal of Biological Chemistry*, 289: 30880-88.

Concepcion, Axel R., Larry E. Wagner, Jingjie Zhu, Anthony Y. Tao, Jun Yang, Alireza Khodadadi-Jamayran, Yin-Hu Wang, Menghan Liu, Rebecca E. Rose, Drew R. Jones, William A. Coetzee, David I. Yule, and Stefan Feske. 2022. 'The volume-regulated anion channel LRRC8C suppresses T cell function by regulating cyclic dinucleotide transport and STING–p53 signaling', *Nature Immunology*, 23: 287-302.

Cordova, Anthony F., Christopher Ritchie, Volker Böhnert, and Lingyin Li. 2021. 'Human SLC46A2 Is the Dominant cGAMP Importer in Extracellular cGAMP-Sensing Macrophages and Monocytes', *ACS Central Science*, 7: 1073-88.

Cordova, Anthony F., Christopher Ritchie, Volker Böhnert, Rachel E. Mardjuki, and Lingyin Li. 2020. 'Murine M1 macrophages are among the direct responders to tumor-derived extracellular cGAMP and their human counterparts use SLC46A2 to import cGAMP', *bioRxiv*: 2020.04.15.043299.

Corrales, L., L. H. Glickman, S. M. McWhirter, D. B. Kanne, K. E. Sivick, G. E. Katibah, S. R. Woo, E. Lemmens, T. Banda, J. J. Leong, K. Metchette, T. W. Dubensky, Jr., and T. F. Gajewski. 2015. 'Direct Activation of STING in the Tumor Microenvironment Leads to Potent and Systemic Tumor Regression and Immunity', *Cell Rep*, 11: 1018-30.

'Crown Human Genome Center'. 2022. Weizman Institute of Science, Accessed 20.12.2022. https://www.genecards.org/.

Crunchbase. 2022. 'Angarus Therapeutics', Accessed 20.12.2022. https://www.crunchbase.com/organization/angarus-therapeutics.

Danastas, K., M. Miranda-Saksena, and A. L. Cunningham. 2020. 'Herpes Simplex Virus Type 1 Interactions with the Interferon System', *Int J Mol Sci*, 21.

Davis, Meredith E., and Michaela U. Gack. 2015. 'Ubiquitination in the antiviral immune response', *Virology*, 479-480: 52-65.

de Reuver, R., S. Verdonck, E. Dierick, J. Nemegeer, E. Hessmann, S. Ahmad, M. Jans, G. Blancke, F. Van Nieuwerburgh, A. Botzki, L. Vereecke, G. van Loo, W. Declercq, S. Hur,

P. Vandenabeele, and J. Maelfait. 2022. 'ADAR1 prevents autoinflammation by suppressing spontaneous ZBP1 activation', *Nature*, 607: 784-89.

De Salis, Sophie K. F., Lanxin Li, Zheng Chen, Kam W. Lam, Kristen K. Skarratt, Thomas Balle, and Stephen J. Fuller. 2022. "Alternatively Spliced Isoforms of the P2X7 Receptor: Structure, Function and Disease Associations." In *International Journal of Molecular Sciences*.

Deets, K. A., and R. E. Vance. 2021. 'Inflammasomes and adaptive immune responses', *Nat Immunol*.

Dempsey, A., and A. G. Bowie. 2015. 'Innate immune recognition of DNA: A recent history', *Virology*, 479-480: 146-52.

Deneka, Dawid, Marta Sawicka, Andy K. M. Lam, Cristina Paulino, and Raimund Dutzler. 2018. 'Structure of a volume-regulated anion channel of the LRRC8 family', *Nature*, 558: 254-59.

Deng, Zimu, Zhenlu Chong, Christopher S. Law, Kojiro Mukai, Frances O. Ho, Tereza Martinu, Bradley J. Backes, Walter L. Eckalbar, Tomohiko Taguchi, and Anthony K. Shum. 2020. 'A defect in COPI-mediated transport of STING causes immune dysregulation in COPA syndrome', *bioRxiv*: 2020.05.20.106500.

Di Virgilio, Francesco, Alba Clara Sarti, Simonetta Falzoni, Elena De Marchi, and Elena Adinolfi. 2018. 'Extracellular ATP and P2 purinergic signalling in the tumour microenvironment', *Nature Reviews Cancer*, 18: 601-18.

Ding, Bei, Lauren Soblosky, Khoi Nguyen, Junqing Geng, Xinglong Yu, Ayyalusamy Ramamoorthy, and Zhan Chen. 2013. 'Physiologically-Relevant Modes of Membrane Interactions by the Human Antimicrobial Peptide, LL-37, Revealed by SFG Experiments', *Scientific Reports*, 3: 1854.

Dobbs, Nicole, Nikolay Burnaevskiy, Didi Chen, Vijay K Gonugunta, Neal M Alto, and Nan Yan. 2015. 'STING Activation by Translocation from the ER Is Associated with Infection and Autoinflammatory Disease', *Cell Host & Microbe*, 18: 157-68.

Dodantenna, Niranjan, Lakmal Ranathunga, W. A. Gayan Chathuranga, Asela Weerawardhana, Ji-Won Cha, Ashan Subasinghe, Nuwan Gamage, D. K. Haluwana, YongKwan Kim, WeonHwa Jheong, Haryoung Poo, and Jong-Soo Lee. 2022. 'African Swine Fever Virus EP364R and C129R Target Cyclic GMP-AMP To Inhibit the cGAS-STING Signaling Pathway', *Journal of Virology*, 96: e0102222-e22.

Döhner, K., A. Wolfstein, U. Prank, C. Echeverri, D. Dujardin, R. Vallee, and B. Sodeik. 2002. 'Function of dynein and dynactin in herpes simplex virus capsid transport', *Molecular biology of the cell*, 13: 2795-809.

Doitsh, G., N. L. Galloway, X. Geng, Z. Yang, K. M. Monroe, O. Zepeda, P. W. Hunt, H. Hatano, S. Sowinski, I. Muñoz-Arias, and W. C. Greene. 2014. 'Cell death by pyroptosis drives CD4 T-cell depletion in HIV-1 infection', *Nature*, 505: 509-14.

Donnelly-Roberts, Diana L., Marian T. Namovic, Ping Han, and Michael F. Jarvis. 2009. 'Mammalian P2X7 receptor pharmacology: comparison of recombinant mouse, rat and human P2X7 receptors', *British journal of pharmacology*, 157: 1203-14.

Dou, Lei, Yi-Fa Chen, Peter J. Cowan, and Xiao-Ping Chen. 2018. 'Extracellular ATP signaling and clinical relevance', *Clinical Immunology*, 188: 67-73.

Dou, Z., K. Ghosh, M. G. Vizioli, J. Zhu, P. Sen, K. J. Wangensteen, J. Simithy, Y. Lan, Y. Lin, Z. Zhou, B. C. Capell, C. Xu, M. Xu, J. E. Kieckhaefer, T. Jiang, M. Shoshkes-Carmel, Kmaa Tanim, G. N. Barber, J. T. Seykora, S. E. Millar, K. H. Kaestner, B. A. Garcia, P. D. Adams, and S. L. Berger. 2017. 'Cytoplasmic chromatin triggers inflammation in senescence and cancer', *Nature*, 550: 402-06.

Drill, Matthew, Nigel C. Jones, Martin Hunn, Terence J. O'Brien, and Mastura Monif. 2021. 'Antagonism of the ATP-gated P2X7 receptor: a potential therapeutic strategy for cancer', *Purinergic Signalling*, 17: 215-27.

Du, Mingjian, and Zhijian J. Chen. 2018. 'DNA-induced liquid phase condensation of cGAS activates innate immune signaling', *Science*, 361: 704.

Dunphy, G., S. M. Flannery, J. F. Almine, D. J. Connolly, C. Paulus, K. L. Jønsson, M. R. Jakobsen, M. M. Nevels, A. G. Bowie, and L. Unterholzner. 2018. 'Non-canonical Activation of the DNA Sensing Adaptor STING by ATM and IFI16 Mediates NF-κB Signaling after Nuclear DNA Damage', *Mol Cell*, 71: 745-60.e5.

Eaglesham, J. B., Y. Pan, T. S. Kupper, and P. J. Kranzusch. 2019. 'Viral and metazoan poxins are cGAMP-specific nucleases that restrict cGAS-STING signalling', *Nature*, 566: 259-63.

Egan, Terrance M., and Baljit S. Khakh. 2004. 'Contribution of Calcium Ions to P2X Channel Responses', *The Journal of Neuroscience*, 24: 3413.

Ehlers, Bernhard, Judit Küchler, Nezlisah Yasmum, Güzin Dural, Sebastian Voigt, Jonas Schmidt-Chanasit, Thomas Jäkel, Franz-Rainer Matuschka, Dania Richter, Sandra Essbauer, David J. Hughes, Candice Summers, Malcolm Bennett, James P. Stewart, and Rainer G. Ulrich. 2007. 'Identification of novel rodent herpesviruses, including the first gammaherpesvirus of Mus musculus', *Journal of Virology*, 81: 8091-100.

Ehrlich, Paul. 1957. 'The Collected Papers of Paul Ehrlich', *Proceedings of the Royal Society of Medicine*, 50: 210-10.

El-Jesr, M., M. Teir, and C. Maluquer de Motes. 2020. 'Vaccinia Virus Activation and Antagonism of Cytosolic DNA Sensing', *Front Immunol*, 11: 568412.

Ensemble. 2022. 'Ensemble', Accessed 20.12.2022. https://www.ensembl.org/index.html.

Fang, R., Q. Jiang, Y. Guan, P. Gao, R. Zhang, Z. Zhao, and Z. Jiang. 2021. 'Golgi apparatus-synthesized sulfated glycosaminoglycans mediate polymerization and activation of the cGAMP sensor STING', *Immunity*, 54: 962-75.e8.

Fenteany, G., R. F. Standaert, W. S. Lane, S. Choi, E. J. Corey, and S. L. Schreiber. 1995. 'Inhibition of proteasome activities and subunit-specific amino-terminal threonine modification by lactacystin', *Science*, 268: 726-31.

Ferguson, B. J., D. S. Mansur, N. E. Peters, H. Ren, and G. L. Smith. 2012. 'DNA-PK is a DNA sensor for IRF-3-dependent innate immunity', *eLife*, 1: e00047.

Ferrari, D., P. Chiozzi, S. Falzoni, M. Dal Susino, L. Melchiorri, O. R. Baricordi, and F. Di Virgilio. 1997. 'Extracellular ATP triggers IL-1 beta release by activating the purinergic P2Z receptor of human macrophages', *J Immunol*, 159: 1451-8.

Feske, S., C. Picard, and A. Fischer. 2010. 'Immunodeficiency due to mutations in ORAI1 and STIM1', *Clin Immunol*, 135: 169-82.

Fitzgerald, Katherine A., and Jonathan C. Kagan. 2020. 'Toll-like Receptors and the Control of Immunity', *Cell*, 180: 1044-66.

Fore, Faith, Cut Indriputri, Janet Mamutse, and Jusak Nugraha. 2020. 'TLR10 and Its Unique Anti-Inflammatory Properties and Potential Use as a Target in Therapeutics', *Immune network*, 20: e21-e21.

Friard, J., M. Tauc, M. Cougnon, V. Compan, C. Duranton, and I. Rubera. 2017. 'Comparative Effects of Chloride Channel Inhibitors on LRRC8/VRAC-Mediated Chloride Conductance', *Front Pharmacol*, 8: 328.

Friard, Jonas, Alain Corinus, Marc Cougnon, Michel Tauc, Didier F. Pisani, Christophe Duranton, and Isabelle Rubera. 2019. 'LRRC8/VRAC channels exhibit a noncanonical permeability to glutathione, which modulates epithelial-to-mesenchymal transition (EMT)', *Cell death & disease*, 10: 925-25.

Fu, J., D. B. Kanne, M. Leong, L. H. Glickman, S. M. McWhirter, E. Lemmens, K. Mechette, J. J. Leong, P. Lauer, W. Liu, K. E. Sivick, Q. Zeng, K. C. Soares, L. Zheng, D. A. Portnoy, J. J. Woodward, D. M. Pardoll, T. W. Dubensky, Jr., and Y. Kim. 2015. 'STING agonist formulated cancer vaccines can cure established tumors resistant to PD-1 blockade', *Sci Transl Med*, 7: 283ra52.

Fuhrmann, M., A. Castinel, D. Cheslett, D. Furones Nozal, and R. J. Whittington. 2019. 'L'impact des microvariants du virus herpétique ostreid herpesvirus 1 sur la culture d'huîtres creuses dans les hémisphères Nord et Sud depuis 2008', *Rev Sci Tech*, 38: 491-509.

Gaidt, Moritz M., Alyssa Morrow, Marian R. Fairgrieve, Jonathan P. Karr, Nir Yosef, and Russell E. Vance. 2021. 'Self-guarding of MORC3 enables virulence factor-triggered immunity', *Nature*, 600: 138-42.

Gaitán-Peñas, H., A. Gradogna, L. Laparra-Cuervo, C. Solsona, V. Fernández-Dueñas, A. Barrallo-Gimeno, F. Ciruela, M. Lakadamyali, M. Pusch, and R. Estévez. 2016. 'Investigation of LRRC8-Mediated Volume-Regulated Anion Currents in Xenopus Oocytes', *Biophys J*, 111: 1429-43.

Ganser-Pornillos, Barbie K., and Owen Pornillos. 2019. 'Restriction of HIV-1 and other retroviruses by TRIM5', *Nature reviews. Microbiology*, 17: 546-56.

Gao, D., T. Li, X. D. Li, X. Chen, Q. Z. Li, M. Wight-Carter, and Z. J. Chen. 2015. 'Activation of cyclic GMP-AMP synthase by self-DNA causes autoimmune diseases', *Proc Natl Acad Sci U S A*, 112: E5699-705.

Gao, Pu, Manuel Ascano, Yang Wu, Winfried Barchet, Barbara L Gaffney, Thomas Zillinger, Artem A Serganov, Yizhou Liu, Roger A Jones, Gunther Hartmann, Thomas Tuschl, and Dinshaw J Patel. 2013. 'Cyclic [G(2′,5′)pA(3′,5′)p] Is the Metazoan Second Messenger Produced by DNA-Activated Cyclic GMP-AMP Synthase', *Cell*, 153: 1094-107.

Gentili, M., J. Kowal, M. Tkach, T. Satoh, X. Lahaye, C. Conrad, M. Boyron, B. Lombard, S. Durand, G. Kroemer, D. Loew, M. Dalod, C. Thery, and N. Manel. 2015. 'Transmission of innate immune signaling by packaging of cGAMP in viral particles', *Science*, 349: 1232-6.

Geraghty, R. J., C. Krummenacher, G. H. Cohen, R. J. Eisenberg, and P. G. Spear. 1998. 'Entry of alphaherpesviruses mediated by poliovirus receptor-related protein 1 and poliovirus receptor', *Science*, 280: 1618-20.

Ghiringhelli, François, Lionel Apetoh, Antoine Tesniere, Laetitia Aymeric, Yuting Ma, Carla Ortiz, Karim Vermaelen, Theocharis Panaretakis, Grégoire Mignot, Evelyn Ullrich, Jean-Luc Perfettini, Frédéric Schlemmer, Ezgi Tasdemir, Martin Uhl, Pierre Génin, Ahmet Civas, Bernhard Ryffel, Jean Kanellopoulos, Jürg Tschopp, Fabrice André, Rosette Lidereau, Nicole M. McLaughlin, Nicole M. Haynes, Mark J. Smyth, Guido Kroemer, and Laurence Zitvogel. 2009. 'Activation of the NLRP3 inflammasome in dendritic cells induces IL-1β–dependent adaptive immunity against tumors', *Nature Medicine*, 15: 1170-78.

Gombault, Aurélie, Ludivine Baron, and Isabelle Couillin. 2013. 'ATP release and purinergic signaling in NLRP3 inflammasome activation', *Frontiers in Immunology*, 3: 414-14.

Goodsell, David. 2011. 'Toll-like receptors warn us about bacterial and viral infection', *RCSB PDB*, November 2011.

Gossman, David G., and Hong-Bo Zhao. 2008. 'Hemichannel-mediated inositol 1,4,5-trisphosphate (IP3) release in the cochlea: a novel mechanism of IP3 intercellular signaling', *Cell communication & adhesion*, 15: 305-15.

Gray, E. E., P. M. Treuting, J. J. Woodward, and D. B. Stetson. 2015. 'Cutting Edge: cGAS Is Required for Lethal Autoimmune Disease in the Trex1-Deficient Mouse Model of Aicardi-Goutières Syndrome', *J Immunol*, 195: 1939-43.

Green, Jack P., Tessa Swanton, Lucy V. Morris, Lina Y. El-Sharkawy, James Cook, Shi Yu, James Beswick, Antony D. Adamson, Neil E. Humphreys, Richard Bryce, Sally Freeman, Catherine Lawrence, and David Brough. 2020. 'LRRC8A is essential for hypotonicity-, but not for DAMP-induced NLRP3 inflammasome activation', *eLife*, 9: e59704.

Greenbaum, Benjamin D., Arnold J. Levine, Gyan Bhanot, and Raul Rabadan. 2008. 'Patterns of Evolution and Host Gene Mimicry in Influenza and Other RNA Viruses', *PLOS Pathogens*, 4: e1000079.

Grose, C., and P. A. Brunel. 1978. 'Varicella-zoster virus: isolation and propagation in human melanoma cells at 36 and 32 degrees C', *Infect Immun*, 19: 199-203.

Gruffat, Henri, Roberta Marchione, and Evelyne Manet. 2016. 'Herpesvirus Late Gene Expression: A Viral-Specific Pre-initiation Complex Is Key', *Frontiers in microbiology*, 7: 869-69.

Gui, X., H. Yang, T. Li, X. Tan, P. Shi, M. Li, F. Du, and Z. J. Chen. 2019. 'Autophagy induction via STING trafficking is a primordial function of the cGAS pathway', *Nature*, 567: 262-66.

Gulen, M. F., U. Koch, S. M. Haag, F. Schuler, L. Apetoh, A. Villunger, F. Radtke, and A. Ablasser. 2017. 'Signalling strength determines proapoptotic functions of STING', *Nat Commun*, 8: 427.

Guo, H., R. P. Gilley, A. Fisher, R. Lane, V. J. Landsteiner, K. B. Ragan, C. M. Dovey, J. E. Carette, J. W. Upton, E. S. Mocarski, and W. J. Kaiser. 2018. 'Species-independent contribution of ZBP1/DAI/DLM-1-triggered necroptosis in host defense against HSV1', *Cell death & disease*, 9: 816.

Guo, X., J. Ma, J. Sun, and G. Gao. 2007. 'The zinc-finger antiviral protein recruits the RNA processing exosome to degrade the target mRNA', *Proc Natl Acad Sci U S A*, 104: 151-6.

Haag, Simone M., Muhammet F. Gulen, Luc Reymond, Antoine Gibelin, Laurence Abrami, Alexiane Decout, Michael Heymann, F. Gisou van der Goot, Gerardo Turcatti, Rayk Behrendt, and Andrea Ablasser. 2018. 'Targeting STING with covalent small-molecule inhibitors', *Nature*, 559: 269-73.

Hall, Justin, Erik C. Ralph, Suman Shanker, Hong Wang, Laura J. Byrnes, Reto Horst, Jimson Wong, Amy Brault, Darren Dumlao, James F. Smith, Leslie A. Dakin, Daniel C. Schmitt,

John Trujillo, Fabien Vincent, Matt Griffor, and Ann E. Aulabaugh. 2017. 'The catalytic mechanism of cyclic GMP-AMP synthase (cGAS) and implications for innate immunity and inhibition', *Protein science : a publication of the Protein Society*, 26: 2367-80.

Hansen, A. L., G. J. Buchan, M. Rühl, K. Mukai, S. R. Salvatore, E. Ogawa, S. D. Andersen, M. B. Iversen, A. L. Thielke, C. Gunderstofte, M. Motwani, C. T. Møller, A. S. Jakobsen, K. A. Fitzgerald, J. Roos, R. Lin, T. J. Maier, R. Goldbach-Mansky, C. A. Miner, W. Qian, J. J. Miner, R. E. Rigby, J. Rehwinkel, M. R. Jakobsen, H. Arai, T. Taguchi, F. J. Schopfer, D. Olagnier, and C. K. Holm. 2018. 'Nitro-fatty acids are formed in response to virus infection and are potent inhibitors of STING palmitoylation and signaling', *Proc Natl Acad Sci U S A*, 115: E7768-e75.

Hansen, Ann-Brit E., Hanne T. Vestergaard, Ram B. Dessau, Jacob Bodilsen, Nanna S. Andersen, Lars H. Omland, Claus B. Christiansen, Svend Ellermann-Eriksen, Lene Nielsen, Thomas Benfield, Henrik T. Sørensen, Christian Ø Andersen, Anne-Mette Lebech, and Niels Obel. 2020. 'Long-Term Survival, Morbidity, Social Functioning and Risk of Disability in Patients with a Herpes Simplex Virus Type 1 or Type 2 Central Nervous System Infection, Denmark, 2000-2016', *Clinical epidemiology*, 12: 745-55.

Harding, S. M., J. L. Benci, J. Irianto, D. E. Discher, A. J. Minn, and R. A. Greenberg. 2017. 'Mitotic progression following DNA damage enables pattern recognition within micronuclei', *Nature*, 548: 466-70.

Hayes, C. K., D. R. Wilcox, Y. Yang, G. K. Coleman, M. A. Brown, and R. Longnecker. 2021. 'ASC-dependent inflammasomes contribute to immunopathology and mortality in herpes simplex encephalitis', *PLoS Pathog*, 17: e1009285.

Heinemann, Udo, and Yvette Roske. 2020. "Symmetry in Nucleic-Acid Double Helices." In *Symmetry*.

Hemmi, Hiroaki, Osamu Takeuchi, Taro Kawai, Tsuneyasu Kaisho, Shintaro Sato, Hideki Sanjo, Makoto Matsumoto, Katsuaki Hoshino, Hermann Wagner, Kiyoshi Takeda, and Shizuo Akira. 2000. 'A Toll-like receptor recognizes bacterial DNA', *Nature*, 408: 740-45.

Hennessy, Elizabeth J., Andrew E. Parker, and Luke A. J. O'Neill. 2010. 'Targeting Toll-like receptors: emerging therapeutics?', *Nature Reviews Drug Discovery*, 9: 293-307.

Hernández-Carballo, C. Y., J. A. De Santiago-Castillo, T. Rosales-Saavedra, P. Pérez-Cornejo, and J. Arreola. 2010. 'Control of volume-sensitive chloride channel inactivation by the coupled action of intracellular chloride and extracellular protons', *Pflugers Arch*, 460: 633-44.

Herold, B. C., D. WuDunn, N. Soltys, and P. G. Spear. 1991. 'Glycoprotein C of herpes simplex virus type 1 plays a principal role in the adsorption of virus to cells and in infectivity', *J Virol*, 65: 1090-8.

Hertzog, Jonny, Antonio Gregorio Dias Junior, Rachel E. Rigby, Claire L. Donald, Alice Mayer, Erdinc Sezgin, Chaojun Song, Boquan Jin, Philip Hublitz, Christian Eggeling, Alain Kohl,

and Jan Rehwinkel. 2018. 'Infection with a Brazilian isolate of Zika virus generates RIG-I stimulatory RNA and the viral NS5 protein blocks type I IFN induction and signaling', *European Journal of Immunology*, 48: 1120-36.

Hertzog, Jonny, and Jan Rehwinkel. 2020. 'Regulation and inhibition of the DNA sensor cGAS', *EMBO reports*, 21: e51345.

Hong, Z., J. Mei, C. Li, G. Bai, M. Maimaiti, H. Hu, W. Yu, L. Sun, L. Zhang, D. Cheng, Y. Liao, S. Li, Y. You, H. Sun, J. Huang, X. Liu, J. Lieberman, and C. Wang. 2021. 'STING inhibitors target the cyclic dinucleotide binding pocket', *Proc Natl Acad Sci U S A*, 118.

Hooy, Richard M, Guido Massaccesi, Kimberly E Rousseau, Michael A Chattergoon, and Jungsan Sohn. 2020. 'Allosteric coupling between Mn2+ and dsDNA controls the catalytic efficiency and fidelity of cGAS', *Nucleic Acids Research*, 48: 4435-47.

Horan, K. A., K. Hansen, M. R. Jakobsen, C. K. Holm, S. Søby, L. Unterholzner, M. Thompson, J. A. West, M. B. Iversen, S. B. Rasmussen, S. Ellermann-Eriksen, E. Kurt-Jones, S. Landolfo, B. Damania, J. Melchjorsen, A. G. Bowie, K. A. Fitzgerald, and S. R. Paludan. 2013. 'Proteasomal degradation of herpes simplex virus capsids in macrophages releases DNA to the cytosol for recognition by DNA sensors', *J Immunol*, 190: 2311-9.

Hornung, V., J. Ellegast, S. Kim, K. Brzózka, A. Jung, H. Kato, H. Poeck, S. Akira, K. K. Conzelmann, M. Schlee, S. Endres, and G. Hartmann. 2006. '5'-Triphosphate RNA is the ligand for RIG-I', *Science*, 314: 994-7.

Hornung, V., R. Hartmann, A. Ablasser, and K. P. Hopfner. 2014. 'OAS proteins and cGAS: unifying concepts in sensing and responding to cytosolic nucleic acids', *Nat Rev Immunol*, 14: 521-8.

Hoshino, K., O. Takeuchi, T. Kawai, H. Sanjo, T. Ogawa, Y. Takeda, K. Takeda, and S. Akira. 1999. 'Cutting edge: Toll-like receptor 4 (TLR4)-deficient mice are hyporesponsive to lipopolysaccharide: evidence for TLR4 as the Lps gene product', *J Immunol*, 162: 3749-52.

Hristova, Dayana B., Katharina B. Lauer, and Brian J. Ferguson. 2020. 'Viral interactions with non-homologous end-joining: a game of hide-and-seek', *Journal of General Virology*, 101: 1133-44.

Hu, Hongbo, and Shao-Cong Sun. 2016. 'Ubiquitin signaling in immune responses', *Cell research*, 26: 457-83.

Hu, Jiaxiang, Xiaoxue Wang, Yanling Xing, Enguang Rong, Mengfei Ning, Jacqueline Smith, and Yinhua Huang. 2018. 'Origin and development of oligoadenylate synthetase immune system', *BMC Evolutionary Biology*, 18: 201.

Hu, Ming-Ming, and Hong-Bing Shu. 2017. 'Multifaceted roles of TRIM38 in innate immune and inflammatory responses', *Cellular & Molecular Immunology*, 14: 331-38.

Hubbard, Nicholas W., Joshua M. Ames, Megan Maurano, Lan H. Chu, Kim Y. Somfleth, Nandan S. Gokhale, Margo Werner, Jessica M. Snyder, Katrina Lichauco, Ram Savan, Daniel B. Stetson, and Andrew Oberst. 2022. 'ADAR1 mutation causes ZBP1-dependent immunopathology', *Nature*, 607: 769-75.

Ibáñez, F. J., M. A. Farías, M. P. Gonzalez-Troncoso, N. Corrales, L. F. Duarte, A. Retamal-Díaz, and P. A. González. 2018. 'Experimental Dissection of the Lytic Replication Cycles of Herpes Simplex Viruses in vitro', *Frontiers in microbiology*, 9: 2406.

Idriss, H. T., and J. H. Naismith. 2000. 'TNF alpha and the TNF receptor superfamily: structure-function relationship(s)', *Microsc Res Tech*, 50: 184-95.

Isaacs, A., R. A. Cox, and Z. Rotem. 1963. 'Foreign nucleic acids as the stimulus to make interferon', *Lancet*, 2: 113-6.

Ishii, K. J., C. Coban, H. Kato, K. Takahashi, Y. Torii, F. Takeshita, H. Ludwig, G. Sutter, K. Suzuki, H. Hemmi, S. Sato, M. Yamamoto, S. Uematsu, T. Kawai, O. Takeuchi, and S. Akira. 2006. 'A Toll-like receptor-independent antiviral response induced by double-stranded B-form DNA', *Nat Immunol*, 7: 40-8.

Ishikawa, H., and G. N. Barber. 2008. 'STING is an endoplasmic reticulum adaptor that facilitates innate immune signalling', *Nature*, 455: 674-8.

Ishikawa, H., Z. Ma, and G. N. Barber. 2009. 'STING regulates intracellular DNA-mediated, type I interferon-dependent innate immunity', *Nature*, 461: 788-92.

Ivashkiv, Lionel B., and Laura T. Donlin. 2014. 'Regulation of type I interferon responses', *Nature Reviews Immunology*, 14: 36-49.

James, Charlotte, Manale Harfouche, Nicky J. Welton, Katherine Me Turner, Laith J. Abu-Raddad, Sami L. Gottlieb, and Katharine J. Looker. 2020. 'Herpes simplex virus: global infection prevalence and incidence estimates, 2016', *Bulletin of the World Health Organization*, 98: 315-29.

Janeway, C. A., Jr. 1989. 'Approaching the asymptote? Evolution and revolution in immunology', *Cold Spring Harb Symp Quant Biol*, 54 Pt 1: 1-13.

Jefferies, C. A. 2019. 'Regulating IRFs in IFN Driven Disease', *Front Immunol*, 10: 325.

Jeffries, Austin M., Alexander J. Suptela, and Ian Marriott. 2022. 'Z-DNA binding protein 1 mediates necroptotic and apoptotic cell death pathways in murine astrocytes following herpes simplex virus-1 infection', *Journal of Neuroinflammation*, 19: 109.

Jesus, Sónia A., Marcus G. Doherr, and Thomas B. Hildebrandt. 2021. "Elephant Endotheliotropic Herpesvirus Impact in the European Asian Elephant (Elephas maximus) Population: Are Hereditability and Zoo-Associated Factors Linked with Mortality?" In *Animals*.

Jiao, Huipeng, Laurens Wachsmuth, Simone Wolf, Juliane Lohmann, Masahiro Nagata, Göksu Gökberk Kaya, Nikos Oikonomou, Vangelis Kondylis, Manuel Rogg, Martin Diebold, Simon E. Tröder, Branko Zevnik, Marco Prinz, Christoph Schell, George R. Young, George Kassiotis, and Manolis Pasparakis. 2022. 'ADAR1 averts fatal type I interferon induction by ZBP1', *Nature*, 607: 776-83.

Jin, T., A. Perry, J. Jiang, P. Smith, J. A. Curry, L. Unterholzner, Z. Jiang, G. Horvath, V. A. Rathinam, R. W. Johnstone, V. Hornung, E. Latz, A. G. Bowie, K. A. Fitzgerald, and T. S. Xiao. 2012. 'Structures of the HIN domain:DNA complexes reveal ligand binding and activation mechanisms of the AIM2 inflammasome and IFI16 receptor', *Immunity*, 36: 561-71.

Jinek, Martin, Krzysztof Chylinski, Ines Fonfara, Michael Hauer, Jennifer A. Doudna, and Emmanuelle Charpentier. 2012. 'A Programmable Dual-RNA–Guided DNA Endonuclease in Adaptive Bacterial Immunity', *Science*, 337: 816-21.

Johnson, Zachary Lee, and Jue Chen. 2017. 'Structural Basis of Substrate Recognition by the Multidrug Resistance Protein MRP1', *Cell*, 168: 1075-85.e9.

Josephson, A., and M. E. Gombert. 1988. 'Airborne transmission of nosocomial varicella from localized zoster', *J Infect Dis*, 158: 238-41.

Judge, A. D., V. Sood, J. R. Shaw, D. Fang, K. McClintock, and I. MacLachlan. 2005. 'Sequence-dependent stimulation of the mammalian innate immune response by synthetic siRNA', *Nat Biotechnol*, 23: 457-62.

Kager, Leo, Meyling Cheok, Wenjian Yang, Gianluigi Zaza, Qing Cheng, John C. Panetta, Ching-Hon Pui, James R. Downing, Mary V. Relling, and William E. Evans. 2005. 'Folate pathway gene expression differs in subtypes of acute lymphoblastic leukemia and influences methotrexate pharmacodynamics', *The Journal of Clinical Investigation*, 115: 110-17.

Karaba, Andrew H., Alexis Figueroa, Guido Massaccesi, Sara Botto, Victor R. DeFilippis, and Andrea L. Cox. 2020. 'Herpes simplex virus type 1 inflammasome activation in proinflammatory human macrophages is dependent on NLRP3, ASC, and caspase-1', *PLoS One*, 15: e0229570.

Karasawa, Akira, and Toshimitsu Kawate. 2018. 'High-throughput YO-PRO-1 Uptake Assay for P2X7 Receptors Expressed in HEK Cells', *Bio-protocol*, 8: e2943.

Karki, R., S. M. Man, R. K. S. Malireddi, P. Gurung, P. Vogel, M. Lamkanfi, and T. D. Kanneganti. 2015. 'Concerted activation of the AIM2 and NLRP3 inflammasomes orchestrates host protection against Aspergillus infection', *Cell Host Microbe*, 17: 357-68.

Karlin, S., W. Doerfler, and L. R. Cardon. 1994. 'Why is CpG suppressed in the genomes of virtually all small eukaryotic viruses but not in those of large eukaryotic viruses?', *Journal of Virology*, 68: 2889.

Karlin, S., and J. Mrázek. 1997. 'Compositional differences within and between eukaryotic genomes', *Proceedings of the National Academy of Sciences of the United States of America*, 94: 10227-32.

Karmakar, Mausita, Michael A. Katsnelson, George R. Dubyak, and Eric Pearlman. 2016. 'Neutrophil P2X7 receptors mediate NLRP3 inflammasome-dependent IL-1β secretion in response to ATP', *Nature Communications*, 7: 10555.

Kasuya, Go, Takanori Nakane, Takeshi Yokoyama, Yanyan Jia, Masato Inoue, Kengo Watanabe, Ryoki Nakamura, Tomohiro Nishizawa, Tsukasa Kusakizako, Akihisa Tsutsumi, Haruaki Yanagisawa, Naoshi Dohmae, Motoyuki Hattori, Hidenori Ichijo, Zhiqiang Yan, Masahide Kikkawa, Mikako Shirouzu, Ryuichiro Ishitani, and Osamu Nureki. 2018. 'Cryo-EM structures of the human volume-regulated anion channel LRRC8', *Nature Structural & Molecular Biology*, 25: 797-804.

Kato, H., O. Takeuchi, E. Mikamo-Satoh, R. Hirai, T. Kawai, K. Matsushita, A. Hiiragi, T. S. Dermody, T. Fujita, and S. Akira. 2008. 'Length-dependent recognition of double-stranded ribonucleic acids by retinoic acid-inducible gene-I and melanoma differentiation-associated gene 5', *J Exp Med*, 205: 1601-10.

Kerur, N., M. V. Veettil, N. Sharma-Walia, V. Bottero, S. Sadagopan, P. Otageri, and B. Chandran. 2011. 'IFI16 acts as a nuclear pathogen sensor to induce the inflammasome in response to Kaposi Sarcoma-associated herpesvirus infection', *Cell Host Microbe*, 9: 363-75.

Kilchert, Cornelia, Sina Wittmann, and Lidia Vasiljeva. 2016. 'The regulation and functions of the nuclear RNA exosome complex', *Nature Reviews Molecular Cell Biology*, 17: 227-39.

Kim, Ki Yeon, Gwanghee Lee, Minsang Yoon, Eun Hye Cho, Chan-Sik Park, and Moon Gyo Kim. 2015. 'Expression Analyses Revealed Thymic Stromal Co-Transporter/Slc46A2 Is in Stem Cell Populations and Is a Putative Tumor Suppressor', *Molecules and cells*, 38: 548-61.

Kim, T., S. Pazhoor, M. Bao, Z. Zhang, S. Hanabuchi, V. Facchinetti, L. Bover, J. Plumas, L. Chaperot, J. Qin, and Y. J. Liu. 2010. 'Aspartate-glutamate-alanine-histidine box motif (DEAH)/RNA helicase A helicases sense microbial DNA in human plasmacytoid dendritic cells', *Proc Natl Acad Sci U S A*, 107: 15181-6.

Kimberlin, David W., Chin-Yu Lin, Richard F. Jacobs, Dwight A. Powell, Lawrence Corey, William C. Gruber, Mobeen Rathore, John S. Bradley, Pamela S. Diaz, Mary Kumar, Ann M. Arvin, Kathleen Gutierrez, Mark Shelton, Leonard B. Weiner, John W. Sleasman, Teresa Murguía de Sierra, Stephen Weller, Seng-Jaw Soong, Jan Kiell, Fred D. Lakeman, Richard J. Whitley, Allergy the National Institute of, and Groupa Infectious Diseases Collaborative Antiviral Study. 2001. 'Safety and Efficacy of High-Dose Intravenous Acyclovir in the Management of Neonatal Herpes Simplex Virus Infections', *Pediatrics*, 108: 230-38.

Kirchhoff, Christian, and Heribert Cypionka. 2017. 'Propidium ion enters viable cells with high membrane potential during live-dead staining', *Journal of Microbiological Methods*, 142: 79-82.

Klafack, Sandro, Lars Schröder, Yeonhwa Jin, Matthias Lenk, Pei-Yu Lee, Walter Fuchs, Jean-Christophe Avarre, and Sven M. Bergmann. 2022. 'Development of an attenuated vaccine against Koi Herpesvirus Disease (KHVD) suitable for oral administration and immersion', *npj Vaccines*, 7: 106.

Kolde, R., S. Laur, P. Adler, and J. Vilo. 2012. 'Robust rank aggregation for gene list integration and meta-analysis', *Bioinformatics*, 28: 573-80.

Komuro, Akihiko, and Curt M. Horvath. 2006. 'RNA- and Virus-Independent Inhibition of Antiviral Signaling by RNA Helicase LGP2', *Journal of Virology*, 80: 12332-42.

Kondo, Takeshi, Junya Kobayashi, Tatsuya Saitoh, Kenta Maruyama, Ken J. Ishii, Glen N. Barber, Kenshi Komatsu, Shizuo Akira, and Taro Kawai. 2013. 'DNA damage sensor MRE11 recognizes cytosolic double-stranded DNA and induces type I interferon by regulating STING trafficking', *Proceedings of the National Academy of Sciences*, 110: 2969.

Konno, H., K. Konno, and G. N. Barber. 2013. 'Cyclic dinucleotides trigger ULK1 (ATG1) phosphorylation of STING to prevent sustained innate immune signaling', *Cell*, 155: 688-98.

Koshizuka, Tetsuo, Fumi Goshima, Hiroki Takakuwa, Naoki Nozawa, Tohru Daikoku, Osamu Koiwai, and Yukihiro Nishiyama. 2002. 'Identification and characterization of the UL56 gene product of herpes simplex virus type 2', *Journal of Virology*, 76: 6718-28.

Kranzusch, P. J., S. C. Wilson, A. S. Lee, J. M. Berger, J. A. Doudna, and R. E. Vance. 2015. 'Ancient Origin of cGAS-STING Reveals Mechanism of Universal 2',3' cGAMP Signaling', *Mol Cell*, 59: 891-903.

Kranzusch, Philip J, Amy Si-Ying Lee, James M Berger, and Jennifer A Doudna. 2013. 'Structure of Human cGAS Reveals a Conserved Family of Second-Messenger Enzymes in Innate Immunity', *Cell Reports*, 3: 1362-68.

Kranzusch, Philip J. 2019. 'cGAS and CD-NTase enzymes: structure, mechanism, and evolution', *Current Opinion in Structural Biology*, 59: 178-87.

Krug, A., G. D. Luker, W. Barchet, D. A. Leib, S. Akira, and M. Colonna. 2004. 'Herpes simplex virus type 1 activates murine natural interferon-producing cells through toll-like receptor 9', *Blood*, 103: 1433-7.

Kujirai, Tomoya, Christian Zierhut, Yoshimasa Takizawa, Ryan Kim, Lumi Negishi, Nobuki Uruma, Seiya Hirai, Hironori Funabiki, and Hitoshi Kurumizaka. 2020. 'Structural basis for the inhibition of cGAS by nucleosomes', *Science*, 370: 455.

Kumar, Lalit, Janet Chou, Christina S. K. Yee, Arturo Borzutzky, Elisabeth H. Vollmann, Ulrich H. von Andrian, Shin-Young Park, Georg Hollander, John P. Manis, P. Luigi Poliani, and Raif S. Geha. 2014. 'Leucine-rich repeat containing 8A (LRRC8A) is essential for T lymphocyte development and function', *The Journal of experimental medicine*, 211: 929-42.

Kuriakose, Teneema, Si Ming Man, R. K. Subbarao Malireddi, Rajendra Karki, Sannula Kesavardhana, David E. Place, Geoffrey Neale, Peter Vogel, and Thirumala-Devi Kanneganti. 2016. 'ZBP1/DAI is an innate sensor of influenza virus triggering the NLRP3 inflammasome and programmed cell death pathways', *Science Immunology*, 1: aag2045.

Lahaye, X., M. Gentili, A. Silvin, C. Conrad, L. Picard, M. Jouve, E. Zueva, M. Maurin, F. Nadalin, G. J. Knott, B. Zhao, F. Du, M. Rio, J. Amiel, A. H. Fox, P. Li, L. Etienne, C. S. Bond, L. Colleaux, and N. Manel. 2018. 'NONO Detects the Nuclear HIV Capsid to Promote cGAS-Mediated Innate Immune Activation', *Cell*, 175: 488-501.e22.

Lahey, Lauren J., Xianlan Wen, Rachel E. Mardjuki, Volker Böhnert, Gaelen T. Hess, Christopher Ritchie, Jacqueline A. Carozza, Merritt Maduke, Michael C. Bassik, and Lingyin Li. 2020. 'The LRRC8A:C Heteromeric Channel Is a cGAMP Transporter and the Dominant cGAMP Importer in Human Vasculature Cells', *bioRxiv*: 2020.02.13.948273.

Laird, Dale W. 2006. 'Life cycle of connexins in health and disease', *The Biochemical journal*, 394: 527-43.

Lande, Roberto, Josh Gregorio, Valeria Facchinetti, Bithi Chatterjee, Yi-Hong Wang, Bernhard Homey, Wei Cao, Yui-Hsi Wang, Bing Su, Frank O. Nestle, Tomasz Zal, Ira Mellman, Jens-Michael Schröder, Yong-Jun Liu, and Michel Gilliet. 2007. 'Plasmacytoid dendritic cells sense self-DNA coupled with antimicrobial peptide', *Nature*, 449: 564-69.

Larkin, B., V. Ilyukha, M. Sorokin, A. Buzdin, E. Vannier, and A. Poltorak. 2017. 'Cutting Edge: Activation of STING in T Cells Induces Type I IFN Responses and Cell Death', *J Immunol*, 199: 397-402.

Layden, Michael J., Fabian Rentzsch, and Eric Röttinger. 2016. 'The rise of the starlet sea anemone Nematostella vectensis as a model system to investigate development and regeneration', *WIREs Developmental Biology*, 5: 408-28.

Lazarowski, E. R. 2012. 'Vesicular and conductive mechanisms of nucleotide release', *Purinergic Signal*, 8: 359-73.

Leclair, J. M., J. A. Zaia, M. J. Levin, R. G. Congdon, and D. A. Goldmann. 1980. 'Airborne transmission of chickenpox in a hospital', *N Engl J Med*, 302: 450-3.

Lee, C. C., Y. Sun, S. Qian, and H. W. Huang. 2011. 'Transmembrane pores formed by human antimicrobial peptide LL-37', *Biophys J*, 100: 1688-96.

Lefèvre, Fabrice, Marie-Hélène Rémy, and Jean-Michel Masson. 1997. 'Alanine-stretch scanning mutagenesis: a simple and efficient method to probe protein structure and function', *Nucleic Acids Research*, 25: 447-48.

Lemaitre, B., E. Nicolas, L. Michaut, J. M. Reichhart, and J. A. Hoffmann. 1996. 'The dorsoventral regulatory gene cassette spätzle/Toll/cactus controls the potent antifungal response in Drosophila adults', *Cell*, 86: 973-83.

Li, J., M. A. Duran, N. Dhanota, W. K. Chatila, S. E. Bettigole, J. Kwon, R. K. Sriram, M. P. Humphries, M. Salto-Tellez, J. A. James, M. G. Hanna, J. C. Melms, S. Vallabhaneni, K. Litchfield, I. Usaite, D. Biswas, R. Bareja, H. W. Li, M. L. Martin, P. Dorsaint, J. A. Cavallo, P. Li, C. Pauli, L. Gottesdiener, B. J. DiPardo, T. J. Hollmann, T. Merghoub, H. Y. Wen, J. S. Reis-Filho, N. Riaz, S. M. Su, A. Kalbasi, N. Vasan, S. N. Powell, J. D. Wolchok, O. Elemento, C. Swanton, A. N. Shoushtari, E. E. Parkes, B. Izar, and S. F. Bakhoum. 2021. 'Metastasis and Immune Evasion from Extracellular cGAMP Hydrolysis', *Cancer Discov*, 11: 1212-27.

Li, L., Q. Yin, P. Kuss, Z. Maliga, J. L. Millan, H. Wu, and T. J. Mitchison. 2014. 'Hydrolysis of 2'3'-cGAMP by ENPP1 and design of nonhydrolyzable analogs', *Nat Chem Biol*, 10: 1043-8.

Li, Ning, Jing Sun, Zachary L. Benet, Ze Wang, Souhaila Al-Khodor, Sinu P. John, Bin Lin, Myong-Hee Sung, and Iain D. C. Fraser. 2015. 'Development of a cell system for siRNA screening of pathogen responses in human and mouse macrophages', *Scientific Reports*, 5: 9559.

Li, Tuo, Tuozhi Huang, Mingjian Du, Xiang Chen, Fenghe Du, Junyao Ren, and Zhijian J. Chen. 2021. 'Phosphorylation and chromatin tethering prevent cGAS activation during mitosis', *Science*: eabc5386.

Li, Wei, Han Xu, Tengfei Xiao, Le Cong, Michael I. Love, Feng Zhang, Rafael A. Irizarry, Jun S. Liu, Myles Brown, and X. Shirley Liu. 2014. 'MAGeCK enables robust identification of essential genes from genome-scale CRISPR/Cas9 knockout screens', *Genome Biology*, 15: 554.

Lian, H., J. Wei, R. Zang, W. Ye, Q. Yang, X. N. Zhang, Y. D. Chen, Y. Z. Fu, M. M. Hu, C. Q. Lei, W. W. Luo, S. Li, and H. B. Shu. 2018. 'ZCCHC3 is a co-sensor of cGAS for dsDNA recognition in innate immune response', *Nat Commun*, 9: 3349.

Liang, Y., J. L. Vogel, A. Narayanan, H. Peng, and T. M. Kristie. 2009. 'Inhibition of the histone demethylase LSD1 blocks alpha-herpesvirus lytic replication and reactivation from latency', *Nat Med*, 15: 1312-7.

Liao, Chen-Yang, Cao-Qi Lei, and Hong-Bing Shu. 2020. 'PCBP1 modulates the innate immune response by facilitating the binding of cGAS to DNA', *Cellular & Molecular Immunology*.

Liddicoat, B. J., R. Piskol, A. M. Chalk, G. Ramaswami, M. Higuchi, J. C. Hartner, J. B. Li, P. H. Seeburg, and C. R. Walkley. 2015. 'RNA editing by ADAR1 prevents MDA5 sensing of endogenous dsRNA as nonself', *Science*, 349: 1115-20.

Liu, G., and M. U. Gack. 2020. 'Distinct and Orchestrated Functions of RNA Sensors in Innate Immunity', *Immunity*, 53: 26-42.

Liu, N., X. Pang, H. Zhang, and P. Ji. 2021. 'The cGAS-STING Pathway in Bacterial Infection and Bacterial Immunity', *Front Immunol*, 12: 814709.

Liu, Shu-Guang, Chao Gao, Rui-Dong Zhang, Xiao-Xi Zhao, Lei Cui, Wei-Jing Li, Zhen-Ping Chen, Zhi-Xia Yue, Yuan-Yuan Zhang, Min-Yuan Wu, Jian-Xiang Wang, Zhi-Gang Li, and Hu-Yong Zheng. 2017. 'Polymorphisms in methotrexate transporters and their relationship to plasma methotrexate levels, toxicity of high-dose methotrexate, and outcome of pediatric acute lymphoblastic leukemia', *Oncotarget*, 8.

Liu, Y., A. A. Jesus, B. Marrero, D. Yang, S. E. Ramsey, G. A. M. Sanchez, K. Tenbrock, H. Wittkowski, O. Y. Jones, H. S. Kuehn, C. R. Lee, M. A. DiMattia, E. W. Cowen, B. Gonzalez, I. Palmer, J. J. DiGiovanna, A. Biancotto, H. Kim, W. L. Tsai, A. M. Trier, Y. Huang, D. L. Stone, S. Hill, H. J. Kim, C. St Hilaire, S. Gurprasad, N. Plass, D. Chapelle, I. Horkayne-Szakaly, D. Foell, A. Barysenka, F. Candotti, S. M. Holland, J. D. Hughes, H. Mehmet, A. C. Issekutz, M. Raffeld, J. McElwee, J. R. Fontana, C. P. Minniti, S. Moir, D. L. Kastner, M. Gadina, A. C. Steven, P. T. Wingfield, S. R. Brooks, S. D. Rosenzweig, T. A. Fleisher, Z. Deng, M. Boehm, A. S. Paller, and R. Goldbach-Mansky. 2014. 'Activated STING in a vascular and pulmonary syndrome', *N Engl J Med*, 371: 507-18.

Liu, Ying, Pengbiao Xu, Sophie Rivara, Chong Liu, Jonathan Ricci, Xuefeng Ren, James H. Hurley, and Andrea Ablasser. 2022. 'Clathrin-associated AP-1 controls termination of STING signalling', *Nature*, 610: 761-67.

Liu, Zhao-Shan, Hong Cai, Wen Xue, Miao Wang, Tian Xia, Wan-Jin Li, Jia-Qing Xing, Ming Zhao, Yi-Jiao Huang, Shuai Chen, Sheng-Ming Wu, Xinzheng Wang, Xin Liu, Xue Pang, Zi-Yu Zhang, Tingting Li, Jiang Dai, Fangting Dong, Qing Xia, Ai-Ling Li, Tao Zhou, Zheng-gang Liu, Xue-Min Zhang, and Tao Li. 2019. 'G3BP1 promotes DNA binding and activation of cGAS', *Nature Immunology*, 20: 18-28.

Livak, K. J., and T. D. Schmittgen. 2001. 'Analysis of relative gene expression data using real-time quantitative PCR and the 2(-Delta Delta C(T)) Method', *Methods*, 25: 402-8.

Loiselle, Alayna E., Jean X. Jiang, and Henry J. Donahue. 2013. 'Gap junction and hemichannel functions in osteocytes', *Bone*, 54: 205-12.

Lück, J. C., D. Puchkov, F. Ullrich, and T. J. Jentsch. 2018. 'LRRC8/VRAC anion channels are required for late stages of spermatid development in mice', *J Biol Chem*, 293: 11796-808.

Luo, W. W., S. Li, C. Li, H. Lian, Q. Yang, B. Zhong, and H. B. Shu. 2016. 'iRhom2 is essential for innate immunity to DNA viruses by mediating trafficking and stability of the adaptor STING', *Nat Immunol*, 17: 1057-66.

Luteijn, Rutger D., Shivam A. Zaver, Benjamin G. Gowen, Stacia K. Wyman, Nick E. Garelis, Liberty Onia, Sarah M. McWhirter, George E. Katibah, Jacob E. Corn, Joshua J. Woodward, and David H. Raulet. 2019. 'SLC19A1 transports immunoreactive cyclic dinucleotides', *Nature*, 573: 434-38.

Lutter, Darius, Florian Ullrich, Jennifer C. Lueck, Stefan Kempa, and Thomas J. Jentsch. 2017. 'Selective transport of neurotransmitters and modulators by distinct volume-regulated LRRC8 anion channels', *Journal of Cell Science*, 130: 1122.

Mackenzie, K. J., P. Carroll, C. A. Martin, O. Murina, A. Fluteau, D. J. Simpson, N. Olova, H. Sutcliffe, J. K. Rainger, A. Leitch, R. T. Osborn, A. P. Wheeler, M. Nowotny, N. Gilbert, T. Chandra, M. A. M. Reijns, and A. P. Jackson. 2017. 'cGAS surveillance of micronuclei links genome instability to innate immunity', *Nature*, 548: 461-65.

Maelfait, J., L. Liverpool, A. Bridgeman, K. B. Ragan, J. W. Upton, and J. Rehwinkel. 2017. 'Sensing of viral and endogenous RNA by ZBP1/DAI induces necroptosis', *Embo j*, 36: 2529-43.

Maltbaek, Joanna H., Jessica M. Snyder, and Daniel B. Stetson. 2021. 'ABCC1/MRP1 exports cGAMP and modulates cGAS-dependent immunity', *bioRxiv*: 2021.12.03.470980.

Mammas, I. N., and D. A. Spandidos. 2016. 'Paediatric Virology in the Hippocratic Corpus', *Exp Ther Med*, 12: 541-49.

Mankan, Arun K., Tobias Schmidt, Dhruv Chauhan, Marion Goldeck, Klara Höning, Moritz Gaidt, Andrew V. Kubarenko, Liudmila Andreeva, Karl-Peter Hopfner, and Veit Hornung. 2014. 'Cytosolic RNA:DNA hybrids activate the cGAS–STING axis', *The EMBO Journal*, 33: 2937-46.

Mannion, N. M., S. M. Greenwood, R. Young, S. Cox, J. Brindle, D. Read, C. Nellåker, C. Vesely, C. P. Ponting, P. J. McLaughlin, M. F. Jantsch, J. Dorin, I. R. Adams, A. D. Scadden, M. Ohman, L. P. Keegan, and M. A. O'Connell. 2014. 'The RNA-editing enzyme ADAR1 controls innate immune responses to RNA', *Cell Rep*, 9: 1482-94.

Marcus, Assaf, Amy J. Mao, Monisha Lensink-Vasan, LeeAnn Wang, Russell E. Vance, and David H. Raulet. 2018. 'Tumor-Derived cGAMP Triggers a STING-Mediated Interferon Response in Non-tumor Cells to Activate the NK Cell Response', *Immunity*, 49: 754-63.e4.

Mariathasan, S., D. S. Weiss, K. Newton, J. McBride, K. O'Rourke, M. Roose-Girma, W. P. Lee, Y. Weinrauch, D. M. Monack, and V. M. Dixit. 2006. 'Cryopyrin activates the inflammasome in response to toxins and ATP', *Nature*, 440: 228-32.

Marié, I., J. E. Durbin, and D. E. Levy. 1998. 'Differential viral induction of distinct interferon-alpha genes by positive feedback through interferon regulatory factor-7', *Embo j*, 17: 6660-9.

Marugen, Koi Farm. 2018. 'New World Record 203Million Yen 101cm Sakai Kohaku – S Legend', Marugen Koi Farm, Accessed 23. 12. 2022. https://marugenfishfarm.com/category/koi-auction/.

Matzinger, P. 1994. 'Tolerance, Danger, and the Extended Family', *Annual Review of Immunology*, 12: 991-1045.

———. 2001. 'Essay 1: The Danger Model in Its Historical Context', *Scandinavian Journal of Immunology*, 54: 4-9.

Matzinger, Polly. 2002. 'The Danger Model: A Renewed Sense of Self', *Science*, 296: 301-05.

Mayer, A., J. Maelfait, A. Bridgeman, and J. Rehwinkel. 2017. 'Purification of Cyclic GMP-AMP from Viruses and Measurement of Its Activity in Cell Culture', *Methods Mol Biol*, 1656: 143-52.

Medzhitov, R., P. Preston-Hurlburt, and C. A. Janeway, Jr. 1997. 'A human homologue of the Drosophila Toll protein signals activation of adaptive immunity', *Nature*, 388: 394-7.

Meric-Bernstam, Funda, Randy F. Sweis, F. Stephen Hodi, Wells A. Messersmith, Robert H. I. Andtbacka, Matthew Ingham, Nancy Lewis, Xinhui Chen, Marc Pelletier, Xueying Chen, Jincheng Wu, Sarah M. McWhirter, Thomas Müller, Nitya Nair, and Jason J. Luke. 2021. 'Phase I Dose-Escalation Trial of MIW815 (ADU-S100), an Intratumoral STING Agonist, in Patients with Advanced/Metastatic Solid Tumors or Lymphomas', *Clinical Cancer Research*, 28: 677-88.

Metchnikoff, Élie. 1902. 'Immunität bei Infektionskrankheiten', *Jena: Verlag von Gustav Fischer*: 1–456.

———. 1908. 'My stay in messina (in Russian).', *Russk Vedomosti*, 31:302.

Michalski, Sebastian, Carina C. de Oliveira Mann, Che A. Stafford, Gregor Witte, Joseph Bartho, Katja Lammens, Veit Hornung, and Karl-Peter Hopfner. 2020. 'Structural basis for sequestration and autoinhibition of cGAS by chromatin', *Nature*, 587: 678-82.

Miller, J. F. 1961. 'Immunological function of the thymus', *Lancet*, 2: 748-9.

Miller, J. F., and G. F. Mitchell. 1968. 'Cell to cell interaction in the immune response. I. Hemolysin-forming cells in neonatally thymectomized mice reconstituted with thymus or thoracic duct lymphocytes', *J Exp Med*, 128: 801-20.

Mitchell, G. F., and J. F. Miller. 1968a. 'Cell to cell interaction in the immune response. II. The source of hemolysin-forming cells in irradiated mice given bone marrow and thymus or thoracic duct lymphocytes', *J Exp Med*, 128: 821-37.

———. 1968b. 'Immunological activity of thymus and thoracic-duct lymphocytes', *Proc Natl Acad Sci U S A*, 59: 296-303.

Mitoma, H., S. Hanabuchi, T. Kim, M. Bao, Z. Zhang, N. Sugimoto, and Y. J. Liu. 2013. 'The DHX33 RNA helicase senses cytosolic RNA and activates the NLRP3 inflammasome', *Immunity*, 39: 123-35.

Monroe, K. M., Z. Yang, J. R. Johnson, X. Geng, G. Doitsh, N. J. Krogan, and W. C. Greene. 2014. 'IFI16 DNA sensor is required for death of lymphoid CD4 T cells abortively infected with HIV', *Science*, 343: 428-32.

Morchikh, M., A. Cribier, R. Raffel, S. Amraoui, J. Cau, D. Severac, E. Dubois, O. Schwartz, Y. Bennasser, and M. Benkirane. 2017. 'HEXIM1 and NEAT1 Long Non-coding RNA Form a Multi-subunit Complex that Regulates DNA-Mediated Innate Immune Response', *Mol Cell*, 67: 387-99.e5.

Morrison, L. A., A. E. Lukacher, V. L. Braciale, D. P. Fan, and T. J. Braciale. 1986. 'Differences in antigen presentation to MHC class I-and class II-restricted influenza virus-specific cytolytic T lymphocyte clones', *J Exp Med*, 163: 903-21.

Mouchess, M. L., N. Arpaia, G. Souza, R. Barbalat, S. E. Ewald, L. Lau, and G. M. Barton. 2011. 'Transmembrane mutations in Toll-like receptor 9 bypass the requirement for ectodomain proteolysis and induce fatal inflammation', *Immunity*, 35: 721-32.

Müller, Christa E., and Vigneshwaran Namasivayam. 2022. 'Agonists, Antagonists, and Modulators of P2X7 Receptors.' in Annette Nicke (ed.), *The P2X7 Receptor: Methods and Protocols* (Springer US: New York, NY).

Nakamura, T., H. Miyabe, M. Hyodo, Y. Sato, Y. Hayakawa, and H. Harashima. 2015. 'Liposomes loaded with a STING pathway ligand, cyclic di-GMP, enhance cancer immunotherapy against metastatic melanoma', *J Control Release*, 216: 149-57.

Neil, S. J., T. Zang, and P. D. Bieniasz. 2008. 'Tetherin inhibits retrovirus release and is antagonized by HIV-1 Vpu', *Nature*, 451: 425-30.

Netea, Mihai G., Jorge Domínguez-Andrés, Luis B. Barreiro, Triantafyllos Chavakis, Maziar Divangahi, Elaine Fuchs, Leo A. B. Joosten, Jos W. M. van der Meer, Musa M. Mhlanga, Willem J. M. Mulder, Niels P. Riksen, Andreas Schlitzer, Joachim L. Schultze, Christine Stabell Benn, Joseph C. Sun, Ramnik J. Xavier, and Eicke Latz. 2020. 'Defining trained immunity and its role in health and disease', *Nature Reviews Immunology*, 20: 375-88.

Nicoll, M. P., W. Hann, M. Shivkumar, L. E. Harman, V. Connor, H. M. Coleman, J. T. Proença, and S. Efstathiou. 2016. 'The HSV-1 Latency-Associated Transcript Functions to Repress Latent Phase Lytic Gene Expression and Suppress Virus Reactivation from Latently Infected Neurons', *PLoS Pathog*, 12: e1005539.

Nies, A. T., G. Jedlitschky, J. König, C. Herold-Mende, H. H. Steiner, H. P. Schmitt, and D. Keppler. 2004. 'Expression and immunolocalization of the multidrug resistance proteins, MRP1–MRP6 (ABCC1–ABCC6), in human brain', *Neuroscience*, 129: 349-60.

O'Connor, Christine M., and Ganes C. Sen. 2021. "Innate Immune Responses to Herpesvirus Infection." In *Cells*.

Ohkuri, T., A. Ghosh, A. Kosaka, J. Zhu, M. Ikeura, M. David, S. C. Watkins, S. N. Sarkar, and H. Okada. 2014. 'STING contributes to antiglioma immunity via triggering type I IFN signals in the tumor microenvironment', *Cancer Immunol Res*, 2: 1199-208.

Oka, Y., H. Varmark, K. Vitting-Seerup, P. Beli, J. Waage, A. Hakobyan, M. Mistrik, C. Choudhary, M. Rohde, S. Bekker-Jensen, and N. Mailand. 2014. 'UBL5 is essential for pre-mRNA splicing and sister chromatid cohesion in human cells', *EMBO Rep*, 15: 956-64.

Olagnier, David, Aske M. Brandtoft, Camilla Gunderstofte, Nikolaj L. Villadsen, Christian Krapp, Anne L. Thielke, Anders Laustsen, Suraj Peri, Anne Louise Hansen, Lene Bonefeld, Jacob Thyrsted, Victor Bruun, Marie B. Iversen, Lin Lin, Virginia M. Artegoitia, Chenhe Su, Long Yang, Rongtuan Lin, Siddharth Balachandran, Yonglun Luo, Mette Nyegaard, Bernadette Marrero, Raphaela Goldbach-Mansky, Mona Motwani, Dylan G. Ryan, Katherine A. Fitzgerald, Luke A. O'Neill, Anne K. Hollensen, Christian K. Damgaard, Frank v de Paoli, Hanne C. Bertram, Martin R. Jakobsen, Thomas B. Poulsen, and Christian K. Holm. 2018. 'Nrf2 negatively regulates STING indicating a link between antiviral sensing and metabolic reprogramming', *Nature Communications*, 9: 3506.

Oroskar, A. A., and G. S. Read. 1987. 'A mutant of herpes simplex virus type 1 exhibits increased stability of immediate-early (alpha) mRNAs', *J Virol*, 61: 604-6.

Paik, D., A. Monahan, D. R. Caffrey, R. Elling, W. E. Goldman, and N. Silverman. 2017. 'SLC46 Family Transporters Facilitate Cytosolic Innate Immune Recognition of Monomeric Peptidoglycans', *J Immunol*, 199: 263-70.

Palmer, Caroline V. 2018. 'Immunity and the coral crisis', *Communications biology*, 1: 91-91.

Parvatiyar, Kislay, Zhiqiang Zhang, Rosane M. Teles, Songying Ouyang, Yan Jiang, Shankar S. Iyer, Shivam A. Zaver, Mirjam Schenk, Shang Zeng, Wenwan Zhong, Zhi-Jie Liu, Robert L. Modlin, Yong-jun Liu, and Genhong Cheng. 2012. 'The helicase DDX41 recognizes the bacterial secondary messengers cyclic di-GMP and cyclic di-AMP to activate a type I interferon immune response', *Nature Immunology*, 13: 1155-61.

Patel, Suraj J., Kevin R. King, Monica Casali, and Martin L. Yarmush. 2009. 'DNA-triggered innate immune responses are propagated by gap junction communication', *Proceedings of the National Academy of Sciences*, 106: 12867-72.

Pathare, G. R., A. Decout, S. Glück, S. Cavadini, K. Makasheva, R. Hovius, G. Kempf, J. Weiss, Z. Kozicka, B. Guey, P. Melenec, B. Fierz, N. H. Thomä, and A. Ablasser. 2020. 'Structural mechanism of cGAS inhibition by the nucleosome', *Nature*, 587: 668-72.

Pellegatti, P., L. Raffaghello, G. Bianchi, F. Piccardi, V. Pistoia, and F. Di Virgilio. 2008. 'Increased level of extracellular ATP at tumor sites: in vivo imaging with plasma membrane luciferase', *PLoS One*, 3: e2599.

Pépin, Geneviève, Dominic De Nardo, Christina L. Rootes, Tomalika R. Ullah, Sumaiah S. Al-Asmari, Katherine R. Balka, Hong-Mei Li, Kylie M. Quinn, Fiona Moghaddas, Stephane Chappaz, Benjamin T. Kile, Eric F. Morand, Seth L. Masters, Cameron R. Stewart, Bryan R. G. Williams, and Michael P. Gantier. 2020. 'Connexin-Dependent Transfer of cGAMP to Phagocytes Modulates Antiviral Responses', *mBio*, 11: e03187-19.

Perregaux, D., and C. A. Gabel. 1994. 'Interleukin-1 beta maturation and release in response to ATP and nigericin. Evidence that potassium depletion mediated by these agents is a necessary and common feature of their activity', *J Biol Chem*, 269: 15195-203.

Pestal, K., C. C. Funk, J. M. Snyder, N. D. Price, P. M. Treuting, and D. B. Stetson. 2015. 'Isoforms of RNA-Editing Enzyme ADAR1 Independently Control Nucleic Acid Sensor MDA5-Driven Autoimmunity and Multi-organ Development', *Immunity*, 43: 933-44.

Peters, N. E., B. J. Ferguson, M. Mazzon, A. S. Fahy, E. Krysztofinska, R. Arribas-Bosacoma, L. H. Pearl, H. Ren, and G. L. Smith. 2013. 'A mechanism for the inhibition of DNA-PK-mediated DNA sensing by a virus', *PLoS Pathog*, 9: e1003649.

Petti, S., and G. Lodi. 2019. 'The controversial natural history of oral herpes simplex virus type 1 infection', *Oral Dis*, 25: 1850-65.

Pichlmair, A., O. Schulz, C. P. Tan, T. I. Näslund, P. Liljeström, F. Weber, and C. Reis e Sousa. 2006. 'RIG-I-mediated antiviral responses to single-stranded RNA bearing 5'-phosphates', *Science*, 314: 997-1001.

Pichlmair, A., O. Schulz, C. P. Tan, J. Rehwinkel, H. Kato, O. Takeuchi, S. Akira, M. Way, G. Schiavo, and C. Reis e Sousa. 2009. 'Activation of MDA5 requires higher-order RNA structures generated during virus infection', *J Virol*, 83: 10761-9.

Planells-Cases, R., D. Lutter, C. Guyader, N. M. Gerhards, F. Ullrich, D. A. Elger, A. Kucukosmanoglu, G. Xu, F. K. Voss, S. M. Reincke, T. Stauber, V. A. Blomen, D. J. Vis, L. F. Wessels, T. R. Brummelkamp, P. Borst, S. Rottenberg, and T. J. Jentsch. 2015. 'Subunit composition of VRAC channels determines substrate specificity and cellular resistance to Pt-based anti-cancer drugs', *Embo j*, 34: 2993-3008.

Platanias, Leonidas C. 2005. 'Mechanisms of type-I- and type-II-interferon-mediated signalling', *Nature Reviews Immunology*, 5: 375-86.

Poltorak, A., X. He, I. Smirnova, M. Y. Liu, C. Van Huffel, X. Du, D. Birdwell, E. Alejos, M. Silva, C. Galanos, M. Freudenberg, P. Ricciardi-Castagnoli, B. Layton, and B. Beutler. 1998.

'Defective LPS signaling in C3H/HeJ and C57BL/10ScCr mice: mutations in Tlr4 gene', *Science*, 282: 2085-8.

Powell, Timothy J., Jonathan D. Silk, Jane Sharps, Ervin Fodor, and Alain R. M. Townsend. 2012. 'Pseudotyped influenza A virus as a vaccine for the induction of heterotypic immunity', *Journal of Virology*, 86: 13397-406.

Prabakaran, T., A. Troldborg, S. Kumpunya, I. Alee, E. Marinković, S. J. Windross, R. Nandakumar, R. Narita, B. C. Zhang, M. Carstensen, P. Vejvisithsakul, M. H. S. Marqvorsen, M. B. Iversen, C. K. Holm, L. J. Østergaard, F. S. Pedersen, T. Pisitkun, R. Behrendt, P. Pisitkun, and S. R. Paludan. 2021. 'A STING antagonist modulating the interaction with STIM1 blocks ER-to-Golgi trafficking and inhibits lupus pathology', *EBioMedicine*, 66: 103314.

Qin, Yue, Mao-Tian Zhou, Ming-Ming Hu, Yun-Hong Hu, Jing Zhang, Lin Guo, Bo Zhong, and Hong-Bing Shu. 2014. 'RNF26 Temporally Regulates Virus-Triggered Type I Interferon Induction by Two Distinct Mechanisms', *PLOS Pathogens*, 10: e1004358.

Qiu, Andong, Michaela Jansen, Antoinette Sakaris, Sang Hee Min, Shrikanta Chattopadhyay, Eugenia Tsai, Claudio Sandoval, Rongbao Zhao, Myles H. Akabas, and I. David Goldman. 2006. 'Identification of an Intestinal Folate Transporter and the Molecular Basis for Hereditary Folate Malabsorption', *Cell*, 127: 917-28.

Qiu, Zhaozhu, Adrienne E Dubin, Jayanti Mathur, Buu Tu, Kritika Reddy, Loren J Miraglia, Jürgen Reinhardt, Anthony P Orth, and Ardem Patapoutian. 2014. 'SWELL1, a Plasma Membrane Protein, Is an Essential Component of Volume-Regulated Anion Channel', *Cell*, 157: 447-58.

Quicke, K. M., K. Y. Kim, C. M. Horvath, and M. S. Suthar. 2019. 'RNA Helicase LGP2 Negatively Regulates RIG-I Signaling by Preventing TRIM25-Mediated Caspase Activation and Recruitment Domain Ubiquitination', *J Interferon Cytokine Res*, 39: 669-83.

Radtke, Kerstin, Daniela Kieneke, André Wolfstein, Kathrin Michael, Walter Steffen, Tim Scholz, Axel Karger, and Beate Sodeik. 2010. 'Plus- and Minus-End Directed Microtubule Motors Bind Simultaneously to Herpes Simplex Virus Capsids Using Different Inner Tegument Structures', *PLOS Pathogens*, 6: e1000991.

Ran, Y., M. G. Xiong, Z. S. Xu, W. W. Luo, S. Y. Wang, and Y. Y. Wang. 2019. 'YIPF5 Is Essential for Innate Immunity to DNA Virus and Facilitates COPII-Dependent STING Trafficking', *J Immunol*, 203: 1560-70.

Rao, V. V., J. L. Dahlheimer, M. E. Bardgett, A. Z. Snyder, R. A. Finch, A. C. Sartorelli, and D. Piwnica-Worms. 1999. 'Choroid plexus epithelial expression of MDR1 P glycoprotein and multidrug resistance-associated protein contribute to the blood-cerebrospinal-fluid drug-permeability barrier', *Proc Natl Acad Sci U S A*, 96: 3900-5.

Rathinam, Vijay A. K., Zhaozhao Jiang, Stephen N. Waggoner, Shruti Sharma, Leah E. Cole, Lisa Waggoner, Sivapriya Kailasan Vanaja, Brian G. Monks, Sandhya Ganesan, Eicke Latz,

Veit Hornung, Stefanie N. Vogel, Eva Szomolanyi-Tsuda, and Katherine A. Fitzgerald. 2010. 'The AIM2 inflammasome is essential for host defense against cytosolic bacteria and DNA viruses', *Nature Immunology*, 11: 395-402.

Read, G. S., and N. Frenkel. 1983. 'Herpes simplex virus mutants defective in the virion-associated shutoff of host polypeptide synthesis and exhibiting abnormal synthesis of alpha (immediate early) viral polypeptides', *J Virol*, 46: 498-512.

Rehwinkel, Jan, and Michaela U. Gack. 2020. 'RIG-I-like receptors: their regulation and roles in RNA sensing', *Nature Reviews Immunology*, 20: 537-51.

Reus, J. B., G. S. Trivino-Soto, L. I. Wu, K. Kokott, and E. S. Lim. 2020. 'SV40 Large T Antigen Is Not Responsible for the Loss of STING in 293T Cells but Can Inhibit cGAS-STING Interferon Induction', *Viruses*, 12.

Rice, G. I., P. R. Kasher, G. M. Forte, N. M. Mannion, S. M. Greenwood, M. Szynkiewicz, J. E. Dickerson, S. S. Bhaskar, M. Zampini, T. A. Briggs, E. M. Jenkinson, C. A. Bacino, R. Battini, E. Bertini, P. A. Brogan, L. A. Brueton, M. Carpanelli, C. De Laet, P. de Lonlay, M. del Toro, I. Desguerre, E. Fazzi, A. Garcia-Cazorla, A. Heiberg, M. Kawaguchi, R. Kumar, J. P. Lin, C. M. Lourenco, A. M. Male, W. Marques, Jr., C. Mignot, I. Olivieri, S. Orcesi, P. Prabhakar, M. Rasmussen, R. A. Robinson, F. Rozenberg, J. L. Schmidt, K. Steindl, T. Y. Tan, W. G. van der Merwe, A. Vanderver, G. Vassallo, E. L. Wakeling, E. Wassmer, E. Whittaker, J. H. Livingston, P. Lebon, T. Suzuki, P. J. McLaughlin, L. P. Keegan, M. A. O'Connell, S. C. Lovell, and Y. J. Crow. 2012. 'Mutations in ADAR1 cause Aicardi-Goutières syndrome associated with a type I interferon signature', *Nat Genet*, 44: 1243-8.

Riedel, T., G. Schmalzing, and F. Markwardt. 2007. 'Influence of Extracellular Monovalent Cations on Pore and Gating Properties of P2X7 Receptor-Operated Single-Channel Currents', *Biophysical Journal*, 93: 846-58.

Rima, B. K., and N. V. McFerran. 1997. 'Dinucleotide and stop codon frequencies in single-stranded RNA viruses', *J Gen Virol*, 78 (Pt 11): 2859-70.

Ritchie, Christopher, Anthony F. Cordova, Gaelen T. Hess, Michael C. Bassik, and Lingyin Li. 2019. 'SLC19A1 Is an Importer of the Immunotransmitter cGAMP', *Molecular Cell*, 75: 372-81.e5.

Ritchie, Christopher, Anthony F. Cordova, and Lingyin Li. 2019. 'In response to Luteijn et al.: Concerns regarding cGAMP uptake assay and evidence that SLC19A1 is not the major cGAMP importer in human PBMCs', *bioRxiv*: 798397.

Roberts, C. M., J. R. Pfister, and S. J. Spear. 2003. 'Increasing proportion of herpes simplex virus type 1 as a cause of genital herpes infection in college students', *Sex Transm Dis*, 30: 797-800.

Rotem, Z., R. A. Cox, and A. Isaacs. 1963. 'Inhibition of virus multiplication by foreign nucleic acid', *Nature*, 197: 564-6.

Rothenfusser, S., N. Goutagny, G. DiPerna, M. Gong, B. G. Monks, A. Schoenemeyer, M. Yamamoto, S. Akira, and K. A. Fitzgerald. 2005. 'The RNA helicase Lgp2 inhibits TLR-independent sensing of viral replication by retinoic acid-inducible gene-I', *J Immunol*, 175: 5260-8.

Rowe, A. M., A. J. St Leger, S. Jeon, D. K. Dhaliwal, J. E. Knickelbein, and R. L. Hendricks. 2013. 'Herpes keratitis', *Prog Retin Eye Res*, 32: 88-101.

Sabbah, A., T. H. Chang, R. Harnack, V. Frohlich, K. Tominaga, P. H. Dube, Y. Xiang, and S. Bose. 2009. 'Activation of innate immune antiviral responses by Nod2', *Nat Immunol*, 10: 1073-80.

Salameh, Aida, and Stefan Dhein. 2005. 'Pharmacology of Gap junctions. New pharmacological targets for treatment of arrhythmia, seizure and cancer?', *Biochimica et Biophysica Acta (BBA) - Biomembranes*, 1719: 36-58.

Sancho-Vaello, Enea, David Gil-Carton, Patrice François, Eve-Julie Bonetti, Mohamed Kreir, Karunakar Reddy Pothula, Ulrich Kleinekathöfer, and Kornelius Zeth. 2020. 'The structure of the antimicrobial human cathelicidin LL-37 shows oligomerization and channel formation in the presence of membrane mimics', *Scientific Reports*, 10: 17356.

Sandgren, Staffan, Anders Wittrup, Fang Cheng, Mats Jönsson, Erik Eklund, Susann Busch, and Mattias Belting. 2004. 'The Human Antimicrobial Peptide LL-37 Transfers Extracellular DNA Plasmid to the Nuclear Compartment of Mammalian Cells via Lipid Rafts and Proteoglycan-dependent Endocytosis*', *Journal of Biological Chemistry*, 279: 17951-56.

Sanjana, N. E., O. Shalem, and F. Zhang. 2014. 'Improved vectors and genome-wide libraries for CRISPR screening', *Nat Methods*, 11: 783-84.

Satoh, T., J. Arii, T. Suenaga, J. Wang, A. Kogure, J. Uehori, N. Arase, I. Shiratori, S. Tanaka, Y. Kawaguchi, P. G. Spear, L. L. Lanier, and H. Arase. 2008. 'PILRalpha is a herpes simplex virus-1 entry coreceptor that associates with glycoprotein B', *Cell*, 132: 935-44.

Satoh, T., H. Kato, Y. Kumagai, M. Yoneyama, S. Sato, K. Matsushita, T. Tsujimura, T. Fujita, S. Akira, and O. Takeuchi. 2010. 'LGP2 is a positive regulator of RIG-I- and MDA5-mediated antiviral responses', *Proc Natl Acad Sci U S A*, 107: 1512-7.

Schmidt, A., T. Schwerd, W. Hamm, J. C. Hellmuth, S. Cui, M. Wenzel, F. S. Hoffmann, M. C. Michallet, R. Besch, K. P. Hopfner, S. Endres, and S. Rothenfusser. 2009. '5'-triphosphate RNA requires base-paired structures to activate antiviral signaling via RIG-I', *Proc Natl Acad Sci U S A*, 106: 12067-72.

Schober, Alexandra L., Corinne S. Wilson, and Alexander A. Mongin. 2017. 'Molecular composition and heterogeneity of the LRRC8-containing swelling-activated osmolyte channels in primary rat astrocytes', *The Journal of Physiology*, 595: 6939-51.

Shang, Guijun, Conggang Zhang, Zhijian J. Chen, Xiao-chen Bai, and Xuewu Zhang. 2019. 'Cryo-EM structures of STING reveal its mechanism of activation by cyclic GMP–AMP', *Nature*, 567: 389-93.

Silva, L., A. Cliffe, L. Chang, and D. M. Knipe. 2008. 'Role for A-type lamins in herpesviral DNA targeting and heterochromatin modulation', *PLoS Pathog*, 4: e1000071.

Sirianant, Lalida, Podchanart Wanitchakool, Jiraporn Ousingsawat, Roberta Benedetto, Anna Zormpa, Ines Cabrita, Rainer Schreiber, and Karl Kunzelmann. 2016. 'Non-essential contribution of LRRC8A to volume regulation', *Pflügers Archiv - European Journal of Physiology*, 468: 805-16.

Slavik, Kailey M., Benjamin R. Morehouse, Adelyn E. Ragucci, Wen Zhou, Xianlong Ai, Yuqiang Chen, Lihua Li, Ziming Wei, Heike Bähre, Martin König, Roland Seifert, Amy S. Y. Lee, Hua Cai, Jean-Luc Imler, and Philip J. Kranzusch. 2021. 'cGAS-like receptors sense RNA and control 3’2’-cGAMP signalling in Drosophila', *Nature*, 597: 109-13.

Sliter, Danielle A., Jennifer Martinez, Ling Hao, Xi Chen, Nuo Sun, Tara D. Fischer, Jonathon L. Burman, Yan Li, Zhe Zhang, Derek P. Narendra, Huaibin Cai, Max Borsche, Christine Klein, and Richard J. Youle. 2018. 'Parkin and PINK1 mitigate STING-induced inflammation', *Nature*, 561: 258-62.

Sodeik, B., M. W. Ebersold, and A. Helenius. 1997. 'Microtubule-mediated transport of incoming herpes simplex virus 1 capsids to the nucleus', *J Cell Biol*, 136: 1007-21.

Soh, T. K., C. T. R. Davies, J. Muenzner, L. M. Hunter, H. G. Barrow, V. Connor, C. R. Bouton, C. Smith, E. Emmott, R. Antrobus, S. C. Graham, M. P. Weekes, and C. M. Crump. 2020. 'Temporal Proteomic Analysis of Herpes Simplex Virus 1 Infection Reveals Cell-Surface Remodeling via pUL56-Mediated GOPC Degradation', *Cell Rep*, 33: 108235.

Sørensen, O. E., P. Follin, A. H. Johnsen, J. Calafat, G. S. Tjabringa, P. S. Hiemstra, and N. Borregaard. 2001. 'Human cathelicidin, hCAP-18, is processed to the antimicrobial peptide LL-37 by extracellular cleavage with proteinase 3', *Blood*, 97: 3951-9.

Srikanth, S., J. S. Woo, B. Wu, Y. M. El-Sherbiny, J. Leung, K. Chupradit, L. Rice, G. J. Seo, G. Calmettes, C. Ramakrishna, E. Cantin, D. S. An, R. Sun, T. T. Wu, J. U. Jung, S. Savic, and Y. Gwack. 2019. 'The Ca(2+) sensor STIM1 regulates the type I interferon response by retaining the signaling adaptor STING at the endoplasmic reticulum', *Nat Immunol*, 20: 152-62.

St-Pierre, M. V., T. Stallmach, A. Freimoser Grundschober, J. F. Dufour, M. A. Serrano, J. J. G. Marin, Y. Sugiyama, and P. J. Meier. 2004. 'Temporal expression profiles of organic anion transport proteins in placenta and fetal liver of the rat', *American Journal of Physiology-Regulatory, Integrative and Comparative Physiology*, 287: R1505-R16.

Stetson, D. B., J. S. Ko, T. Heidmann, and R. Medzhitov. 2008. 'Trex1 prevents cell-intrinsic initiation of autoimmunity', *Cell*, 134: 587-98.

Stetson, D. B., and R. Medzhitov. 2006a. 'Recognition of cytosolic DNA activates an IRF3-dependent innate immune response', *Immunity*, 24: 93-103.

———. 2006b. 'Type I interferons in host defense', *Immunity*, 25: 373-81.

Stuhlmann, Till, Rosa Planells-Cases, and Thomas J. Jentsch. 2018. 'LRRC8/VRAC anion channels enhance β-cell glucose sensing and insulin secretion', *Nature Communications*, 9: 1974.

Sun, Lijun, Jiaxi Wu, Fenghe Du, Xiang Chen, and Zhijian J. Chen. 2013. 'Cyclic GMP-AMP Synthase Is a Cytosolic DNA Sensor That Activates the Type I Interferon Pathway', *Science*, 339: 786-91.

Suzich, Jon B., and Anna R. Cliffe. 2018. 'Strength in diversity: Understanding the pathways to herpes simplex virus reactivation', *Virology*, 522: 81-91.

Swan, Norman. 2011. "Celebrating a scientific breakthrough." In.

Takabe, K., R. H. Kim, J. C. Allegood, P. Mitra, S. Ramachandran, M. Nagahashi, K. B. Harikumar, N. C. Hait, S. Milstien, and S. Spiegel. 2010. 'Estradiol induces export of sphingosine 1-phosphate from breast cancer cells via ABCC1 and ABCG2', *J Biol Chem*, 285: 10477-86.

Takata, Matthew A., Daniel Gonçalves-Carneiro, Trinity M. Zang, Steven J. Soll, Ashley York, Daniel Blanco-Melo, and Paul D. Bieniasz. 2017. 'CG dinucleotide suppression enables antiviral defence targeting non-self RNA', *Nature*, 550: 124-27.

Tanaka, T., M. Narazaki, and T. Kishimoto. 2014. 'IL-6 in inflammation, immunity, and disease', *Cold Spring Harb Perspect Biol*, 6: a016295.

Tassia, Michael G., Nathan V. Whelan, and Kenneth M. Halanych. 2017. 'Toll-like receptor pathway evolution in deuterostomes', *Proceedings of the National Academy of Sciences*, 114: 7055.

Thapa, R. J., J. P. Ingram, K. B. Ragan, S. Nogusa, D. F. Boyd, A. A. Benitez, H. Sridharan, R. Kosoff, M. Shubina, V. J. Landsteiner, M. Andrake, P. Vogel, L. J. Sigal, B. R. tenOever, P. G. Thomas, J. W. Upton, and S. Balachandran. 2016. 'DAI Senses Influenza A Virus Genomic RNA and Activates RIPK3-Dependent Cell Death', *Cell Host Microbe*, 20: 674-81.

Thomas, Suzanne, Linta Kuncheria, Victoria Roulstone, Joan N. Kyula, David Mansfield, Praveen K. Bommareddy, Henry Smith, Howard L. Kaufman, Kevin J. Harrington, and Robert S. Coffin. 2019. 'Development of a new fusion-enhanced oncolytic immunotherapy platform based on herpes simplex virus type 1', *Journal for immunotherapy of cancer*, 7: 214-14.

"TIME." In. 1982. *TIME*. TIME.

Totland, M. Z., N. L. Rasmussen, L. M. Knudsen, and E. Leithe. 2020. 'Regulation of gap junction intercellular communication by connexin ubiquitination: physiological and pathophysiological implications', *Cell Mol Life Sci*, 77: 573-91.

Townsend, A. R., J. Rothbard, F. M. Gotch, G. Bahadur, D. Wraith, and A. J. McMichael. 1986. 'The epitopes of influenza nucleoprotein recognized by cytotoxic T lymphocytes can be defined with short synthetic peptides', *Cell*, 44: 959-68.

Trompouki, E., E. Hatzivassiliou, T. Tsichritzis, H. Farmer, A. Ashworth, and G. Mosialos. 2003. 'CYLD is a deubiquitinating enzyme that negatively regulates NF-kappaB activation by TNFR family members', *Nature*, 424: 793-6.

Tsuchiya, S., Y. Kobayashi, Y. Goto, H. Okumura, S. Nakae, T. Konno, and K. Tada. 1982. 'Induction of maturation in cultured human monocytic leukemia cells by a phorbol diester', *Cancer Res*, 42: 1530-6.

Tsuchiya, S., M. Yamabe, Y. Yamaguchi, Y. Kobayashi, T. Konno, and K. Tada. 1980. 'Establishment and characterization of a human acute monocytic leukemia cell line (THP-1)', *Int J Cancer*, 26: 171-6.

Tsuji, Y. 2020. 'Transmembrane protein western blotting: Impact of sample preparation on detection of SLC11A2 (DMT1) and SLC40A1 (ferroportin)', *PLoS One*, 15: e0235563.

Turner, J., Y. Cho, N. N. Dinh, A. J. Waring, and R. I. Lehrer. 1998. 'Activities of LL-37, a cathelin-associated antimicrobial peptide of human neutrophils', *Antimicrob Agents Chemother*, 42: 2206-14.

Uggenti, C., A. Lepelley, M. Depp, A. P. Badrock, M. P. Rodero, M. T. El-Daher, G. I. Rice, S. Dhir, A. P. Wheeler, A. Dhir, W. Albawardi, M. L. Frémond, L. Seabra, J. Doig, N. Blair, M. J. Martin-Niclos, E. Della Mina, A. Rubio-Roldán, J. L. García-Pérez, D. Sproul, J. Rehwinkel, J. Hertzog, A. Boland-Auge, R. Olaso, J. F. Deleuze, J. Baruteau, K. Brochard, J. Buckley, V. Cavallera, C. Cereda, L. M. H. De Waele, A. Dobbie, D. Doummar, F. Elmslie, M. Koch-Hogrebe, R. Kumar, K. Lamb, J. H. Livingston, A. Majumdar, C. M. Lorenço, S. Orcesi, S. Peudenier, K. Rostasy, C. A. Salmon, C. Scott, D. Tonduti, G. Touati, M. Valente, H. van der Linden, Jr., H. Van Esch, M. Vermelle, K. Webb, A. P. Jackson, M. A. M. Reijns, N. Gilbert, and Y. J. Crow. 2020. 'cGAS-mediated induction of type I interferon due to inborn errors of histone pre-mRNA processing', *Nat Genet*, 52: 1364-72.

Unknown. 13th Century. "Untitled." In. Fresco in the crypt of the Cathedral, Anagni, Italy.

Valiunas, V. 2013. 'Cyclic nucleotide permeability through unopposed connexin hemichannels', *Front Pharmacol*, 4: 75.

Van Damme, N., D. Goff, C. Katsura, R. L. Jorgenson, R. Mitchell, M. C. Johnson, E. B. Stephens, and J. Guatelli. 2008. 'The interferon-induced protein BST-2 restricts HIV-1 release and is downregulated from the cell surface by the viral Vpu protein', *Cell Host Microbe*, 3: 245-52.

van Maanen, J. M. S., J. Retèl, J. de Vries, and H. M. Pinedo. 1988. 'Mechanism of Action of Antitumor Drug Etoposide: A Review', *JNCI: Journal of the National Cancer Institute*, 80: 1526-33.

Van, Valen. 1973. 'A new evolutionary law'.

Vance, Russell E. 2016. 'Cytosolic DNA Sensing: The Field Narrows', *Immunity*, 45: 227-28.

Vandamme, Dieter, Bart Landuyt, Walter Luyten, and Liliane Schoofs. 2012. 'A comprehensive summary of LL-37, the factotum human cathelicidin peptide', *Cellular Immunology*, 280: 22-35.

Vasiliou, Vasilis, Konstandinos Vasiliou, and Daniel W. Nebert. 2009. 'Human ATP-binding cassette (ABC) transporter family', *Human genomics*, 3: 281-90.

Venkataraman, T., M. Valdes, R. Elsby, S. Kakuta, G. Caceres, S. Saijo, Y. Iwakura, and G. N. Barber. 2007. 'Loss of DExD/H box RNA helicase LGP2 manifests disparate antiviral responses', *J Immunol*, 178: 6444-55.

Verhoeft, K. R., H. L. Ngan, and V. W. Y. Lui. 2016. 'The cylindromatosis (CYLD) gene and head and neck tumorigenesis', *Cancers Head Neck*, 1: 10.

Vinken, Mathieu. 2015. 'Introduction: connexins, pannexins and their channels as gatekeepers of organ physiology', *Cellular and Molecular Life Sciences*, 72: 2775-78.

Voss, Felizia K., Florian Ullrich, Jonas Münch, Katina Lazarow, Darius Lutter, Nancy Mah, Miguel A. Andrade-Navarro, Jens P. von Kries, Tobias Stauber, and Thomas J. Jentsch. 2014. 'Identification of LRRC8 Heteromers as an Essential Component of the Volume-Regulated Anion Channel VRAC', *Science*, 344: 634.

Waltzek, T. B., G. O. Kelley, M. E. Alfaro, T. Kurobe, A. J. Davison, and R. P. Hedrick. 2009. 'Phylogenetic relationships in the family Alloherpesviridae', *Dis Aquat Organ*, 84: 179-94.

Wang, J., P. Li, Y. Yu, Y. Fu, H. Jiang, M. Lu, Z. Sun, S. Jiang, L. Lu, and M. X. Wu. 2020. 'Pulmonary surfactant-biomimetic nanoparticles potentiate heterosubtypic influenza immunity', *Science*, 367.

Wang, Penghua, Shu Zhu, Long Yang, Shuang Cui, Wen Pan, Ruaidhri Jackson, Yunjiang Zheng, Anthony Rongvaux, Qiangming Sun, Guang Yang, Shandian Gao, Rongtuan Lin, Fuping You, Richard Flavell, and Erol Fikrig. 2015. 'Nlrp6 regulates intestinal antiviral innate immunity', *Science (New York, N.Y.)*, 350: 826-30.

Wang, Q., X. Liu, Y. Cui, Y. Tang, W. Chen, S. Li, H. Yu, Y. Pan, and C. Wang. 2014. 'The E3 ubiquitin ligase AMFR and INSIG1 bridge the activation of TBK1 kinase by modifying the adaptor STING', *Immunity*, 41: 919-33.

Warner, M. S., R. J. Geraghty, W. M. Martinez, R. I. Montgomery, J. C. Whitbeck, R. Xu, R. J. Eisenberg, G. H. Cohen, and P. G. Spear. 1998. 'A cell surface protein with herpesvirus

entry activity (HveB) confers susceptibility to infection by mutants of herpes simplex virus type 1, herpes simplex virus type 2, and pseudorabies virus', *Virology*, 246: 179-89.

Wei, J., H. Lian, W. Guo, Y. D. Chen, X. N. Zhang, R. Zang, L. Zhong, Q. Yang, M. M. Hu, W. W. Luo, H. B. Shu, and S. Li. 2018. 'SNX8 modulates innate immune response to DNA virus by mediating trafficking and activation of MITA', *PLoS Pathog*, 14: e1007336.

Wei, X., L. Zhang, Y. Yang, Y. Hou, Y. Xu, Z. Wang, H. Su, F. Han, J. Han, P. Liu, S. Hu, M. D. Koci, X. Sun, and C. Zhang. 2022. 'LL-37 transports immunoreactive cGAMP to activate STING signaling and enhance interferon-mediated host antiviral immunity', *Cell Rep*, 39: 110880.

Wertheim, Joel O., Martin D. Smith, Davey M. Smith, Konrad Scheffler, and Sergei L. Kosakovsky Pond. 2014. 'Evolutionary Origins of Human Herpes Simplex Viruses 1 and 2', *Molecular Biology and Evolution*, 31: 2356-64.

Whitbeck, J. C., C. Peng, H. Lou, R. Xu, S. H. Willis, M. Ponce de Leon, T. Peng, A. V. Nicola, R. I. Montgomery, M. S. Warner, A. M. Soulika, L. A. Spruce, W. T. Moore, J. D. Lambris, P. G. Spear, G. H. Cohen, and R. J. Eisenberg. 1997. 'Glycoprotein D of herpes simplex virus (HSV) binds directly to HVEM, a member of the tumor necrosis factor receptor superfamily and a mediator of HSV entry', *J Virol*, 71: 6083-93.

Whiteley, Aaron T., James B. Eaglesham, Carina C. de Oliveira Mann, Benjamin R. Morehouse, Brianna Lowey, Eric A. Nieminen, Olga Danilchanka, David S. King, Amy S. Y. Lee, John J. Mekalanos, and Philip J. Kranzusch. 2019. 'Bacterial cGAS-like enzymes synthesize diverse nucleotide signals', *Nature*, 567: 194-99.

Whitley, R, and J Baines. 2018. 'Clinical management of herpes simplex virus infections: past, present, and future [version 1; peer review: 2 approved]', *F1000Research*, 7.

Wong, R., W. Chen, X. Zhong, J. T. Rutka, Z. P. Feng, and H. S. Sun. 2018. 'Swelling-induced chloride current in glioblastoma proliferation, migration, and invasion', *J Cell Physiol*, 233: 363-70.

Wu, J., T. Fernandes-Alnemri, and E. S. Alnemri. 2010. 'Involvement of the AIM2, NLRC4, and NLRP3 inflammasomes in caspase-1 activation by Listeria monocytogenes', *J Clin Immunol*, 30: 693-702.

Wu, J., L. Sun, X. Chen, F. Du, H. Shi, C. Chen, and Z. J. Chen. 2013. 'Cyclic GMP-AMP is an endogenous second messenger in innate immune signaling by cytosolic DNA', *Science*, 339: 826-30.

Xhindoli, Daniela, Sabrina Pacor, Monica Benincasa, Marco Scocchi, Renato Gennaro, and Alessandro Tossi. 2016. 'The human cathelicidin LL-37 — A pore-forming antibacterial peptide and host-cell modulator', *Biochimica et Biophysica Acta (BBA) - Biomembranes*, 1858: 546-66.

Yamasaki, Kenshi, Jürgen Schauber, Alvin Coda, Henry Lin, Robert A. Dorschner, Norman M. Schechter, Chrystelle Bonnart, Pascal Descargues, Alain Hovnanian, and Richard L. Gallo. 2006. 'Kallikrein-mediated proteolysis regulates the antimicrobial effects of cathelicidins in skin', *The FASEB Journal*, 20: 2068-80.

Yang, Binbin, David Good, Tamim Mosaiab, Wei Liu, Guoying Ni, Jasmine Kaur, Xiaosong Liu, Calvin Jessop, Lu Yang, Rushdi Fadhil, Zhengjun Yi, and Ming Q. Wei. 2020. 'Significance of LL-37 on Immunomodulation and Disease Outcome', *BioMed Research International*, 2020: 8349712.

Yang, Pengyuan, Huazhang An, Xingguang Liu, Mingyue Wen, Yuanyuan Zheng, Yaocheng Rui, and Xuetao Cao. 2010. 'The cytosolic nucleic acid sensor LRRFIP1 mediates the production of type I interferon via a β-catenin-dependent pathway', *Nature Immunology*, 11: 487-94.

Yin, J. Y., Q. Huang, Y. Yang, J. T. Zhang, M. Z. Zhong, H. H. Zhou, and Z. Q. Liu. 2009. 'Characterization and analyses of multidrug resistance-associated protein 1 (MRP1/ABCC1) polymorphisms in Chinese population', *Pharmacogenet Genomics*, 19: 206-16.

Yoneyama, Mitsutoshi, Mika Kikuchi, Takashi Natsukawa, Noriaki Shinobu, Tadaatsu Imaizumi, Makoto Miyagishi, Kazunari Taira, Shizuo Akira, and Takashi Fujita. 2004. 'The RNA helicase RIG-I has an essential function in double-stranded RNA-induced innate antiviral responses', *Nature Immunology*, 5: 730-37.

Yoon, Sung-Hyun, Inhwa Hwang, Eunju Lee, Hyo-Joung Cho, Ju Hee Ryu, Tae-Gyun Kim, and Je-Wook Yu. 2021. 'Antimicrobial Peptide LL-37 Drives Rosacea-Like Skin Inflammation in an NLRP3-Dependent Manner', *Journal of Investigative Dermatology*, 141: 2885-94.e5.

Yuan, S. S., M. F. Hou, Y. C. Hsieh, C. Y. Huang, Y. C. Lee, Y. J. Chen, and S. Lo. 2012. 'Role of MRE11 in cell proliferation, tumor invasion, and DNA repair in breast cancer', *J Natl Cancer Inst*, 104: 1485-502.

Zahid, Ayesha, Hazrat Ismail, Bofeng Li, and Tengchuan Jin. 2020. 'Molecular and Structural Basis of DNA Sensors in Antiviral Innate Immunity', *Frontiers in Immunology*, 11: 613039-39.

Zerboni, Leigh, Nandini Sen, Stefan L. Oliver, and Ann M. Arvin. 2014. 'Molecular mechanisms of varicella zoster virus pathogenesis', *Nature Reviews Microbiology*, 12: 197-210.

Zhang, C., G. Shang, X. Gui, X. Zhang, X. C. Bai, and Z. J. Chen. 2019. 'Structural basis of STING binding with and phosphorylation by TBK1', *Nature*, 567: 394-98.

Zhang, H., Z. Deng, D. Zhang, H. Li, L. Zhang, J. Niu, W. Zuo, R. Fu, L. Fan, J. H. Ye, and J. She. 2018. 'High expression of leucine-rich repeat-containing 8A is indicative of a worse outcome of colon cancer patients by enhancing cancer cell growth and metastasis', *Oncol Rep*, 40: 1275-86.

Zhang, J., M. M. Hu, Y. Y. Wang, and H. B. Shu. 2012. 'TRIM32 protein modulates type I interferon induction and cellular antiviral response by targeting MITA/STING protein for K63-linked ubiquitination', *J Biol Chem*, 287: 28646-55.

Zhang, L., N. Wei, Y. Cui, Z. Hong, X. Liu, Q. Wang, S. Li, H. Liu, H. Yu, Y. Cai, Q. Wang, J. Zhu, W. Meng, Z. Chen, and C. Wang. 2018. 'The deubiquitinase CYLD is a specific checkpoint of the STING antiviral signaling pathway', *PLoS Pathog*, 14: e1007435.

Zhang, Qi-Yu, Zhi-Bin Yan, Yue-Ming Meng, Xiang-Yu Hong, Gang Shao, Jun-Jie Ma, Xu-Rui Cheng, Jun Liu, Jian Kang, and Cai-Yun Fu. 2021. 'Antimicrobial peptides: mechanism of action, activity and clinical potential', *Military Medical Research*, 8: 48.

Zhang, Qixiang, Xuyuan Zhang, Yalan Zhu, Panpan Sun, Liwei Zhang, Junxiao Ma, Yong Zhang, Lingan Zeng, Xiaohua Nie, Yina Gao, Zhaolong Li, Songqing Liu, Jizhong Lou, Ang Gao, Liguo Zhang, and Pu Gao. 2022. 'Recognition of cyclic dinucleotides and folates by human SLC19A1', *Nature*, 612: 170-76.

Zhang, Shen-Ying, Emmanuelle Jouanguy, Sophie Ugolini, Asma Smahi, Gaëlle Elain, Pedro Romero, David Segal, Vanessa Sancho-Shimizu, Lazaro Lorenzo, Anne Puel, Capucine Picard, Ariane Chapgier, Sabine Plancoulaine, Matthias Titeux, Céline Cognet, Horst von Bernuth, Cheng-Lung Ku, Armanda Casrouge, Xin-Xin Zhang, Luis Barreiro, Joshua Leonard, Claire Hamilton, Pierre Lebon, Bénédicte Héron, Louis Vallée, Lluis Quintana-Murci, Alain Hovnanian, Flore Rozenberg, Eric Vivier, Frédéric Geissmann, Marc Tardieu, Laurent Abel, and Jean-Laurent Casanova. 2007. 'TLR3 Deficiency in Patients with Herpes Simplex Encephalitis', *Science*, 317: 1522-27.

Zhang, Yanhui, Litao Xie, Susheel K. Gunasekar, Dan Tong, Anil Mishra, William J. Gibson, Chuansong Wang, Trevor Fidler, Brodie Marthaler, Aloysius Klingelhutz, E. Dale Abel, Isaac Samuel, Jessica K. Smith, Lei Cao, and Rajan Sah. 2017. 'SWELL1 is a regulator of adipocyte size, insulin signalling and glucose homeostasis', *Nature cell biology*, 19: 504-17.

Zhang, Z., B. Yuan, M. Bao, N. Lu, T. Kim, and Y. J. Liu. 2011. 'The helicase DDX41 senses intracellular DNA mediated by the adaptor STING in dendritic cells', *Nat Immunol*, 12: 959-65.

Zhao, Baoyu, Pengbiao Xu, Chesley M. Rowlett, Tao Jing, Omkar Shinde, Yuanjiu Lei, A. Phillip West, Wenshe Ray Liu, and Pingwei Li. 2020. 'The molecular basis of tight nuclear tethering and inactivation of cGAS', *Nature*, 587: 673-77.

Zhao, R., R. G. Russell, Y. Wang, L. Liu, F. Gao, B. Kneitz, W. Edelmann, and I. D. Goldman. 2001. 'Rescue of embryonic lethality in reduced folate carrier-deficient mice by maternal folic acid supplementation reveals early neonatal failure of hematopoietic organs', *J Biol Chem*, 276: 10224-8.

Zhao, Rongbao, and I. David Goldman. 2013. 'Folate and thiamine transporters mediated by facilitative carriers (SLC19A1-3 and SLC46A1) and folate receptors', *Molecular Aspects of Medicine*, 34: 373-85.

Zhao, Y., Z. Dai, Y. Liang, M. Yin, K. Ma, M. He, H. Ouyang, and C. B. Teng. 2014. 'Sequence-specific inhibition of microRNA via CRISPR/CRISPRi system', *Sci Rep*, 4: 3943.

Zheng, Zhou-Qin, Yu-Zhi Fu, Su-Yun Wang, Zhi-Sheng Xu, Hong-Mei Zou, and Yan-Yi Wang. 2022. 'Herpes simplex virus protein UL56 inhibits cGAS-Mediated DNA sensing to evade antiviral immunity', *Cell Insight*, 1: 100014.

Zhong, B., L. Zhang, C. Lei, Y. Li, A. P. Mao, Y. Yang, Y. Y. Wang, X. L. Zhang, and H. B. Shu. 2009. 'The ubiquitin ligase RNF5 regulates antiviral responses by mediating degradation of the adaptor protein MITA', *Immunity*, 30: 397-407.

Zhou, C., X. Chen, R. Planells-Cases, J. Chu, L. Wang, L. Cao, Z. Li, K. I. Lopez-Cayuqueo, Y. Xie, S. Ye, X. Wang, F. Ullrich, S. Ma, Y. Fang, X. Zhang, Z. Qian, X. Liang, S. Q. Cai, Z. Jiang, D. Zhou, Q. Leng, T. S. Xiao, K. Lan, J. Yang, H. Li, C. Peng, Z. Qiu, T. J. Jentsch, and H. Xiao. 2020. 'Transfer of cGAMP into Bystander Cells via LRRC8 Volume-Regulated Anion Channels Augments STING-Mediated Interferon Responses and Anti-viral Immunity', *Immunity*.

Zhou, Y., M. Fei, G. Zhang, W. C. Liang, W. Lin, Y. Wu, R. Piskol, J. Ridgway, E. McNamara, H. Huang, J. Zhang, J. Oh, J. M. Patel, D. Jakubiak, J. Lau, B. Blackwood, D. D. Bravo, Y. Shi, J. Wang, H. M. Hu, W. P. Lee, R. Jesudason, D. Sangaraju, Z. Modrusan, K. R. Anderson, S. Warming, M. Roose-Girma, and M. Yan. 2020. 'Blockade of the Phagocytic Receptor MerTK on Tumor-Associated Macrophages Enhances P2X7R-Dependent STING Activation by Tumor-Derived cGAMP', *Immunity*, 52: 357-73.e9.

Zhu, S., S. Ding, P. Wang, Z. Wei, W. Pan, N. W. Palm, Y. Yang, H. Yu, H. B. Li, G. Wang, X. Lei, M. R. de Zoete, J. Zhao, Y. Zheng, H. Chen, Y. Zhao, K. A. Jurado, N. Feng, L. Shan, Y. Kluger, J. Lu, C. Abraham, E. Fikrig, H. B. Greenberg, and R. A. Flavell. 2017. 'Nlrp9b inflammasome restricts rotavirus infection in intestinal epithelial cells', *Nature*, 546: 667-70.

List of Figures

Figure 1 - Evolution of Immunology. A) Élie Metchnikov drawings of silver nitrate stained bacteria being digested by phagocytes (Metchnikoff 1902). B) Paul Ehrlich's drawings depicting side chain theory. His diagram shows cells producing many receptors. He thought side chains that bind toxins (in black) become so abundant they are released into the extracellular milieu providing protection to the host (Ehrlich 1957). C) Charles Janeway's remarkably accurate diagram of pattern recognition receptors from 1989. In: 1 – pre-vertebrates who only possess PRRs; 2 and 3 – vertebrates that possess both PRRs and clonal receptors (Janeway 1989).

Figure 2 – Toll-like Receptor signalling. A) Structure of TLR4's LRR domain (blue) in complex with LPS (red) determined by X-Ray crystallography. MD-2, a TLR4 accessory required for detection of LPS is shown in green. The transmembrane domain and TIR domain are shown schematically. The Illustration is adapted from Goodsell (2011). B) The 10 human TLRs signal through the myddosome and triffosome to drive production of proinflammatory cytokines.

Figure 3 – Intracellular RNA sensors. A schematic showing known cytosolic RNA sensors discussed in section I.3. RNA PRRs are grouped into three classes - RNA sensing restriction factors, RIG-I like receptors and sensors of Z-RNA.

Figure 4 – DNA sensing by cGAS. A) The presence of mislocalised or pathogen associated dsDNA in the cytoplasm is detected by cGAS. Upon DNA binding, cGAS undergoes phase separation and generates the cyclic dinucleotide 2'3'-cGAMP required by the central hub of DNA sensing – STING – to translocate from the ER towards ERGIC. Here, STING recruits TBK1 to phosphorylate the master transcriptional regulators of innate immune activation - IRF3 and NF-κB. This results in the production of proinflammatory cytokines, primarily type I IFNs but also IL-6 and TNF-α. B) Schematic showing structural domains within human cGAS. C) Structure of human cGAS in complex with DNA resolved by X-ray crystallography. Adapted from Ablasser and Chen (2019).

Figure 5 – Intracellular DNA sensors. A schematic showing known cytosolic DNA sensors discussed in section I.4. DNA PRRs are split into four groups - cGAS dependent sensors, putative DNA sensors, DNA-PK mediated sensing and inflammasome activators. A) Funeral given to putative DNA sensors after the discovery of cGAS lifted from Vance (2016). B) Crystal structure of A, B and Z -form DNA adapted from Heinemann and Roske (2020).

Figure - 6 structure of STING. A) picture of starlet sea anemone (*Nematostella vectensis*) lifted from Layden, Rentzsch, and Röttinger (2016). B) Amino acid sequence of STING showing: starts codons in blue, potential serine phosphorylation sites in purple, potential lysine ubiquitination sites in orange and polymorphic sites in red and green. C) Topological diagram of STING's domains, showing the cyclic dinucleotide binding domain (CBD) and C- terminal tail (CTT). D) Structure of human STING dimer resolved by cryo-EM. Individual subunits are coloured green and yellow, with the ligand binding pocket shown in pink. Figure adapted from Shang et al. (2019).

Figure 7 - Accessories of STING. Positive regulators of STING are shown in red and negative in blue. Where possible regulators are shown at their subcellular site of action. A description and reference for the individual STING regulators shown is given in supplementary Table 1.

Figure 8 - Posttranslational modification of STING. Diagram showing the residues within STING targeted by ubiquitin ligases, SUMOylases, DUBs and kinases to regulate signalling. A description and reference for the individual STING regulators shown is given in supplementary Table 1.

Figure 9 - STING associated diseases. Schematic showing diseases where STING signalling is thought to contribute to pathology. The table is adapted from Ablasser and Chen (2019).

Figure 10 – Interferon signalling. Viral invasion releases nucleic acids into the cell cytosol that can be detected by toll-like receptors (TLRs), RIG-I like receptors (RLRs) and cytoplasmic DNA receptors (CDRs). This leads to the production of type I interferons, which act through the IFNAR receptor in both an autocrine and paracrine manner to drive ISG expression. ISGs then act to restrict viral replication.

Figure 11 – Extracellular 2'3'-cGAMP transport. Schematic showing the mechanisms by which 2'3'-cGAMP can be transferred between cells. A) Within viral particles. B) Through gap junctions. C) Import and export through LRRC8A:C heterodimers which are activated by hypotonicity and S1P. D) Export through ABCC1. E) Transport through the ATP gated pore P2X7. F) Import through SLC19A1. G) Import through SLC46A2. H) 2'3'-cGAMP shuttling by LL-37. I) 2'3'-cGAMP hydrolysis by ENPP1.

Figure 12 – Structure of SLC19A1 in complex with 2'3'-cGAMP. A) Cryo-EM density map of human SLC19A1(blue)-Fab(grey) complex bound to two molecules of 2'3'-cGAMP (green and purple). B) The overall structures of hSLC19A1 bound to 2'3'-cGAMP in the inward-open conformation. The N-terminal domain (NTD) is coloured yellow and C-terminal domain (CTD) coloured blue. Two bound 2'3'-cGAMP molecules are shown as a space-filling representation and are coloured (green and purple). Adapted from Zhang et al. (2022).

Figure 13 – P2X7 mediated 2'3'-cGAMP uptake during MERTK blockade. Dying cancer cells are cleared by efferocytosis where the MerTK receptor present on tumour associated macrophages (TAMs) recognises "eat me" signals Gas6/ProS. This leads to immunologically silent cell death by engulfment and digestion of the cellular corpse. Blockade of MerTK activity with an anti-MerTK antibody result in accumulation of dying cancer cells. Likely as a result of membrane disintegration, 2'3'-cGAMP and ATP are released into the tumour microenvironment. ATP activates the P2X7 pore expressed by TAMs allowing 2'3'-cGAMP to passively move across the plasma membrane and drive type I IFN production through STING.

Figure 14 – Structure and function of VRACs. A) Diagram showing regulatory volume decrease. Hypotonic conditions cause cells to swell as water molecules cross the plasma membrane through osmosis. Cell swelling opens VRAC channels, leading to export of small anionic species such as Cl^-. The reduction in anionic solutes within the cell reduces its osmolarity and allows for cell shrinkage. B) Topology of LRRC8A. Depicted is the transmembrane domains, Extracellular loops (EL), intracellular loops (IL) and leucine rich repeats (LRR). Cryo-EM density map of hexameric channel formed by human LRRC8A. Structure adapted from Kasuya et al. (2018).

Figure 15 – Structure of ABCC1. A) Diagram depicting topology of ABCC1 with its transmembrane domains (TM) and nucleotide binding domains (NBD) shown. B) Cartoon showing structure of bovine ABCC1 based upon a Cryo-EM density map. Lifted from Johnson and Chen (2017).

Figure 16 – (Natural) history of HSV-1. A) Depiction of Hippocrates (Unknown 13th Century). B) TIME magazine August 2nd, 1982 ("TIME" 1982). C) Kōhaku, the most expensive koi carp in the world, sold for $1.8 million (Marugen 2018). D) HSV-1 initially infects the oral mucosa, infecting sensory neurons and travelling by anterograde transport to the trigeminal ganglion, the site of viral latency. Further spread into the central nervous system can lead to encephalitis. Reactivation allows trafficking by retrograde transport back to the oral mucosa and lytic infection.

Figure 17 – HSV-1 replication cycle. HSV-1 associates with the cell surface through interaction with heparan-sulphate proteoglycans then binds to an entry receptor to trigger membrane fusion. Molecular motor proteins traffic virions through the microtubule-organising centre (MTOC) to the nuclear pore complex (NPC). HSV-1 genes are expressed temporally leading to the production of the structural proteins needed for capsid assembly which are loaded with viral genomes and then traffic to early endosomes (EE). Exocytosis allows for progeny viral particles to be released.

Figure 18 – Antagonism of cGAS-STING signalling by HSV-1. cGAS-STING pathway and the known antagonists encoded by HSV-1. Adapted from Danastas, Miranda-Saksena, and Cunningham (2020).

Figure 19 - A) Schematic of the lentiviral construct used in the GeCKO v2 library. Showing the: U6 promoter, single guide RNA (sgRNA), elongation factor-1α short promoter (EFS), *Streptococcus pyogenes* CRISPR associated protein 9 (spCas9), FLAG octapeptide tag (FLAG), 2A self-cleaving peptide (P2A), puromycin

selection marker (Puro) and post transcriptional regulatory element (WPRE). B) Composition of the GeCKO v2 library of sgRNAs.

Figure 20 – CRISPR screen looking to identify regulators of STING. A) Lentiviral constructs encoding the GeCKO v2 library of sgRNAs were used to transduce p125 THP-1 cells engineered to express GFP from an IFN-β promoter. After puromycin selection cells were differentiated with PMA (5ng/ml) for 24 hours then permeabilised with digitonin buffer (0.001%) containing 2'3'-cGAMP (0.4 ng/ul). 6 hours later cells were then FACS sorted into GFP- and GFP+ populations. DNA was extracted and sgRNAs amplified by PCR using U6 forward and EFS reverse primers. A custom python pipeline was used to count sgRNA abundance within the GFP- and GFP+ populations. Statistical analysis designed to identify guides enriched within GFP- population was done with the statistical analysis programme MAGeCK. B) Negative bimodal model of guide enrichment. Each data point represents a sgRNA and those statistically significant are shown in red. STING and IRF7 are annotated. C) sgRNAs targeting genes known to enhance STING signalling that reach statistical significance. D) sgRNAs targeting genes known to augment STING signalling that don't reach statistical significance. E) sgRNAs targeting genes unrelated to *2'3'*-cGAMP driven STING activation that don't reach statistical significance. Statistics at the individual sgRNA level was done using an alpha-modified robust rank aggregation method. Each bar represents one of the six sgRNAs used to target a gene. The bars show its individual enrichment score (n=1).

Figure 21 – Statistical analysis of CRISPR screen. Gene ontology analysis revealed amongst 177 genes that reach statistical significance of these 100 are involved in gene expression and 12 in mitochondrial function or energy metabolism. These pathways are crucial to protein translation likely effecting GFP production independently of STING activation and so were excluded. This left 58 genes displayed in this figure that were investigated further. Statistics at the individual sgRNA level was done using an alpha-modified Robust Rank Aggregation Method. Each bar represents one of the six sgRNAs used to target a gene. The bars show the individual enrichment score (n=1).

Figure 22 – Crystal violet viability assay. A) THP-1 cells were transfected with non-targeting (NT) or STING targeting siRNAs using Viromere Blue. 48 hours post transfection the indicated cells were differentiated with PMA (50 ng/ml). The abundance of STING was assessed at the indicated time points by western blotting (n=1). A) The indicated number of THP-1 cells were differentiated with PMA (50ng/ml) in the presence or absence of etoposide. 24 hours later cells were fixed and stained with crystal violet dye. Retention of crystal violet was then measured by resolubilising the dye in MeOH and reading absorbance at 570nm. C) Point at which linear increase between cell number and absorbance started was determined (purple cross section). This was set as the minimum readable value. The mock is displayed as the mean of three technical replicates with error bars showing SEM. A single reading is displayed for the etoposide conditions hence no error bars are present (n=1).

Figure 23 – Assessing IFN production by siRNA treated THP-1 cells (part 1). A) Cells were transfected with siRNA using Viromere Blue. 48 hours later cells were treated with PMA (50 ng/ml). Then at 72 hours post transfection stimulated with 2'3'-cGAMP (0.4 ng/ul) in permeabilisation buffer (0.001% digitonin). B) 6 hours after 2'3'-cGAMP stimulation supernatants were transferred onto 3C11 cells which express luciferase under an interferon stimulated response element (pIRSE). The recipient 3C11 cells were lysed and luminescence measured on addition of luciferin after 24 hours. Luminescence values were converted to IFN values using a IFN A/D standard. C) THP-1 cells were fixed and stained with crystal violet dye. Retention of crystal violet was then measured by resolubilising the dye in MeOH and reading absorbance at 570nm. D) IFN values were normalised by division to cellular viability.

Figure 24 - Assessing IFN production by siRNA treated THP-1 cells (part 2). THP-1 cells were transfected with indicated siRNAs using Viromere Blue. 48 hours later cells were differentiated with PMA (50 ng/ml). Then at 72 hours post transfection stimulated with 2'3'-cGAMP (0.4 ng/ul) in permiabalisation buffer (0.001% digitonin). 6 hours after 2'3'-cGAMP stimulation supernatants were transferred onto 3C11 cells. A) Cell viability was measured using a crystal violet stain. The limit of detection (LD) defined as the minimum number of cells detectable is displayed. B) luminescence values. C) 3C11 were treated with an IFNA/D standard. Standards from individual bioassays were used to convert luminescence scores to IFN values. The limit of detection (LD) was defined as highest luminescence recorded for media with 0 U/ml of IFN A/D. The saturation point (SP) was defined as the value at which luminescence induction by IFN A/D moved outside of the linear range. Samples being tested were diluted to ensure they could be read within the SP and LD. A representative standard is shown. (D) Luminescence values were converted to IFN values using the IFN A/D standard. (E) Total IFN production

normalised by division to cellular viability. One representative experiment is shown with data points representing technical duplicates (n=3, biological repeats, representative graphs shown). F) STING and MAVS abundance was assessed by western blotting at 72 hours after siRNA treatment (n=2, biological repeats, representative blot shown).

Figure 25 - siRNA Screen (Part 1) - THP-1 cells were transfected with indicated siRNAs using Viromere Blue as described in Figure 24. A) Cell viability was measured using a crystal violet stain. The average viability of the untreated wells and viability limit (VL) defined as the minimum number of cells detectable are displayed. An X indicates each data point excluded in subsequent analysis due to cells not meeting the viability limit (VL). B) Luminescence values were converted to IFN values using a IFN A/D standard. C) Total IFN production normalised to cellular viability. Technical duplicates were recorded and individual data points are displayed. The average value for the positive and negative controls STING and MAVS are displayed. Using these as a reference 13 genes of interest were identified for further testing indicated by pink arrows (n=1).

Figure 26 – siRNA screen (Part 2). Data from Figure 25 replotted as IFN vs Absorbance (viability). Data points show averages of technical duplicates with data points below the viability limit (VL) excluded. The average value for the positive and negative controls STING and MAVS are displayed. Using these as a reference 13 genes of interest were identified for further testing indicated by pink arrows (n=1).

Figure 27 – Overexpression of potential STING acessories in THP-1 cells. A) THP-1 cells were transduced with lentiviruses stably expressing the indicated genes with a C terminal V5 tag and lysed. Protein abundance was then assessed by western blotting (n=1). B) Table showing whether proteins were detected at the expected size. Size predictions estimated by gene card.

Figure 28 – Overexpression of TBK1 in THP-1 cells. (A) RNA was extracted from THP-1 Lucia cells stably expressing the indicated genes and RT-qPCR was performed for the *TBK1* gene. Technical duplicates shown (n=1). THP-1 Lucia cells stably expressing either GFP-V5 or TBK1-V5 were intracellularly stained for V5 and populations quantified by flow cytometry. Gating strategy shown in supplementary Figure 3 (n=1).

Figure 29 – Stimulation of THP-1 cells with 2'3'-cGAMP. THP-1 Lucia cells expressing luciferase under an IRF3-induced promoter were stably transduced with GFP or TBK1. THP-1 cells were differentiated with PMA (50 ng/ml) 24 hours prior to stimulation with: (A) exogenous 2'3'-cGAMP (n=3, biological repeats, representative graph shown); (B) 2'3'-cGAMP in a permeabilisation buffer (0.001% digitonin) (n=2, biological repeats, representative graph shown); (C) transfected VACV dsDNA (n=3, biological repeats, representative graph shown). 24 hours after stimulation luminometry was then used to assess luciferase production.

Figure 30 - Stimulation of THP-1 cells expressing potential STING accessories with 2'3'-cGAMP. THP-1 Lucia cells expressing luciferase under an IRF3-induced promoter were stably transduced with the indicated genes. THP-1 cells were differentiated with PMA (50 ng/ml) 24 hours prior to stimulation with: exogenous 2'3'-cGAMP, 2'3'-cGAMP in a permeabilisation buffer (0.001% digitonin) or transfected VACV dsDNA. 24 hours after stimulation luminometry was used to assess luciferase production. A) Heat map showing fold change of luciferase production relative to GFP for untreated and vehicle controls. B) Heat map showing fold change of luciferase production relative to GFP for different 2'3'-cGAMP stimuli. Left hand column displays average fold change across all stimuli and doses (n=2, average of biological repeats shown).

Figure 31 - Stimulation of THP-1 cells expressing potential STING accessories with exogenous 2'3'-cGAMP. THP-1 Lucia cells expressing luciferase under an IRF3-induced promoter were stably transduced with the indicated genes. The THP-1 cells were differentiated with PMA (50 ng/ml) 24 hours prior to stimulation with exogenous 2'3'-cGAMP at the indicated doses. 24 hours after stimulation luminometry was used to assess luciferase production (n=1).

Figure 32 - Synopsis of cGAMP channels and viruses tested. A) Synopsis of cGAMP channels based upon evidence presented in Chapter I, section I.7. B) Synopsis of viruses used adapted from Zahid et al. (2020).

Figure 33 -Screening for viral degradation of LRRC8A. 293 cells were infected with HSV-1 (MOI – 0.02, 0.006, 0.002), VACV (MOI – 0.2, 0.066, 0.022), AdV (MOI – 1500, 150, 15), HIV-1 (1:10, 1:50, 1:250), HIV-2 (1:10, 1:50,

1:250), ZIKV (MOI – 1, 0.25, 0.06) and IAV (MOI – 10, 5, 2.5). 48 hours later, the cells were lysed and abundance of LRRC8A was assessed by western blotting (n=2, biological repeats).

Figure 34 -Screening for viral degradation of LRRC8C. 293 cells were infected with HSV-1 (MOI – 0.02, 0.006, 0.002), VACV (MOI – 0.2, 0.066, 0.022), AdV (MOI – 1500, 150, 15), HIV-1 (1:10, 1:50, 1:250), HIV-2 (1:10, 1:50, 1:250), ZIKV (MOI – 1, 0.25, 0.06) and IAV (MOI – 10, 5, 2.5). 48 hours later, the cells were lysed and abundance of LRRC8C was assessed by western blotting. Secondary band indicated by * (n=2, biological repeats).

Figure 35 – Overexpression of P2X7, SLC19A1 and SLC46A2. A) A western blot of 293 cells stably transduced with P2X7-V5, SLC46A2-V5 and SLC19A1 (n=3, biological repeats). B/C) Western blots as in (A) boiled for 5 minutes at indicated temperatures and lysed in either NP40 buffer or NP40 buffer supplemented with 7M urea. Pink and blue boxes indicate the stacking and resolving portion of the gel (n=3, biological repeats).

Figure 36 -Screening for viral degradation of P2X7-V5. 293 cells were infected with HSV-1 (MOI – 0.02, 0.006, 0.002), VACV (MOI – 0.2, 0.066, 0.022), AdV (MOI – 1500, 150, 15), HIV-1 (1:10, 1:50, 1:250), HIV-2 (1:10, 1:50, 1:250), ZIKV (MOI – 1, 0.25, 0.06) and IAV (MOI – 10, 5, 2.5). 48 hours later, the cells were lysed and abundance of P2X7-V5 was assessed by western blotting (n=2, biological repeats).

Figure 37 -Screening for viral degradation of SLC19A1-V5. 293 cells were infected with HSV-1 (MOI – 0.02, 0.006, 0.002), VACV (MOI – 0.2, 0.066, 0.022), AdV (MOI – 1500, 150, 15), HIV-1 (1:10, 1:50, 1:250), HIV-2 (1:10, 1:50, 1:250), ZIKV (MOI – 1, 0.25, 0.06) and IAV (MOI – 10, 5, 2.5). 48 hours later, the cells were lysed and abundance of SLC46A2-V5 was assessed by western blotting (n=1).

Figure 38 -Screening for viral degradation of SLC46A2-V5. 293 cells were infected with HSV-1 (MOI – 0.02, 0.006, 0.002), VACV (MOI – 0.2, 0.066, 0.022), AdV (MOI – 1500, 150, 15), HIV-1 (1:10, 1:50, 1:250), HIV-2 (1:10, 1:50, 1:250), ZIKV (MOI – 1, 0.25, 0.06) and IAV (MOI – 10, 5, 2.5). 48 hours later, the cells were lysed and abundance of SLC46A2-V5 was assessed by western blotting (n=1).

Figure 39 – Resolving ABCC1 by polyacrylamide gel electrophoresis. 293 cell lysates were boiled for 5 minutes at indicated temperatures after lysis in either NP40 buffer or NP40 buffer supplemented with 7M urea. Pink and blue boxes indicate the stacking and resolving portion of the gel (n=3, biological repeats).

Figure 40 -Screening for viral degradation of ABCC1. 293 cells were infected with HSV-1 (MOI – 0.02, 0.006, 0.002), VACV (MOI – 0.2, 0.066, 0.022), AdV (MOI – 1500, 150, 15), HIV-1 (1:10, 1:50, 1:250), HIV-2 (1:10, 1:50, 1:250), ZIKV (MOI – 1, 0.25, 0.06) and IAV (MOI – 10, 5, 2.5). 48 hours later, the cells were lysed and abundance of ABCC1 was assessed by western blotting (n=2, biological repeats).

Figure 41 - Summary of cGAMP channel abundance during viral infection with viruses. Values indicate the number of times individual phenotypes were replicated.

Figure 42 – Human LRRC8A:C is degraded by HSV-1. A) 293 cells were infected with HSV-1 at MOI - 0.06, 0.12, 0.25, 0.5 and 1. 24 hpi cells were lysed and LRRC8A:C abundance was quantification by immunblotting. A pink arrow shows the LRRC8C secondary band (n=3, biological repeats). B) MEFs were infected with HSV-1 at MOI – 1, 10, 30 and 100. 24 hpi cells were lysed and LRRC8A:C abundance was quatified by immunblotting (n=2, biological repeats). C) Total RNA was extracted from cells treated as in A. Expression levels of LRRC8A:C were determined by RT-qPCR with samples assayed in technical triplicates. Data were analysed by the comparative Ct method. Densitometry from A is plotted on the right hand Y axis (n=1).

Figure 43 - LRRC8A:C is degraded late during HSV-1 infection. 293 cells were infected with HSV-1 at MOI 1 and lysed at the indicated time points. LRRC8A (A) and LRRC8C (B) abundance was then assessed by immunoblotting. A schematic showing the mechanism by which herpes viruses regulate there genome is also displayed (n=2, biological repeats). C) Densitometry from A and B.

Figure 44 – HSV-2 but not VZV degrade LRRC8A:C. (A) Schematic showing phylogeny of human herpes viruses. (B) 293-T cells were infected with HSV-2 at MOI - 1, 3, 5, and 10. 24 hpi cells were lysed and LRRC8A:C abundance was assessed by immunblotting (n=2, biological repeats). (C) VZV infected MeWo cells were seeded on top of uninfected MeWo (1 infected cell : 5 seeded cells). 1 hour later the infected MeWos were washed off with PBS.

24 hours after VZV exposure cells were lysed and LRRC8A:C abundance was assessed by immunoblotting (n=3, biological repeats).

Figure 45 – Immunoprecipitation of LRRC8C from HSV-1 infected cells. HEK239 cells stably over expressing LRRC8A-V5 (A) or LRRC8C-V5 (B) were infected with HSV-1 at MOI 10. 8 hpi cells were lysed and immunoprecipitated with an α-V5 antibody. Input unbound and IP were subjected to immunoblotting (n=2, biological repeats). The LRRC8C IP samples were analysed by mass spectrometry. PEAKS software was used to identify peptides and align them to the Human UniProt Swissprot database (Alignment ID - 20210911_seq23155) and HSV-1 genome (NCBI database - NC_001806). The progenesis label free quantification software was used to assign relative values of protein abundance. The abundance limit (AL) was set to exclude lowest 3% of host proteins. Nonlinear regression shows average protein abundance where proteins above are enriched and below depleted in HSV-1 infected cells. Peripheral lines show the 95% confidence limits. Proteins associated with DNA-PK, cGAS or LRRC8C are annotated (n=1).

Figure 46 – Narrowing down HSV-1 genes responsible for LRRC8A:C degradation. Schematic showing how the pool of 84 HSV-1 genes was narrowed down to 2 candidate genes using the information gathered in Figure 43, Figure 44, and Figure 45.

Figure 47 – Known functionality of UL56. The arginine rich region (RR) and transmembrane (TM) domain are annotated. PPXY motifs recruit NEDD4 family E3 ligases to ubiquitinate multiple cellular targets. One known target, the trafficking molecule GOPC, is targeted for proteasomal degradation. Mutation of PPXY motifs to AAXA nullifies UL56 mediated NEDD4 E3 ligase activity.

F**igure 48 – UL56 is necessary and sufficient for LRRC8A:C degradation.** A) HEK293 cells were transiently transfected with constructs expressing UL56-GFP or UL6-GFP. To exclude bulk effects, 24 hours after transfection cells were sorted into GFP- and GFP+ populations by FACS sorting. Gating strategy is shown in supplementary Figures 4 and 5. Mock, lipofectamine treated and HSV-1 infected cells (MOI 3 for 24 hours) were lysed without sorting (n=3, biological repeats). B) HEK239 cells were infected with the indicated HSV-1 genotypes (MOI 3) for 24 hours before lysis (n=3, biological repeats). In both cases western blotting was used to assess LRRC8A:C abundance.

Figure 49 – LRRC8A:C is potentially proteasomally degraded. HEK293 GOPC knockout cell lines were lysed and western blotting was used to assess LRRC8A:C abundance (n=3, biological repeats). HEK293 cells were infected with HSV-1 (MOI 3) and one hour later treated with the proteasomal inhibitor lactacystin (20μm). 24 hpi western blotting was used to assess LRRC8A:C abundance (n=2, biological repeats).

Figure 50 - Schematic showing dual luciferase assay. HEK293T cells were transfected with p125-FLuc expressing firefly luciferase under an IFN-β promoter, pRL-TK expressing renilla luciferase under an TK promoter and pcDNA3.2-STING constitutively expressing STING. 24 hours after transfection cells were then treated with 2'3'-cGAMP in a hypotonic buffer to active LRRC8A:C. Luminesce was then read with firefly (indicative of IFN-β production) being divided by renilla to normalise for transfection efficiency.

Figure 51 – Chemical inhibition of LRRC8A:C mediated 2'3'-cGAMP uptake. HEK293T cells were transfected with p125-FLuc (IFNβ promoter reporter), pRL-TK (constitutively expresses renilla luciferase) and pcDNA3.2 STING. IFN-β production was then assessed in response to low salt (NaCl) buffers containing 2'3'-cGAMP. Cells were also treated with DCPIB (20uM) or the vehicle control (DMSO). Graphs display average of three technical replicates statistically evaluated with grouped two-way ANOVA – Tukey. *=p<0.05, **=p<0.01, ***=p<0.001, ****=p<0.0001, ns=not significant (n=3, biological repeats, representative dataset).

Figure 52 – LRRC8A is required for 2'3'-cGAMP uptake. A) HEK293 LRRC8A knockout single cell clones were lysed and western blotting was used to assess LRRC8A abundance (n=3, biological repeats). B) HEK293 LRRC8A KO cells were transfected with p125-FLuc (IFNβ promoter reporter), pRL-TK (constitutively expresses renilla luciferase) and pcDNA3.2-STING. IFN-β production was then assessed in response to low salt (NaCl) buffers containing 2'3'-cGAMP. Graphs display average of three technical replicates statistically evaluated with grouped two-way ANOVA – Tukey. *=p<0.05, **=p<0.01, ***=p<0.001, ****=p<0.0001, ns=not significant (n=3, biological repeats, representative data set).

Figure 53 – UL56 inhibits LRRC8A:C mediated 2'3'-cGAMP uptake. A) HEK293T stably over expressing UL56 and UL56 AXAA mutant constructs were lysed and western blotting (A) was used to assess LRRC8A:C abundance. Densitometry was used to quantify the results (B). Graphs display average (±SEM) of three independent biological repeats statistically evaluated with two-way ANOVA – Tukey (n=3, biological repeats). B) HEK293T cells stably expressing indicated UL56 constructs were transfected with p125-FLuc (IFNβ promoter reporter), pRL-TK (constitutively expresses renilla luciferase) and pcDNA3.2-STING. IFN-β production was then assessed in response to low salt (NaCl) buffers containing 2'3'-cGAMP. Graphs display average of three independent biological repeats statistically evaluated with grouped two-way ANOVA – Tukey. *=p<0.05, **=p<0.01, ***=p<0.001, ****=p<0.0001, ns=not significant (n=3, biological repeats, pooled data for 3 individual experiments shown).

Figure 54 – UL56 degrades SLC46A2. A) HEK293T cells stably expressing SLC46A2 with a C-terminal V5 tag were transiently transfected with a construct expressing UL56-GFP. To exclude bulk effects, cells were FACS sorted into GFP- and GFP+ populations as, shown in supplementary Figure 4 and 5 (n=1, biological repeats). B) HEK293T SLC46A2-V5 cells were infected with the indicated HSV-1 genotypes (MOI 3) for 24 hours before lysis (n=3, biological repeats) (Experiment performed by Jed Avissar under my close supervision). In both A and B western blotting was used to assess LRRC8A:C abundance.

Figure 55 – A model of SLC46A2 mediated 2'3'-cGAMP uptake. A) HEK293T cells stably transduced with SLC46A2-V5 were transfected with p125-FLuc (IFNβ promoter reporter), pRL-TK (constitutively expresses renilla luciferase) and pcDNA3.2-STING. IFN-β production was then assessed in response to extracellular 2'3'-cGAMP. Cells were also treated with SSZ (1mM) or the vehicle control (DMSO). Graphs display average (±SEM) of three technical replicates statistically evaluated with two-way ANOVA – Tukey. *=p<0.05, **=p<0.01, ***=p<0.001, ****=p<0.0001, ns=not significant (n=3, biological repeats, representative dataset) (Experiment performed by Jed Avissar under my close supervision). B) Schematic showing sulfasalazine an antagonist of both SLC46A2 and SLC19A1.

Figure 56 – UL56 inhibits SLC46A2 mediated 2'3'-cGAMP uptake. A) HEK293T SLC46A2-V5 stably over expressing UL56 and UL56 AXAA mutant constructs were lysed and western blotting was used to assess V5 abundance (n=2, biological repeats). B) HEK293T SLC46A2-V5 cells stably expressing the indicated UL56 constructs were transfected with p125-FLuc (IFNβ promoter reporter), pRL-TK (constitutively expresses renilla luciferase) and pcDNA3.2-STING. IFN-β production was then assessed in response to extracellular 2'3'-cGAMP. Graphs display average (±SEM) normalised to R-Luc and then the average of unstimulated groups of three technical replicates statistically evaluated with grouped two-way ANOVA – Tukey. *=p<0.05, **=p<0.01, ***=p<0.001, ****=p<0.0001, ns=not significant (n=3, biological repeats, representative data set shown) (Experiment performed by Jed Avissar under my close supervision).

Figure 57 – UL56 degrades P2X7. A) HEK293T cells stably expressing P2X7 with a C-terminal V5 tag were transiently transfected with a construct expressing UL56-GFP. To exclude bulk effects cells were FACS sorted into GFP- and GFP+ populations as, shown in supplementary Figure 4 and 5 (n=3, biological repeats). B) HEK293T P2X7-V5 cells were infected with the indicated HSV-1 genotypes (MOI 3) for 24 hours before lysis (n=3, biological repeats) (Experiment performed by Jed Avissar under my close supervision). In both A and B, western blotting was used to assess LRRC8A:C abundance.

Figure 58 – P2X7 activity assay. A) Schematic showing YO-PRO-1 uptake through P2X7. B) Indicated HEK293 cells were treated with BzATP (80 μM) in the presence of YO-PRO-1. Immediately after YO-PRO-1 addition, green fluorescence was measured at 45 second intervals before and BzATP was added at 10 minutes indicated by a grey line. Fluorescence levels were normalised to the average fluorescence before BzATP was added (F/F0). Data was statically evaluated with grouped two-way ANOVA – Tukey. *=p<0.05, **=p<0.01, ***=p<0.001, ****=p<0.0001, ns=not significant (n=3, biological repeats, representative data set shown) (Experiment performed by Alex Redmond under my close supervision).

Figure 59 – UL56 inhibits P2X7's activity. HEK293T P2X7-V5 stably over expressing UL56 and UL56 AXAA mutant constructs were treated with BzATP (80 μM) in the presence of YO-PRO-1. Immediately after YO-PRO-1 addition, green fluorescence was measured at 45 second intervals before and BzATP was added at 10 minutes indicated by grey line. Fluorescence levels were normalised to the average fluorescence before BzATP was added (F/F0).

Data was statically evaluated with grouped two-way ANOVA – Tukey. *=p<0.05, **=p<0.01, ***=p<0.001, ****=p<0.0001, ns=not significant (n=3, biological repeats, representative data set shown) (Experiment performed by Jed Avissar under my close supervision).

Figure 60 – UL56 inhibits 2'3'-cGAMP uptake through P2X7. A) HEK293T GFP-V5 or P2X7-V5 cells were transfected with p125-FLuc (IFNβ promoter reporter), pRL-TK (constitutively expresses renilla luciferase) and pcDNA3.2-STING. IFN-β production was then assessed in response to extracellular 2'3'-cGAMP and BzATP at the indicated doses. F-Luc is normalised to R-Luc and then the average of unstimulated groups. Data was statically evaluated with grouped two-way ANOVA – Tukey. *=p<0.05, **=p<0.01, ***=p<0.001, ****=p<0.0001, ns=not significant (n=3, biological repeats, representative data set shown). B) HEK293T P2X7-V5 cells stably expressing the indicated GFP or UL56 constructs were assessed for IFN-β induction as is A (n=1).

Figure 61 – UL56 targets multiple cGAMP channels. The *UL56* gene from HSV-1 targets LRRC8A:C, P2X7 and SLC46A2 for degradation and so antagonises 2'3'-cGAMP transport. Described in Chapters IV, V and VI.

Table 1 – The cell types in which cGAMP channels function and the CDNs they transport. Shown are cell types in which channel deficiency or specific chemical inhibitors prevent STING pathway activation in response to exogenous CDNs. FDA approved drugs are shown in red. Primary cell lines are shown in black and cancer cell lines in blue. Mouse cell lines and channels only tested in mice are shown in italics. * - Not major importer as knockout or chemical inhibition only marginally reduces CDN mediated STING activation. ** - Direct CDN uptake not proven in *vitro* but in *vivo* channel required for STING pathway activation in presence of exogenous CDNs. † - Unclear if imported. †† - Minimal effect of transporter on uptake. # - P2X7 forms a large non-selective pore for hydrophilic substances ~0.9 KDa in size therefore although not formally shown it is assumed there is no CDN specificity. Ψ reviewed by Salameh and Dhein (2005). λ reviewed by Müller and Namasivayam (2022). ω reviewed by Cole (2014).

Table 2– Substrate and tissue specificity of auxiliary VRAC subunits. LRRC8A is thought to be ubiquitously expressed. Tissue expression data was compiled from publicly available transcriptome databases by Abascal and Zardoya (2012).

Appendix

Supplementary Figures and Tables

Supplementary Table 1 (Page 1 of 3) – List of STING accessory proteins. The sites and type of post-translation modification are listed. Additionally, where possible the cellular site of action and domains interacting with STING are also denoted. If the accessory is known regulates both NF-kB and IRF3 dependent signalling is also listed. Related to Chapter I, Section I.5, Figures 7 and 8.

STING accessory	positive or negative Regulator	Description	STING PMT site	type of ubquitination	cellular site of action	regulates NF-kB activity	regulates IRF3 activity	domain of STING accessory interacting with STING	domain of STING interacting with protein	reference
ADAM17 / SEMA4D	neither	Through an unclear mechanism STING activates ADAM17 which cleaves SEMA4D a noncanonical pronflammatory cytokine. This process is independent of both IRF3 and NF-kB activation.	na	na	not tested	no	no	not tested	not tested	(Motani et al., 2018)
AP-1	negative	AP-1 sorts phosphorylated STING into clathrin-coated transport vesicles for delivery to the endolysosomal system, where STING is degraded.	na	na	ERGIC	yes	yes	not tested	(a.a. 342-376)	(Liu et al., 2022)
Atg9a	negative	Atg9a is a protien central to the induction of autophagy. Loss of Atg9a enhances STING mediated innate imune responses. Although Atg9a's mechanism of action is unclear.	na	na	ERGIC	yes	yes	not tested	not tested	(Saitoh et al., 2009)
COPA / SURF4	negative	The coat protein I complex (COP-I) mediates retrograde transport of STING from the Golgi to the ER. COPA is a subunit of the COP-1 complex which interact with STING via the bridging molecule SURF4. This allows for Golgi located STING to move back to the ER preventing aberrant signalling. Interestingly disease causing mutations mean COPA cannot transport STING. Suggesting a link between STING signalling and the pathogenesis of COPA syndrome.	na	na	ER ERGIC	not tested	yes	not tested	not tested	(Mukai et al., 2021) (Deng et al., 2020)
CSK	positive	After DNA stimulation, the non-receptor tyrosine kinase (CSK) phosphorylates STING at Y240 and Y245 driving its activation.	Y240 and Y245	na	not tested	yes	yes	not tested	not tested	(Gao et al., 2020)
CYLD	positive	CYLD is a deubquinatase removing K48 linked polyubqutin chains from K150 on STING. Preventing proteosmal degradation of STING.	K150	K48 linked removed	ERGIC	not tested	yes	not tested	not tested	(Zhang et al., 2018)
EIF3S5	positive	EIF3S5 is recruited to STING by iRhom2 and contributes to STING's stability by removal of K48 linked ubquitin chains.	not tested	K48 linked removed	ER ERGIC	yes	yes	not tested	not tested	(Lou., 2016)
HER2 / AKT1	negative	HER2 assocaites with STING recruiting AKT1 to phosphorylate TBK1 at S510 which inhibits the TBK1 from interacting with STING.	na	na	ER ERGIC	yes	yes	(a.a. 679-1255)	(a.a. 139-379)	(Wu et al., 2019)
Hsp70	negative	STING contains a KEFRQ-like motif critical for chaperone mediated autophagy. Hsp70 is the chaperone that recognises this motif targeting STING for degradation.	na	na	not tested	yes	yes	(a.a. 326-330)	not tested	(Hu et al., 2016)
Hsp90β	positive	Heat shock protien 90 β (Hsp90β) increases the expression of STING at the protien level.	na	na	not tested	not tested	yes	not tested	(a.a. 173-240)	(Sato et al., 2020)
INSIG-1 and AMFR	positive	INSIG-1 recruit the E3 ubquint ligase AMFR to STING wich links K27 polyubquitin chain to STING at K137, K150, K224, K236. K27 linked chains recruit TBK1 to the STING complex.	K137, K150, K224, K236	K27 linked added	not tested	not tested	yes	(a.a. 1 – 259)	(a.a. 1 – 259)	(Wang et al., 2014)
IQGAP1	negative	IQGAP1 interacts with NLRC3 disrupting the NLRC3-STING interaction. Counterintuitively this attunates STINGs activation. As mechanistically it is unclear how blocking NLRC3 (a negative regulator) from binding STING prevents IFN induction.	na	na	ER	yes	no	no interaction known	no interaction known	(Tocker et al., 2017)
iRhom2	positive	iRhom2 binds to STING preventing its proteosomal turnover. iRhom2 also recruits EIF3S5 to STING promoting removal of K48-linked polyubquitin chains maintaining its stability. iRhom2 also recruits TRAPβ to STING.	na	na	ER ERGIC	yes	yes	(a.a. 410–430)	(a.a. 1–190)	(Luo et al., 2016)
lysyl-tRNA	negative	preventing cGAS recognition and producing diadenosine tetraphosphate (Ap4A) which competatively inhibits cGAMP binding to STING.	na	na	not tested	not tested	yes	na	na	Guerra et al., 2020
MUL-1	positive	MUL-1 is an E3 ubquitin ligase linking K63 polyubquitin chains to STING at K224. Aiding STING trafficking from the ER to ERGIC.	K224	K63 linked added	not tested	no	yes	(a.a. 1 – 259)	(a.a. 1- 195)	(Ni et al., 2017)

Supplementary Table 1 (Page 2 of 3) – List of STING accessory proteins.

STING accessory	positive or negative Regulator	Description	STING PMT site	type of ubquitination	cellular site of action	regulates NF-kB activity	regulates IRF3 activity	domain of STING accessory interacting with STING	domain of STING interacting with protein	reference
NLRC3	negative	NLRC3 is constitutively bound to STING. Abberant cytosolic DNA activates the ATPase domain of NLRC3 allowing dissociation from STING. Resulting in more efficient STING trafficking to ERGIC.	na	na	ER	yes	yes	NLRC3's NBD domain	(a.a. 139-344)	(Zhang et al., 2014) (Li et al., 2019)
NLRP3	neither	STING promotes NLRP3 inflammasome activation by directly binding NLRP3 at the ER. This facillitates removal of K-48 and K-63 polyubquitin chains locking NLRP3 into an inactive state. Interestingly the inflamasome complex like STING also asscociates with SCAP and translocates to the Golgi.	na	na	ER ERGIC	not tested	not tested	NACHT and LRR domains	(a.a. 151-160)	(Wang et al., 2020)
NLRX1	negative	NLRX1 associates with STING preventing recruitment of TBK1 and so proinflammatory cytokine production.	na	na	Mitochondrialy located	yes	yes	NBD domain	not tested	(Guo et al., 2016)
OTUD5	positive	Dubiquitinase removing K48 linked chains at K347 that target STING for proteosomal degradation.	K347	K48	not tested	not tested	yes	(a.a. 1–220)	(a.a. 153–339)	(Guo et al., 2021)
PPM1A	negative	Phosphotase that dephosphorillates both STING and TBK1.	not tested	na	not tested	not tested	yes	not tested	not tested	(Li et al., 2015)
PPP6C	negative	Dephophorolase that removes phosphates from STING reducing its activation.	not tested	na	not tested	no	yes	C terminus (a.a. not annotated)	(a.a. 181-379)	(Ni et al., 2020)
RAB2B-GARIL5	positive	The GTPase RAB2B and GARIL5 colocalise with STING at ERGIC specifically aiding phophorillation of IRF3.	na	na	ERGIC	not tested	yes	not tested	not tested	(Takahama et al., 2017)
RNF26	negative / positive	RNF26 is an E3 ubquitin ligase linking K11 polyubiquitin chains to STING at K150. This decreases STING activation early during infection but promotes STING signalling later during infection.	K150	K11 linked added	ER and minor fraction at mitochondria.	yes	yes	not tested	not tested	(Qin et al ., 2014)
RNF5	negative	RNF5 is an E3 ubquitin ligase which forms K48 linked polyubquitin chains at K150 on STING. K48 linked chains trigger proteosomal degradation of STING.	K150	K48 linked added	mitochondrialy located STING	yes	yes	(a.a. 168-180)	(aa. 111-150).	(Zhong et al., 2009)
SCAP	positive	SCAP binds STING and trafficks with STING to ERGIC. SCAP does not enhance trafficking but instead enhances recruitment of IRF3 to STING. Interestingly INSIG1 directly interacts with SCAP.	na	na	ER ERGIC	not tested	yes	(a.a. 1–735)	(a.a. 1–175)	(Chen et al., 2016)
SEC5	positive	Sec5 is a component of the exocyst 8 subunit complex that participates in the vesicular transport process.	na	na	ERGIC	yes	not tested	not tested	not tested	(Ishikawa et al., 2009)
Senp2	negative	Phosphorillation of STING at S365 during the late stages of infection triggers recruitment of Senp2. Senp2 desumoylates both STING and cGAS wich leads to subsequent proteosomal or autophagocytic degradation respectively.	na	na	not tested	yes	yes	not tested	not tested	(Hu et al., 2016)
SNX8 / VSP34		SNX8 recruits the class III phosphatylinositol 3-kinase VPS34 to STING which facillitating translocation to ERGIC.	na	na	ER ERGIC	yes	yes	(a.a. 1-180)	(a.a. 1-190)	(Wei et al., 2018)
SQSTM1	negative	Aids targeting of STING for authophagic degradation. KO results increased type I IFN production.	na	na	ERGIC	not tested	yes	not tested	not tested	(Prabakaran et al., 2018)
STIM1	negative	STIM1 binds to STING and retains it in an inactive state at the ER. This role is independent of STIM1's known role in store operated calcium release which is critical to effective adaptive immune responses.	na	na	ER	yes	yes	(two separate interactions a.a. 1-24	(a.a. 1-136)	(Srikanth et al., 2019)
TMED2	positive	TMED2 binds STING facillitating dimerisation and trafficking to ERGIC. Mechanistically TMED2 recruits STING into COPII complex (containing: Sar1B, Sec23B and Sec24C) which drives vesicle formation. TMED2 is also shown to interact with TRAPβ and iRhom2.	na	na	ER ERGIC	yes	yes	(a.a. 30-168)	(a.a. 1–81)	(Sun et al., 2018)

Supplementary Table 1 (Page 3 of 3) – List of STING accessory proteins.

STING accessory	positive or negative Regulator	Description	STING PMT site	type of ubquitination	cellular site of action	regulates NF-kB activity	regulates IRF3 activity	domain of STING accessory interacting with STING	domain of STING interacting with protein	reference
TMEM230	positive	TMEM203 binds STING and also STIM1 facillitating STING trafficking to ERGIC. STIM1 is a negative regulator of STING and may compete with TMEM203 to control STING trafficking.	na	na	ER ERGIC lysosomes	not tested	yes	(a.a. 1-51)	(a.a. 1-147)	(Deng et al., 2016)
TOLLIP / IRE1α	positive	lysomal degradation mediated by IRE1-α. TOLLIP co-immunoprecipitates with STING. Treatment of MEFs with cyclo hexamide shows that tollip reduces turn over of STING.	na	na	not tested	yes	yes	(a.a. 180 -229)	(a.a. 1-139)	(Pokatayev et al., 2020)
TRAPβ / SEC61β	positive	the ER translocon (comprisied of SEC61α, SEC61β and SEC61γ) resposible for import of cytolically translated proteins into the ER.	na	na	ER	yes	not tested	not tested	not tested	(Ishikawa et al., 2008)
TRIM29	negative	TRIM29 is an E3 ubquitin ligase linking K48 polyubquitin chains to STING at K370, K338 and K289. Targeting STING for proteosomal degradation.	K370, K338 and K289	K48 linked removed	ER and ERGIC	yes	yes	(a.a. 1 – 259)	(a.a. 1 – 259)	(Li et al., 2018)
TRIM30α	negative	polyubquitin chains to STING on K275. Targeting STING for proteosomal degradation.	K275	K48 linked added	ER and ERGIC	yes	yes	(a.a. 1 – 259)	(a.a. 136-338)	(Wang et al., 2015)
TRIM32	positive	TRIM32 is an E3 ubquitin ligase linking K63 polubquitin chains to STING at K20, K150, K224and K236. Enabling recruitment of TBK1 to STING.	K20, K150, K224, K236	K63 linked added	ER and mitochondrially located STING.	yes	yes	C terminal NHL domain	(a.a. 1-240).	(Zhang et al., 2012)
TRIM38	positive	TRIM38 is an E3 ubquitin ligase that targets cGAS for SUMOylation preventing its polyubquitination and degradation. Similalry TRIM38 sumoylates STING at K338 promoting both STING activation and protien stability. STING stability is increased as sumoylation masks the KEFRQ-like motif within STING preventing chaperone mediated autophagy by HSP70.	K338	na	not tested	yes	yes	not tested	not tested	(Hu et al., 2016)
UBXN38 and TRIM56	positive	UBXN38 facilitates an intereaction between the TRIM56 and STING. TRIM56 is an E3 ubquitin ligase catalysing K63 linked polyubquitination at K150 on STING. The K63 polyubquition aids STINGs dimerisation and TBK1 recruitment.	K150	K63 linked added	ER and ERGIC	yes	yes	TRIM56 (a.a. 1-208) UBXN38 (a.a. 122 – 275)	(aa. 174-379)	(Yang et al., 2018)
ULK1 (AKA ATG1)	negative	After trafficking of STING to ERGIC, ULK1 phosphorylates STING at S336, leading to STINGs degradation by an unknown mechanism. ULK1s activity is repressed by AMPKα a factor inactivated by cGAMP through an unknown mechanism. Providing a direct negative feedback loop upon cGAS activation.	S336	na	ERGIC	no	yes	not tested	not tested	(Konno., 2013)
USP13	negative	USP13 is a deubquitinase interacting with STING deconjugating K27 linked ubquitin chains. This prevents recruitment of TBK1.	not tested	K27 linked removed	not tested	yes	yes	(a.a. 1-624) and (a.a. 625-863)	transmembrane domain	(Sun et al., 2017)
USP18 and USP20	positive	USP18 recruits the deubquitinase USP20 to STING removing K48 linked ubquitin chains.	not tested	K48 linked removed	not tested	yes	yes	(a.a. 51- 150)	(a.a. 1_160)	(Zhang., 2016)
USP21	negative	Phophorylation of the deubquitinase USP21 at Ser538 by p38 triggers removal of K27 and K63 linked polyubquitin chains from STING. This prevents translocation from the ER to ERGIC.	not tested	K27 and K63 linked removed	ER	yes	yes	(a.a. 495-565)	(a.a. 221-341)	(Chen et al., 2017)
USP44	positive	USP44 is a deubqutinase removing K48 linked ubquitin chains from STING at K236. This prevents proetsomal degradation of STING.	K236 and posibly K150 and K224	K48 linked removed	not tested	yes	yes	not tested	not tested	(Zhang et al., 2020)
USP49	negative	UL49 deconjugates K63-linked ubquitin chains from STING. This inhibits STING aggregation at ERGIC.	not tested	K63	not tested	not tested	yes	not tested	not tested	(Ye et al., 2019)
YIPF5 and COPII complex	positive	Primarily YIPF5 interacts with both STING and components of COPII complex (contaning: SAR1, SEC13, SEC23, SEC31) facilitating vesicles trafficiking from the ER to ERGIC. YIPF5 is also thought important for STING mediated autophagy.	na	na	not tested	yes	yes	(a.a. 125-257)	(a.a. 111-379)	(Ran et al., 2019)
ZDHHC1	positive	ZDHHC1 is a member of the DHHC palmitoyl transferase family that facilitates the dimerisation and trafficking of STING to ERGIC. Interestingly the palmitoyl transferase activity of ZDHHC1 was not required for STING activation.	na	na	ER ERGIC	yes	yes	(a.a. 1-271)	(a.a. 1-190)	(Zhou et al., 2014)

Supplementary Table 2 (Page 1 of 4) – Table of siRNA sequences. Related to Chapter II, section II.2.16. Custom smart pool siRNA libraries were ordered from DharmaFECT.

Pool Catalog Number	Duplex Catalog Number	Gene Symbol	GENE ID	Gene Accession	GI Number	Sequence
D-001810-01	D-001810-01	ON-TARGETplus Non-targeting Control	0		0	UGGUUUACAUGUCGACUAA
D-001810-02	D-001810-02	ON-TARGETplus Non-targeting Control	0		0	UGGUUUACAUGUUGUGUGA
D-001810-03	D-001810-03	ON-TARGETplus Non-targeting Control	0		0	UGGUUUACAUGUUUUCUGA
D-001810-04	D-001810-04	ON-TARGETplus Non-targeting Control	0		0	UGGUUUACAUGUUUUCCUA
L-024333-00	J-024333-05	TMEM173	340061	NM_198282	38093658	GGUCAUAUUACAUCGGAUA
L-024333-00	J-024333-06	TMEM173	340061	NM_198282	38093658	AACAUUCGCUUCCUGGAUA
L-024333-00	J-024333-07	TMEM173	340061	NM_198282	38093658	GCAUCAAGGAUCGGGUUUA
L-024333-00	J-024333-08	TMEM173	340061	NM_198282	38093658	GCACCUGUGUCCUGGAGUA
L-024237-00	J-024237-05	MAVS	57506	NM_020746	83776597	AAGUAUAUCUGCCGCAAUU
L-024237-00	J-024237-06	MAVS	57506	NM_020746	83776597	CAUCCAAAGUGCCUACUAG
L-024237-00	J-024237-07	MAVS	57506	NM_020746	83776597	GCAAUGUGGAUGUUGUAGA
L-024237-00	J-024237-08	MAVS	57506	NM_020746	83776597	CAUCCAAAUUGCCCAUCAA
L-009566-01	J-009566-09	ACO2	50	NM_001098	46411160	CAGCCAGGAAAUUGAGCGA
L-009566-01	J-009566-10	ACO2	50	NM_001098	46411160	GAGACGAGAACUACGGCGA
L-009566-01	J-009566-11	ACO2	50	NM_001098	46411160	CGGAGAAGAUUGUGUAUGG
L-009566-01	J-009566-12	ACO2	50	NM_001098	46411160	GCUCAAGUUCCGUGGGCAC
L-180653-01	J-180653-13	AGAP5	729092	NM_001144000	221136913	ACACAAAGAGAUGCAGAUA
L-180653-01	J-180653-14	AGAP5	729092	NM_001144000	221136913	CGUUGAAGUUGGUGAGGAC
L-180653-01	J-180653-15	AGAP5	729092	NM_001144000	221136913	GCGUCAGCCUCGAGUUUGA
L-180653-01	J-180653-16	AGAP5	729092	NM_001144000	221136913	AGGAGAUGCCUGAAGCUUU
L-009276-01	J-009276-09	ALAS1	211	NM_199166	40316938	GACCACACCUAUCGAGUUU
L-009276-01	J-009276-10	ALAS1	211	NM_199166	40316938	AGAAGAGCUCCUACGGAUU
L-009276-01	J-009276-11	ALAS1	211	NM_199166	40316938	GCACCAGCGCAACGUCAAA
L-009276-01	J-009276-12	ALAS1	211	NM_199166	40316938	ACAUAACAUCUACGUGCAA
L-010376-00	J-010376-06	ALDOA	226	NM_184041	34577109	CCUAUUAAGCGGAGGUGUU
L-010376-00	J-010376-07	ALDOA	226	NM_184041	34577109	GGACAAAUGGCGAGACUAC
L-010376-00	J-010376-08	ALDOA	226	NM_184041	34577109	GGAGGAGUAUGUCAAGCGA
L-010376-00	J-010376-09	ALDOA	226	NM_184041	34577109	CAAGGAAAGUACACUCCGA
L-020426-00	J-020426-05	ATP13A1	57130	NM_020410	9966896	GAGAGUACGCCCAUUGUGA
L-020426-00	J-020426-06	ATP13A1	57130	NM_020410	9966896	GUGCUUGCCUCGUAUGAGA
L-020426-00	J-020426-07	ATP13A1	57130	NM_020410	9966896	GCGAGUGGCGCUCCAUUGA
L-020426-00	J-020426-08	ATP13A1	57130	NM_020410	9966896	GGACCGGAUUCAACACAUC
L-008131-01	J-008131-09	ATP13A3	79572	XM_931948	88967173	GGUCAUAAUUAUCGAGUCU
L-008131-01	J-008131-10	ATP13A3	79572	XM_931948	88967173	AGAAACACAUAAACGACAU
L-008131-01	J-008131-11	ATP13A3	79572	XM_931948	88967173	CAAUUGACCCAGAGGCUAU
L-008131-01	J-008131-12	ATP13A3	79572	XM_931948	88967173	AGUCUUCUCUCGUAGGUUA
L-004569-02	J-004569-17	ATP1B3	483	NM_001679	49574492	CAGUGACCGCAUUGGAAUA
L-004569-02	J-004569-18	ATP1B3	483	NM_001679	49574492	UCAUUCACGAUGUGGGUUA
L-004569-02	J-004569-19	ATP1B3	483	NM_001679	49574492	CCCUUGUAUUCUUGUGAAA
L-004569-02	J-004569-20	ATP1B3	483	NM_001679	49574492	CUGAAUUAGCCUCGAUCUU
L-013987-02	J-013987-17	C3orf17	25871	NM_001025073	75812963	GGGUCAUCGUAGUGAAUUA
L-013987-02	J-013987-18	C3orf17	25871	NM_001025073	75812963	GUGCAUAAGUCCCUAUUAA
L-013987-02	J-013987-19	C3orf17	25871	NM_001025073	75812963	CAGAGAAAGUUGCAGUCGA
L-013987-02	J-013987-20	C3orf17	25871	NM_001025073	75812963	GAGUUUAGAUGUUCGUUCA
L-010900-03	J-010900-18	C9orf114	51490	NM_016390	359718908	AGGCAGAGUGGGCGACAAU
L-010900-03	J-010900-19	C9orf114	51490	NM_016390	359718908	CAAAGGAUUGAGUGGCGAA
L-010900-03	J-010900-20	C9orf114	51490	NM_016390	359718908	GCACCUACUUGGCCGGUCA
L-010900-03	J-010900-21	C9orf114	51490	NM_016390	359718908	GCACUAACAACCUGAUCGU
L-011990-00	J-011990-05	CAPZB	832	NM_004930	4826658	GGAGUGAUCCUCAUAAAGA
L-011990-00	J-011990-06	CAPZB	832	NM_004930	4826658	GAAGUACGCUGAACGAGAU
L-011990-00	J-011990-07	CAPZB	832	NM_004930	4826658	CAAAGGAUAUCGUCAAUGG
L-011990-00	J-011990-08	CAPZB	832	NM_004930	4826658	CACCAUGGAGUAACAAGUA
L-029590-00	J-029590-05	CCNK	8812	NM_003858	38176157	UUUCAUCGCUUCUAUAUGU
L-029590-00	J-029590-06	CCNK	8812	NM_003858	38176157	GCGCUCGGUUCAUCUUUGA
L-029590-00	J-029590-07	CCNK	8812	NM_003858	38176157	CAAAGCAACUCAAAGGUGA
L-029590-00	J-029590-08	CCNK	8812	NM_003858	38176157	CAAGUUUGAUUUACAGGUA
L-003243-00	J-003243-09	CDK9	1025	NM_001261	17017983	GGCCAAACGUGGACAACUA
L-003243-00	J-003243-10	CDK9	1025	NM_001261	17017983	GUAUAUACCUGGUGUUCGA
L-003243-00	J-003243-11	CDK9	1025	NM_001261	17017983	GGACAUGAAGGCUGCUAAU
L-003243-00	J-003243-12	CDK9	1025	NM_001261	17017983	UAUAACCGCUGCAAGGGUA
L-011494-00	J-011494-05	COPS3	8533	NM_003653	23238221	GCACAAGUGUAUUCAACCA
L-011494-00	J-011494-06	COPS3	8533	NM_003653	23238221	CAAUGCAUACCACGAGUUA
L-011494-00	J-011494-07	COPS3	8533	NM_003653	23238221	CAAACCAGCUGACCUCAAU
L-011494-00	J-011494-08	COPS3	8533	NM_003653	23238221	GAAUUGGCAUCCUUAAGCA
L-021037-02	J-021037-17	COPS4	51138	NM_016129	38373689	CAAUAGUCCACGAAAGUGA
L-021037-02	J-021037-18	COPS4	51138	NM_016129	38373689	CAGUCCAGGCAGAGGCUUA
L-021037-02	J-021037-19	COPS4	51138	NM_016129	38373689	AAUGAUAACCGAAGGACGU
L-021037-02	J-021037-20	COPS4	51138	NM_016129	38373689	CAACGUGGGAUAAGCAGAU
L-015831-02	J-015831-18	COPS8	10920	NM_006710	40805828	GAAAUGAGUUGUAUGGUGA
L-015831-02	J-015831-19	COPS8	10920	NM_006710	40805828	GCAUAUUAGAACAAGGAUG
L-015831-02	J-015831-20	COPS8	10920	NM_006710	40805828	GAGACGGUCCAGCCAAUUA
L-015831-02	J-015831-21	COPS8	10920	NM_006710	40805828	CAAGCUGAUUCCACCACAA
L-031994-01	J-031994-09	CRCP	27297	NM_014478	27552758	UCUCAGUAACUACGAGGUA
L-031994-01	J-031994-10	CRCP	27297	NM_014478	27552758	GCAAUGUGGCAAUGGACGA
L-031994-01	J-031994-11	CRCP	27297	NM_014478	27552758	AUCUGAAAGAGCAGCGUAA
L-031994-01	J-031994-12	CRCP	27297	NM_014478	27552758	UCACCUAUGAAACGUUAAA
L-008290-00	J-008290-06	DBR1	51163	NM_016216	56549112	GACAAAUGCUUACCACAUA
L-008290-00	J-008290-07	DBR1	51163	NM_016216	56549112	CCAUGUAACUUUAGUGUAA
L-008290-00	J-008290-08	DBR1	51163	NM_016216	56549112	GGAGGAAUCAAGCCAUUUA
L-008290-00	J-008290-09	DBR1	51163	NM_016216	56549112	CAAAUGCAGCUGAUUCAUA
L-013167-01	J-013167-09	DHX36	170506	NM_020865	18497285	CGGCAUGUGGUACGCGAAA
L-013167-01	J-013167-10	DHX36	170506	NM_020865	18497285	GAUCAUAUAUUGACCGAGA
L-013167-01	J-013167-11	DHX36	170506	NM_020865	18497285	GUAAGGGAACUGCGAAGAA

Supplementary Table 2 (Page 2 of 4) – Table of siRNA sequences.

Pool Catalog Number	Duplex Catalog Number	Gene Symbol	GENE ID	Gene Accession	GI Number	Sequence
L-013167-01	J-013167-12	DHX36	170506	NM_020865	18497285	AGAAGAGGAUGGUGCGAUA
L-016975-01	J-016975-09	EXOSC2	23404	NM_014285	39725699	GCACAGUGUUACAGUCGAA
L-016975-01	J-016975-10	EXOSC2	23404	NM_014285	39725699	CGCCAGAGUUCUCGCUGAA
L-016975-01	J-016975-11	EXOSC2	23404	NM_014285	39725699	CCUCAGUGAUUCUCGGUAA
L-016975-01	J-016975-12	EXOSC2	23404	NM_014285	39725699	GAUACAAUCACUACGGACA
L-013004-01	J-013004-09	EXOSC6	118460	NM_058219	32484988	GGACUUAAGGACAUCGAAU
L-013004-01	J-013004-10	EXOSC6	118460	NM_058219	32484988	GCGUGGAGAUGUACGACCU
L-013004-01	J-013004-11	EXOSC6	118460	NM_058219	32484988	CGCUCAUGCCUGUGCUGAA
L-013004-01	J-013004-12	EXOSC6	118460	NM_058219	32484988	CAGUUUGCGUCGAGAAUUC
L-014160-01	J-014160-09	EXOSC7	23016	NM_015004	39725632	AUACCAAGGGUUCGAGUUU
L-014160-01	J-014160-10	EXOSC7	23016	NM_015004	39725632	UAAAAGCAGUGUCGACUUA
L-014160-01	J-014160-11	EXOSC7	23016	NM_015004	39725632	GCAAGGGAGUUGUGACGUG
L-014160-01	J-014160-12	EXOSC7	23016	NM_015004	39725632	CGGAGAAGGUGUACAUCGU
L-012782-02	J-012782-09	EXOSC8	11340	NM_181503	224465145	ACACUGUGCACAAACGUUU
L-012782-02	J-012782-10	EXOSC8	11340	NM_181503	224465145	UGAUAAAGGAUACGUUGUU
L-012782-02	J-012782-11	EXOSC8	11340	NM_181503	224465145	UUGCUUUGCUAGCGGCUUU
L-012782-02	J-012782-17	EXOSC8	11340	NM_181503	224465145	CCUUAACAAUAGUAAUGGA
L-008181-02	J-008181-18	G6PD	2539	NM_001042351	108773792	ACAGAUACAAGAACGUGAA
L-008181-02	J-008181-19	G6PD	2539	NM_001042351	108773792	CCGUGUACACCAAGAUGAU
L-008181-02	J-008181-20	G6PD	2539	NM_001042351	108773792	CAGAUAGGCUGGAACCGCA
L-008181-02	J-008181-21	G6PD	2539	NM_001042351	108773792	AUUCACGAGUCCUGCAUGA
L-004253-00	J-004253-06	GAPDH	2597	NM_002046	83641890	CAACGGAUUUGGUCGUAUU
L-004253-00	J-004253-07	GAPDH	2597	NM_002046	83641890	GACCUGACCUGCCGUCUAG
L-004253-00	J-004253-08	GAPDH	2597	NM_002046	83641890	CAAUAUGAUUCCACCCAUG
L-004253-00	J-004253-09	GAPDH	2597	NM_002046	83641890	GCGAUGCUGGGCGUGAGUA
L-004329-00	J-004329-06	GPS2	2874	NM_004489	53832030	CAAGUGACCAUCAGAUUAU
L-004329-00	J-004329-07	GPS2	2874	NM_004489	53832030	AUAAGAUGAUGGAACAGAA
L-004329-00	J-004329-08	GPS2	2874	NM_004489	53832030	GAACUCAUCUCCUCAGCAU
L-004329-00	J-004329-09	GPS2	2874	NM_004489	53832030	GAUGGAACAUGCUAACCAG
L-006731-00	J-006731-05	GUCY1A3	2982	NM_000856	67763815	CCACAUCGCUAUUCUGCAA
L-006731-00	J-006731-06	GUCY1A3	2982	NM_000856	67763815	GGAAUAGAUUAGCAACCUA
L-006731-00	J-006731-07	GUCY1A3	2982	NM_000856	67763815	GAAGUGGAAGUGUCGUUAA
L-006731-00	J-006731-08	GUCY1A3	2982	NM_000856	67763815	CAAAGACUGUCCUGGUUUC
L-017609-00	J-017609-06	HSPA8	3312	NM_153201	24234685	CGUAAUACCACCAUUCCUA
L-017609-00	J-017609-07	HSPA8	3312	NM_153201	24234685	GAUAACAACCUGCUUGGCA
L-017609-00	J-017609-08	HSPA8	3312	NM_153201	24234685	GACCUUCACUACCUAUUCU
L-017609-00	J-017609-09	HSPA8	3312	NM_153201	24234685	UGAAACUGCUGGUGGAGUC
L-011810-00	J-011810-07	IRF7	3665	NM_004030	4809285	GCACAAGGUGUACGCGCUC
L-011810-00	J-011810-08	IRF7	3665	NM_004030	4809285	CAACUUCCGCUGCGCACUG
L-011810-00	J-011810-09	IRF7	3665	NM_004030	4809285	GCGCGCAUCUUCAAGGCCU
L-011810-00	J-011810-10	IRF7	3665	NM_004030	4809285	CAGGCACGGACCAGACUGA
L-006214-00	J-006214-06	KCNA4	3739	NM_002233	25952084	GCGGGUGUCUUAACCAUUG
L-006214-00	J-006214-07	KCNA4	3739	NM_002233	25952084	GUGGUUCGCUGCUUUGCUU
L-006214-00	J-006214-08	KCNA4	3739	NM_002233	25952084	GCAGAAUGCAGUCAGUUGU
L-006214-00	J-006214-09	KCNA4	3739	NM_002233	25952084	GGUGAUGAGUGUUCCUACA
L-012453-00	J-012453-05	KEAP1	9817	NM_012289	45269143	GGACAAACCGCCUUAAUUC
L-012453-00	J-012453-06	KEAP1	9817	NM_012289	45269143	CAGCAGAACUGUACCUGUU
L-012453-00	J-012453-07	KEAP1	9817	NM_012289	45269143	GGGAGUACAUCUACAUGCA
L-012453-00	J-012453-08	KEAP1	9817	NM_012289	45269143	CGAAUGAUCACAGCAAUGA
L-022984-01	J-022984-09	KIDINS220	57498	NM_020738	55741640	GUGAGUAGUUGCCGCGUAA
L-022984-01	J-022984-10	KIDINS220	57498	NM_020738	55741640	CAACAAAGCAGGCGAGACU
L-022984-01	J-022984-11	KIDINS220	57498	NM_020738	55741640	GAUGAUAGCUGCCGAACAA
L-022984-01	J-022984-12	KIDINS220	57498	NM_020738	55741640	UGAAAUUGUUCGAGCGCUU
L-008818-00	J-008818-05	MAT2A	4144	NM_005911	46852159	GAAAGUGGUUCGUGAAGCU
L-008818-00	J-008818-06	MAT2A	4144	NM_005911	46852159	GUGUUCAUCUUGACAGAAA
L-008818-00	J-008818-07	MAT2A	4144	NM_005911	46852159	GACCAGGGCUUAAUGUUUG
L-008818-00	J-008818-08	MAT2A	4144	NM_005911	46852159	GAAAGGAUUAUACCAAGGU
L-015607-02	J-015607-17	MB21D1	115004	NM_138441	115511029	GAAGAAACAUGGCGGCUAU
L-015607-02	J-015607-18	MB21D1	115004	NM_138441	115511029	AGGAAGCAACUACGACUAA
L-015607-02	J-015607-19	MB21D1	115004	NM_138441	115511029	AGAACUAGAGUCACCCUAA
L-015607-02	J-015607-20	MB21D1	115004	NM_138441	115511029	CCAAGAAGGCCUGCGCAUU
L-005939-00	J-005939-07	MBTPS1	8720	NM_201268	41350326	AGAAUUAUACCUCGAAACA
L-005939-00	J-005939-08	MBTPS1	8720	NM_201268	41350326	GGAAUUAACAGCUAACAAU
L-005939-00	J-005939-09	MBTPS1	8720	NM_201268	41350326	AAAGAAGAUCGACGUGUUA
L-005939-00	J-005939-10	MBTPS1	8720	NM_201268	41350326	GCUAAAAGACGCUUGUUAA
L-005940-00	J-005940-07	MBTPS2	51360	NM_015884	7706692	GGAAUGGUGUUUGGCGUAA
L-005940-00	J-005940-08	MBTPS2	51360	NM_015884	7706692	GUGCAGGUAUCUGGCAUAA
L-005940-00	J-005940-09	MBTPS2	51360	NM_015884	7706692	GAAACUCACACUCGCUUAA
L-005940-00	J-005940-10	MBTPS2	51360	NM_015884	7706692	GAUCUGUUCACCACUCAUU
L-012976-01	J-012976-09	MORC3	23515	NM_015358	28872811	GGAUCAGACAACCGGAAAU
L-012976-01	J-012976-10	MORC3	23515	NM_015358	28872811	CUUAAUACGUGUCGGUCAU
L-012976-01	J-012976-11	MORC3	23515	NM_015358	28872811	CCAGGAAACCACCGAUAAA
L-012976-01	J-012976-12	MORC3	23515	NM_015358	28872811	GGAACAAAUUCUUAUGCGA
L-009606-00	J-009606-05	NAA10	8260	NM_003491	34222259	GUGAAGUGGAGCCCAAAUA
L-009606-00	J-009606-06	NAA10	8260	NM_003491	34222259	CCAGAGGACCUAAUGAACA
L-009606-00	J-009606-07	NAA10	8260	NM_003491	34222259	UCACUCAGAUGGCCGACGA
L-009606-00	J-009606-08	NAA10	8260	NM_003491	34222259	GAACUUCAAUGCCAAAUAU
L-004581-00	J-004581-05	NAMPT	10135	NM_182790	33386694	GGUAAGAAGUUUCCUGUUA
L-004581-00	J-004581-06	NAMPT	10135	NM_182790	33386694	CAAAUUGGAUUGAGACUAU
L-004581-00	J-004581-07	NAMPT	10135	NM_182790	33386694	UAACUUAGAUGGUCUGGAA
L-004581-00	J-004581-08	NAMPT	10135	NM_182790	33386694	CAAGCAAAGUUUAUUCCUA
L-008951-00	J-008951-05	NMNAT1	64802	NM_022787	20070320	AUGAAUGGAUCGCUAAUGA
L-008951-00	J-008951-06	NMNAT1	64802	NM_022787	20070320	GGGUGGAAGUUGAUACAUG
L-008951-00	J-008951-07	NMNAT1	64802	NM_022787	20070320	AAUCGGAUGUGCUGUGGAA

Supplementary Table 2 (Page 3 of 4) – Table of siRNA sequences.

Pool Catalog Number	Duplex Catalog Number	Gene Symbol	GENE ID	Gene Accession	GI Number	Sequence
L-008951-00	J-008951-08	NMNAT1	64802	NM_022787	20070320	ACAGGAAGGUACACAGUUG
L-019111-00	J-019111-05	OGT	8473	NM_181673	32307149	GGCAGAAGCUUAUUCGAAU
L-019111-00	J-019111-06	OGT	8473	NM_181673	32307149	GCACAAUCCUGAUAAAUUU
L-019111-00	J-019111-07	OGT	8473	NM_181673	32307149	GGCACAAACUUCCGAGUGA
L-019111-00	J-019111-08	OGT	8473	NM_181673	32307149	GUCUUGAGCUUAUUGCUAA
L-012243-01	J-012243-10	PCBP1	5093	NM_006196	14141164	UCGCUAUGAUCAUCGACAA
L-012243-01	J-012243-11	PCBP1	5093	NM_006196	14141164	CAACUUUAUCAUCCGCUAA
L-012243-01	J-012243-12	PCBP1	5093	NM_006196	14141164	CAAAGAGAUCCGCGAGAGU
L-012243-01	J-012243-13	PCBP1	5093	NM_006196	14141164	CUACUCGAUUCAAGGACAA
L-010530-00	J-010530-05	PHB	5245	NM_002634	6031190	GCGACGACCUUACAGAGCG
L-010530-00	J-010530-06	PHB	5245	NM_002634	6031190	AAACUUGGAUGGACUUGUA
L-010530-00	J-010530-07	PHB	5245	NM_002634	6031190	GAACUGGGCACAGAUUGAA
L-010530-00	J-010530-08	PHB	5245	NM_002634	6031190	CUUCAGAUCUCUAAUUAGU
L-018703-00	J-018703-05	PHB2	11331	NM_007273	31543548	GUGAAUAUCUCCCUGCGAG
L-018703-00	J-018703-06	PHB2	11331	NM_007273	31543548	CCACAUCACAGAAUCGUAU
L-018703-00	J-018703-07	PHB2	11331	NM_007273	31543548	CAUCAAACUUCGCAAGAUU
L-018703-00	J-018703-08	PHB2	11331	NM_007273	31543548	CAGAAUAUCUCCAAGACGA
L-011358-00	J-011358-05	PPP1R10	5514	NM_002714	25777670	ACAAUUGGCUGACGUAUUC
L-011358-00	J-011358-06	PPP1R10	5514	NM_002714	25777670	GCAGACCCGUUCACCAGAA
L-011358-00	J-011358-07	PPP1R10	5514	NM_002714	25777670	GAACGAGUAAAUGUGAAUA
L-011358-00	J-011358-08	PPP1R10	5514	NM_002714	25777670	GAAACAACCAGACUAUUCG
L-015361-00	J-015361-05	PPP1R2	5504	NM_006241	34147499	GCCUGGACAUUGUUAAAUA
L-015361-00	J-015361-06	PPP1R2	5504	NM_006241	34147499	GGUAAUUGAUAGGGUAUGA
L-015361-00	J-015361-07	PPP1R2	5504	NM_006241	34147499	GGAAUACCACUGAUUUAGA
L-015361-00	J-015361-08	PPP1R2	5504	NM_006241	34147499	GAAAAGGUAUGUUCAAGUC
L-006979-02	J-006979-09	PRICKLE4	29964	NM_013397	197333762	GGGACCAAACCUCGGUGAA
L-006979-02	J-006979-12	PRICKLE4	29964	NM_013397	197333762	AGACUGGACUCGACCGAAC
L-006979-02	J-006979-17	PRICKLE4	29964	NM_013397	197333762	AGGACAUUGAUGAGCGCUA
L-006979-02	J-006979-18	PRICKLE4	29964	NM_013397	197333762	CCGGAAGCCUCCAAGCAGA
L-006551-00	J-006551-05	RBBP6	5930	NM_032626	38683864	UAUUGGAGGUGUUAAAUCU
L-006551-00	J-006551-06	RBBP6	5930	NM_032626	38683864	AGACAUAUGUUAUAAGUCG
L-006551-00	J-006551-07	RBBP6	5930	NM_032626	38683864	CCUCUAAACUCAACUAUGA
L-006551-00	J-006551-08	RBBP6	5930	NM_032626	38683864	CGAAAGAAGAAUAUACUGA
L-006590-00	J-006590-05	RNF113A	7737	NM_006978	5902157	UUACUUAGGUUUCCCAUAA
L-006590-00	J-006590-06	RNF113A	7737	NM_006978	5902157	GCGAAAGAAUUGAUUGCUA
L-006590-00	J-006590-07	RNF113A	7737	NM_006978	5902157	GGGUGGUGCUUCCGACUUG
L-006590-00	J-006590-08	RNF113A	7737	NM_006978	5902157	GACAAGAUCUAUCGGGGAA
L-012808-00	J-012808-05	SCAP	22937	NM_012235	66932901	GACCUCACCUGCUUAAUUG
L-012808-00	J-012808-06	SCAP	22937	NM_012235	66932901	CGACGCUCUUCAGCUAUUA
L-012808-00	J-012808-07	SCAP	22937	NM_012235	66932901	UGUGGUGGUUAUUGGGUUA
L-012808-00	J-012808-08	SCAP	22937	NM_012235	66932901	UCACACUGGCCAAGAGGUA
L-021503-01	J-021503-09	SEC61A1	29927	NM_013336	60218911	CGGCCAGUCUAUCGUGUAU
L-021503-01	J-021503-10	SEC61A1	29927	NM_013336	60218911	ACUUUGAGAUCUUCGUUAA
L-021503-01	J-021503-11	SEC61A1	29927	NM_013336	60218911	GUGUCAUCCUGCCGGAAAU
L-021503-01	J-021503-12	SEC61A1	29927	NM_013336	60218911	CCAUGCAGUUGUAUACAUA
L-004886-01	J-004886-09	SEC63	11231	NM_007214	47458818	AACAAAGCAUACAGCGAAA
L-004886-01	J-004886-10	SEC63	11231	NM_007214	47458818	CAAGCAGACCAACGGAUAA
L-004886-01	J-004886-11	SEC63	11231	NM_007214	47458818	AGAUCAGAAUGCCGAGCAA
L-004886-01	J-004886-12	SEC63	11231	NM_007214	47458818	GAUGAAGAGUCCCGGAAAA
L-013475-01	J-013475-09	SEH1L	81929	NM_001013437	61743970	UCUCAGGUCUGGCGAGUGA
L-013475-01	J-013475-10	SEH1L	81929	NM_001013437	61743970	GAAUAUAACAGGAACGGUG
L-013475-01	J-013475-11	SEH1L	81929	NM_001013437	61743970	GCGUUAAGGUCUGGGAUAA
L-013475-01	J-013475-12	SEH1L	81929	NM_001013437	61743970	GAGAUCUCAUGUAAGCUAA
L-031902-02	J-031902-09	SKIV2L2	23517	NM_015360	193211479	GCACAUACCUCAGCGGGAA
L-031902-02	J-031902-10	SKIV2L2	23517	NM_015360	193211479	AGGGAAAAGCAGCGUGUAA
L-031902-02	J-031902-12	SKIV2L2	23517	NM_015360	193211479	UUACAGAGGUUCCGAAGUU
L-031902-02	J-031902-17	SKIV2L2	23517	NM_015360	193211479	GAAACUGUGUAUACGCUUU
L-014798-02	J-014798-17	SLC7A6OS	84138	NM_032178	14149860	GAGAAUAACUGGCGCAAUG
L-014798-02	J-014798-18	SLC7A6OS	84138	NM_032178	14149860	GGACAUUUACGACGAUGAA
L-014798-02	J-014798-19	SLC7A6OS	84138	NM_032178	14149860	GCAGAAGGAGUUCGGCUAU
L-014798-02	J-014798-20	SLC7A6OS	84138	NM_032178	14149860	GCACAGAAGACGUCGGAGG
L-019716-00	J-019716-05	SRP72	6731	NM_006947	40789255	CAAAAUAUCUGCCAGUUUA
L-019716-00	J-019716-06	SRP72	6731	NM_006947	40789255	GAGAAUGCCUUGAAGACAA
L-019716-00	J-019716-07	SRP72	6731	NM_006947	40789255	CUACAUACAUUCGGAAGAA
L-019716-00	J-019716-08	SRP72	6731	NM_006947	40789255	GAUCAACAAAGAUGACGUA
L-020389-01	J-020389-09	STRN4	29888	NM_013403	89886476	CUGUAUAAAUAACGGGAUU
L-020389-01	J-020389-10	STRN4	29888	NM_013403	89886476	GGCCAAGGUCUUCGUAUGA
L-020389-01	J-020389-11	STRN4	29888	NM_013403	89886476	AGAAGGCGGUCACGGCCAA
L-020389-01	J-020389-12	STRN4	29888	NM_013403	89886476	CUGGAAAGCCGUCGGGUCA
L-008088-01	J-008088-09	TLR4	7099	NM_138554	88758616	UGGUGGAAGUUGAACGAAU
L-008088-01	J-008088-10	TLR4	7099	NM_138554	88758616	GUUUAGAAGUCCAUCGUUU
L-008088-01	J-008088-11	TLR4	7099	NM_138554	88758616	CAUUGAAGAAUUCCGAUUA
L-008088-01	J-008088-12	TLR4	7099	NM_138554	88758616	GGAAAAUGGUGUAGCCGUU
L-020272-01	J-020272-09	TMEM30A	55754	NM_018247	52694667	GCGAUGAACUAUAACGCGA
L-020272-01	J-020272-10	TMEM30A	55754	NM_018247	52694667	CCAUCGUCGUUACGUGAAA
L-020272-01	J-020272-11	TMEM30A	55754	NM_018247	52694667	GCACAGAGGAUGUCGCUAA
L-020272-01	J-020272-12	TMEM30A	55754	NM_018247	52694667	GCGAGAUCGAGAUUGAUUA
L-014320-00	J-014320-05	UBL5	59286	NM_024292	42476283	GGGAAGAAGGUCCGCGUUA
L-014320-00	J-014320-06	UBL5	59286	NM_024292	42476283	GGGAUGAACCUGGAGCUUU
L-014320-00	J-014320-07	UBL5	59286	NM_024292	42476283	AAGAAGUGGUACACGAUUU
L-014320-00	J-014320-08	UBL5	59286	NM_024292	42476283	GACCUUAAGAAGCUGAUUG
L-014822-00	J-014822-05	WDR24	84219	NM_032259	14149986	GAACACAAGCGCACGGUAA
L-014822-00	J-014822-06	WDR24	84219	NM_032259	14149986	CGACGUACCUGCCGACUAC
L-014822-00	J-014822-07	WDR24	84219	NM_032259	14149986	GGGACGUGCAGUUCAGUAU

Supplementary Table 2 (Page 4 of 4) – Table of siRNA sequences.

Pool Catalog Number	Duplex Catalog Number	Gene Symbol	GENE ID	Gene Accession	GI Number	Sequence
L-014822-00	J-014822-08	WDR24	84219	NM_032259	14149986	GUUCACAGCCCACAACGGA
L-022683-00	J-022683-05	WDR59	79726	NM_030581	58331265	GAGCUGAAGUGUUGAAGUU
L-022683-00	J-022683-06	WDR59	79726	NM_030581	58331265	CAUAUUAGAUGGUGUUGAU
L-022683-00	J-022683-07	WDR59	79726	NM_030581	58331265	GAGCGGAAAUCAAGACGAU
L-022683-00	J-022683-08	WDR59	79726	NM_030581	58331265	AAACGUGGUUGUAGAGUUC
L-005752-00	J-005752-05	XPR1	9213	NM_004736	19923271	ACACUAAGGUAUUGAUAGA
L-005752-00	J-005752-06	XPR1	9213	NM_004736	19923271	UCGAUUACCUCUACAACUU
L-005752-00	J-005752-07	XPR1	9213	NM_004736	19923271	GCUUGCCGCUGUAUUUAAA
L-005752-00	J-005752-08	XPR1	9213	NM_004736	19923271	GGCCUUUCCUCAUUUAGUU
L-010491-00	J-010491-05	XRCC5	7520	NM_021141	12408650	GCAUGGAUGUGAUUCAACA
L-010491-00	J-010491-06	XRCC5	7520	NM_021141	12408650	CGAGUAACCAGCUCAUAAA
L-010491-00	J-010491-07	XRCC5	7520	NM_021141	12408650	GAGCAGCGCUUUAACAACU
L-010491-00	J-010491-08	XRCC5	7520	NM_021141	12408650	AAACUUCCGUGUUCUAGUG
L-013754-01	J-013754-09	XRN1	54464	NM_019001	40254886	CUUCAUAGUUGGUCGGUAU
L-013754-01	J-013754-10	XRN1	54464	NM_019001	40254886	GAACAUAUUACAUGACGAA
L-013754-01	J-013754-11	XRN1	54464	NM_019001	40254886	AAUAAGAAGGUGCGAGUAA
L-013754-01	J-013754-12	XRN1	54464	NM_019001	40254886	AAUAAUUACCUCAGCGUUA

Evidence	HSV-2 degrades LRRC8A (Figure 44B).	VZV does not degade LRRC8A (Figure 44C).	LRRC8A:C is degraded late during viral infection (Figure 43).	Gene detectable in LRRC8C IP from HSV-1 infected cells (Figure 45).	Gene detectable at a high abundance within LRRC8C IP from HSV-1 infected cells (Figure 45).
Exclusion critieria	HSV-1 genes with no homolog in HSV-2	HSV-1 genes with a homolog in VZV	Genes in immediate early (α) or early (β) kinetic class	Not detected in LRRC8C IP	Detected in LRRC8C IP at low abundance
HSV-1 Gene Name and Aliases	**HSV-2 Gene Name and Aliases**	**VZV Gene Name and Aliases**	**Kinetic Class**	**Detected in LRRC8C IP**	Detected in LRRC8C IP > Abundance Limit
UL56	UL56	No homolog	Leaky late γ1 - (Ushijima et al., 2008 & Koshhizuka et al., 2002)	yes	yes
US6, gD	US6, gD	No homolog	Leaky late γ1 - (Garvey et al., 2014 & Fox et al., 2017)	yes	yes
US11	US11	No homolog	True late γ2 - (Liu et al., 2019)	yes	yes
UL45, EV45	UL45	No homolog	True late γ2 - (Visalli & Brandt 2008)	yes	
US2	US2	No homolog	True late γ2 - (Fox et al., 2017)	yes	
γ134.5	γ134.5	No homolog	Leaky late γ1 - (Chou & Roizman 1986)		
UL9.5	Unclear if homolog exists	Unclear if homolog exists	True late γ2 - (Baradaran et al., 1994)		
UL27.5	UL27.5	No homolog	True late γ2 - (Chang et al., 1998)		
UL43.5	UL43.5	No homolog	Late γ - (Ward et al., 1996)		
US4, gG	US4, gG	No homolog	Leaky late γ1 - (Garvey et al., 2014)		
US5, gJ	US5, gJ	No homolog	Leaky late γ1 - (Aubert et al., 2008)		
US8.5	US8.5	No homolog	Leaky late γ1 - (Georgopoulou et al., 1995)		
UL12.5	UL12.5	No homolog	Early β - (Reuven et al., 2004 & Draper et al., 1986)		
US12, α47, ICP47	US12, α47, ICP47	No homolog	Immediate early α - (Chen et al., 2020)		
α0, ICP0 RL2	α0, ICP0	α0, ICP0 RL2			
α4, ICP4	α4, ICP4	α4, ICP4		yes	
US3	US3	US3		yes	yes
US1, α 22, ICP22	US1, α 22, ICP22	US1, α 22, ICP22		yes	
US1.5	US1.5	US1.5			
US7, gI	US7, gI	US7, gI		yes	yes
US8, gE	US8, gE	US8, gE		yes	
US9	US9	US9			
US10	US10	US10		yes	
UL1, gL	UL1, gL	UL1, gL		yes	
UL2	UL2	UL2			
UL3, NP03	UL3	UL3		yes	
UL4	UL4	UL4			
UL5	UL5	UL5			
UL6	UL6	UL6		yes	yes
UL7	UL7	UL7			
UL8	UL8	UL8			
UL8.5	UL8.5	UL8.5			
UL9, OBP	UL9	UL9		yes	
UL10	UL10	UL10			
UL11	UL11	UL11			
UL12, AN	UL12	UL12		yes	
UL13	UL13	UL13		yes	
UL14	UL14	UL14			
UL15	UL15	UL15			
UL15.5	UL15.5	UL15.5			
UL16	UL16	UL16			
UL17	UL17	UL17			
UL18, TRX2	UL18	UL18		yes	
UL19, MCP, VP5	UL19	UL19		yes	
UL20	UL20	UL20			
UL21	UL21	UL21			
UL22, gH	UL22	UL22		yes	yes
UL23, KITH, TK	UL23	UL23		yes	
UL24	UL24	UL24		yes	
UL25, CVC2	UL25	UL25		yes	
UL26, SCAF	UL26	UL26		yes	
UL26.5	UL26.5	UL26.5			
UL27 gB	UL27	UL27		yes	
UL28	UL28	UL28			
UL29	UL29	UL29			
UL30, DPOL	UL30	UL30		yes	
UL31 NEC1	UL31	UL31		yes	yes
UL32	UL32	UL32			
UL33	UL33	UL33			
UL34, NEC2	UL34	UL34		yes	
UL35	UL35	UL35			
UL36	UL36	UL36			
UL37	UL37	UL37		yes	
UL38	UL38	UL38		yes	
UL39, RIR1	UL39	UL39		yes	
UL40, RIR2	UL40	UL40		yes	
UL41 vhs, SHUT	UL41	UL41		yes	yes
UL42	UL42	UL42		yes	
UL43	UL43	UL43			
UL44, gC	UL44	UL44		yes	
UL46, TEG1	UL46	UL46		yes	yes
UL47 TEG5	UL47	UL47		yes	yes
UL48 vp16	UL48	UL48		yes	yes
UL49 vp22	UL49	UL49		yes	yes
UL49.5	UL49.5	UL49.5			
UL50, DUT	UL50	UL50		yes	yes
UL51	UL51	UL51			
UL52	UL52	UL52			
UL53	UL53	UL53			
UL54, α27	UL54, α27	UL54, α27		yes	yes
UL55, TEG6	UL55	UL55		yes	
ORF-O	No homolog	No homolog			
ORF-P	No homolog	No homolog			
UL20.5	No homolog	No homolog			

Supplementary Table 3 - Showing the 84 known HSV-1 genes and their homologs in HSV-2 and VZV.
Related to Chapter V, section V.3, Figure 46. Genes were excluded (highlighted grey) as the gene causing LRRC8A:C depletion based on the experimental evidence outlined in the top two rows. Genes kinetic class and whether they are detectable above the abundance limit (displayed in Figure 45) are also shown.

Supplementary Table 4 (Page 1 of 9) – List of detected proteins immunoprecipitated from HSV-1 infected cells. Related to Chapter V, section V.2, Figure 45.

Gene	Accession	Species	Confidence score	Mass	Unique Peptides	Peptide Count	Control Raw Protien Abundance	HSV-1 Raw Protien Abundance	Control Normalised Protien Abundance	HSV-1 Normalised Protien Abundance
AN	P04294	HHV11	351.58	67508.32	6	6	105	52442	105	45345
CVC2	P10209	HHV11	540.93	62670.08	11	11	111	97816	111	84580
DPOL	P04293	HHV11	496.04	136420.88	11	11	472	49705	472	42979
DUT	P10234	HHV11	444.6	39127.918	8	8	24449	100397	24449	86811
EV45	P10229	HHV11	80.16	18179.979	1	1	2666	139033	2666	120219
GB	P10211	HHV11	2745.83	100292.445	47	49	408	6441895	408	5570156
GC	P10228	HHV11	376.25	54998.246	4	5	2059	97158	2059	84011
GD	Q69091	HHV11	180.11	43346.9	3	3	11449	143053	11449	123695
GE	P04488	HHV11	320.4	59093.67	5	5	255	336468	255	290936
GH	P06477	HHV11	633.11	90366.164	11	11	5494	395016	5494	341561
GI	P06487	HHV11	112.15	41369.543	3	3	1287	203129	1287	175641
GL	P10185	HHV11	474.41	24933.533	9	9	70512	887587	70512	767476
ICP0	P08393	HHV11	1118.27	78456.516	19	20	1958	522447	1958	451748
ICP22	P04485	HHV11	354.57	46524.812	7	7	87	318917	87	275760
ICP27	P10238	HHV11	1378.41	55253.145	21	21	3893	3083214	3893	2665983
ICP4	P08392	HHV11	1261.51	132843.86	15	23	31	176477	31	152596
ICP4	P90493	HHV2H	427.67	135103.27	1	9	2079	15267	2079	13201
ITP	P10221	HHV11	156.77	120556.06	4	4	497	25406	497	21968
KITH	P03176	HHV11	165.66	40971.996	3	3	474	177356	474	153356
MCP	P06491	HHV11	1380.21	149083.39	24	24	927	212317	927	183586
NEC1	P10215	HHV11	472.07	33953.11	9	9	3188	673819	3188	582635
NEC2	P10218	HHV11	434.23	29790.305	7	7	1780	1059961	1780	916523
NP03	P10187	HHV11	37.75	25609.037	1	1	0	10176	0	8799
OBP	P10193	HHV11	82.03	94261.67	2	2	489	25347	489	21917
PAP	P10226	HHV11	276.69	51159.25	6	6	1239	77960	1239	67410
PORTL	P10190	HHV11	1017.66	74091.58	18	18	5009	263406	5009	227761
RIR1	P08543	HHV11	1073.33	124050.41	22	22	204	195784	204	169290
RIR2	P10224	HHV11	99.65	38019.223	2	2	350	29590	350	25586
RNB	P04487	HHV11	364.72	17757.076	7	7	32345	7697468	32345	6655821
SCAF	P10210	HHV11	62.18	66470.82	1	1	0	21250	0	18374
SHUT	P10225	HHV11	691.37	54917.78	12	13	236963	990144	236963	856154
TEG1	P10230	HHV11	2300.74	78241.43	39	40	15610	9311711	15610	8051619
TEG5	P10231	HHV11	3825.19	73816.92	56	62	13986	37769379	13986	32658298
TEG6	P10239	HHV11	59.5	20492.555	2	2	253	49971	253	43209
TRX1	P32888	HHV11	370.95	50263.395	6	6	5855	315281	5855	272616
TRX2	P10202	HHV11	108.49	34270.76	2	2	0	19111	0	16525
UL13	P04290	HHV11	605.94	57196.883	12	12	3491	390504	3491	337660
UL24	P10208	HHV11	272.17	29476.389	6	6	213	437141	213	377985
UL56	P10240	HHV11	204.01	25320.521	4	4	9789	212453	9789	183703
US02	P06485	HHV11	328.04	32470.814	5	5	98	202309	98	174932
US02	P13292	HHV2H	43.98	32780.58	1	1	2719	189162	2719	163564
US03	P04413	HHV11	828.42	52834.64	13	13	11711	530962	11711	459111
US10	P06486	HHV11	364.28	34055.7	7	7	6564	134910	6564	116654
VP16	P06492	HHV11	889.9	54345.434	13	13	7081	990684	7081	856621
VP22	P10233	HHV11	1395.62	32253.994	19	19	53665	17580463	53665	15201415
1433B	P31946	HUMAN	167.95	28082.387	1	4	765	4885	765	4224
1433E	P62258	HUMAN	175.59	29173.883	2	4	14667	38225	14667	33052
AAR2	Q9Y312	HUMAN	71.88	43472.223	1	1	3379	17109	3379	14793
AATF	Q9NY61	HUMAN	114.99	63133.016	2	2	11580	26586	11580	22989
ABC3A	P31941	HUMAN	41.17	23011.996	1	1	1252	10968	1252	9484
ABCF1	Q8NE71	HUMAN	57.23	95925.734	1	1	10615	9238	10615	7988
ABT1	Q9ULW3	HUMAN	38.56	31078.938	1	1	9219	5952	9219	5146
ACTB	P60709	HUMAN	661.3	41736.754	6	11	402509	209678	402509	181303
ADT2	P05141	HUMAN	442.57	32852.242	3	10	375796	393993	375796	340677
ADT3	P12236	HUMAN	429.93	32866.273	2	9	204467	216102	204467	186859
AFF4	Q9UHB7	HUMAN	63.65	127458.98	1	1	14135.95605	0	14135.95605	0
AGO2	Q9UKV8	HUMAN	119.95	97208.1	3	3	16405	10364	16405	8962
AIFM1	O95831	HUMAN	230.74	66900.68	4	5	1138484	1328190	1138484	1148454
AKAP8	O43823	HUMAN	47.92	76108.43	1	1	4418	24789	4418	21435
AKIP	Q9NWT8	HUMAN	37.03	22354.248	1	1	67134	65342	67134	56500
AKP8L	Q9ULX6	HUMAN	87.86	71639.85	2	2	29031	37659	29031	32563
ALBU	P02768	HUMAN	168.62	69366.805	4	4	40372	30186	40372	26101
ALDOA	P04075	HUMAN	44.85	39420.03	1	1	10573	616	10573	533
ANM1	Q99873	HUMAN	50.6	42461.664	1	1	22537	9205	22537	7959
ANXA2	P07355	HUMAN	574.27	38604.05	11	11	144201	72835	144201	62979
AP2A1	O95782	HUMAN	812.25	107545.86	14	16	135596	55724	135596	48184
AP2B1	P63010	HUMAN	644.34	104552.53	14	14	219214	68301	219214	59058
AP2M1	Q96CW1	HUMAN	386.36	49654.754	8	8	152238	95918	152238	82938
AP2S1	P53680	HUMAN	39.09	17017.693	1	1	45404	8253	45404	7136
AR6P4	Q66PJ3	HUMAN	58.82	44915.45	1	1	51534	11171	51534	9660
ARF	Q8N726	HUMAN	43.57	13903.234	1	1	21024	9201	21024	7956
ARF3	P61204	HUMAN	168.15	20600.76	1	3	6471	39766	6471	34385
ARF4	P18085	HUMAN	146.13	20510.773	1	3	3654	8014	3654	6929
ARGI1	P05089	HUMAN	302.57	34734.973	6	6	25907746	29772687	25907746	25743746
ARHG2	Q92974	HUMAN	42.53	111542.555	1	1	13596	14148	13596	12233
AROS	Q86WX3	HUMAN	48.94	15433.816	1	1	14118	10509	14118	9087
ASCC3	Q8N3C0	HUMAN	535.37	251458	10	11	43028	29441	43028	25457
ASPH	Q12797	HUMAN	231.4	85862.62	4	4	72261	55266	72261	47788
ATD3A	Q9NVI7	HUMAN	725.56	71369.2	7	15	14940	57054	14940	49333
ATD3B	Q5T9A4	HUMAN	369.79	72572.98	1	9	11674	29286	11674	25323
ATPA	P25705	HUMAN	239.47	59750.66	5	5	38652	33243	38652	28744
ATPG	P36542	HUMAN	199.38	32996.035	4	4	28711	42183	28711	36474
ATX2L	Q8WWM7	HUMAN	726.64	113373.734	16	17	73907	107768	73907	93184
B3GT6	Q96L58	HUMAN	41.18	37137.6	1	1	5496	12689	5496	10972
BCLF1	Q9NYF8	HUMAN	1334.59	106122.17	24	25	189785	188574	189785	163055
BIP	P11021	HUMAN	1228.14	72333.055	19	21	189482	180304	189482	155905
BLMH	Q13867	HUMAN	87.7	52562.3	2	2	43025	31544	43025	27275

Supplementary Table 4 (Page 2 of 9) – List of detected proteins immunoprecipitated from HSV-1 infected cells.

Gene	Accession	Species	Confidence score	Mass	Unique Peptides	Peptide Count	Control Raw Protien Abundance	HSV-1 Raw Protien Abundance	Control Normalised Protien Abundance	HSV-1 Normalised Protien Abundance
BMS1	Q14692	HUMAN	309.78	145806.81	6	6	11035	37865	11035	32741
BOP1	Q14137	HUMAN	426.78	83629.51	10	10	17628	66987	17628	57922
BPIA1	Q9NP55	HUMAN	36.08	26712.67	1	1	0	37450	0	32382
BRI3	O95415	HUMAN	63.89	13644.964	1	1	6347	9272	6347	8017
BRI3B	Q8WY22	HUMAN	75.3	27835.533	1	1	35836	43251	35836	37398
BRX1	Q8TDN6	HUMAN	626.03	41401.383	12	12	61358	161806	61358	139910
BUD13	Q9BRD0	HUMAN	293.94	70520.86	6	6	20137	37233	20137	32194
BYST	Q13895	HUMAN	43.93	49601.395	1	1	2805	13254	2805	11461
C1QBP	Q07021	HUMAN	466.95	31362.22	7	7	1396793	1341157	1396793	1159668
CALL5	Q9NZT1	HUMAN	128.02	15892.504	2	2	98474	52595	98474	45478
CAPR1	Q14444	HUMAN	590.54	78366.3	12	12	290878	257064	290879	222277
CASPE	P31944	HUMAN	159.06	27679.518	4	4	87950	67521	87950	58384
CATA	P04040	HUMAN	246.19	59756.223	5	5	47540	19411	47540	16784
CATD	P07339	HUMAN	69.59	44552.254	2	2	46257	26533	46257	22943
CCD86	Q9H6F5	HUMAN	124.11	40235.63	3	3	33701	36657	33701	31697
CD2B2	O95400	HUMAN	154.79	37646.484	4	4	38069	22785	38069	19702
CDC5L	Q99459	HUMAN	1515.35	92250.67	29	29	116454	257981	116454	223070
CDSN	Q15517	HUMAN	144.62	51522.11	2	2	335903	80979	335903	70021
CE170	Q5SW79	HUMAN	148.5	175292.06	4	4	23888	21271	23888	18393
CEBPZ	Q03701	HUMAN	209.79	120973.78	5	5	6155	33999	6155	29398
CENPV	Q7Z7K6	HUMAN	425.94	29945.91	7	7	208803	121534	208803	105088
CEP78	Q5JTW2	HUMAN	99.41	76396.47	2	2	17179	13473	17179	11649
CETN2	P41208	HUMAN	115.44	19738.428	2	2	28550	20609	28550	17820
CG050	Q9BRJ6	HUMAN	635.82	22083.36	10	10	820074	649980	820074	562023
CH033	Q9H7E9	HUMAN	181.31	24992.496	4	4	18587	27147	18587	23473
CH60	P10809	HUMAN	335.32	61054.73	7	7	52073	67612	52073	58462
CHD1	O14646	HUMAN	87.83	196686.56	2	2	1509	6880	1509	5949
CHTOP	Q9Y3Y2	HUMAN	359.37	26396.584	6	6	55798	186406	55798	161181
CI114	Q5T280	HUMAN	51.8	42008.676	1	1	9957	25425	9957	21985
CK098	E9PRG8	HUMAN	103.91	14233.721	2	2	49944	59669	49944	51594
CKAP2	Q8WWK9	HUMAN	44.74	76986.78	1	1	10751	14373	10751	12428
CKAP4	Q07065	HUMAN	445.36	66022.54	8	8	63599	77663	63599	67154
CLAP2	O75122	HUMAN	59.68	141063.08	1	1	12526	10412	12526	9003
CNBP	P62633	HUMAN	106.28	19462.688	2	2	35444	22616	35444	19556
CNDG2	Q86XI2	HUMAN	65.65	130960.01	1	1	9875	9293	9875	8035
CNIH4	Q9P003	HUMAN	65.19	16093.348	1	1	156830	205256	156830	177480
COIL	P38432	HUMAN	115.77	62608.36	2	2	4884	29673	4884	25657
CPSF6	Q16630	HUMAN	158.97	59209.91	3	3	30284	27549	30284	23821
CPSF7	Q8N684	HUMAN	95.33	52050.113	2	2	10271	16719	10271	14456
CSDE1	O75534	HUMAN	67.42	88884.734	2	2	15078	11448	15078	9899
CSTOS	Q96C57	HUMAN	41.17	28170.492	1	1	0	14752	0	12756
CYTA	P01040	HUMAN	231.12	11006.488	4	4	559019	236010	559019	204072
DCA13	Q9NV06	HUMAN	104.7	51402.242	2	2	12244	30707	12244	26552
DCAF7	P61962	HUMAN	39.72	38926.195	1	1	6747	4078	6747	3526
DCD	P81605	HUMAN	131.09	11283.856	3	3	596837	445666	596837	385357
DDB1	Q16531	HUMAN	973.26	126967.76	22	22	71005	168219	71005	145455
DDX1	Q92499	HUMAN	216.91	82432.2	4	4	12968	12165	12968	10519
DDX10	Q13206	HUMAN	69.26	100887.84	2	2	6299	8306	6299	7182
DDX17	Q92841	HUMAN	1774.17	80272.64	25	33	453263	1016662	453263	879084
DDX18	Q9NVP1	HUMAN	1111.88	75406.86	19	19	84401	198192	84401	171372
DDX21	Q9NR30	HUMAN	2558.62	87344.48	39	42	667619	1016248	667619	878726
DDX23	Q9BUQ8	HUMAN	104.33	95582.52	3	3	9768	5242	9768	4532
DDX24	Q9GZR7	HUMAN	813.92	96331.73	15	15	83266	120489	83266	104184
DDX27	Q96GQ7	HUMAN	714.39	89835.266	13	14	238714	305310	238714	263995
DDX28	Q9NUL7	HUMAN	49.64	59581.3	1	1	4018	16516	4018	14281
DDX31	Q9H8H2	HUMAN	261.17	94087.12	6	6	10175	26368	10175	22800
DDX3X	O00571	HUMAN	764.73	73243.57	13	15	111164	177256	111164	153269
DDX41	Q9UJV9	HUMAN	761.7	69837.7	15	15	64094	84943	64094	73448
DDX46	Q7L014	HUMAN	131.72	117361.92	4	4	13965	7833	13965	6773
DDX47	Q9H0S4	HUMAN	263.07	50646.58	6	6	28588	25832	28588	22336
DDX5	P17844	HUMAN	1303.87	69148.2	17	25	140313099	183343199	140313104	158532576
DDX50	Q9BQ39	HUMAN	1066.81	82565.07	18	21	110113	104326	110113	90208
DDX52	Q9Y2R4	HUMAN	427.16	67498.164	9	9	121513	75738	121513	65489
DDX54	Q8TDD1	HUMAN	534.12	98594.94	13	13	33158	55680	33158	48146
DDX55	Q8NHQ9	HUMAN	43.52	68546.88	1	1	8728	7597	8728	6569
DDX56	Q9NY93	HUMAN	69.41	61589.625	2	2	9311	13888	9311	12009
DEK	P35659	HUMAN	97.09	42674.34	2	2	8349	12835	8349	11098
DESP	P15924	HUMAN	3949.39	331774.38	79	79	588220	201818	588220	174507
DHX15	O43143	HUMAN	1126.04	90932.836	20	22	153931	245089	153931	211923
DHX30	Q7L2E3	HUMAN	2256.44	133938.02	45	45	220931	359765	220931	311081
DHX33	Q9H6R0	HUMAN	64.47	78874.17	1	1	15938	31037	15938	26837
DHX36	Q9H2U1	HUMAN	491.87	114760.01	8	9	67058	63666	67058	55050
DHX57	Q6P158	HUMAN	313.17	155603.72	7	8	35924	47831	35924	41358
DHX9	Q08211	HUMAN	2897.05	140957.98	50	50	676188	1176813	676188	1017563
DIDO1	Q9BTC0	HUMAN	46.47	243869.75	2	2	3256	7954	3256	6878
DIM1	Q9UNQ2	HUMAN	430.79	35236.402	9	9	166246	212728	166246	183941
DJB11	Q9UBS4	HUMAN	372.11	40513.98	7	7	109181	134826	109181	116581
DJC10	Q8IXB1	HUMAN	49.58	91079.78	1	1	16795	20183	16795	17452
DKC1	O60832	HUMAN	408.31	57674.223	8	8	30131	74280	30131	64228
DNJA1	P31689	HUMAN	391.45	44868.246	5	5	185854	195409	185854	168965
DNJA2	O60884	HUMAN	531.41	45745.65	11	11	49492	54895	49492	47467
DNJA3	Q96EY1	HUMAN	117.08	52488.71	2	2	33094	37958	33094	32821
DNJB6	O75190	HUMAN	81.41	36087.023	2	2	19827	16311	19827	14104
DNJC9	Q8WXX5	HUMAN	438.73	29909.705	8	8	121733	178	121733	154
DPM1	O60762	HUMAN	100.06	29634.281	2	2	34628	51707	34628	44710
DRG1	Q9Y295	HUMAN	168.97	40542.188	3	3	30837	21570	30837	18651
DSC1	Q08554	HUMAN	377.26	99986.87	5	5	384371	98801	384371	85431

Supplementary Table 4 (Page 3 of 9) – List of detected proteins immunoprecipitated from HSV-1 infected cells.

Gene	Accession	Species	Confidence score	Mass	Unique Peptides	Peptide Count	Control Raw Protien Abundance	HSV-1 Raw Protien Abundance	Control Normalised Protien Abundance	HSV-1 Normalised Protien Abundance
DSC3	Q14574	HUMAN	47.65	99969.03	1	1	41846	15887	41847	13737
DSG1	Q02413	HUMAN	918.83	113747.6	17	18	699853	188514	699853	163004
DSRAD	P55265	HUMAN	344.55	136066.22	7	7	33779	51329	33779	44383
EAF6	Q9HAF1	HUMAN	110.88	21634.879	2	2	15240	14280	15240	12347
EBP2	Q99848	HUMAN	509.27	34851.957	11	11	192870	531524	192870	459596
ECM1	Q16610	HUMAN	83.29	60674.203	2	2	14614	4239	14614	3665
EF1A1	P68104	HUMAN	636.61	50140.918	12	12	563820	507749	563820	439039
EF2	P13639	HUMAN	121.32	95338.22	2	4	11029	13391	11029	11579
EI2BA	Q14232	HUMAN	57.06	33712.203	1	1	10080	9476	10080	8193
ELAV1	Q15717	HUMAN	350.24	36091.887	6	7	293812	163680	293812	141530
ELAV2	Q12926	HUMAN	210.83	39503.938	4	5	32789	7490	32789	6477
ELOA1	Q14241	HUMAN	284.39	89908.914	6	6	39027	41557	39027	35934
EMAL3	Q32P44	HUMAN	47.28	95196.75	2	2	58425	59270	58425	51249
EMD	P50402	HUMAN	296.84	28993.854	5	5	29177	64443	29177	55722
ENOA	P06733	HUMAN	58.29	47168.996	1	1	24460	20654	24460	17859
ERD22	P33947	HUMAN	98.88	24421.945	2	2	9098	13569	9098	11732
ERH	P84090	HUMAN	108.7	12258.929	2	2	96213	126742	96213	109591
ESF1	Q9H501	HUMAN	135.06	98796.11	3	3	11642	16389	11642	14171
EST1A	Q86US8	HUMAN	129.97	160461.05	3	3	12965	9779	12965	8455
EWS	Q01844	HUMAN	190.72	68478.266	3	3	86434	80766	86434	69836
EXOS1	Q9Y3B2	HUMAN	147.13	21451.748	3	3	61645	88329	61645	76376
EXOS2	Q13868	HUMAN	473.78	32789.004	8	8	131828	163398	131828	141286
EXOS3	Q9NQT5	HUMAN	292.07	29572.176	5	5	87106	104529	87106	90383
EXOS4	Q9NPD3	HUMAN	297.16	26382.959	7	7	41961	52522	41961	45415
EXOS5	Q9NQT4	HUMAN	70.76	25248.936	2	2	25247	34753	25247	30050
EXOS6	Q5RKV6	HUMAN	301.99	28235.15	5	5	83756	105145	83756	90916
EXOS7	Q15024	HUMAN	211.84	31821.416	3	3	95364	139238	95364	120396
EXOS8	Q96B26	HUMAN	225.82	30039.576	4	4	115962	120275	115962	103999
EXOS9	Q06265	HUMAN	399.42	48949.1	7	7	145596	92365	145596	79866
EXOSX	Q01780	HUMAN	1141.48	100831.17	22	22	117509	147212	117509	127291
F111B	Q6SJ93	HUMAN	82.31	84674.41	2	2	22075	4791	22075	4143
F120A	Q9NZB2	HUMAN	479.84	121887.73	9	9	40964	49411	40964	42725
F207A	Q9NSI2	HUMAN	59.43	25456.254	1	1	0	21102	0	18247
FA98A	Q8NCA5	HUMAN	57.36	55272.414	1	1	1399	5832	1399	5043
FABP5	Q01469	HUMAN	41.34	15164.424	1	1	136436	92523	136436	80002
FBRL	P22087	HUMAN	418.07	33784.227	6	7	104548	219283	104548	189609
FHL1	Q13642	HUMAN	217.69	36263.027	5	5	315215	148072	315215	128034
FILA	P20930	HUMAN	390.35	435180.3	9	10	223375	73482	223375	63538
FILA2	Q5D862	HUMAN	593.03	248071.53	10	10	617200	214915	617200	185832
FMR1	Q06787	HUMAN	1605.17	71174.516	24	28	544657	858080	544657	741962
FUBP2	Q92945	HUMAN	132.89	73115.4	2	2	29738	19546	29738	16901
FUS	P35637	HUMAN	375.46	53425.86	4	6	268898	415363	268898	359155
FXR1	P51114	HUMAN	2237.6	69720.84	32	35	1132937	1789486	1132937	1547327
FXR2	P51116	HUMAN	2078.43	74223.36	29	35	786190	1369743	786190	1184385
G3BP1	Q13283	HUMAN	520.21	52164.26	8	9	249581	170483	249581	147413
G3BP2	Q9UN86	HUMAN	543.79	54121.156	9	10	255851	275160	255851	237925
G3P	P04406	HUMAN	538.07	36053.223	10	10	320684	130044	320684	112446
GANAB	Q14697	HUMAN	45.66	106874.01	1	1	3640	21032	3640	18186
GAR1	Q9NY12	HUMAN	78.91	22347.896	2	2	41159	80612	41159	69703
GGCT	O75223	HUMAN	143.3	21007.719	3	3	30178	14518	30178	12554
GGYF2	Q6Y7W6	HUMAN	1922.23	150069.64	32	32	89492	637505	89492	551235
GLYR1	Q49A26	HUMAN	240.09	60547.43	5	5	48227	61783	48227	53422
GNL3	Q9BVP2	HUMAN	549.9	61993.273	10	10	111134	181994	111134	157366
GPTC4	Q5T3I0	HUMAN	438.5	50381.23	8	8	68342	67177	68342	58086
GRB2	P62993	HUMAN	84.48	25206.346	2	2	855	18947	855	16383
GRP75	P38646	HUMAN	546.92	73680.57	11	12	72391	48781	72391	42180
GRSF1	Q12849	HUMAN	98.58	53126.39	2	2	66287	63189	66287	54638
GRWD1	Q9BQ67	HUMAN	708.29	49419.195	12	12	496108	647402	496108	559793
GSDMA	Q96QA5	HUMAN	132.39	49364.926	2	2	52876	39182	52876	33880
GTPB1	O00178	HUMAN	84	72453.94	2	2	14089	12390	14089	10713
H10	P07305	HUMAN	166.99	20862.92	3	3	69667	62570	69667	54103
H11	Q02539	HUMAN	681.36	21842.078	1	10	11269	14043	11269	12143
H12	P16403	HUMAN	1056.01	21364.732	5	17	1412855	1630291	1412855	1409675
H13	P16402	HUMAN	1016.87	22349.887	5	17	722052	833175	722052	720427
H14	P10412	HUMAN	1060.86	21865.252	5	17	1423923	1643063	1423923	1420718
H1X	Q92522	HUMAN	750.64	22487.107	12	12	903411	1239849	903411	1072069
H2A1B	P04908	HUMAN	166.06	14135.485	2	4	1197570	1134607	1197570	981069
H2AZ	P0C0S5	HUMAN	104.62	13552.729	1	3	38438	25761	38438	22275
H2B1K	O60814	HUMAN	291.09	13890.133	6	6	699413	697981	699413	603528
H31	P68431	HUMAN	35.93	15404.08	1	1	254507	92181	254507	79707
H4	P62805	HUMAN	164.23	11367.339	3	3	445022	246696	445022	213312
HACD3	Q9P035	HUMAN	338.83	43159.58	7	7	65841	76295	65841	65970
HDAC1	Q13547	HUMAN	146.45	55103.082	1	4	2011	1503	2011	1300
HDAC1	Q13547	HUMAN	146.45	55103.082	1	4	2011	1503	2011	1300
HDAC2	Q92769	HUMAN	201.34	55364.293	2	5	27046	15090	27046	13048
HEAT1	Q9H583	HUMAN	310.72	242367.6	7	7	4447	35798	4447	30953
HERC5	Q9UII4	HUMAN	56.85	116852.27	1	1	24014	23262	24014	20114
HNRC2	B2RXH8	HUMAN	447.49	32072.299	2	9	1174777	1777637	1174777	1537081
HNRDL	O14979	HUMAN	98.54	46437.504	2	2	22618	32732	22618	28302
HNRH1	P31943	HUMAN	1210.36	49229.457	10	19	532395	1066125	532395	921854
HNRH2	P55795	HUMAN	617.03	49263.56	3	10	90245	200837	90245	173659
HNRL1	Q9BUJ2	HUMAN	1715.48	95738.8	30	30	756979	968880	756979	837768
HNRL2	Q1KMD3	HUMAN	86.93	85104.875	2	2	15288	23629	15288	20432
HNRPC	P07910	HUMAN	878.74	33670	8	15	127620	1394693	127620	1205959
HNRPD	Q14103	HUMAN	119.8	38434.156	2	2	37612	48872	37612	42258
HNRPF	P52597	HUMAN	1156.98	45671.86	13	16	1228963	1711685	1228963	1480054
HNRPK	P61978	HUMAN	995.21	50976.273	18	18	322099	845750	322099	731300

Supplementary Table 4 (Page 4 of 9) – List of detected proteins immunoprecipitated from HSV-1 infected cells.

Gene	Accession	Species	Confidence score	Mass	Unique Peptides	Peptide Count	Control Raw Protien Abundance	HSV-1 Raw Protien Abundance	Control Normalised Protien Abundance	HSV-1 Normalised Protien Abundance
HNRPL	P14866	HUMAN	331.29	64132.832	9	9	66403	121893	66403	105398
HNRPM	P52272	HUMAN	4671.76	77515.51	85	86	1205703	5427936	1205703	4693410
HNRPQ	O60506	HUMAN	642.1	69602.664	7	12	205597	121744	205597	105270
HNRPR	O43390	HUMAN	908.36	70943.125	11	16	160925	245223	160925	212039
HNRPU	Q00839	HUMAN	1200.09	90584.625	21	21	1211720	1142519	1211720	987910
HORN	Q86YZ3	HUMAN	2646.92	282389.1	26	27	2307685	428029	2307685	370107
HP1B3	Q5SSJ5	HUMAN	337.59	61207.074	7	7	32346	48297	32346	41761
HS71A	P0DMV8	HUMAN	1089.33	70052.375	14	18	328436	335150	328436	289796
HS90B	P08238	HUMAN	286.56	83264.234	4	6	71474	52066	71474	45021
HSP7C	P11142	HUMAN	1765.99	70898.25	21	28	927132	933371	927132	807064
HSPB1	P04792	HUMAN	116.66	22782.523	2	2	168624	119870	168624	103649
IF2A	P05198	HUMAN	486.03	36112.18	9	9	100306	78527	100306	67900
IF2B	P20042	HUMAN	168	38388.414	3	3	72847	52044	72847	45001
IF2B1	Q9NZI8	HUMAN	1432.35	63480.65	24	25	819934	1394243	819934	1205569
IF2B2	Q9Y6M1	HUMAN	910.51	66121.484	16	17	364240	409460	364240	354050
IF2B3	O00425	HUMAN	726.66	63705.117	12	14	178935	252103	178935	217988
IF2G	P41091	HUMAN	614.17	51109.566	10	10	175209	124892	175209	107991
IF4A1	P60842	HUMAN	178.9	46153.97	4	4	18997	26593	18997	22995
IF4A3	P38919	HUMAN	141.95	46871.074	3	3	32926	20396	32926	17636
IF4E2	O60573	HUMAN	410.23	28361.963	7	7	3729	275081	3729	237856
IF4H	Q15056	HUMAN	358.95	27385.062	6	7	165274	914126	165274	790423
IF6	P56537	HUMAN	185.03	26599.074	3	3	54954	150895	54954	130476
IGHA1	P01876	HUMAN	167.16	37654.664	3	3	85213	144967	85213	125349
IGKC	P01834	HUMAN	125.08	11765.036	2	2	56013	59057	56013	51065
IGLC2	P0DOY2	HUMAN	99.41	11293.563	2	2	5539	19355	5539	16736
ILF2	Q12905	HUMAN	854.5	43062.184	13	14	493771	599252	493771	518159
ILF3	Q12906	HUMAN	1639.09	95338.79	30	31	418833	601177	418833	519824
IMP3	Q9NV31	HUMAN	97.45	21850.148	2	2	7381	41603	7381	35973
IMP4	Q96G21	HUMAN	156.36	33756.56	3	3	8513	32931	8513	28475
INO1	Q9NPH2	HUMAN	44.44	61067.9	1	1	9455	10152	9455	8778
IRS4	O14654	HUMAN	820.48	133767.48	16	16	138117	29991	138117	25933
K1C10	P13645	HUMAN	7097.3	58827.047	108	123	59401313	25913169	59401312	22406510
K1C14	P02533	HUMAN	2948.67	51561.5	22	53	5713305	1915388	5713306	1656191
K1C16	P08779	HUMAN	2492.7	51267.836	25	47	2225548	1078977	2225548	932966
K1C17	Q04695	HUMAN	1731.37	48105.684	16	32	604624	300231	604624	259603
K1C9	P35527	HUMAN	7304.28	62064.266	124	125	116361224	20959763	116361224	18123416
K1H1	Q15323	HUMAN	655.43	47237.117	5	13	89799	8239	89799	7125
K22E	P35908	HUMAN	5678.04	65432.89	73	96	19635554	5699775	19635554	4928462
K2C1	P04264	HUMAN	9278.13	66038.71	149	170	172631607	44613851	172631600	38576552
K2C1B	Q7Z794	HUMAN	1069.09	61901.414	13	22	136210	73276	136210	63360
K2C5	P13647	HUMAN	3233.19	62378.367	38	64	6243319	1982557	6243319	1714271
K2C6A	P02538	HUMAN	2739.75	60044.984	2	54	1417540	1113654	1417541	962951
K2C6B	P04259	HUMAN	2871.95	60066.992	4	58	730396	449010	730396	388248
K2C75	O95678	HUMAN	785.16	59560.434	1	17	57970	29167	57970	25220
K2C78	Q8N1N4	HUMAN	530.67	56865.863	8	11	239012	99195	239012	85771
K2C8	P05787	HUMAN	657.24	53704.273	1	14	9840	3312	9840	2864
K2C80	Q6KB66	HUMAN	359.36	50525.34	6	7	82541	35132	82541	30378
KCRM	P06732	HUMAN	55.27	43101.133	1	1	91524	31153	91524	26937
KCTD5	Q9NXV2	HUMAN	261.49	26092.537	4	4	41893	67362	41893	58246
KHDR1	Q07666	HUMAN	189.11	48227.348	4	4	86841	197637	86841	170892
KI67	P46013	HUMAN	1338.35	358695.03	30	30	644838	332659	644838	287642
KIF23	Q02241	HUMAN	739.03	110058.8	13	13	49533	76055	49533	65763
KNOP1	Q1ED39	HUMAN	226.85	51589.05	5	5	32383	39645	32383	34280
KPRP	Q5T749	HUMAN	74.31	64135.848	2	2	307538	141648	307538	122479
KPYM	P14618	HUMAN	116.56	57936.93	3	3	24996	8418	24996	7279
KRR1	Q13601	HUMAN	35.5	43665.035	1	1	6591	25599	6591	22135
KRT86	O43790	HUMAN	325.31	53500.68	2	8	135993	15678	135993	13556
KT33B	Q14525	HUMAN	451.7	46213.71	1	9	85960	12975	85960	11219
KVD29	A0A075B6S2	HUMAN	111.91	13143.122	2	2	6023032	3834774	6023032	3315840
L10K	Q9UNZ5	HUMAN	128.29	10576.587	4	4	18353	7214	18353	6238
LA	P05455	HUMAN	315.91	46837.1	6	6	43963	36895	43963	31902
LACTB	P83111	HUMAN	964.47	60693.652	17	18	614839	922095	614839	797314
LAP2A	P42166	HUMAN	56.29	75492.07	1	1	5506	13018	5506	11256
LARP1	Q6PKG0	HUMAN	1451.1	123510.35	26	29	1462944	1312763	1462944	1135116
LARP4	Q71RC2	HUMAN	121.5	80596.016	3	3	324708	310221	324708	268241
LAS1L	Q9Y4W2	HUMAN	260.67	83064.94	4	5	8521	16987	8521	14688
LC7L2	Q9Y383	HUMAN	545.43	46513.92	8	12	172523	182993	172523	158229
LC7L3	O95232	HUMAN	407.93	51466.21	7	7	82471	121601	82471	105146
LCN1	P31025	HUMAN	64.22	19250.002	1	2	201535	160537	201535	138813
LENG8	Q96PV6	HUMAN	63.84	88157.33	1	1	17856	23025	17856	19909
LLPH	Q9BRT6	HUMAN	92.23	15225.178	2	2	67979	91280	67979	78928
LN28B	Q6ZN17	HUMAN	69.4	27083.635	2	2	12902	14042	12902	12142
LRC59	Q96AG4	HUMAN	101.84	34930.45	3	3	5789	13939	5789	12052
LRC8A	Q8IWT6	HUMAN	2729.54	94198.63	36	46	2821244	1184810	2821244	1024477
LRC8B	Q6P9F7	HUMAN	322.77	92389.7	3	7	46347	25009	46347	21624
LRC8C	Q8TDW0	HUMAN	10987.02	92449.46	180	190	162538923	194663489	162538928	168320960
LRC8D	Q7L1W4	HUMAN	2146.69	98201.23	36	37	551598	375470	551598	324660
LRC8E	Q6NSJ5	HUMAN	2423.67	90247.15	33	40	1491292	1443278	1491292	1247969
LS14B	Q9BX40	HUMAN	55.77	42070.74	1	1	23854	29642	23854	25630
LSM12	Q3MHD2	HUMAN	58.38	21700.74	1	1	74386	115800	74386	100130
LTV1	Q96GA3	HUMAN	80.22	54855.035	2	2	22947	15446	22947	13356
LUC7L	Q9NQ29	HUMAN	477.66	43727.984	5	9	71562	179541	71562	155245
LYAR	Q9NX58	HUMAN	520.46	43614.844	8	8	137759	225633	137759	195099
LYRIC	Q86UE4	HUMAN	206.55	63837.13	5	5	24685	21488	24685	18580
M2OM	Q02978	HUMAN	263.71	34061.723	5	6	51050	37599	51050	32511
MA7D1	Q3KQU3	HUMAN	109.09	92820.01	2	2	18104	19163	18104	16570
MAGT1	Q9H0U3	HUMAN	67.37	38036.65	2	2	14956	11612	14956	10041

Supplementary Table 4 (Page 5 of 9) – List of detected proteins immunoprecipitated from HSV-1 infected cells.

Gene	Accession	Species	Confidence score	Mass	Unique Peptides	Peptide Count	Control Raw Protien Abundance	HSV-1 Raw Protien Abundance	Control Normalised Protien Abundance	HSV-1 Normalised Protien Abundance
MARK2	Q7KZI7	HUMAN	526.18	87910.8	7	9	46493	53666	46493	46404
MARK3	P27448	HUMAN	355.31	84428.5	6	8	33717	42027	33717	36340
MATR3	P43243	HUMAN	1563.39	94623.15	29	29	73257	700345	73257	605572
MBB1A	Q9BQG0	HUMAN	2987.52	148853.9	51	53	362713	618915	362713	535162
MELK	Q14680	HUMAN	52.04	74642.2	1	1	14295	348	14295	301
MK67I	Q9BYG3	HUMAN	523.96	34222.207	8	8	92031	119150	92031	103026
ML12B	O14950	HUMAN	251.48	19779.145	5	5	55764	28671	55764	24791
MMTA2	Q9BU76	HUMAN	168.97	29411.803	3	3	19416	13078	19416	11309
MOV10	Q9HCE1	HUMAN	1088.19	113671.24	23	23	109464	205813	109464	177962
MPCP	Q00325	HUMAN	268.97	40094.87	7	7	911167	945196	911167	817289
MPH6	Q99547	HUMAN	78.1	19023.697	1	2	2059	4872	2059	4213
MPP10	O00566	HUMAN	209.73	78863.83	5	5	6454	43629	6454	37725
MRM3	Q9HC36	HUMAN	201.81	47020.07	3	3	35821	57111	35821	49383
MRT4	Q9UKD2	HUMAN	590.79	27560.457	12	12	170707	244791	170707	211665
MTR1L	Q13585	HUMAN	52.41	67368.625	1	1	34242	22298	34242	19280
MTREX	P42285	HUMAN	471.08	117804.66	9	9	50424	73304	50424	63384
MYEF2	Q9P2K5	HUMAN	351.56	64121.65	8	8	39099	132222	39099	114329
NAT10	Q9H0A0	HUMAN	1690.48	115729.74	31	34	102100	292028	102100	252510
NCBP1	Q09161	HUMAN	367.03	91839.42	7	7	94812	90819	94812	78529
NCBP3	Q53F19	HUMAN	55.6	70592.64	1	1	7852	17343	7852	14996
NDKM	O00746	HUMAN	100.34	20658.58	3	3	4866	11864	4866	10259
NEUA	Q8NFW8	HUMAN	126.1	48379.297	3	3	21705	30020	21705	25958
NFXL1	Q6ZNB6	HUMAN	48.85	101339.45	1	1	12621	15743	12621	13613
NGDN	Q8NEJ9	HUMAN	209.97	35894.1	3	3	14530	27829	14530	24063
NH2L1	P55769	HUMAN	56.94	14173.538	1	1	20625	106863	20625	92402
NHP2	Q9NX24	HUMAN	121.18	17201.035	2	2	24152	62082	24152	53681
NIP7	Q9Y221	HUMAN	100.28	20462.602	2	2	65098	156932	65098	135696
NKAP	Q8N5F7	HUMAN	135.86	47138.28	3	3	18829	23133	18829	20003
NKRF	O15226	HUMAN	264.9	77672.96	6	7	22538	28449	22538	24599
NLE1	Q9NVX2	HUMAN	43.7	53320.316	1	1	7387	4716	7387	4078
NMNA1	Q9HAN9	HUMAN	422.23	31932.453	7	7	60041	73073	60041	63184
NOB1	Q9ULX3	HUMAN	190.94	46674.98	3	4	16808	26441	16808	22863
NOC2L	Q9Y3T9	HUMAN	81.15	84919.445	2	2	2132	13631	2132	11786
NOC3L	Q8WTT2	HUMAN	73.72	92547.78	3	3	4757	23548	4757	20361
NOC4L	Q9BVI4	HUMAN	65.33	58467.824	2	2	9819	16962	9819	14666
NOG1	Q9BZE4	HUMAN	758.65	73964.62	16	16	61877	134793	61877	116553
NOG2	Q13823	HUMAN	92.67	83654.98	3	3	14878	13710	14878	11855
NOL10	Q9BSC4	HUMAN	208.42	80301.65	5	5	10830	17805	10830	15396
NOL11	Q9H8H0	HUMAN	244.29	81123.61	5	5	3372	37187	3372	32154
NOL12	Q9UGY1	HUMAN	54.95	24662.936	1	1	42233	31422	42233	27169
NOL6	Q9H6R4	HUMAN	318.45	127592.97	6	6	8549	78933	8549	68251
NOLC1	Q14978	HUMAN	113.16	73603.336	2	3	4143	18404	4143	15914
NONO	Q15233	HUMAN	2048.72	54231.547	32	35	1892050	5470051	1892050	4729826
NOP14	P78316	HUMAN	276.14	97668.36	5	5	15253	33478	15253	28948
NOP16	Q9Y3C1	HUMAN	237.86	21188.34	5	5	15845	43651	15845	37744
NOP2	P46087	HUMAN	1057.96	89301.79	20	20	181498	449362	181498	388553
NOP53	Q9NZM5	HUMAN	166.25	54389.24	3	3	24967	51162	24967	44239
NOP56	O00567	HUMAN	1200.28	66050.02	20	20	98947	304580	98947	263364
NOP58	Q9Y2X3	HUMAN	837.92	59578.31	15	15	66603	220001	66603	190230
NP1L1	P55209	HUMAN	421.13	45374.195	7	7	252442	243438	252442	210495
NPA1P	O60287	HUMAN	103.86	254386.45	2	2	0	8542	0	7386
NPM	P06748	HUMAN	2111	32574.996	32	32	3206673	7580697	3206673	6554852
NSD2	O96028	HUMAN	294.44	152258.06	6	6	85999	30185	85999	26101
NUCL	P19338	HUMAN	3394.3	76614.58	62	62	6426312	7645273	6426312	6610689
NUFP2	Q7Z417	HUMAN	929.39	76121.16	16	16	126148	232101	126148	200693
NUMA1	Q14980	HUMAN	602.43	238257.27	10	11	54269	52790	54269	45646
NUSAP	Q9BXS6	HUMAN	341.19	49451.87	7	7	37923	32902	37923	28450
NVL	O15381	HUMAN	1226.31	95050.81	23	23	129312	236997	129312	204926
OST48	P39656	HUMAN	145.33	50800.855	4	4	18441	22589	18441	19532
P53	P04637	HUMAN	168.68	43653.22	4	4	150107	11841	150107	10238
PABP1	P11940	HUMAN	2216.09	70670.78	11	39	1690359	2257160	1690359	1951713
PABP2	Q86U42	HUMAN	91.16	32749.06	2	2	6996	48301	6996	41764
PABP3	Q9H361	HUMAN	999.04	70030.89	1	19	2010751	2579689	2010751	2230597
PABP4	Q13310	HUMAN	1328.23	70782.8	12	25	403598	549980	403598	475555
PAIRB	Q8NC51	HUMAN	188.6	44965.41	4	4	48755	50672	48755	43815
PARP1	P09874	HUMAN	907.31	113083.695	18	18	129947	90986	129947	78674
PCBP1	Q15365	HUMAN	463.57	37497.83	4	9	164862	309986	164862	268037
PCBP2	Q15366	HUMAN	710.21	38580.09	7	12	187824	729142	187824	630472
PCNA	P12004	HUMAN	68.47	28768.773	1	1	30872	31809	30872	27505
PELP1	Q8IZL8	HUMAN	444.76	119699.81	8	8	55524	117925	55524	101967
PESC	O00541	HUMAN	355.73	68002.734	8	8	11264	39476	11264	34134
PGAM5	Q96HS1	HUMAN	313.38	32004.459	7	7	174311	567193	174311	490438
PHF2	O75151	HUMAN	80.61	120774.836	1	2	14141	12874	14141	11131
PHF6	Q8IWS0	HUMAN	353.42	41290.477	7	7	133550	111807	133550	96677
PHF8	Q9UPP1	HUMAN	132.15	117863.91	1	2	27987	19867	27987	17178
PIMT	P22061	HUMAN	92.81	24636.38	3	3	46220	65429	46220	56575
PIP	P12273	HUMAN	192.48	16572.467	4	4	106846	85953	106846	74322
PK1IP	Q9NWT1	HUMAN	177.49	43963.895	3	3	12398	45402	12398	39258
PKP1	Q13835	HUMAN	250.47	82860.58	4	5	192988	42141	192988	36438
PLAK	P14923	HUMAN	1069.23	81744.8	21	21	369765	99312	369765	85873
PLEC	Q15149	HUMAN	63.87	531795.7	2	2	6777	27490	6777	23770
PLOD1	Q02809	HUMAN	51.77	83550.26	1	1	1444	15285	1444	13217
PLRG1	O43660	HUMAN	419.03	57193.93	8	8	26660	111871	26660	96732
PNO1	Q9NRX1	HUMAN	262.01	27924.268	5	5	16269	22423	16269	19388
POF1B	Q8WVV4	HUMAN	48.86	68065.15	1	1	42326	20675	42326	17877
POTEE	Q6S8J3	HUMAN	341.57	121363.39	1	5	4203	4470	4203	3865
PP1G	P36873	HUMAN	170.59	36983.793	4	4	27419	63749	27419	55122

Supplementary Table 4 (Page 6 of 9) – List of detected proteins immunoprecipitated from HSV-1 infected cells.

Gene	Accession	Species	Confidence score	Mass	Unique Peptides	Peptide Count	Control Raw Protien Abundance	HSV-1 Raw Protien Abundance	Control Normalised Protien Abundance	HSV-1 Normalised Protien Abundance
PR38B	Q5VTL8	HUMAN	46.62	64468.02	2	2	13990	17650	13990	15262
PRC1	O43663	HUMAN	163.54	71606.63	4	4	12712	13544	12712	11711
PRC2A	P48634	HUMAN	762.67	228860.75	13	15	67891	125466	67891	108488
PRC2C	Q9Y520	HUMAN	1129.64	316910.66	23	25	109899	88276	109899	76330
PRDX1	Q06830	HUMAN	253.1	22110.348	4	6	76737	52151	76737	45094
PRDX2	P32119	HUMAN	252.53	21891.908	4	5	104107	47010	104107	40649
PRKRA	O75569	HUMAN	289.48	34404.215	6	6	81224	95086	81224	82219
PRP19	Q9UMS4	HUMAN	784.5	55180.85	13	13	438700	950832	438700	822162
PRP4B	Q13523	HUMAN	288.33	116986.7	6	7	34496	39300	34496	33982
PRP6	O94906	HUMAN	303.65	106924.88	6	6	46236	46176	46236	39928
PRP8	Q6P2Q9	HUMAN	2584.15	273598.72	55	55	136430	140480	136430	121470
PSAL	A6NEC2	HUMAN	84.3	53747.31	2	2	13455	7725	13455	6679
PSIP1	O75475	HUMAN	61.33	60103.344	2	2	12839	8736	12839	7554
PSPC1	Q8WXF1	HUMAN	403.47	58743.56	8	10	97955	51650	97955	44661
PTBP1	P26599	HUMAN	442.62	57221.363	7	9	167536	143157	167536	123785
PTN13	Q12923	HUMAN	64.04	276903.2	1	2	2406	74059	2406	64037
PTSS1	P48651	HUMAN	44.06	55527.66	1	1	19486	27542	19486	23815
PUF60	Q9UHX1	HUMAN	601.76	59875.53	11	11	60728	77179	60728	66735
PUM3	Q15397	HUMAN	290.53	73584.47	6	6	7893	65616	7893	56737
PURA	Q00577	HUMAN	409.05	34910.773	6	7	129516	194061	129516	167800
PURB	Q96QR8	HUMAN	316.11	33240.82	6	6	27551	33752	27551	29185
PWP1	Q13610	HUMAN	382.61	55827.96	7	7	133335	190454	133335	164681
PWP2	Q15269	HUMAN	502.27	102451.97	10	11	47123	110489	47123	95538
RACK1	P63244	HUMAN	55.6	35076.74	1	1	39390	60198	39390	52052
RALY	Q9UKM9	HUMAN	301.55	32463.186	7	8	16861	100493	16861	86894
RBBP4	Q09028	HUMAN	128.08	47655.758	3	3	70303	35793	70303	30950
RBM10	P98175	HUMAN	46.82	103532.58	1	1	16759	28797	16759	24900
RBM14	Q96PK6	HUMAN	1032.23	69491.56	20	21	121435	657482	121435	568509
RBM15	Q96T37	HUMAN	75.33	107188.47	2	2	9113	13413	9113	11598
RBM27	Q9P2N5	HUMAN	327.69	118717.75	7	7	12075	29831	12075	25794
RBM28	Q9NW13	HUMAN	602.27	85737.625	12	12	31679	154180	31679	133315
RBM34	P42696	HUMAN	719.85	48564.836	13	13	92100	114196	92100	98743
RBM39	Q14498	HUMAN	512.93	59379.617	9	9	145189	229987	145189	198864
RBM4	Q9BWF3	HUMAN	353.88	40313.83	1	8	26809	33577	26809	29034
RBM4B	Q9BQ04	HUMAN	354.95	40149.613	1	8	6517	9590	6517	8293
RBM8A	Q9Y5S9	HUMAN	154.63	19888.979	3	3	45897	10835	45897	9369
RBMX	P38159	HUMAN	757.09	42331.836	13	13	230541	579041	230541	500683
RBMX2	Q9Y388	HUMAN	75.16	37335.63	2	2	13825	24397	13825	21096
RBP56	Q92804	HUMAN	429.93	61829.867	4	6	45731	127361	45731	110126
RCL1	Q9Y2P8	HUMAN	93.55	40842.664	2	2	13651	29727	13651	25705
RCN1	Q15293	HUMAN	271.13	38890.01	5	5	92951	67506	92951	58371
RCN2	Q14257	HUMAN	460.52	36876.45	8	8	85027	109878	85027	95009
REN3B	Q9BZI7	HUMAN	83.91	57762.18	2	2	16570	11605	16570	10034
RENT1	Q92900	HUMAN	1915.37	124345.33	33	33	229747	241453	229747	208779
REPI1	Q9BWE0	HUMAN	175.87	63574.816	3	3	17234	18874	17234	16320
RFA1	P27694	HUMAN	61.98	68138.3	1	1	11550	20998	11550	18156
RFC1	P35251	HUMAN	525.9	128254.44	9	9	55068	50480	55068	43649
RFC2	P35250	HUMAN	200.9	39157.293	4	4	47829	38422	47829	33222
RFC3	P40938	HUMAN	182.5	40556.297	3	3	36979	42498	36979	36747
RFC4	P35249	HUMAN	350.98	39681.79	6	7	99330	75391	99330	65189
RFC5	P40937	HUMAN	158.81	38496.598	3	3	21577	23022	21577	19907
RFIP1	Q6WKZ4	HUMAN	58.99	137166.97	1	1	6823	23452	6823	20278
RGAP1	Q9H0H5	HUMAN	245.09	71026.62	5	5	32108	33308	32108	28800
RIOX1	Q9H6W3	HUMAN	426.11	71085.734	7	8	36909	503717	36909	435552
RL10	P27635	HUMAN	814.61	24603.879	12	12	3785453	3610593	3785453	3121995
RL10A	P62906	HUMAN	1499.06	24831.297	24	24	7957403	9821425	7957403	8492356
RL11	P62913	HUMAN	529.9	20252.38	11	12	5250531	6379960	5250531	5516603
RL12	P30050	HUMAN	875.65	17818.578	15	15	7907010	9723917	7907010	8408044
RL13	P26373	HUMAN	809.83	24261.463	15	16	5539197	7104434	5539197	6143038
RL13A	P40429	HUMAN	514.06	23577.236	11	11	6901456	8100275	6901457	7004118
RL14	P50914	HUMAN	943.22	23431.826	17	17	6316189	9177035	6316189	7935168
RL15	P61313	HUMAN	723.46	24146.068	13	13	3040195	4151212	3040195	3589456
RL17	P18621	HUMAN	694.16	21397.014	11	11	4539214	5348278	4539214	4624531
RL18	Q07020	HUMAN	577.19	21634.48	11	11	6503054	7957100	6503055	6880318
RL18A	Q02543	HUMAN	753.12	20762.348	16	16	2465936	3159405	2465937	2731863
RL19	P84098	HUMAN	529.91	23465.951	10	10	1741135	2113705	1741135	1827672
RL1D1	O76021	HUMAN	1096.36	54972.63	23	23	220957	517306	220957	447302
RL21	P46778	HUMAN	734.36	18564.828	12	12	4889700	4795194	4889701	4146292
RL22	P35268	HUMAN	243.35	14786.983	5	5	1137178	1606032	1137178	1388699
RL23	P62829	HUMAN	521.85	14865.438	9	9	2620264	2785805	2620264	2408821
RL23A	P62750	HUMAN	815.37	17695.057	15	15	3651919	4305831	3651919	3723151
RL24	P83731	HUMAN	614.02	17778.957	15	15	2663440	3471213	2663441	3001476
RL26	P61254	HUMAN	847.82	17258.201	3	15	1833219	2128178	1833219	1840186
RL26L	Q9UNX3	HUMAN	690.94	17256.229	1	13	392959	456185	392959	394452
RL27	P61353	HUMAN	477.2	15797.716	8	8	6949169	8511530	6949169	7359721
RL27A	P46776	HUMAN	285.78	16561.38	6	6	1859945	2713301	1859945	2346128
RL28	P46779	HUMAN	786.69	15747.497	14	14	3009147	3491805	3009147	3019282
RL29	P47914	HUMAN	600.67	17752.062	11	11	994121	1438747	994121	1244051
RL3	P39023	HUMAN	2703.17	46108.94	45	46	5277692	5892638	5277693	5095226
RL30	P62888	HUMAN	633.11	12784.043	12	12	3482361	4500506	3482361	3891482
RL31	P62899	HUMAN	446.13	14462.857	9	9	1875917	2302249	1875917	1990701
RL32	P62910	HUMAN	281.22	15859.792	4	4	983780	1230639	983780	1064105
RL34	P49207	HUMAN	555.14	13292.948	11	11	3695377	4619565	3695377	3994430
RL35	P42766	HUMAN	225.02	14551.467	5	5	1237314	1581789	1237314	1367736
RL35A	P18077	HUMAN	807.88	12537.664	15	15	4112107	4175597	4112107	3610542
RL36	Q9Y3U8	HUMAN	407.78	12253.694	8	8	3826341	4280395	3826341	3701157
RL36A	P83881	HUMAN	329.8	12440.813	3	7	974436	1027658	974436	888592

Supplementary Table 4 (Page 7 of 9) – List of detected proteins immunoprecipitated from HSV-1 infected cells.

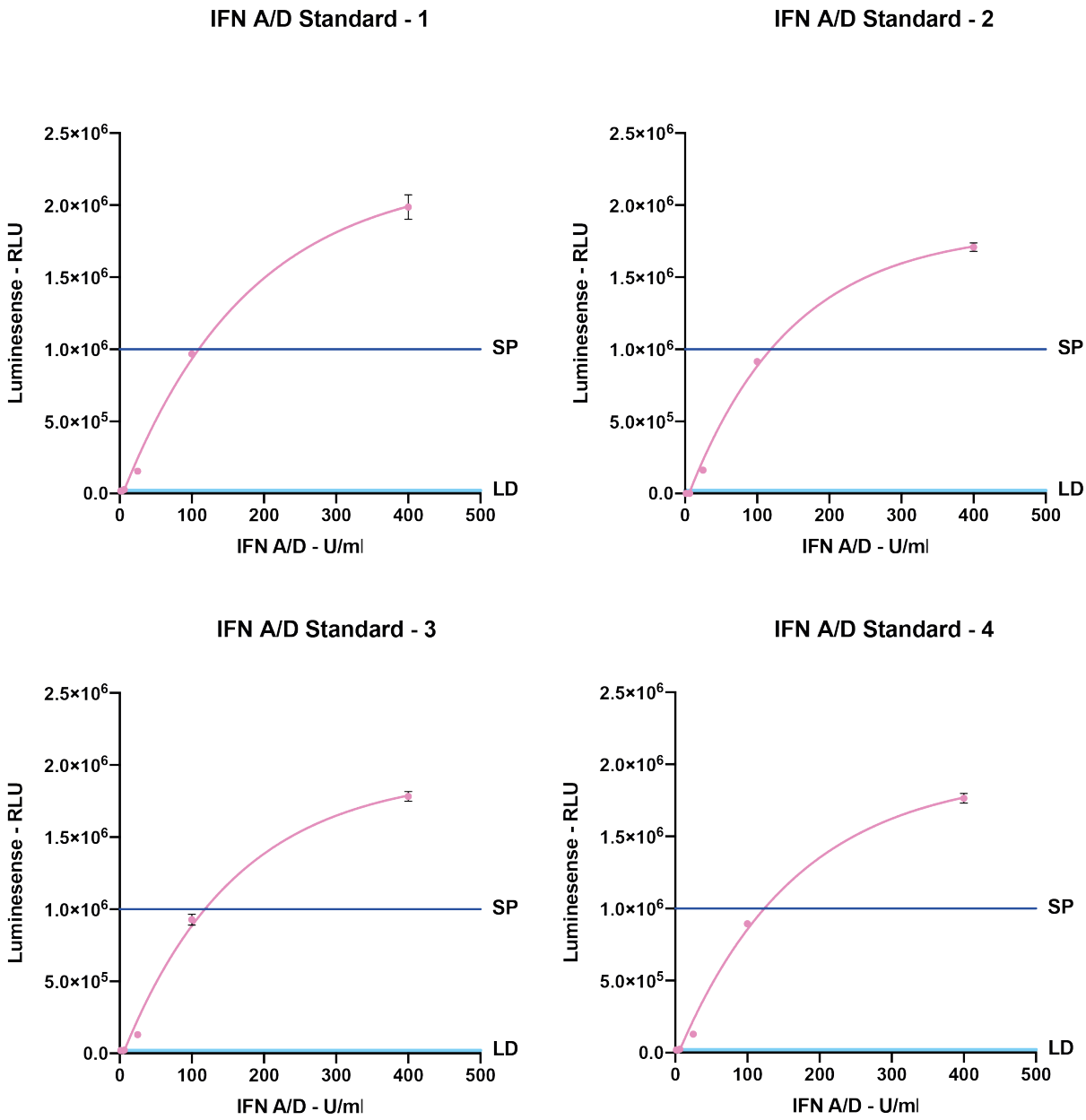
Gene	Accession	Species	Confidence score	Mass	Unique Peptides	Peptide Count	Control Raw Protien Abundance	HSV-1 Raw Protien Abundance	Control Normalised Protien Abundance	HSV-1 Normalised Protien Abundance
RL36L	Q969Q0	HUMAN	245.2	12468.827	2	6	502381	534023	502382	461757
RL37	P61927	HUMAN	181.05	11077.876	5	5	149163	166214	149163	143721
RL37A	P61513	HUMAN	457.54	10275.249	7	7	2702265	3225415	2702265	2788941
RL38	P63173	HUMAN	129.38	8217.883	3	3	176235	167156	176235	144536
RL4	P36578	HUMAN	2364.19	47697.4	40	40	6777747	9284022	6777747	8027677
RL5	P46777	HUMAN	1637.93	34362.613	26	26	5857394	6217109	5857395	5375789
RL6	Q02878	HUMAN	1794.82	32727.934	29	29	7421470	8003561	7421470	6920492
RL7	P18124	HUMAN	1416.97	29225.775	23	23	5319227	6162103	5319227	5328227
RL7A	P62424	HUMAN	1802.75	29995.623	30	30	12175412	14488271	12175412	12527669
RL7L	Q6DKI1	HUMAN	69.24	29669.22	2	2	40076	49618	40076	42903
RL8	P62917	HUMAN	755.65	28024.654	13	13	8172978	8235475	8172978	7121023
RL9	P32969	HUMAN	1085.92	21863.408	14	15	3679457	4863104	3679457	4205013
RLA0	P05388	HUMAN	1530.34	34273.508	25	25	11330225	11706325	11330225	10122185
RLA1	P05386	HUMAN	405.27	11513.929	3	6	259606	477340	259606	412744
RLA2	P05387	HUMAN	776.25	11664.931	8	11	1480770	2338451	1480770	2022004
RM11	Q9Y3B7	HUMAN	279.34	20683.184	6	6	60500	60001	60500	51881
RM22	Q9NWU5	HUMAN	82.06	23640.646	2	2	10397	11823	10397	10223
RM24	Q96A35	HUMAN	53.32	24914.824	1	1	7033	16220	7033	14025
RM54	Q6P161	HUMAN	187.52	15819.155	3	3	63217	88325	63217	76373
RNPS1	Q15287	HUMAN	88.13	34208.25	2	2	59066	48047	59066	41545
ROA0	Q13151	HUMAN	283.24	30840.65	6	6	145164	255712	145164	221108
ROA1	P09651	HUMAN	715.7	38746.656	10	11	384993	318813	384993	275670
ROA2	P22626	HUMAN	498.28	37429.707	9	10	146202	170092	146202	147075
ROA3	P51991	HUMAN	570.3	39594.945	9	9	241869	362056	241869	313062
ROAA	Q99729	HUMAN	140.13	36224.875	2	2	21039	7217	21039	6240
RPA1	O95602	HUMAN	38.75	194809.83	1	1	3014	9648	3014	8343
RPA34	O15446	HUMAN	62.37	54985.676	2	2	14083	49173	14083	42519
RPA49	Q9GZS1	HUMAN	59.37	47260.25	1	1	19813	39748	19813	34369
RPAB1	P19388	HUMAN	112.67	24551.217	2	2	14355	6606	14355	5712
RPAB3	P52434	HUMAN	41.1	17143.293	1	1	10324	12169	10324	10522
RPF2	Q9H7B2	HUMAN	86.69	35582.883	2	2	33217	122725	33217	106117
RPN2	P04844	HUMAN	77.23	69284.08	2	2	18263	23553	18263	20365
RRBP1	Q9P2E9	HUMAN	1435.56	152455.56	25	26	59706	114591	59706	99084
RRP1	P56182	HUMAN	155.86	52839.246	3	3	27112	36425	27112	31496
RRP12	Q5JTH9	HUMAN	106.31	143701.62	1	2	16939	33700	16939	29140
RRP1B	Q14684	HUMAN	1064.36	84427.52	21	22	154521	273693	154521	236656
RRP5	Q14690	HUMAN	1226.31	208698.8	25	25	16583	100025	16583	86489
RRP7A	Q9Y3A4	HUMAN	122.24	32334.037	2	2	17686	48765	17686	42166
RRP8	O43159	HUMAN	182.33	50714.805	4	4	17337	33625	17337	29075
RRS1	Q15050	HUMAN	288.63	41193.324	5	5	41112	174290	41112	150705
RS10	P46783	HUMAN	249.93	18897.77	5	5	188353	206457	188353	178519
RS11	P62280	HUMAN	948.68	18430.715	17	17	2997771	2898980	2997771	2506680
RS12	P25398	HUMAN	149.77	14514.926	3	3	119829	91665	119829	79260
RS13	P62277	HUMAN	510.61	17222.293	10	10	4398917	5599753	4398917	4841976
RS14	P62263	HUMAN	541.58	16272.697	10	10	2394015	3553063	2394015	3072251
RS15	P62841	HUMAN	896.24	17040.088	12	12	1981464	2531130	1981464	2188609
RS15A	P62244	HUMAN	747.06	14839.5	13	13	4915498	5289674	4915498	4573858
RS16	P62249	HUMAN	885.38	16445.307	16	16	3189590	3659689	3189590	3164447
RS17	P08708	HUMAN	766.07	15550.114	10	10	2094242	2950622	2094242	2551334
RS18	P62269	HUMAN	813.72	17718.666	16	16	2955445	3765272	2955445	3255742
RS19	P39019	HUMAN	373.32	16060.491	8	9	549397	859077	549397	742824
RS2	P15880	HUMAN	1307.61	31324.432	20	20	5656282	8488574	5656283	7339871
RS20	P60866	HUMAN	300.91	13372.707	4	4	610227	669151	610227	578599
RS23	P62266	HUMAN	628.11	15807.548	10	10	2428081	3229774	2428081	2792710
RS24	P62847	HUMAN	492.74	15423.179	8	8	1962507	2675864	1962507	2313757
RS25	P62851	HUMAN	474.78	13742.125	10	10	2561306	2658272	2561307	2298546
RS26	P62854	HUMAN	229.49	13015.42	4	5	3731658	4394113	3731658	3799487
RS27	P42677	HUMAN	396.13	9461.116	2	6	1542926	1568334	1542926	1356102
RS27A	P62979	HUMAN	599.64	17964.902	11	11	1171149	1384084	1171149	1196785
RS27L	Q71UM5	HUMAN	289.24	9477.159	1	5	1212720	1169826	1212720	1011521
RS28	P62857	HUMAN	55.76	7841.0215	1	1	208165	152589	208165	131940
RS3	P23396	HUMAN	720.39	26688.326	15	16	798194	829339	798194	717110
RS30	P62861	HUMAN	85.96	6647.856	2	2	2693309	3570319	2693309	3087171
RS3A	P61247	HUMAN	1867.37	29944.91	29	31	4004256	5356849	4004256	4631943
RS4X	P62701	HUMAN	1373.02	29597.73	23	24	6439536	8501078	6439536	7350683
RS5	P46782	HUMAN	319.44	22876.38	7	7	157622	190787	157622	164969
RS6	P62753	HUMAN	1136.58	28680.63	20	20	6550024	8964939	6550025	7751774
RS7	P62081	HUMAN	610.6	22126.844	12	12	2761657	3649804	2761657	3155900
RS8	P62241	HUMAN	994.74	24205.176	16	16	6348209	10114429	6348209	8745710
RS9	P46781	HUMAN	777.62	22591.424	18	18	3886731	4177397	3886731	3612098
RSMB	P14678	HUMAN	120.93	24610.102	4	4	64951	72790	64951	62939
RT18B	Q9Y676	HUMAN	99.99	29395.578	2	2	24584	54673	24584	47275
RT22	P82650	HUMAN	77.1	41280.387	2	2	16043	32489	16043	28093
RT23	Q9Y3D9	HUMAN	41.1	21770.64	1	1	10210	17109	10210	14794
RT25	P82663	HUMAN	84.16	20116.377	2	2	5284	12063	5284	10430
RT26	Q9BYN8	HUMAN	166.86	24211.705	4	4	26025	48157	26025	41640
RT27	Q92552	HUMAN	347.93	47611.4	6	6	25276	56688	25276	49016
RT34	P82930	HUMAN	83.9	25650.469	2	2	14145	30432	14145	26314
RTCB	Q9Y3I0	HUMAN	77.45	55210.316	2	2	8474	6087	8474	5263
RU2A	P09661	HUMAN	93.18	28415.559	2	2	10736	23947	10736	20706
RU2B	P08579	HUMAN	46.14	25486.33	1	1	10673	7982	10673	6902
RUXE	P62304	HUMAN	45.17	10803.593	1	1	199749	163127	199749	141052
S10A7	P31151	HUMAN	63.08	11470.972	1	1	163438	93682	163438	81005
S10A8	P05109	HUMAN	178.83	10834.503	4	4	89774	35887	89774	31030
S10A9	P06702	HUMAN	129.09	13241.983	2	2	131207	27745	131207	23991
SAP18	O00422	HUMAN	126.87	17561.066	3	3	3366	7814	3366	6756
SDA1	Q9NVU7	HUMAN	50.61	79871.31	2	2	20031	24987	20031	21606

Supplementary Table 4 (Page 8 of 9) – List of detected proteins immunoprecipitated from HSV-1 infected cells.

Gene	Accession	Species	Confidence score	Mass	Unique Peptides	Peptide Count	Control Raw Protien Abundance	HSV-1 Raw Protien Abundance	Control Normalised Protien Abundance	HSV-1 Normalised Protien Abundance
SDF2L	Q9HCN8	HUMAN	76.49	23598.318	1	1	23814	41731	23814	36083
SENP3	Q9H4L4	HUMAN	70.05	65009.9	1	1	15155	25182	15155	21774
SERA	O43175	HUMAN	161.63	56650.535	3	3	17763	18256	17763	15786
SF3A1	Q15459	HUMAN	47.94	88886.23	1	1	10634	17296	10634	14955
SF3B1	O75533	HUMAN	510.06	145829.88	10	11	37631	59493	37631	51443
SF3B2	Q13435	HUMAN	647.88	100227.72	11	12	74932	85781	74932	74173
SF3B3	Q15393	HUMAN	656.71	135577.17	14	14	48911	90864	48911	78568
SF3B4	Q15427	HUMAN	64.2	44385.723	1	1	88863	93205	88863	80592
SF3B6	Q9Y3B4	HUMAN	122.8	14584.876	2	2	23159	44987	23159	38899
SFPQ	P23246	HUMAN	2684.94	76149.586	45	46	1378339	4844208	1378339	4188674
SGPL1	O95470	HUMAN	102.95	63523.848	2	2	9139	11648	9139	10072
SLIT2	O94813	HUMAN	92.97	169869.12	2	2	12145	787	12145	680
SMC1A	Q14683	HUMAN	113.68	143232.56	1	3	7586	3967	7586	3431
SMC2	O95347	HUMAN	322.49	135655.77	7	7	15666	7694	15666	6653
SMC3	Q9UQE7	HUMAN	63.2	141541.4	1	1	8951	7228	8951	6249
SMC4	Q9NTJ3	HUMAN	102.11	147181.53	1	2	4957	7301	4957	6313
SMD1	P62314	HUMAN	125.08	13281.563	2	2	188149	214162	188149	185181
SMD2	P62316	HUMAN	167.77	13526.864	4	4	109041	89700	109041	77561
SMD3	P62318	HUMAN	99.27	13916.24	2	2	191611	216579	191611	187271
SMU1	Q2TAY7	HUMAN	123.98	57543.95	3	3	3614	32347	3614	27970
SNR40	Q96DI7	HUMAN	62.26	39310.54	1	1	12484	9829	12484	8498
SNRPA	P09012	HUMAN	60.15	31279.549	2	2	22257	17645	22257	15257
SNUT1	O43290	HUMAN	331.4	90254.84	6	6	35989	29898	35989	25852
SNUT2	Q53GS9	HUMAN	162.62	65380.633	4	4	21974	20030	21974	17319
SNW1	Q13573	HUMAN	144.79	61494.51	3	3	7315	19802	7315	17122
SOGA1	O94964	HUMAN	366.63	159759.4	9	9	59559	39332	59559	34010
SP16H	Q9Y5B9	HUMAN	1146.5	119913.75	23	23	313287	117530	313287	101626
SPAS2	Q86XZ4	HUMAN	132.46	59544.7	1	2	40487	44878	40487	38805
SPB1	Q8IY81	HUMAN	762.67	96558.484	14	15	70769	186558	70769	161312
SPB12	Q96P63	HUMAN	380.98	46276.45	6	6	190237	67674	190237	58516
SPB3	P29508	HUMAN	183.63	44564.617	3	3	46747	25574	46747	22113
SPF45	Q96I25	HUMAN	68.28	44961.598	2	2	31154	19943	31154	17244
SPS2L	Q9NUQ6	HUMAN	549.91	61729.062	10	10	98520	83208	98520	71948
SRP09	P49458	HUMAN	104.24	10111.734	3	3	68983	41009	68983	35459
SRP14	P37108	HUMAN	347.9	14569.933	7	7	508906	284837	508906	246292
SRPK1	Q96SB4	HUMAN	873.45	74324.87	11	16	203986	249958	203986	216133
SRPK2	P78362	HUMAN	410.87	77526.8	6	11	22510	28898	22510	24987
SRRM1	Q8IYB3	HUMAN	729.41	102335.05	12	13	101504	107449	101504	92909
SRRM2	Q9UQ35	HUMAN	208.03	299615.94	4	4	34377	16492	34377	14260
SRS10	O75494	HUMAN	170.74	31300.527	3	3	54349	75518	54349	65298
SRS11	Q05519	HUMAN	50.54	53542.305	1	1	21348	22388	21348	19358
SRSF1	Q07955	HUMAN	610.33	27744.57	10	11	258020	368655	258020	318767
SRSF2	Q01130	HUMAN	323.95	25476.344	7	7	1231971	1417736	1231971	1225884
SRSF3	P84103	HUMAN	493.6	19329.586	10	11	732846	852820	732846	737414
SRSF4	Q08170	HUMAN	569.3	56678.406	4	10	30567	35110	30567	30359
SRSF5	Q13243	HUMAN	508.49	31263.822	8	9	383450	466671	383450	403520
SRSF6	Q13247	HUMAN	863.08	39586.812	9	15	246150	328404	246150	283963
SRSF7	Q16629	HUMAN	310.23	27366.53	5	6	306922	338526	306922	292715
SRSF9	Q13242	HUMAN	160.33	25542.229	4	4	28077	19006	28077	16434
SSBP	Q04837	HUMAN	125.58	17259.658	3	3	48165	100549	48165	86942
SSF1	Q9NQ55	HUMAN	245.73	53193.94	6	6	42079	91398	42079	79030
SSRD	P51571	HUMAN	47.52	18998.604	1	1	15449	17020	15449	14717
SSRP1	Q08945	HUMAN	582.52	81074.91	12	12	301809	108545	301809	93857
STAU1	O95793	HUMAN	1723.37	63182.36	25	29	1173731	685874	1173732	593059
STAU2	Q9NUL3	HUMAN	227.59	62608.527	2	6	17889	21742	17889	18800
STRAP	Q9Y3F4	HUMAN	227.68	38438.344	5	5	38878	24297	38878	21009
SUGP2	Q8IX01	HUMAN	997.34	120207.1	20	20	16963	123666	16963	106932
SURF6	O75683	HUMAN	107.04	41450.42	2	2	11068	39093	11068	33803
SYQ	P47897	HUMAN	63.68	87798.766	1	1	8190	13009	8190	11249
TADBP	Q13148	HUMAN	191.02	44739.766	4	4	17392	12229	17392	10574
TBA1B	P68363	HUMAN	1145.78	50151.684	3	20	952602	934598	952602	808125
TBA1C	Q9BQE3	HUMAN	984.41	49895.38	1	18	92137	90396	92137	78163
TBA8	Q9NY65	HUMAN	644.25	50093.605	1	11	548113	657727	548113	568721
TBAL3	A6NHL2	HUMAN	173.38	49908.785	1	3	10049	12582	10049	10879
TBB4B	P68371	HUMAN	1425.02	49831.047	4	23	390090	465049	390090	402117
TBB5	P07437	HUMAN	1500.45	49670.855	6	25	1193975	1293017	1193975	1118041
TBB6	Q9BUF5	HUMAN	418.33	49857.145	1	8	9231	10585	9231	9152
TBL2	Q9Y4P3	HUMAN	269.55	49797.867	5	5	32813	53395	32813	46169
TBL3	Q12788	HUMAN	709.02	89034.65	12	12	41077	86107	41077	74455
TCOF	Q13428	HUMAN	39.15	152105.42	1	1	17220	35924	17220	31062
TCP4	P53999	HUMAN	118.19	14395.331	3	3	108737	5269	108737	4556
TDIF2	Q5QJE6	HUMAN	122.16	84469.13	3	3	11673	29890	11673	25845
TDRD3	Q9H7E2	HUMAN	227.64	73184.82	5	5	17236	16525	17236	14289
TECR	Q9NZ01	HUMAN	151.27	36034.406	4	4	27613	28367	27613	24528
TEX10	Q9NXF1	HUMAN	198.21	105674.02	4	4	13849	36296	13849	31384
TGM1	P22735	HUMAN	141.49	89786.74	3	3	29495	17689	29495	15295
TGM3	Q08188	HUMAN	422.4	76631.875	9	9	101001	53387	101001	46162
THIO	P10599	HUMAN	151.09	11737.491	3	3	176278	120734	176278	104396
THOC2	Q8NI27	HUMAN	146.82	182773.55	3	3	3341	13685	3341	11833
THOC4	Q86V81	HUMAN	699.95	26887.898	12	12	496075	778741	496075	673359
TIA1	P31483	HUMAN	40.82	42963.11	1	1	20474	15093	20474	13051
TIF1B	Q13263	HUMAN	577.62	88549.67	11	11	124187	46249	124187	39991
TIRR	Q9BRJ7	HUMAN	47.5	23338.252	1	1	1030	14425	1030	12473
TMA16	Q96EY4	HUMAN	58.91	23864.273	2	2	44984	29340	44984	25370
TOP1	P11387	HUMAN	1142.08	90725.69	22	22	396963	482742	396963	417415
TOP2A	P11388	HUMAN	3755.92	174384.25	56	70	710142	542201	710142	468828
TOP2B	Q02880	HUMAN	2781.95	183266.1	35	49	237467	182186	237467	157532

Supplementary Table 4 (Page 9 of 9) – List of detected proteins immunoprecipitated from HSV-1 infected cells.

Gene	Accession	Species	Confidence score	Mass	Unique Peptides	Peptide Count	Control Raw Protien Abundance	HSV-1 Raw Protien Abundance	Control Normalised Protien Abundance	HSV-1 Normalised Protien Abundance
TOP3B	O95985	HUMAN	206.73	96662.02	5	5	13020	27630	13020	23891
TPM3	P06753	HUMAN	39.42	32949.96	1	1	50898	20790	50898	17977
TR150	Q9Y2W1	HUMAN	725.43	108665.81	13	14	93957	137109	93957	118555
TRA2A	Q13595	HUMAN	195.41	32688.63	2	4	30135	44239	30135	38252
TRA2B	P62995	HUMAN	316.35	33665.67	4	6	113462	168225	113462	145460
TRAM1	Q15629	HUMAN	43.34	43071.61	1	1	9105	10350	9105	8950
TRFE	P02787	HUMAN	124.57	77063.97	2	2	26776	35087	26776	30339
TRFL	P02788	HUMAN	192.01	78181.99	4	4	37477	31122	37477	26911
TRI25	Q14258	HUMAN	409.32	70973.52	9	9	107576	103690	107576	89658
TRI26	Q12899	HUMAN	445.64	62166.023	9	9	75134	150708	75134	130314
TRM1L	Q7Z2T5	HUMAN	489.92	81747.4	9	9	222105	263050	222105	227453
TRM2A	Q8IZ69	HUMAN	37.18	68725.63	1	1	4743	5867	4743	5073
TRY1	P07477	HUMAN	611.44	26558.076	8	13	20695941	19157156	20695940	16564745
TRY3	P35030	HUMAN	175.91	32528.826	3	4	492288	166013	492288	143548
TRY6	Q8NHM4	HUMAN	291.22	26537.229	1	6	4310	4708	4310	4071
TSR1	Q2NL82	HUMAN	601.66	91810.086	11	11	73529	73841	73529	63848
TXTP	P53007	HUMAN	148.76	34012.715	3	3	27844	41182	27844	35609
U2AF2	P26368	HUMAN	888.96	53501.047	14	15	879070	1262514	879070	1091666
U2AF5	P0DN76	HUMAN	327.71	27872.05	7	7	317493	431771	317493	373342
U3IP2	O43818	HUMAN	163.51	51840.69	4	5	392057	310277	392057	268289
U520	O75643	HUMAN	2249.67	244505.17	44	44	85431	97844	85431	84603
U5S1	Q15029	HUMAN	1202.36	109435.695	21	23	91521	577150	91521	499048
UBP2L	Q14157	HUMAN	411.19	114534.34	8	8	17700	26540	17700	22948
UBP36	Q9P275	HUMAN	52.78	122907.836	1	1	3557	9979	3557	8629
URB2	Q14146	HUMAN	48.9	170543.05	1	1	249	9199	249	7954
UT14A	Q9BVJ6	HUMAN	307.25	87977.84	7	7	12339	29258	12339	25298
UTP15	Q8TED0	HUMAN	419.11	58415.32	10	10	12136	62151	12136	53741
UTP18	Q9Y5J1	HUMAN	430.79	62003.656	7	7	62705	83787	62705	72448
UTP20	O75691	HUMAN	336.22	318384.72	6	6	14053	21039	14053	18192
UTP4	Q969X6	HUMAN	292.87	76890.195	6	6	7381	42665	7381	36891
UTP6	Q9NYH9	HUMAN	91.23	70193.984	2	2	2179	22690	2179	19619
VIME	P08670	HUMAN	818.4	53651.746	12	15	256669	122822	256669	106202
VSIG8	P0DPA2	HUMAN	40.5	43890.78	1	1	30963	3117	30963	2695
VTNC	P04004	HUMAN	54.58	54305.594	1	1	17291	26951	17291	23304
WDR12	Q9GZL7	HUMAN	467.33	47708.008	10	10	22767	65374	22767	56527
WDR18	Q9BV38	HUMAN	266.88	47405.273	6	6	44630	66862	44630	57814
WDR3	Q9UNX4	HUMAN	600.32	106098.9	11	11	27040	75624	27040	65390
WDR33	Q9C0J8	HUMAN	41.7	145891.44	1	1	0	2479	0	2143
WDR36	Q8NI36	HUMAN	577.02	105322.02	11	11	59542	108704	59542	93994
WDR43	Q15061	HUMAN	154.04	74890.73	4	4	6679	37266	6679	32223
WDR46	O15213	HUMAN	183.83	68071.125	4	4	9655	33127	9655	28644
WDR5	P61964	HUMAN	220.81	36588.51	4	4	27422	34816	27422	30104
WDR74	Q6RFH5	HUMAN	85.01	42441.258	2	2	7172	15545	7172	13442
WDR75	Q8IWA0	HUMAN	150.39	94498.77	5	5	18169	46086	18169	39849
XRCC1	P18887	HUMAN	35.81	69476.586	1	1	6702	7639	6702	6605
XRCC5	P13010	HUMAN	342.6	82704.58	6	6	69572	60506	69572	52318
XRCC6	P12956	HUMAN	584.88	69843.16	12	12	49017	56060	49017	48474
XRN2	Q9H0D6	HUMAN	361.83	108582.516	7	7	23174	37887	23174	32760
YBOX1	P67809	HUMAN	1074.82	35924.207	11	16	1346996	1819240	1346996	1573054
YBOX3	P16989	HUMAN	750.9	40089.973	6	11	339905	379588	339905	328220
YTDC2	Q9H6S0	HUMAN	478.46	160247.67	11	11	28277	30806	28277	26637
YTHD2	Q9Y5A9	HUMAN	221.63	62334.24	4	4	73973	22096	73973	19106
ZA2G	P25311	HUMAN	215.41	34258.71	4	4	121955	75139	121955	64971
ZC21A	Q96GY0	HUMAN	44.04	35092.164	1	1	8705	18002	8705	15566
ZC3HF	Q8WU90	HUMAN	82.79	48602.57	2	2	11546	12250	11546	10592
ZCCHV	Q7Z2W4	HUMAN	1210.42	101431.336	23	23	156150	188288	156150	162809
ZCH18	Q86VM9	HUMAN	257.94	106378.54	4	4	24680	19874	24680	17185
ZCHC3	Q9NUD5	HUMAN	563.54	43547.418	9	9	127496	278659	127496	240950
ZN326	Q5BKZ1	HUMAN	247.52	65653.94	4	4	1152	118001	1152	102033
ZN486	Q96H40	HUMAN	122.67	53630.67	3	3	14027	5242	14027	4533
ZN512	Q96ME7	HUMAN	49.44	64682.22	2	2	16278	17034	16278	14729
ZN598	Q86UK7	HUMAN	340.84	98636.99	7	7	3689	90971	3689	78660
ZN787	Q6DD87	HUMAN	43.94	40428.383	1	1	9400	10214	9400	8832
ZO2	Q9UDY2	HUMAN	365.43	133957.89	8	8	37966	14078	37966	12173



Supplementary Figure 1 – IFN A/D Standard. Corresponds to results summarised in Figure 24 and discussed in section III.2. 3C11 cells that express luciferase under an interferon stimulated response element were treated with an IFNA/D standard. Standards from individual bioassays were used to convert luminescence scores to IFN values. The limit of detection (LD) was defined as highest luminescence recorded for media with 0 U/ml of IFN A/D. The saturation point (SP) was defined as the value at which luminescence induction by IFN A/D moved outside of the linear range. Samples being tested were diluted to ensure they could be read within the SP and LD (n=3, SEM displayed, biological repeats, representative graph set shown).

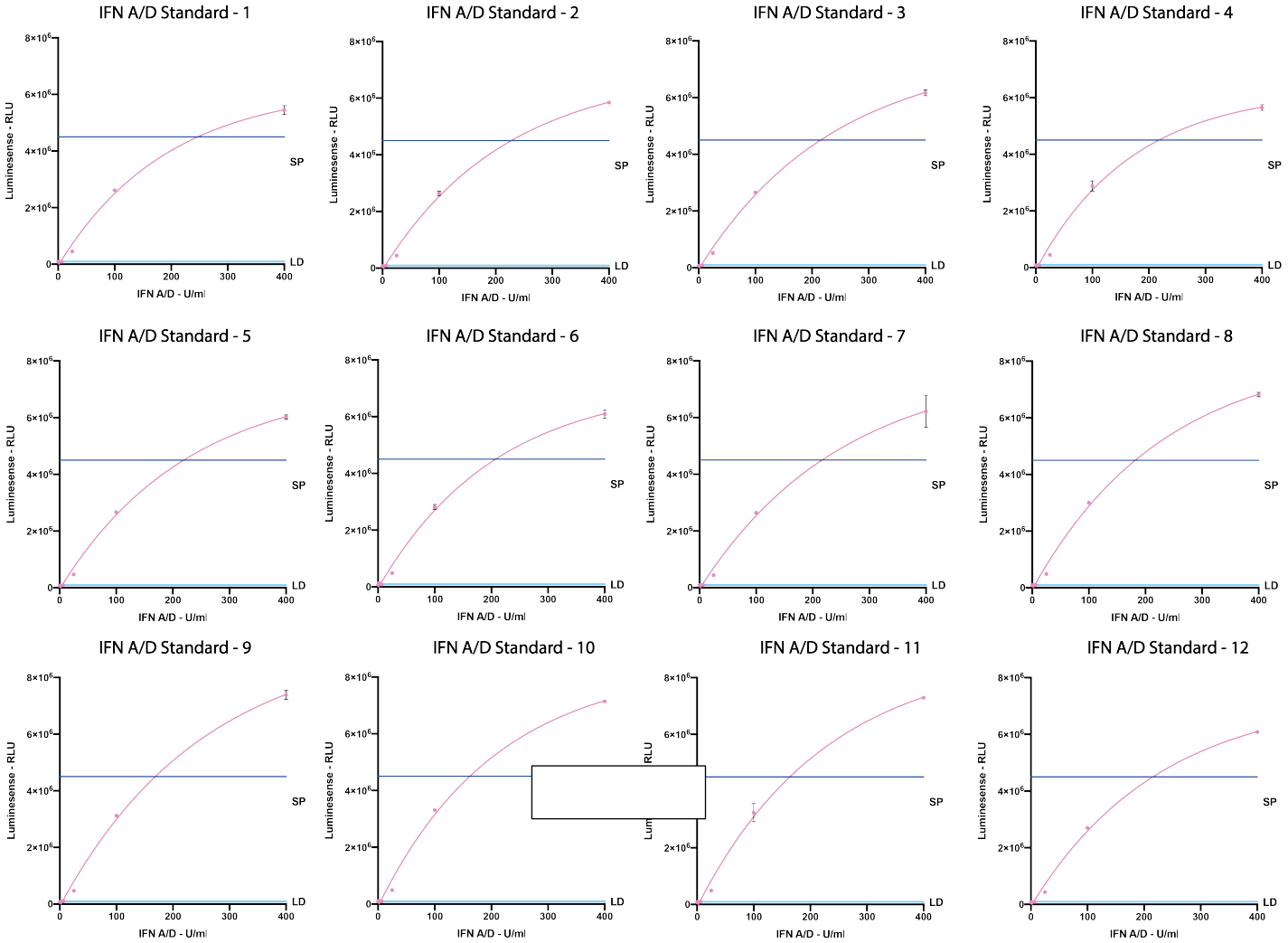
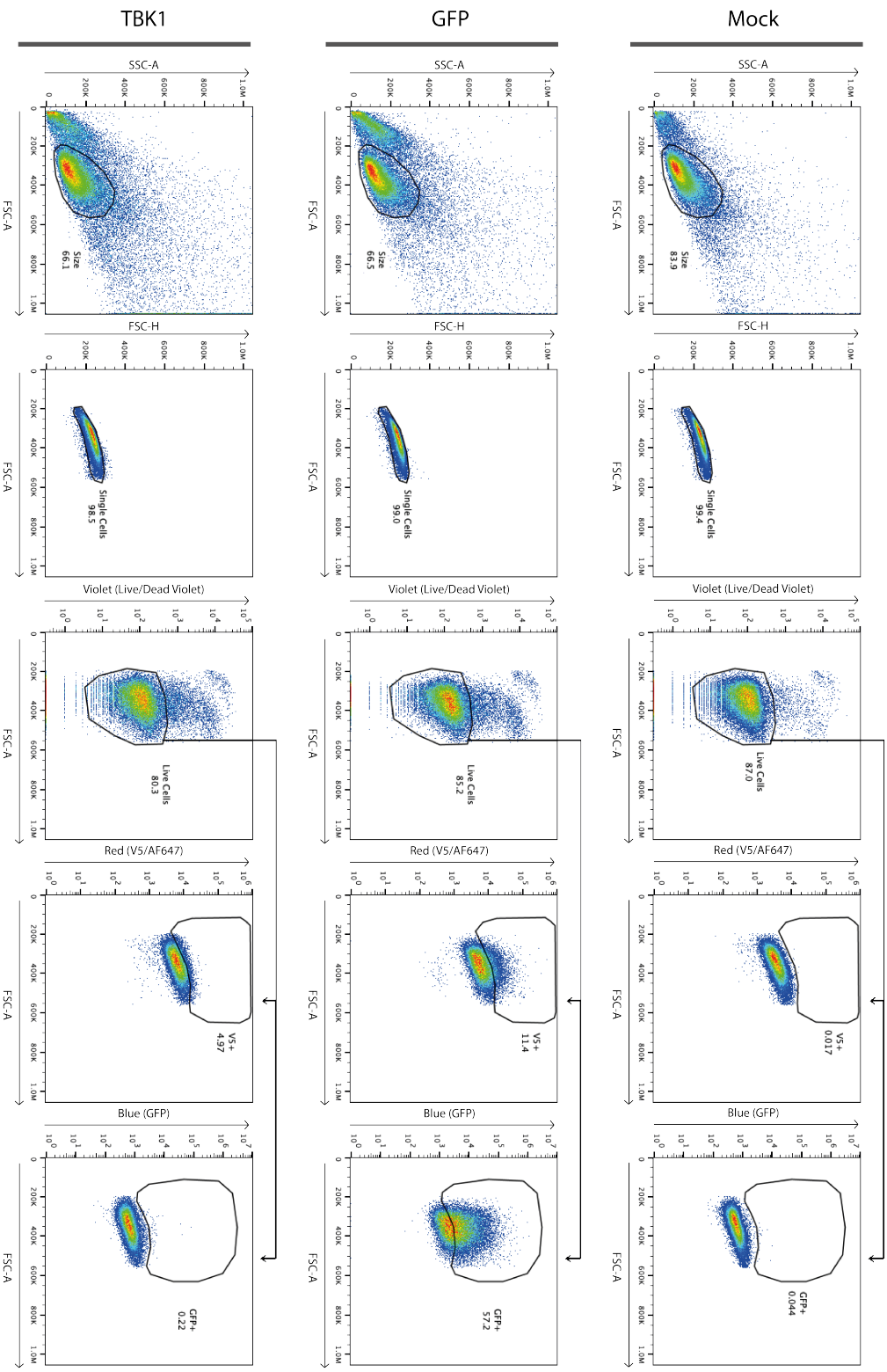
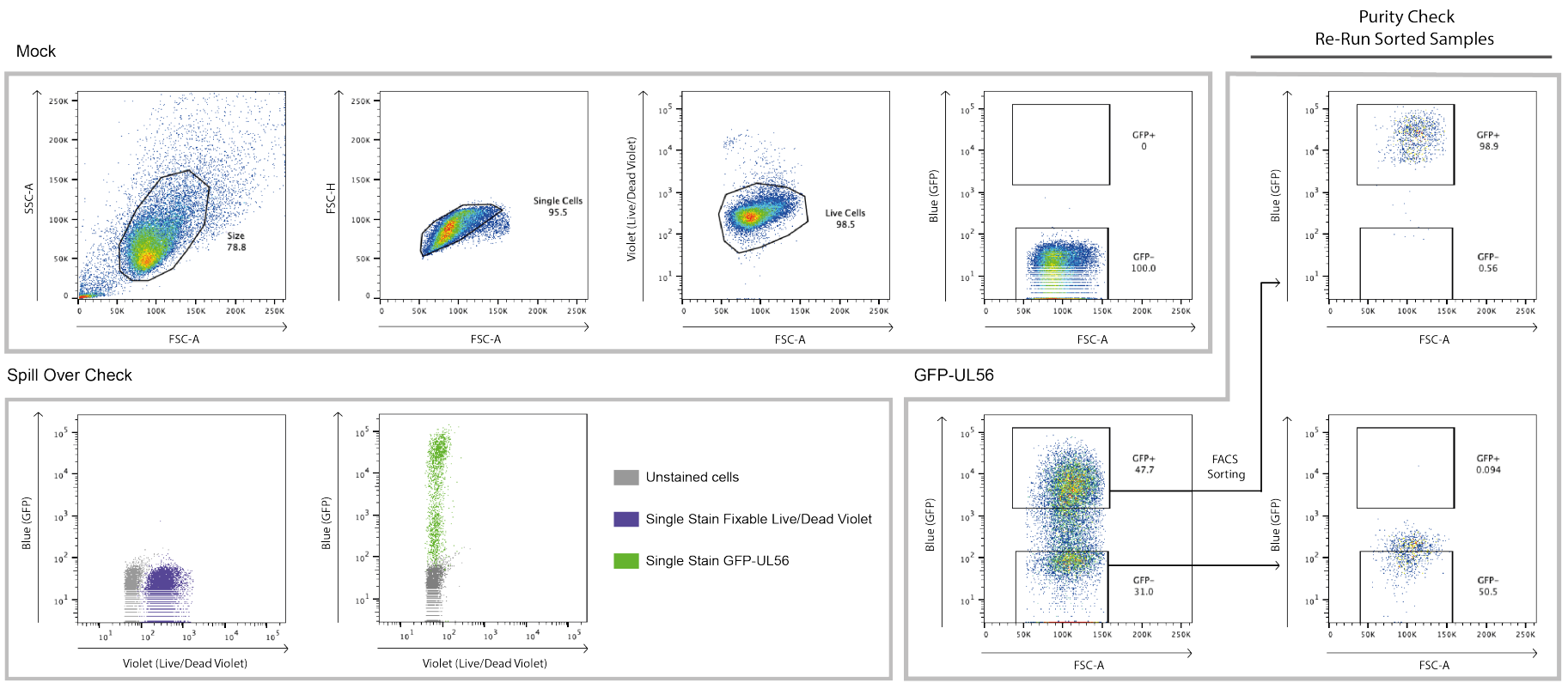


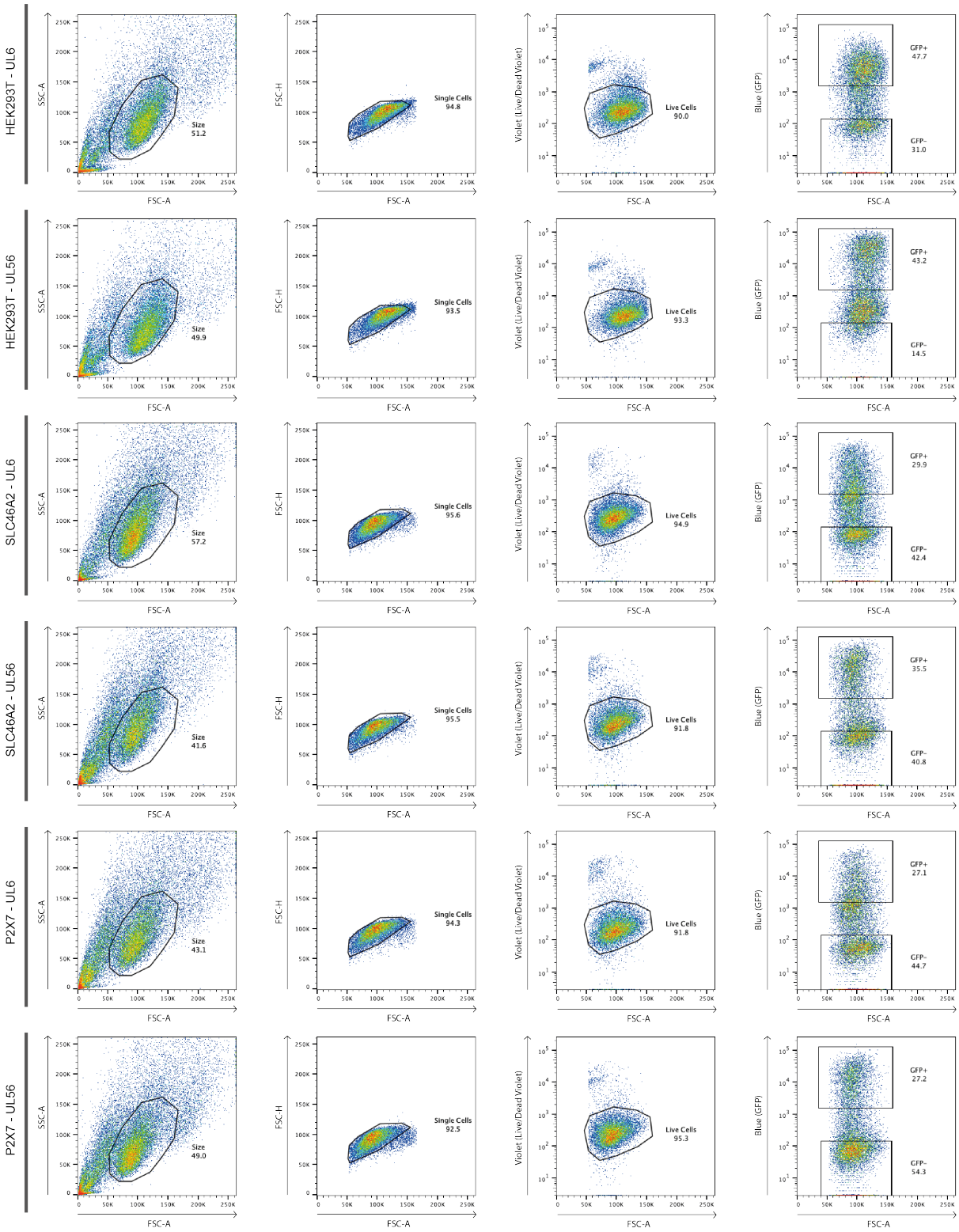
Figure 2 – IFN A/D Standard. Corresponds to results summarised in Figure 25 and discussed in section III.3. 3C11 cells that express luciferase under an interferon stimulated response element were treated with an IFNA/D standard. Standards from individual bioassays were used to convert luminescence scores to IFN values. The limit of detection (LD) was defined as highest luminescence recorded for media with 0 U/ml of IFN A/D. The saturation point (SP) was defined as the value at which luminescence induction by IFN A/D moved outside of the linear range. Samples being tested were diluted to ensure they could be read within the SP and LD (SEM displayed, n=1).



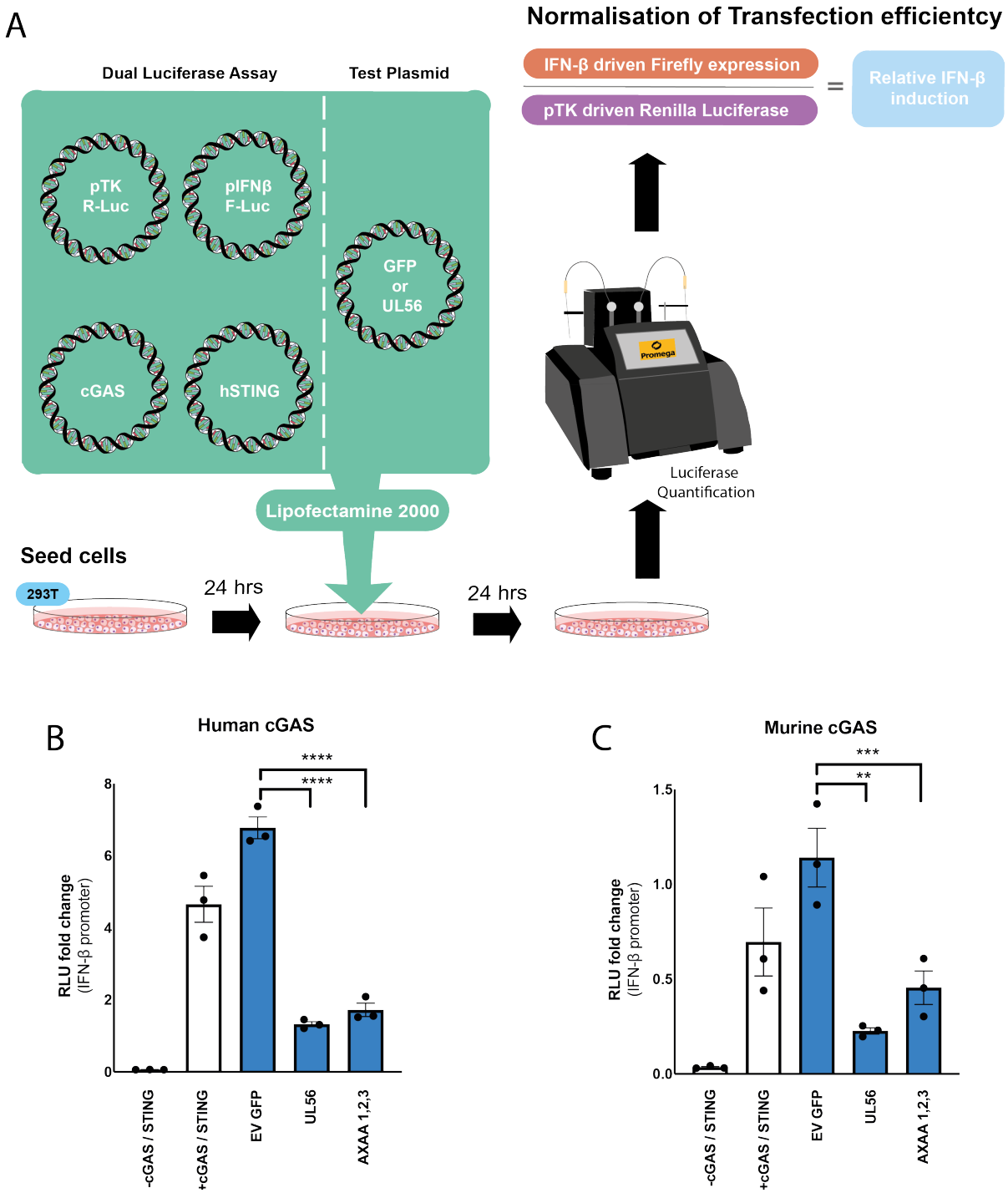
Supplementary Figure 3 – Gating strategy. Corresponds to results summarised in Figure 28 and discussed in section III.4. THP1 cells stably over expressing the indicated genes were assessed for GFP and V5 expression by flow cytometry (n=1).



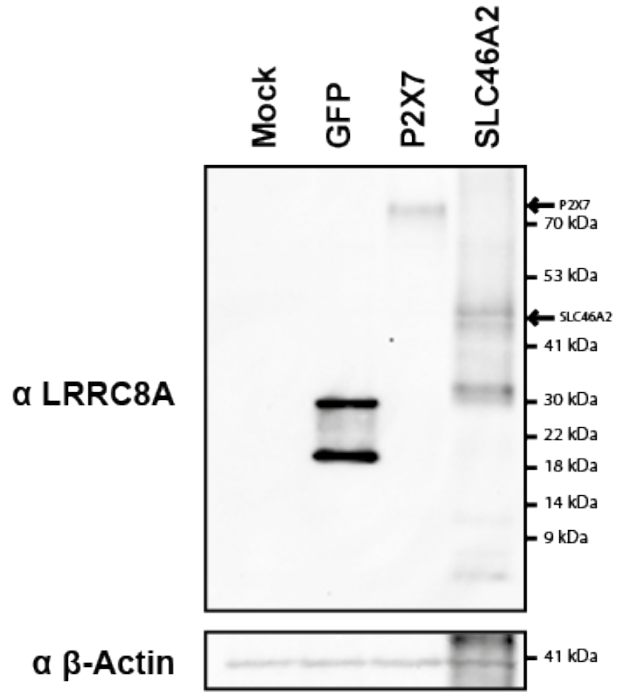
Supplementary Figure 4 - Gating strategy. Corresponds to FACS sorting preformed in Figures 48, 54 and 57 and discussed in Chapters V.3, VI.1 and VI.4. HEK293T cells were stained with fixable live/dead violet and negative and positive gates set. Single stained controls were used to compensate for spill over between flourophores. Cells transfected with GFP tagged HSV-1 genes were sorted into GFP- and GFP+ populations. A small proportion of the sorted cells were purity checked by re-running the samples on the sorter (n=3, biological repeats, representative figure shown).



Supplementary Figure 5 – Cell sorting. FACS plots of cells from Figures 48, 64 and 57 discussed in Chapters V.3 and VI.1 and VI.4. Untransduced HEK293Ts (WT) or cells stably expressing P2X7-V5 or SLC46A2-V5 were transfected with GFP-UL56 or the control gene GFP-UL6. Cells were then sorted into GFP- and GFP+ populations to be lysed and protein abundance assessed by western blotting (n=3, biological repeats, representative plots shown).



Supplementary Figure 6 – UL56 inhibits cGAS independet of its PPXY motifs. A) HEK293T cells were transfected with p125-FLuc (IFN-β promoter reporter), pRL-TK (constitutively expresses renilla luciferase), pcDNA3.2-STING and plenti6.2-hcGAS (B) or pcDNA3-mcGAS (C). Simultaneously test plenti6.2 plasmids encoding GFP, UL56 or UL56 AXAA123 were co-transfected to assess their effect on cGAS activity. IFN-β production was then assessed 24 hours after transfection. Graphs display average of three technical replicates statistically evaluated by one-way ANOVA – Dunnett's multiple comparison test. *=p<0.05, **=p<0.01, ***=p<0.001, ****=p<0.0001, ns=not significant (n=1).



Supplementary Figure 7 – Blastacistidin resistant HEK293T cells overexpressing P2X7 and SLC46A2. A western blot of HEK293T cell stably exspressing GFP-V5, P2X7-V5 and SLC46A2-V5. Cells were transduced using the plenti6.2-V5 (BLAST) lentiviral constructs. (Experiment performed by Jed Avissar under my close supervision) (n=3, biological repeats).